



UNIVERSITÀ DELLA CALABRIA



# UNIVERSITY of CALABRIA

Department of Civil Engineering

**Doctoral School “Pitagora” in Engineering Sciences**

*Doctoral Thesis in Material and Structural Engineering*

This work was supported from  
the European Social Fund and the Region of Calabria

*Cycle XXVII (2011-2014)*

## **ADVANCED STRUCTURAL ANALYSES OF CABLE SUPPORTED BRIDGES**

*Sector ICAR/08 – Structural Mechanics*



**Course Coordinator:** Prof. Renato Sante Olivito

**Thesis Advisor:** Prof. Paolo Lonetti

**PhD Student:** Arturo Pascuzzo



UNIVERSITÀ DELLA CALABRIA



# UNIVERSITY of CALABRIA

Department of Civil Engineering

**Doctoral School “Pitagora” in Engineering Sciences**

*Doctoral Thesis in Material and Structural Engineering*

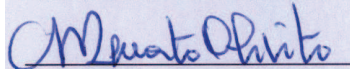
This work was supported from  
the European Social Fund and the Region of Calabria

*Cycle XXVII (2011-2014)*

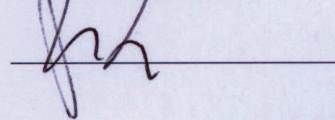
## **ADVANCED STRUCTURAL ANALYSES OF CABLE SUPPORTED BRIDGES**

*Sector ICAR/08 – Structural Mechanics*

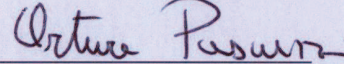
**Course Coordinator**  
Prof. Renato Sante Olivito



**Thesis Advisor**  
Prof. Paolo Lonetti



**Author**  
Arturo Pascuzzo





This thesis is co-financed by the European Commission, the European Social Fund and the Region of Calabria. The author is solely responsible for this thesis and the European Commission and the Region of Calabria are not responsible for any use that may be made of the information contained therein.

La presente tesi è cofinanziata con il sostegno della Commissione Europea, Fondo Sociale Europeo e della Regione Calabria. L'autore è il solo responsabile di questa tesi e la Commissione Europea e la Regione Calabria declinano ogni responsabilità sull'uso che potrà essere fatto delle informazioni in essa contenute.

Arturo Pascuzzo

# CONTENTS

<b>LIST OF FIGURES.....</b>	<b>I</b>
<b>LIST OF TABLES.....</b>	<b>XIII</b>
<b>NOMENCLATURE .....</b>	<b>XV</b>
<b>ABSTRACT/SOMMARIO .....</b>	<b>XIX</b>
<b>1. INTRODUCTION .....</b>	<b>1</b>
1.1. Current issues in the field of cable supported bridges.....	1
1.2. Background of cable supported bridges .....	2
1.2.1. Suspension scheme .....	3
1.2.2. Cable-stayed scheme.....	9
1.2.3. Hybrid cable-stayed suspension scheme .....	13
1.2.4. Self-anchored cable-stayed suspension scheme.....	18
1.3 The longest suspension and cable-stayed bridges built to date .....	22

## CONTENTS

---

1.4. Literature review.....	25
1.4.1. Design methodologies .....	25
1.4.2. Moving loads and damage mechanisms .....	27
1.4.3. Nonlinear behavior of cable supported bridges.....	27
1.5. Objectives and motivations of the thesis .....	31
1.6. Thesis structure.....	35
<b>2. OPTIMUM DESIGN METHODOLOGY.....</b>	<b>39</b>
2.1. Introduction .....	39
2.1.1. The unit load method (ULM) .....	40
2.1.2. The zero displacement method (ZDM) .....	42
2.1.3. The force equilibrium method (FEM) .....	44
2.1.4. The optimization method (OM) .....	46
2.2. The proposed design methodology .....	49
2.2.1. Hybrid cable-stayed suspension bridge scheme .....	50
2.2.2. Cable-stayed and suspension schemes – Pure systems .....	61
2.2.3. Self-anchored cable-stayed suspension bridge scheme .....	63
2.2.4. Application on the intermediate erection stages.....	64
2.3. Bridge formulation .....	66
2.3.1. Girder and pylons formulation .....	66
2.3.2. Cable formulation.....	68
2.4. Finite element implementation .....	69
2.5. Numerical implementation of the design methodology .....	74
2.6. Numerical implementation of the design methodology .....	77
2.6.1. Validation of the proposed design method based on design methodologies available from literature.....	78
2.6.2. Robustness test: the self-anchored cable-stayed suspension scheme with reduced number of cable elements.....	86

CONTENTS

---

2.6.3. The long span bridges case: comparisons between hybrid and pure systems.....	93
2.6.4. The long span bridges case: the self-anchored cable-stayed suspension scheme.....	78
<b>3. VULNERABILITY AND FAILURE ANALYSIS OF CABLE SUPPORTED BRIDGES SUBJECTED TO DAMAGE MECHANISMS UNDER THE ACTION OF MOVING LOADS</b>	
<b>.....</b>	<b>111</b>
3.1. Introduction .....	111
3.1.1. Code prescriptions.....	120
3.2. The proposed analysis model .....	124
3.3. Damage formulation.....	125
3.4. Moving load formulation.....	127
3.5. Bridge formulation .....	130
3.5.1. Girder and pylons.....	130
3.5.2. Cable elements .....	133
3.6. Finite element implementation.....	136
3.7. Dynamic amplification factors definition.....	141
3.8. Results .....	143
3.8.1. Investigation on cable-stayed bridges subjected to an accidental failure in the cable system .....	144
3.8.2. Comparisons between pure and hybrid cable system configurations .....	161
3.8.2.1. Initial configuration of bridges .....	165
3.8.2.2. Damage analysis .....	170

CONTENTS

---

<b>4. NONLINEAR BEHAVIOR OF SELF-ANCHORED CABLE-STAYED SUSPENSION BRIDGES (S.A.C.S.) .....</b>	<b>191</b>
4.1. Introduction .....	191
4.2. The proposed analysis model.....	196
4.3. The formulation of nonlinear material behaviors .....	197
4.3.1. Girder and pylons .....	197
4.3.2. Cable elements .....	199
4.4. Bridge and geometric nonlinear formulations .....	203
4.4.1. Girder and pylons .....	203
4.4.2. Cable elements .....	205
4.5. Finite element implementation .....	206
4.6. Results .....	212
4.6.1. Loads and combinations.....	212
4.6.2. Investigation on the influence of material nonlinear behavior of bridge components .....	214
4.6.3. Parametric study.....	223
<b>5. CONCLUSIONS .....</b>	<b>235</b>
<b>BIBLIOGRAPHY .....</b>	<b>247</b>

# LIST OF FIGURES

## Chapter 1

- Fig. 1.1 Suspension Bridge
- Fig. 1.2 The Golden Gate Bridge
- Fig. 1.3 Three-span, suspension bridge cable system
- Fig. 1.4 Loading case for maximum hanger force
- Fig. 1.5 Loading case for maximum main cable force
- Fig. 1.6 Horizontal equilibrium at the pylon top
- Fig. 1.7 Cable-stayed bridge systems: (top) pure fan system; (centre) semi-fan system; (bottom) harp system
- Fig. 1.8 The Russky Bridge
- Fig. 1.9 Pylon types for cable-stayed bridges: (left) H-frame; (centre) A-frame; (right) Y-frame
- Fig. 1.10 Structural scheme of the Hybrid cable-stayed suspension bridge
- Fig. 1.11 The Brooklyn Bridge
- Fig. 1.12 Structural scheme of the self-anchored cable-stayed suspension bridge
- Fig. 1.13 The Zhuanghe Jianshe Bridge



- Fig. 1.14 Structural scheme for maximum main cable force
- Fig. 1.15 The design proposal for the Portland-Milwaukie Light Rail Bridge

## **Chapter 2**

- Fig. 2.1 Post-tensioning forces in cables. Basic system
- Fig. 2.2 Displacements and control variables for “zero configuration”
- Fig. 2.3 Model of a cable-stayed bridge
- Fig. 2.4 Rigid simple supports model
- Fig. 2.5 Design and control variables to be determined in hybrid cable-stayed suspension bridge scheme
- Fig. 2.6 Identification of the performance factors and design variables on the bridge scheme
- Fig. 2.7 Flowchart of the optimization procedure
- Fig. 2.8 Design and control variables to be determined in cable-stayed and suspension schemes
- Fig. 2.9 Identification of the variables involved in the design procedure
- Fig. 2.10 Girder cross-section notations
- Fig. 2.11 Cable connection
- Fig. 2.12 FE model of an hybrid cable-stayed suspension bridge
- Fig. 2.13 Quincy Bayview Bridge Wilson and Gravelle (1991)
- Fig. 2.14 Geometry of the Quincy Bayview Bridge
- Fig. 2.15 Finite element modeling of the structural scheme of the Quincy Bayview Bridge
- Fig. 2.16 Live load cases used in the optimization design technique

- 
- Fig. 2.17 Comparisons with results obtained in [19] in terms of cross-section distribution of the cables ( $A_i$ ), total steel quantity ( $Q$ ) as a function of the number of iterations.
- Fig. 2.18 Comparisons in terms of maximum stresses produced by live loads and percentage error ( $e$ ) with the values determined in [19].
- Fig. 2.19 Synoptic representation of the live load configurations, maximum stresses and comparison with data obtained in [19].
- Fig. 2.20 Comparisons in terms of girder displacements produced by live loads with values determined in [19], convergence behavior of the cross-sections, maximum and initial post-tensioning stresses as a function of the percentage value of the iteration steps ( $nIT\%$ ).
- Fig. 2.21 Comparisons in terms of pylon displacements produced by live loads with values determined in [19], convergence behavior of the cross-sections, maximum and initial post-tensioning stresses as a function of the percentage value of the iteration steps ( $nIT\%$ ).
- Fig. 2.22 Synoptic representation of the self-anchored cable-stayed suspension scheme
- Fig. 2.23 Cross-section distribution: initial and final evaluations
- Fig. 2.24 Convergence behavior of the cross-sections as a function of the iteration number
- Fig. 2.25 Envelope of the girder deflections under DL and LL
- Fig. 2.26 Comparisons between initial and final evaluations of the girder deflections, convergence behavior of the top pylon horizontal displacement and midspan vertical deflections
- Fig. 2.27 Stress and displacement optimization factors: initial and final prediction

- Fig. 2.28 Distribution of the initial stresses (SI) under DL and convergence behavior of the values observed in the main cable as a function of the percentage value of the iteration steps (nIT%)
- Fig. 2.29 Distribution of the maximum stresses under LL and convergence behavior of the maximum stresses as a function of the iteration percentage number (nIT%).
- Fig. 2.30 HCS bridges: distribution of the cable cross-sections and envelope of the stresses in the cable-system in the stays, hangers and main cable.
- Fig. 2.31 HCS bridges: convergence behavior of the predicted maximum stresses in the cable system as a function of the iteration steps
- Fig. 2.32 HCS bridges: convergence behavior of the girder and pylon displacements in the cable systems as a function of the iteration steps.
- Fig. 2.33 HCS bridges: comparisons between maximum stresses in the cable system and vertical displacements in the girder at discrete points of the bridges as a function of the iteration steps.
- Fig. 2.34 Comparisons between predicted values of the cross-sections in the cable-system between hybrid cable-suspension (HCS), cable-stayed (CS) and suspension (SP) bridges.
- Fig. 2.35 Comparisons between predicted values of the maximum stresses in the cable-system between hybrid cable-suspension (HCS), cable-stayed (CS) and suspension (SP) bridges.
- Fig. 2.36 Structural model of the long span self-anchored cable-stayed suspension bridge
- Fig. 2.37 Normalized cross-sections distribution (AiSA/gL) in the cable-system as a function of the normalized position on the girder projection (X/LT)

- Fig. 2.38 Initial stresses ( $S/S_A$ ) in the cable-system as a function of the normalized position on the girder projection ( $X/LT$ )
- Fig. 2.39 Normalized girder ( $U_3^G/L$ ) displacements produced by live loads; convergence behavior of the cross-sections and the displacements as a function of the percentage value of the iteration steps ( $n_{IT}\%$ ).
- Fig. 2.40 Normalized pylon ( $U_1^G/L$ ) displacements produced by live loads; convergence behavior of the cross-sections and the displacements as a function of the percentage value of the iteration steps ( $n_{IT}\%$ ).
- Fig. 2.41 Normalized maximum tensile stresses ( $\max(S_{LL})/S_A$ ) under live loads
- Fig. 2.42 Normalized maximum tensile stresses ( $\max(S_{LL})/S_A$ ) evolution as a function of the percentage value of the iteration steps ( $n_{IT}\%$ )

### Chapter 3

- Fig. 3.1 Hydrogen embrittlement mechanisms and failure of a hard chromium-plated chain conveyor bolt
- Fig. 3.2 SCC propagation: (a) intergranular SCC of an Inconel heat exchanger tube (X500 micrography); (b) transgranular: the micrography (X300) illustrates SCC in a 316 stainless steel chemical processing piping system
- Fig. 3.3 Pitting corrosion
- Fig. 3.4 The Mid-Hudson Bridge
- Fig. 3.5 Partial removal of wrapping wires
- Fig. 3.6 Expanded Inspection area
- Fig. 3.7 Pitting effect on a wire
- Fig. 3.8 The PTI and SETRA method

- Fig. 3.9 Damage definition and regions affected by the damage scenarios
- Fig. 3.10 Moving load description and girder kinematic
- Fig. 3.11 Displacements of the cross-section
- Fig. 3.12 Initial and current configurations of the cable, support motion due to girder (G) and pylon (P) deformation.
- Fig. 3.13 Cable-stayed bridge scheme: bridge kinematic, pylons, girder and cable system characteristics.
- Fig. 3.14 Dynamic amplification factors of the midspan vertical displacement for a bridge structure with A-shaped pylon as a function of the normalized speed parameter: effect of the failure mechanism, moving load schematization
- Fig. 3.15 Dynamic amplification factors of the midspan vertical displacement for a bridge structure with H-shaped pylon as a function of the normalized speed parameter: effect of the failure mechanism, moving load schematization
- Fig. 3.16 Dynamic amplification factors of the midspan bending moment for a bridge structure with A-shaped tower as a function of the normalized speed parameter: effect of the failure mechanism and moving load schematization.
- Fig. 3.17 Dynamic amplification factors of the midspan bending moment for a bridge structure with H-shaped tower as a function of the normalized speed parameter: effect of the failure mechanism and moving load schematization.
- Fig. 3.18 (a) Dynamic amplification factors and maximum value of the midspan torsional rotation as a function of the normalized speed parameter  $\Theta$ . (b) Schematic deformation produced by the failure mechanism.
- Fig. 3.19 Dynamic amplification factors of the midspan vertical displacement for a bridge structure with A-shaped tower:

- response of damaged and undamaged bridge structures as a function of the bridge size parameter  $a$ .
- Fig. 3.20 Dynamic amplification factors of the midspan vertical displacement for a bridge structure with H-shaped tower: response of damaged and undamaged bridge structures as a function of the bridge size parameter  $a$ .
- Fig. 3.21 Dynamic amplification factors of the midspan bending moment for a bridge structure with A-shaped tower: response of damaged and undamaged bridge structures as a function of the bridge size parameter  $a$ .
- Fig. 3.22 Dynamic amplification factors of the midspan bending moment for a bridge structure with H-shaped tower: response of damaged and undamaged bridge structures as a function of the bridge size parameter  $a$ .
- Fig. 3.23 Dynamic amplification factors of the undamaged anchor stay axial stress for A-shaped tower bridge configurations: damaged and undamaged bridge response as a function of the bridge size parameter  $a$ .
- Fig. 3.24 Dynamic amplification factors of the undamaged anchor stay axial stress for H-shaped tower bridge configurations: damaged and undamaged bridge response as a function of the bridge size parameter  $a$ .
- Fig. 3.25 Synoptic representation of the failure modes: A) failure in the lateral anchor stay, B) failure in the central part of the cable system.
- Fig. 3.26 Time history of the dimensionless midspan displacement and evaluation of the DAFs: comparisons between damaged and undamaged A-shaped bridge configurations.

- Fig. 3.27 Time history of the dimensionless midspan displacement and evaluation of the DAFs: comparisons between damaged and undamaged H-shaped bridge configurations.
- Fig. 3.28 Time history of the dimensionless midspan bending moment and evaluation of the DAFs: comparisons between damaged and undamaged A-shaped bridge configurations.
- Fig. 3.29 Time history of the dimensionless midspan bending moment and evaluation of the DAFs: comparisons between damaged and undamaged H-shaped bridge configurations.
- Fig. 3.30 Time history of the dimensionless midspan torsional rotation: comparisons in terms of the failure mode and tower typology.
- Fig. 3.31 Time history of the dimensionless of the undamaged anchor stay axial force: comparisons in terms of the failure mode and tower typology
- Fig. 3.32 Cable supported bridge considered
- Fig. 3.33 Damage scenarios considered in the cable-system
- Fig. 3.34 Flow-chart of the optimization procedure for cable system dimensioning
- Fig. 3.35 Stress distribution and cable dimensioning in the initial configuration
- Fig. 3.36 Maximum stresses in the stays during the iteration steps and total steel quantity
- Fig. 3.37 Maximum stresses in the hangers during the iteration steps and total steel quantity
- Fig. 3.38 Change of the stresses in the cable-system for the application of type 11 loading scheme (Appendix D, [30]) and comparison with maximum admissible value for fatigue requirement.
- Fig. 3.39 Comparisons between Cable-Stayed bridge (CS) and Hybrid Cable-Stayed Suspension bridge (HCS) in terms of the girder

---

deformability under the action of dead loads (DL) for the damage scenarios SC1.

- Fig. 3.40 Comparisons between Cable-Stayed bridge (CS) and Hybrid Cable-Stayed Suspension bridge (HCS) in terms of the girder deformability under the action of dead loads (DL) for the damage scenarios SC2.
- Fig. 3.41 Comparisons between Cable-Stayed bridge (CS) and Hybrid Cable-Stayed Suspension bridge (HCS) in terms of time histories of dimensionless midspan vertical displacement and torsional rotation
- Fig. 3.42 Comparisons between Cable-Stayed bridge (CS) and Hybrid Cable-Stayed Suspension bridge (HCS) in terms of envelope of stress distribution in the cable systems under the action of dead loads (DL) for the damage scenario SC1
- Fig. 3.43 Comparisons between bridges typologies in terms of the girder deformability under the action of live loads (LL) for the damage scenarios SC1
- Fig. 3.44 Comparisons between bridges typologies in terms of the girder deformability under the action of live loads (LL) for the damage scenarios SC2
- Fig. 3.45 Comparisons between bridges typologies in terms of the girder deformability under the action of live loads (LL) for the damage scenario SC3.
- Fig. 3.46 Comparisons between bridges typologies in terms of the girder deformability under the action of live loads (LL) for the damage scenario SC4
- Fig. 3.47 Normalized vertical displacements and dynamic amplification factors of the maximum vertical displacement for damage scenario SC1 as a function of the normalized speed parameter:



- comparisons between Cable-Stayed bridge (CS) and Hybrid Cable-Stayed Suspension bridge
- Fig. 3.48 Normalized vertical displacements and Dynamic amplification factors of the maximum vertical displacement for damage scenarios SC3 as a function of the normalized speed parameter: comparisons between Suspension Bridge (SP) and Hybrid Cable-Stayed Suspension Bridge (HCS)
- Fig. 3.49 Cable-Stayed Bridge: Envelope stress distribution in the cable systems under the action of live loads (LL) and vulnerability behavior for the damage scenario SC1
- Fig. 3.50 Hybrid Cable-Stayed Suspension bridge: Stress distribution in the cable systems under the action of live loads (LL) and vulnerability behavior for the damage scenario SC1
- Fig. 3.51 Hybrid Cable-Stayed Suspension/Cable stayed bridges: envelope bending moments distribution of the stiffness girder under the action of live loads (LL) for the damage scenarios SC1 and SC2
- Fig. 3.52 Hybrid Cable-Stayed Suspension/Cable stayed bridges: diagrams representing the path traced over time by the stress resultant (M,N) in the girder and pylons for SC1 and SC2 damage scenarios
- Fig. 3.53 Suspension Bridge: Envelope stress distribution in the cable systems under the action of live loads (LL) and vulnerability behavior for the damage scenario SC4
- Fig. 3.54 Hybrid Cable-Stayed Suspension bridge: Envelope stress distribution in the cable systems under the action of live loads (LL) and vulnerability behavior for the damage scenario SC4
- Fig. 3.55 Envelope of vertical displacements of CS(a) and HCS (b) produced by damage scenarios SC1 and SC2, considered individually and simultaneously

Fig. 3.56 Envelope of vertical displacements of SP (c) and HCS (d) produced by damage scenarios SC3 and SC4, considered individually and simultaneously

## Chapter 4

- Fig. 4.1 Spatially suspended elastic catenary cable
- Fig. 4.2 Nonlinear tangent stiffness matrix for a three-dimensional beam-column element
- Fig. 4.3 Flexural stiffness reduction model for refined plastic hinge analysis
- Fig. 4.4 Full plastification surface of AISC-LRFD
- Fig. 4.5 Girder cross-section notations
- Fig. 4.6 Finite element modelling of the structural scheme
- Fig. 4.7 Load cases
- Fig. 4.8 Load-displacement curve for LC1: Analysis on material nonlinear behavior
- Fig. 4.9 Load-displacement curve for LC2: Analysis on material nonlinear behavior
- Fig. 4.10 Evolution of the bridge deformed shapes – FMI
- Fig. 4.11 Force-state parameter and dimensionless reduction parameters ; Maximum cable stresses – LC1
- Fig. 4.12 Force-state parameter and dimensionless reduction parameters ; Maximum cable stresses – LC2
- Fig. 4.13 Force-state parameter and dimensionless reduction parameters for LC1 and LC2
- Fig. 4.14 Load-anchor cable stress curve for LC1 and LC2

- Fig. 4.15 Variability of the length of cable-stayed portion, for several values of relative bending stiffness  $\varepsilon_F$
- Fig. 4.16 Percentage error (e %) of EMB, CMI and BMI models with respect to the FMI model
- Fig. 4.17 Variability of the cable-stayed system configuration
- Fig. 4.18 Variability of tower to girder bending stiffness ratio  $I_r$ , for several values of relative girder bending stiffness  $\varepsilon_F$  and height-span ratio  $\mu$ .
- Fig. 4.19 Variability of the midspan length

# LIST OF TABLES

## Chapter 1

- Tab. 1.1 List of longest suspension bridge spans
- Tab. 1.2 List of longest cable-stayed bridge spans
- Tab. 1.3 List of longest suspension bridge spans
- Tab. 1.4 List of longest cable-stayed bridge spans

## Chapter 2

- Tab. 2.1 Mechanical and geometric properties of Quincy Bayview Bridge
- Tab. 2.2 Bridge parameters of the girder and pylons
- Tab. 2.3 Parametric study: mechanical and geometric properties of bridge

## Chapter 3

- Tab. 3.1 High speed trains
- Tab. 3.2 DAFs of the midspan bending moments as a function of the normalized time of failure on the bridge development comparisons in terms of A and H shaped

- Tab. 3.3 DAFs of the midspan vertical displacements as a function of the normalized time of failure on the bridge development comparisons in terms of A and H shaped
- Tab. 3.4 Mechanical and geometric properties of bridges
- Tab. 3.5 Dynamic amplification effects for the damage scenario SC1 in terms of bending moments at fixed cross-sections of the girder for the cable-stayed and HCS configurations
- Tab. 3.6 Dynamic amplification effects for the damage scenario SC2 in terms of bending moments at fixed cross-sections of the girder for the cable-stayed and HCS configurations
- Tab. 3.7 Dynamic amplification effects for the damage scenario SC1 in terms of bending moments at the lowest cross-sections of the pylons for the cable-stayed and HCS configurations

## Chapter 4

- Tab. 4.1 Geometric and mechanical properties utilized for the analysis of the influence of nonlinear material behavior
- Tab. 4.2 Models utilized for the analysis of the influence of nonlinear material behavior
- Tab. 4.3 Influence of nonlinear material behavior: main cable dimensionless maximum stress ( $S/S_u$ )
- Tab. 4.4 Load multiplier as a function of  $c$  parameter and relative bending stiffness for  $I_r = 25$  and  $\mu = 0.4$
- Tab. 4.5 Variability of load multiplier with respect of cable-stayed system configuration

## NOMENCLATURE

- $(\cdot)^G$  Stiffening girder variable
- $(\cdot)^P$  Pylon variable
- $(\cdot)^C$  Cable system variable
- $(\cdot)^m$  Moving mass variable
- $(\cdot)^0$  Variables associated to the initial configuration
- $A_i^S$  Cross sectional area of main cable
- $A^G$  Girder cross sectional area
- $A^P$  Pylon cross sectional area
- $A_i^S$  Stay cross sectional area of the i-th cable
- $A_0^S$  Anchor stay cross sectional area
- b Half girder cross section width
- c Moving system speed
- $C^{G,P}$  Elasticity modulus of the girder (G) or of the pylon (P)
- $C^C$  Cable elastic modulus

**CE Constraint Equation**

e Eccentricity of the moving loads with respect to the girder geometric axis

$E_1$  Green-Lagrange strain

H Pylon height

$I_i$  Moment of inertia with respect to the i axis

$I_{0i}$  Polar moment of inertia around the i axis

$J_t$  Factor torsional stiffness

$\angle$  Lateral bridge span

L Central bridge span

$L_0$  Development of the cable element

$L_p$  Length of the moving loads

$L_T$  Total length of the girder

m Exponential coefficient of the damage function

$M_{0i}^G$  Limit elastic bending moment of the girder along i-th axis

$M_{0i}^P$  Limit elastic bending moment of the pylon along i-th axis

$N_0^G$  Limit elastic normal stress resultant of the girder

p Live loads

$S_g$  Design stay stress under self-weight loading

$S_a$  Allowable stay stress

$S_1$  Piola- Kirchhoff stress

***SNOPT* Sparse Nonlinear OPTimize**

$U_i$  Component of the displacement field along i-axis

- 
- $t_0$  starting time of the damage mechanism
- $t_f$  Duration of the failure mechanism
- $\alpha$  Relative position of the damage region
- $\beta$  Extent of the damage region
- $\Delta$  Stay spacing step
- $\gamma$  Stay specific weight
- $\lambda_{ML}$  Moving load mass per unit length
- $\lambda_{ML}^0$  Torsional polar mass moment of moving load per unit length
- $\mu^C$  Stay mass per unit length
- $\mu^G$  Girder self-weight per unit length
- $\xi_d$  Static value of the damage variable
- $\xi_d$  Dynamic function of the damage variable
- $\Psi_i$  Component of the rotation field around i axis



## **ABSTRACT**

Cable supported bridges are complex structures presenting optimum use of structural materials, efficient aesthetic and structural characteristics and low maintenance costs. Because of their large size and different features of structural elements, which are essentially girder, cable system and pylons, cable supported bridges present several problems that need to be addressed.

One concerns the definition of the initial geometrical configuration of the structure. As a matter of fact, especially for long spans, cable supported bridges are defined through a large number of cable elements, which lead to highly statically indeterminate structures. As a result, post-tensioning forces and cross-section dimensions of cables can be considered as design variables which must be determined.

Another one concerns the vulnerability assessment for extreme loading conditions as the transit of moving loads or the effects produced by damage mechanisms in the cable system, such as corrosion, which strongly reduce the structural integrity. Such phenomena produce high dynamic amplification

effects in terms of stress and displacement variables. However, effects produced by the action of moving load or by damage mechanisms are not independent. As a matter of fact, corrosion mechanisms make the structure more sensitive to the action of moving loads. On the other hand, moving load induced vibrations can cause the deterioration of cables by fatigue or abrasion effects according to the known phenomenon of the "fretting-fatigue corrosion". Therefore, moving load and damage mechanisms problems should be studied together.

The last one is relative to the geometric and material nonlinear effects on bridge structure behavior. As a matter of fact, geometric and material nonlinearities affect cable supported bridges and, as a consequence, the maximum load carrying capacity. Material nonlinearities come from the nonlinear stress–strain behavior of materials, whereas geometric nonlinearities result from the cable “sag” effect, large displacements and axial force–bending moment interaction in the girder and pylon (beam-column effect).

The aim of the present thesis is to develop advanced structural models of cable supported bridges to address previous issues. To this end, a refined formulation based on FE approach is adopted to reproduce the structural behavior of the main long span cable supported bridges. In particular, the bridge formulation is developed by using a geometric nonlinear formulation, in which the effects of local vibrations of the cable elements and of large displacements in the girder and the pylons are taken into account.

As far as the definition of the initial geometrical configuration, a design methodology to predict optimum post-tensioning forces and dimensioning of the cable system for cable supported bridges is proposed. The model is based on a combination of the previous FE model with an iterative optimization procedure. Such iterative procedure is utilized to optimize the shape of post-tensioning forces as well as the geometry of the cable system to achieve minimum deflections, lowest steel quantity involved in the cable system and maximum performance of the cables under live load configurations. In this framework, results are proposed in terms of comparisons with existing formulations to validate the proposed methodology. Moreover, parametric studies on more complex long span structures are also developed to verify existing cable-dimensioning rules and to analyze between hybrid cable-stayed

suspension bridges and conventional cable-stayed or suspension systems. Furthermore, results concerning the self-anchored cable-stayed suspension scheme case are presented in detail.

In order to analyze the structural behavior of cable supported bridges subjected to moving loads and affected by damage mechanisms in the cable suspension system, further formulations have been added in the FE base model. In particular, the coupling effects arising from the interaction between bridge deformations and moving system parameters has been taken into account, which allow to reproduce the influence of the inertial characteristics of the moving loads. Moreover, damage and failure phenomena on the cable system elements, produced by preexisting corrosion phenomena or unexpected failure mechanisms, are analyzed by using stationary or time dependent explicit laws, developed in the framework of the Continuum Damage Mechanics theory.

At first, analysis focused attention on the dynamic behavior of cable-stayed bridges affected by an accidental failure in the cable suspension system. Sensitivity analyses of typical design bridge variables are proposed. In particular, the effects produced by the moving system characteristics, the tower typologies, and the failure mode characteristics involved in the cable system are investigated by means of comparisons between damaged and undamaged bridge configurations. Subsequently, the behavior of hybrid cable-stayed suspension bridge is investigated. To this end, a parametric study is carried out on four damage scenarios involving damage mechanisms in the hangers, main cable and stays. In particular, in order to point out the advantages presented by such bridge topology, comparisons with bridge schemes based on pure cable-stayed and suspension cable system are proposed. Results are expressed in terms of dynamic amplification factors of typical kinematic and stress design variables.

The problem of the influence on the maximum load carrying capacity of the geometric and material nonlinearities is presented with reference to the self-anchored cable-stayed suspension scheme. The material nonlinear behavior for the girder and pylons elements is accounted for by a refined finite element formulation which combine the a gradual yielding theory based on the (CRC) tangent modulus concept and a plastic hinge model, whereas for cable elements, the finite plasticity theory of Green and Naghdi is adopted. In the framework of

geometric nonlinearities, since the FE base model takes into account large displacement and cable “sag” effect, which is reproduced by adopting a multiple truss element approach, further contributions to reproduce beam-column effect are added. The analysis is based on a limit point instability approach. Since the bridge behavior is mostly influenced by the post-tensioning force distributions in the cable system, the initial geometrical configuration of the bridge under the action of dead loads, is defined in advance. Results are devoted to analyze the influence of the nonlinear material behavior as well as the geometrical and structural parameters of the bridge on the maximum load capacity of the structure.

## SOMMARIO

I ponti di grande luce sono strutture complesse che presentano un utilizzo ottimale dei materiali strutturali, caratteristiche estetiche e costruttive efficienti e bassi costi di manutenzione. A causa delle loro grandi dimensioni e delle diverse caratteristiche degli elementi strutturali, che sono essenzialmente la trave di irrigidimento, i piloni e il sistema dei cavi, i ponti di grande luce presentano diversi problemi che devono essere analizzati.

Uno riguarda la definizione della configurazione iniziale della struttura. I ponti di grande luce, infatti, specialmente per lunghezze elevate, presentano un gran numero di cavi, che determinano strutture altamente iperstatiche. Come risultato, le forze di pretensione e le dimensioni delle sezioni trasversali dei cavi possono essere considerati come variabili di progetto che devono essere determinati.

Un altro riguarda la valutazione della vulnerabilità strutturale nei riguardi di condizioni di carico estreme come il transito di carichi mobili o gli effetti prodotti da meccanismi di danneggiamento del sistema dei cavi, come la corrosione, che riducono fortemente l'integrità strutturale. Tali fenomeni

producono significativi effetti di amplificazione dinamica in termini variabili tensionali e di spostamento. Tuttavia, gli effetti prodotti dall'azione dei carichi mobili o da meccanismi di danno non sono indipendenti. L'effetto della corrosione rende la struttura più sensibile all'azione di carichi mobili. D'altra parte, le vibrazioni indotte dal transito dei veicoli possono causare il deterioramento dei cavi per fatica o abrasione. Per queste ragioni, i problemi dei carichi mobili e dei meccanismi di danno dovrebbero essere studiati congiuntamente.

L'ultimo è relativo agli effetti delle nonlinearità geometriche e dei materiali sul comportamento strutturale dei ponti. Le nonlinearità geometriche e dei materiali, infatti, influenzano la risposta dei ponti di grande luce e, di conseguenza, anche la massima capacità portante. Le nonlinearità dei materiali derivano dal legame sforzo-deformazione dei materiali, mentre le nonlinearità geometriche sono dovute all'effetto "sag" dei cavi, ai grandi spostamenti e ai fenomeni di interazione sforzo assiale-momento flettente che insorgono nella trave di irrigidimento e nei piloni (effetto beam-column).

Obiettivo della presente tesi di dottorato è quello di sviluppare modelli strutturali avanzati per l'analisi delle problematiche dei ponti di grande luce precedentemente descritte. A tal fine, è stato fatto ricorso alla metodologia degli elementi finiti per riprodurre il comportamento strutturale dei principali ponti di grande luce. In particolare, è stata adottata una formulazione di tipo nonlineare geometrico, che ben si presta a riprodurre gli effetti delle vibrazioni locali dei cavi e i grandi spostamenti a cui sono soggetti la trave d'irrigidimento e i piloni.

Per quanto riguarda la definizione della configurazione geometrica iniziale, viene elaborata una metodologia di progettazione per l'ottimizzazione delle forze di pretensione e per il dimensionamento delle sezioni trasversali dei cavi. La metodologia è data dalla combinazione del modello strutturale agli elementi finiti descritto in precedenza con una procedura di ottimizzazione iterativa. Tale procedura iterativa è utilizzata per ottimizzare la distribuzione delle forze di pretensione e le dimensioni delle sezioni trasversali al fine di minimizzare la quantità di acciaio e massimizzare le performance strutturali sotto l'azione di carichi di natura accidentale. In tale ambito, sono stati elaborati dei risultati per validare la metodologia proposta per mezzo di confronti con

formulazioni presenti in letteratura. Inoltre, sono stati sviluppati risultati parametrici con riferimento a ponti di conformazione più complessa per verificare le regole di dimensionamento e per confrontare i ponti a configurazione mista sospesa strallata con le convenzionali configurazioni sospese e strallate. Inoltre, dettagliati risultati sono proposti con riferimento al caso dei ponti misti auto-ancorati sospesi strallati.

Al fine di analizzare il comportamento strutturale di ponti di grande luce in presenza di meccanismi di danneggiamento del sistema dei cavi, sotto l'azione di carichi viaggianti, al modello agli elementi finiti sono aggiunte ulteriori formulazioni. In particolare, sono presi in considerazione gli effetti di accoppiamento flessio-torsionale della struttura da ponte e quelli associati ai contributi di carico e di massa derivanti dal sistema mobile. Inoltre, gli effetti di fenomeni di danneggiamento di elementi del sistema dei cavi, prodotti da preesistenti fenomeni di corrosione o rotture improvvise, vengono analizzati per mezzo di leggi esplicite in funzione del tempo, sviluppate nell'ambito della teoria della meccanica del danneggiamento. Inizialmente, le analisi hanno focalizzato l'attenzione sul comportamento dinamico di ponti strallati in presenza di rottura improvvisa di elementi costituenti il sistema dei cavi. In tale contesto sono proposti dei risultati ricavati da analisi sensitive delle variabili dei ponti di grande luce. In particolare, l'influenza dalle caratteristiche dei carichi mobili, delle tipologia dei piloni e dello scenario di danneggiamento sono studiati per mezzo di confronti tra configurazioni del ponte danneggiate e non danneggiate. Successivamente, viene analizzato il comportamento dei ponti misti strallati sospesi. E' sviluppato uno studio parametrico sulla base di quattro scenari di danneggiamento che prevedono il danneggiamento degli stralli, dei pendini e del cavo principale. In particolare, al fine di evidenziare i vantaggi presentati dalla configurazione mista, vengono proposti dei risultati sotto forma di confronto con sistemi puri strallati e sospesi. I risultati sono espressi in termini di fattori di amplificazione dinamica delle tipiche variabili cinematiche e tensionali di progetto.

Il problema della influenza sulla capacità massima di carico delle non linearità geometriche e del materiale è presentato con riferimento allo schema di sospensione strallato-sospeso auto-ancorato. Il comportamento non

lineare del materiale della trave di irrigidimento e dei piloni è rappresentato da una raffinata formulazione agli elementi finiti che combina la teoria alla base del modulo tangente con un modello di cerniera plastica, mentre per i cavi viene adottata la teoria della plasticità per deformazioni finite. Nel quadro della non linearità geometrica, dal momento che il modello strutturale di base agli elementi finiti riproduce i grandi spostamenti e l'effetto "sag" dei cavi, che viene riprodotto per mezzo di un approccio multi truss element, sono aggiunti ulteriori contributi per riprodurre l'effetto di interazione sforzo normale-momento flettente presente nelle pile e nella trave di irrigidimento. L'analisi si basa su un'analisi nonlineare al passo. Poiché il comportamento strutturale del ponte è fortemente influenzato dalle distribuzioni delle forze di pretensione del sistema dei cavi, come primo step viene determinata la configurazione geometrica iniziale del ponte sotto l'azione di carichi permanenti. I risultati sono finalizzati ad analizzare l'influenza sulla massima capacità di carico del comportamento nonlineare del materiale nonché dei parametri geometrici e strutturali.



# 1

## INTRODUCTION

### 1.1 Current issues in the field of cable supported bridges

With the advent of high-strength materials for use in the cables and the development of digital computers for the structural analysis, great progress has been made in cable supported bridges.

As a consequence, during the last years many problems have been resolved and nowadays new research objectives have been identified.

Most of the current research issues in the field of cable supported bridges are addressed to reduce the construction costs of the new structures and to analyze the structural performance of the bridges built in the past.

Furthermore, since the structural analyses of cable supported bridges are produced mainly by finite element methodologies, more accurate models based on advanced formulations are developed to get more realistic simulations.

Therefore, the majority of the last research works have focused on the following topics:

- Development of new design methods to get maximum structural performance as well as reduced costs;
- Analysis of the structural behavior in the presence of damage mechanisms;
- Implementation of advanced computational models able to reproduce all source of nonlinearity.
- Produce more accurate theories to better simulate the effects of the worst external actions.

The present thesis aims to be a scientific contribution to the development of these topics.

## **1.2 Background of cable supported bridges**

Cable supported bridges are typically employed to overcome medium or long spans, because of their structural, economical and aesthetic properties. Such characteristics arise from an enhanced combination of the structural components of the bridge, which are essentially girder, cable system and pylons.

Cable supported bridges differ from each other by cable system configuration. Typically, cable systems are based on suspension or cable-stayed schemes, known as pure systems, which were employed in the most cable supported bridges built to date. Furthermore, the cable system may assume hybrid configurations, provided by the combination of classical ones.

The most famous hybrid cable supported bridge is the Brooklyn Bridge designed by Roebling in the 1870. Based on his work experiences, Roebling guessed that a cable-stayed system is stiffer than a suspension system and a combination of them could lead good benefits (Gimsing & Georgakis, 2012).

In the case of the Brooklyn Bridge, such hybrid configuration was the best solution against the wind induced vibrations.

An evolution of the Roebling's system was proposed by Dischinger in 1938. The Dischinger's system can be obtained by Roebling's system by taking out the hangers in the regions where stay cables are present.

Although Dischinger has proposed his scheme on several occasions, it was never used. Furthermore, hybrid systems have not been chosen for construction of a major bridge since the days of the Brooklyn Bridge.

Nevertheless, the interest on hybrid schemes has never stopped and recent studies have improved knowledge about structural behavior of such bridge typology.

The ultimate proposal of hybrid scheme, whose is receiving considerable attention, is consistent with a self-anchored cable-stayed suspension scheme. Such cable system configuration combines the best properties of pure cable-stayed and suspension systems leading to considerable structural and economic advantages (Zhang, Wang, Qin, & Ge, 2009; Konstantakopoulos & Michaltsos, 2010).

As a matter of fact, self-anchored cable-stayed suspension bridge, which can be regarded as a self-anchored Dischinger's system, can provide a stiffer and cheaper structure than traditional ones based on pure suspension or cable-stayed systems and for this reason it is considered a good solution for overcoming long spans.

### **1.2.1 Suspension System**

The suspension system comprises a parabolic main cable and vertical hanger cables connecting the deck to the main cable. The most common suspension bridge system has three spans: a large main span flanked by shorter side spans. The three-span bridge is in most cases symmetrical with side spans of equal size, but where special conditions apply, the side spans can have different lengths. However, to transmit the horizontal component of the main cable pull acting at the pylon tops, the main cable will have to continue as free backstays to the anchor blocks.

In the traditional earth anchored suspension bridge each main cable is supported at four points: at the two anchor blocks and on the two pylon tops.



**Figure 1.1** Suspension Bridge

The supporting points at the anchor blocks can generally be assumed to be completely fixed both vertically and horizontally, whereas the supporting points at the pylon tops often are represented best by longitudinally movable bearings (due to the horizontal flexibility of the slender pylon legs).

Therefore the general arrangement of the suspension bridge cable system will be as shown in Fig. 1.1.

An excellent example of suspension bridge is the Golden Gate Bridge whose spans the Golden Gate strait, the mile-wide, three-mile-long channel between San Francisco Bay and the Pacific Ocean (Fig. 1.2). The structure links the U.S. city of San Francisco, on the northern tip of the San Francisco Peninsula, to Marin County, bridging both U.S. Route 101 and California State Route 1 across the strait. The bridge is one of the most internationally recognized symbols of San Francisco, and the United States.

It has been declared one of the Wonders of the Modern World by the American Society of Civil Engineers.



**Figure 1.2** The Golden Gate Bridge

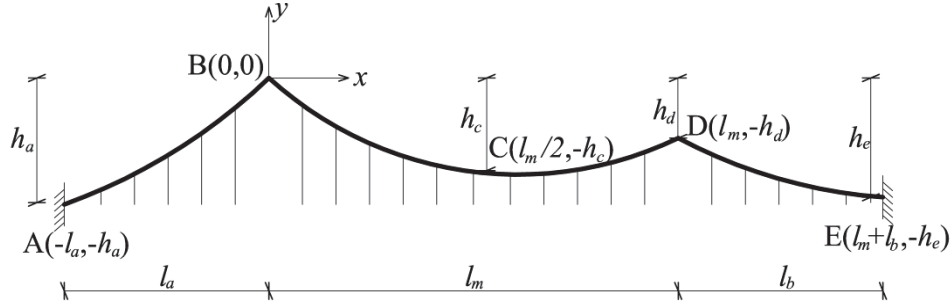


**Figure 1.3** Three-span, suspension bridge cable system

The geometry of the cable system in the dead load condition is generally chosen so that the deck and the pylons are moment-free. To achieve this, the cable curve must coincide with the funicular curve of the total dead load.

The main cable geometry can then be expressed by the following equations:

$$y = \begin{cases} -\frac{M_a(x)}{H} + \frac{h_A}{l_a}x & -l_a < x < 0 \\ -\frac{M_m(x)}{H} + \frac{h_D}{l_m}x & 0 < x < l_m \\ -\frac{M_b(x)}{H} + \frac{h_D - h_E}{l_b}(x - l_m) - h_D & l_m < x < l_m + l_b \end{cases} \quad (1.1)$$

where  $M_a(x)$ ,  $M_m(x)$  and  $M_b(x)$  are the moments of simply supported beams with lengths  $l_a$ ,  $l_m$  and  $l_b$  subjected to the total dead load of main cable, hangers, and deck.

It is worth nothing that, although the contribution from the dead load of the deck and hangers should be applied to the main cable as concentrated forces acting at each cable clamp position and the dead load of the main cable itself should be applied as a distributed load, since in suspension bridges hangers are spaced very closely, the dead load can be assumed to act as a distributed load.

Besides stipulating the position of the supporting points A, B, D and E, the general geometric conditions of the bridge often lead to a predetermined position of the midspan point C in the main span.

The horizontal force H can then be found from:

$$H = \frac{M_m(l_m/2)}{h_c - h_d/2} \quad (1.2)$$

where  $M_m(l_m/2)$  is the simple moment at the main span center and  $h_c - h_d/2$  the cable sag at midspan. Eq.s (1.1) and (1.2) now define the total cable curve when the dead load distribution is known.

A preliminary determination of the maximum hanger force can be based on the assumption that the hanger carries the distributed load acting on a length of the deck equal to the hanger spacing  $\Delta$ :

$$T_h = (g + p)\Delta \quad (1.3)$$

and the cross-sectional area  $A_h$  of the hanger:

$$A_h = \frac{T_h}{f_y} = \frac{(g + p)\Delta}{f_y} \quad (1.4)$$

where  $f_y$  is the allowable stress of the cable steel.

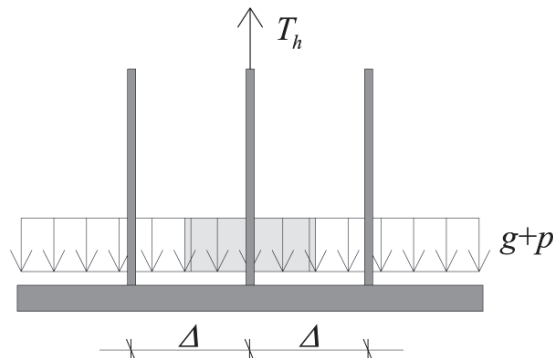


**Figure 1.4** Loading case for maximum hanger force

The maximum force  $T_m$  of the main cable in the main span can be determined by assuming the dead load of the deck and the distributed traffic load acting uniformly in the entire main span.

In the preliminary investigation the dead load of the hangers might be ignored as this contribution is quite insignificant. As a further approximation, the dead load of the main cable  $g_c$  is assumed to be uniformly distributed horizontally. The simplifying assumptions regarding the dead load of the cable system are slightly on the unsafe side, but this is to a large extent balanced out by assuming the dead load geometry instead of the deflected geometry.

For a horizontal main cable, as shown in Fig.1.5, the maximum horizontal force  $H_m$  becomes:

$$H_m = \frac{(g + p + g_c)l_m^2}{8f_m} \quad (1.5)$$

and the maximum cable force  $T_m$  (at the pylon):

$$T_m = H_m \frac{\sqrt{(l_m^2 + 16f_m^2)}}{l_m} = [(g + p)l_m + g_c l_m] \frac{\sqrt{l_m^2 + 16f_m^2}}{8f_m} \quad (1.6)$$

This expression is based on the simplifying assumption that the cable curve is a second order parabola.

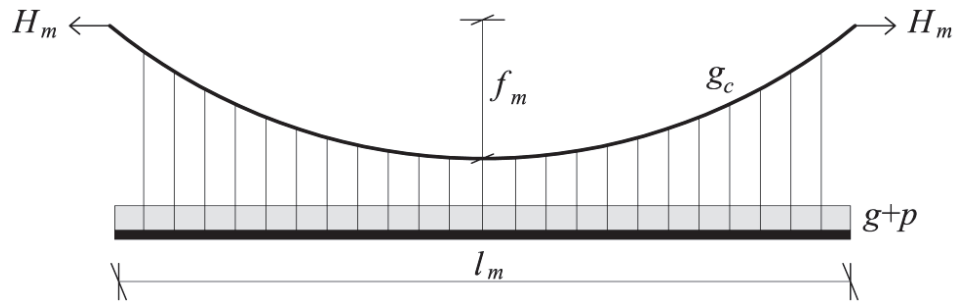


**Figure 1.5** Loading case for maximum main cable force

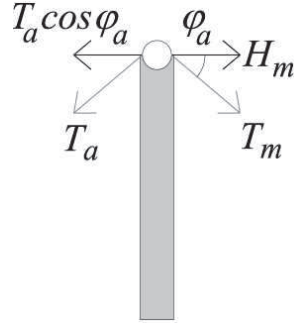


**Figure 1.6** Horizontal equilibrium at the pylon top

The main cable area  $A_m$  is now found from Eq.(1.6) by replacing  $T_m = A_m f_y$  and  $g_c = A_m \gamma_c$ , where  $\gamma_c$  is the density of the cable material:

$$A_m = \frac{[(g + p)l_m] \sqrt{l_m^2 + 16f_m^2}}{8f_y f_m - \gamma_{cb} l_m \sqrt{l_m^2 + 16f_m^2}} \quad (1.7)$$

The maximum tension  $T_a$  in the side span main cable is determined by expressing horizontal equilibrium at the pylon top, as indicated in Fig. 1.5:

$$T_a = \frac{H_m}{\cos \varphi_a} \quad (1.8)$$

where  $H_m$  is the maximum horizontal force from, with  $g_c = A_m \gamma_c$  found from Eq.(1.7). The preliminary cross-section area  $A_a$  of the side span cable thus becomes:

$$A_a = \frac{T_a}{f_y} = \frac{H_m}{f_y \cos \varphi_a} \quad (1.9)$$



### 1.2.2 Cable-stayed scheme

The cable-stayed systems (Fig. 1.6) contain straight cables connecting the deck to the pylons (De Miranda, 1980; Troitsky, 1988).

Three basic arrangements have been developed for the layout of the stay cables: fan system, harp system and semi-fan system.

In the fan system all cables are leading to the top of the pylon. Structurally, this arrangement is perhaps the best, as by taking all cables to the pylon top the maximum inclination to the horizontal is achieved and consequently it need the smallest amount of steel.

The cables carry the maximum component of the dead and live load forces, and the axial component of the deck structure is at a minimum.

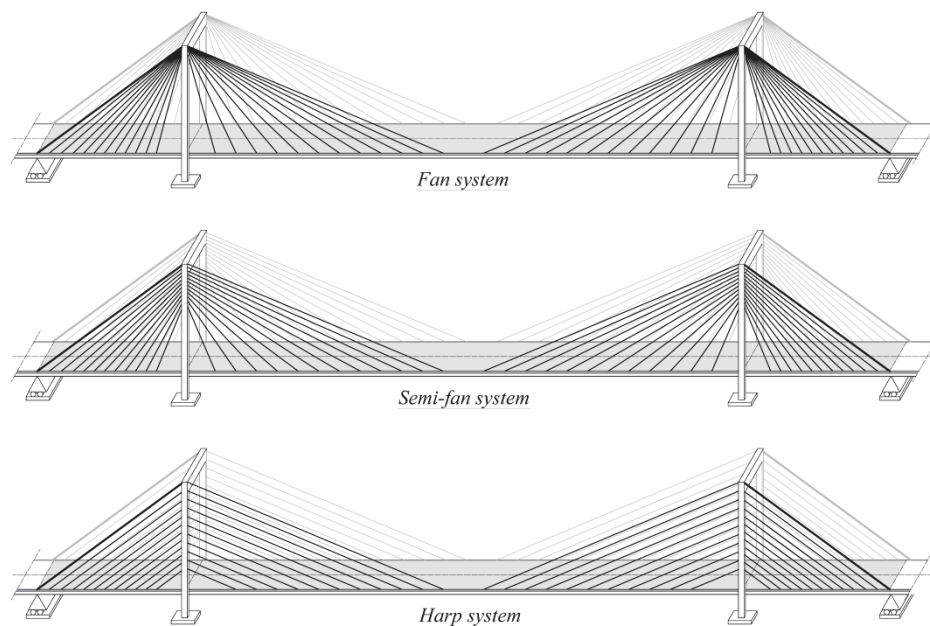


**Figure 1.7** Cable-stayed bridge systems:  
(top) pure fan system; (centre) semi-fan system; (bottom) harp system

However, where a number of cables are taken to the top of the pylon, the cable supports or saddles within the pylon may be very congested and a considerable vertical force has to be transferred. Thus the detailing becomes rather complex.

In the harp system the cables are connected to the pylon at different heights, and placed parallel to each other. This system may be preferred from an aesthetic point of view. However, it causes bending moments in the pylon. In addition, it is necessary to study whether the support of the lower cables can be fixed at the pylon leg or must be made movable in a horizontal direction. The harp-shaped cables give an excellent stiffness for the main span. The quantity of steel required for a harp-shaped cable arrangement is slightly higher than for a fan-shaped arrangement. The curve of steel quantity suggests choosing a higher pylon which will also increase the stiffness of the cable system against deflections.

The semi-fan intermediate stay cable arrangement represents a modification of the harp system. The forces of the stays remain small so that single ropes could be used. All ropes have fixed connections in the pylon.

The Russky Bridge is the world's longest cable-stayed bridge and it is based on a semi-fan cable system configuration Fig. 1.8. The Russky Bridge is built across the Eastern Bosphorus strait, to serve the Asia-Pacific Economic Cooperation conference that took place in Vladivostok in 2012.



**Figure 1.8** The Russky Bridge

The bridge connects the mainland part of the city (Nazimov peninsula) with Russky Island, where the main activities of the summit took place. The bridge was completed in July 2012 and opened by Russian Prime Minister Dmitry Medvedev. Furthermore, the Russky bridge also has the second highest pylons after the Millau Viaduct.

With respect to the pylon types, cable-stayed bridges can be characterized by three main shapes: H-frame, A-frame and Y-frame shape.

The H-frame type pylons were used in the design of early cable-stayed bridges. The A-frame pylon is suitable for inclined stay arrangements. A variation of the A-frame is the inverted Y-frame where the vertical leg, containing the stay anchors, extends above the bifurcation point.

With respect to the various positions in space which may be adopted for planes in which the cable stays are disposed there are two basic arrangements: two-planes system and single-plane system.

In the first case, the cable system may be composed by two vertical or inclined planes which linked the external edge of the girder to the pylons, whereas, in the last case, the cables are located in a single vertical strip. In particular, a single-plane system requires a hollow box main girder with considerable torsional rigidity in order to keep the change of cross-section deformation due to eccentric live load within allowable limits.

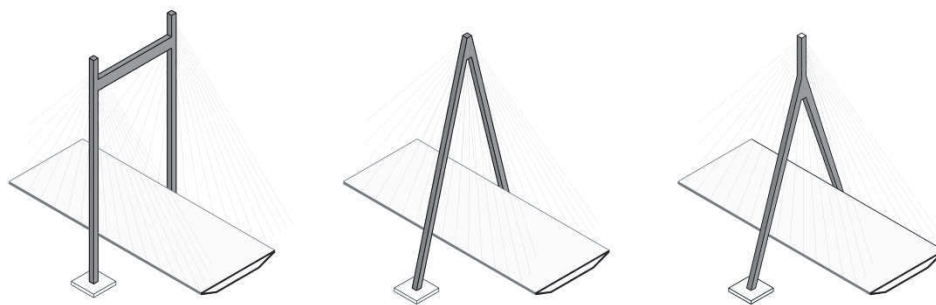


**Figure 1.9** Pylon types for cable-stayed bridges: (left) H-frame; (centre) A-frame; (right) Y-frame

It is worth nothing that, all possible variations regarding the longitudinal arrangements of the cables used with two plane bridges are also applied to single plane central girder bridge.

The cross sectional stay areas are designed so that the dead loads ( $g$ ) produce constant stress over all the distributed elements, which are assumed equal to a fixed design value, namely  $\sigma_g$ . As a result, the geometric area of the stays varies along the girder, but the safety factors are practically constant for each element of the cable system.

Moreover, for the anchor stays, the cross-section geometric area, that is  $A_{s0}$ , is designed in such a way that the allowable stress is obtained in the static case, for live loads applied to the central span only.

Therefore, the geometric measurement for the cable system can be expressed by the following equations:

$$A_s = \frac{g\Delta}{\sigma_g \sin \alpha} \quad (1.10)$$

$$A_{s0} = \frac{gl}{2\sigma_g} \left[ 1 + \left( \frac{l}{H} \right)^2 \right]^{1/2} \left[ \left( \frac{L}{2l} \right)^2 - 1 \right]$$

where  $\alpha$  is the slope of a generic stay element with respect to the reference system,  $L$ ,  $l$  and  $H$  are representative geometric lengths of the bridge structure, and  $\Delta$  is the stay spacing step.

The bridge analysis is based on the following assumptions:

- The stress increments in the stays are proportional to the live loads,  $p$ ;
- A long span fan shaped bridge is characterized by a dominant truss behavior. In this framework, the tension and  $\sigma_{g0}$  for distributed and anchor stays, respectively, can be expressed by the following relations:

$$\sigma_g = \frac{g}{g+p} \sigma_a$$

$$\sigma_{g0} = \sigma_a \left\{ 1 + \frac{p}{g} \left[ 1 - \left( \frac{2L}{l} \right)^2 \right]^{-1} \right\}^{-1} \quad (1.11)$$

It is worth noting that the allowable stay stress,  $\sigma_a$ , represents a known variable of the cable system in terms of which the design tension under dead loading can be determined by the use of Eq. (1.11).

### 1.2.3 Hybrid cable-stayed Suspension scheme

The bridge scheme, reported in Fig. 1.10, is consistent with a long span bridge typology, in which the cable system is composed by the combination of suspension and cable-stayed configurations.

Suspension and cable-stayed cable systems are based on earth and self-anchored schemes and consist of a double layer of cables arranged in the plane containing girder and pylon extremities. The hanger rods and the stays are hinged, at both ends, to the girder and main cable or to the girder and pylons, whereas the main cable is supported at the top pylon cross-sections consistently to a saddle connection.

The Brooklyn Bridge (Fig. 1.11) is the most famous hybrid cable-stayed suspension bridge in New York City and is one of the oldest bridges of either type in the United States. Completed in 1883, it connects the boroughs of Manhattan and Brooklyn by spanning the East River. The stay and hanger cross-sections of an hybrid cable-stayed suspension bridge are designed in such a way that the self-weight loads produce constant tension over all distributed elements and equal to a fixed value, namely  $\sigma_g$ . Moreover, a proper erection procedure is assumed to dispatch the girder's self-weight load with a rate  $r$  ( $0 < r < 1$ ), namely coupling stayed-suspension parameter, in both bearing systems (Gimsing & Georgakis, 2012; Konstantakopoulos & Michaltsos, 2010; Bruno, Greco, & Lonetti, 2008)

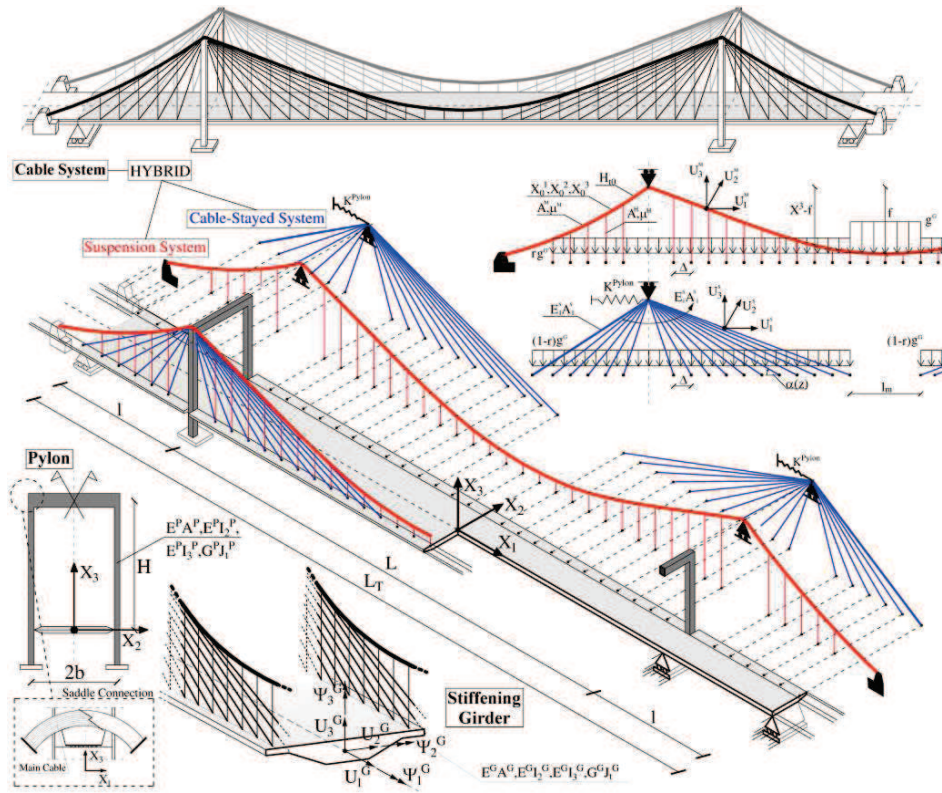


Figure 1.10 Structural scheme of the Hybrid cable-stayed suspension bridge



Figure 1.11 The Brooklyn Bridge

This hypothesis is in agreement with the main theory on combined supported bridges, which considers the dead load distribution spitted into equivalent loads depending on the amount required of the cable steel quantity involved in the cable system (Gimsing & Georgakis, 2012; Gimsing, 1991).

The constant distribution of the dead loads can be viewed as a realistic approximation of the actual solution from an engineering point of view, because it is frequently assumed the dead loading is undertaken by equally distributed elements, i.e. hangers and stays. From an analytical point of view it corresponds to a dead loads distribution factor, equal to the fraction of the total girder dead load taken by the suspension system in the regions where both suspension and cable stayed systems are present.

Therefore, the girder self-weight amounts applied to the cable-stayed (*st*) and the suspension (*sp*) systems, i.e.,  $g_{st}$  and  $g_{sp}$ , respectively, are defined by the following expressions:

$$\begin{aligned} g_{st} &= (1-r)g \\ g_{sp} &= rg \end{aligned} \tag{1.12}$$

where  $g$  represents the girder self-weight loads per unit length.

A generic stay or hanger initial cross-section area is dimensioned by means of the following equations:

$$\begin{aligned} A_s &= \frac{g_{st} \Delta}{\sigma_g \sin \alpha} = (1-r) \bar{A}_s \\ A_h &= \frac{g_{sp} \Delta}{\sigma_g} = r \bar{A}_h \end{aligned} \tag{1.13}$$

where  $\sigma_g$  is the self-weight design tension for a generic stay,  $\Delta$  is the stay and hangers spacing step,  $\alpha$  is the stay orientation angle with respect to the horizontal direction (Fig. 1.10).  $\bar{A}_s$  and  $\bar{A}_h$  are, respectively, the cross-section area dimensions expressed by Eq.s (1.4) and (1.11).

Similarly for the anchor stays, the geometric area is determined in such a way that the corresponding allowable stress, i.e.  $\sigma_{g0}$ , is reached in the static case for live loads applied on the central span only:

$$A_0 = \frac{g_s l}{2\sigma_{g0}} \left[ 1 + \left( \frac{l}{H} \right)^2 \right]^{1/2} \left[ \left( \frac{L}{2l} \right)^2 - 1 \right] = (1-r)\bar{A}_0 \quad (1.14)$$

From a practical point of view, the design parameter  $r$  is an indicator of the ratio between the suspension system steel quantity and that involved in the combined bridges. As an example, assuming that  $r$  is equal to 0 or 1, the combined bridge tends to a perfect cable-stayed or suspension bridge scheme, respectively, and consequently,  $A_s = \bar{A}_s$ ,  $A_{s0} = \bar{A}_{s0}$  and  $A_h = \bar{A}_h$ . Assuming that the stress increments in the stays are proportional to live loads,  $p$ , the self-weight design tension for a generic stay, and the anchor ones, i.e.  $\sigma_g$  and  $\sigma_{g0}$ , respectively, can be expressed by the following equations:

$$\begin{aligned} \sigma_g &= \frac{g}{g+p} \sigma_a \\ \sigma_{g0} &= \frac{\left( \frac{L}{2l} \right)^2 - 1}{\left( 1 + \frac{p}{g} \right) \left( \frac{L}{2l} \right)^2 - 1} \sigma_a \end{aligned} \quad (1.15)$$

where  $\sigma_a$  is the allowable stay stress. The cable stayed system, especially for long spans, is affected by high stiffness reduction due to Dischinger effects (Irvine, 1981).

The stays are supposed to be distributed on a reduced portion of the main span, namely  $2l + L - l_m$  (Fig. 1.10), which can be estimated, approximately, by the following relationship (Gimsing & Georgakis, 2012):

$$l_m = L - L \left[ 1 + \left( \frac{g_{sp} + g_c}{g} \right)^{1/2} \right]^{-1} \quad (1.16)$$



where  $g_c$  is the self-weight main cable suspension distributed loads.

In the framework of long span bridges, the ratio between sag and horizontal main cable projection length, i.e.  $f/L$ , is usually small and it vary in the range between 0.1 and 0.2. Therefore, the initial main cable configuration ( $y$ ) and the corresponding horizontal axial force ( $H_{i0}$ ) can be determined in closed form, utilizing a parabolic approximation of the cable profile (Pugsley, 1968), as:

$$y(z) = -\frac{M(z)}{H_{i0}} \quad (1.17)$$

$$H_{i0} = \frac{1}{s} \left[ (g_c + rg) \frac{L^2}{8} + g_{st} \frac{l_m}{4} \left( L - \frac{l_m}{2} \right) \right]$$

where  $M(z)$  is a fictitious bending moment due to distributed self-weight loads taken by the suspension system calculated as for a simply supported beam and  $s$  is the main cable sag.

In the dead load configuration, the main cable is subjected to the transferring stresses arising from the girder, which can be assumed differently distributed between the cable-stayed and the suspension systems as a function of a dead load factor ( $r$ ), typically assumed in the range between 0.2 and 0.4 for design purposes.

The main cable dimensioning quantifies the geometric area, in terms of maximum main cable axial force, allowable tension, and slope of main cable profile, as (Gimsing & Georgakis, 2012):

$$A_c = \frac{H_{tq}}{\sigma_a \cos(\phi)} \quad (1.18)$$

where  $\phi$  is the orientation angle formed by the main cable tangent at pylon intersection and the vertical direction (Fig. 1.10) and  $H_{tq}$  is the horizontal main cable force related to live loads applied to the whole central span.

### 1.2.4 Self-anchored cable-stayed suspension bridge

The structural scheme, reported in Fig.1.12, is consistent with a self-anchored cable-stayed suspension bridge in which the cable system is based on the combination of suspension and cable-stayed configurations (Wang, Tan, Qin, & Zhang, 2013). Suspension and cable-stayed cable systems consist of a double layer of cables arranged in the plane containing girder and pylon extremities. In particular, the cable-stayed system is based on discrete stays, which are mainly arranged in the region close to the pylons, whereas, the suspension system is composed by a main cable and several hangers located in the central span of the main span.

The hanger rods and the stays are hinged, at both ends, to the girder and to the main cable or to the girder and pylons and they are spaced at constant step  $\Delta^G$  along the entire girder length.

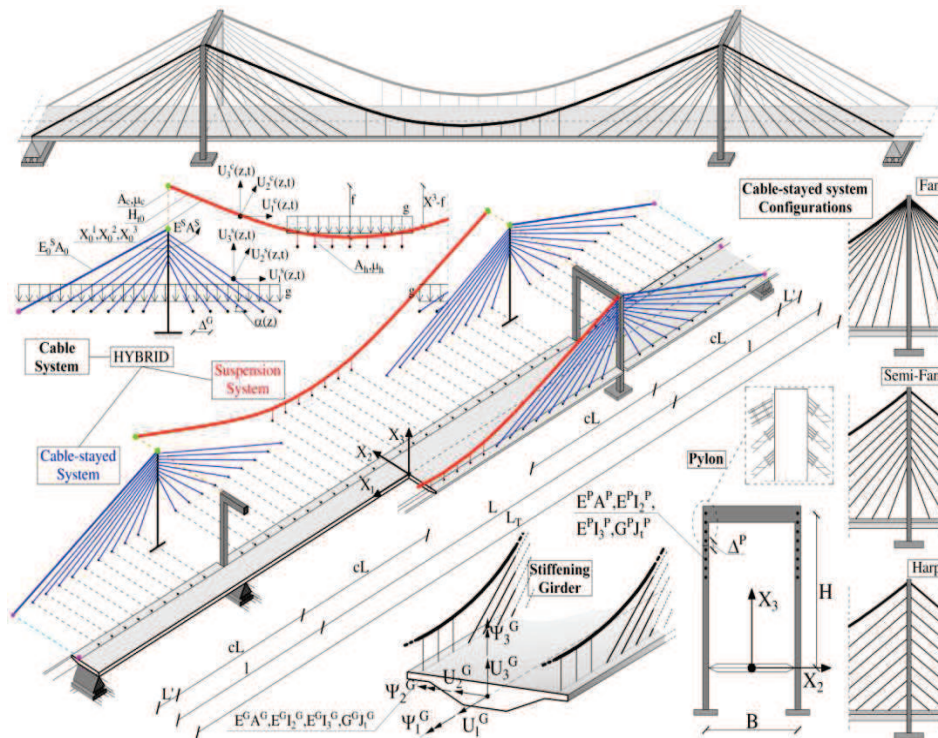


Figure 1.12 Structural scheme of the self-anchored cable-stayed suspension bridge

Furthermore, the stays are spaced at constant step  $\Delta^p$  along the pylons height and, depending on this step size, the cable-stayed system can be characterized by a fan, a semi-fan or an harp configuration. The main cable is in the main span only and it is hinged at top pylons. The whole system results as self-anchored by an anchor cable which connect stiffening girder extremities to the top of the pylons. The stiffening girder is simply supported at its ends and at the pylons connections, which are formed by H-shaped.



**Figure 1.13** The Zhuanghe Jianshe Bridge

One of the last self-anchored cable-stayed suspension bridges built is the Zhuanghe Jianshe Bridge. The entire bridge is 202 m long, and has a central span of 110 m and two side spans of 46 m. The suspended part and the stayed part of the central span are 38.4 m and 39 m, respectively. The pylon and stiffening girders are both of concrete structures. The main parameters characterizing the self-anchored cable-stayed suspension bridge scheme are defined as follows (Zhang, Wang, Qin, & Ge, 2009):

- 1) The main span length  $L$ ;
- 2) The pylon height  $H$ ;
- 3) The rise-span ratio of main cable  $\zeta$ , that is  $f/L$ , which vary between 0.1 and 0.2;
- 4) The length of cable-stayed portion of the main span  $c$ , which vary between 0 and 0.5;
- 5) The height-span ratio  $\mu$ , i.e.  $h/cL$ , which vary between 0.4 and 0.5;
- 6) The distance between the anchor points and the nearest stay  $L'$ .

It is worth nothing that, the cable system has to be designed considering that the total load is carried by the cable-stayed system in the region near pylons and by suspension system in the center of the main span (Wang, Qin, Zhang, Huang, & Xu, 2010). For this reason, the initial main cable configuration ( $y$ ) and the corresponding horizontal axial force ( $H_{t0}$ ) can be determined in closed form, utilizing a parabolic approximation of the cable profile (Fig. 1.14):

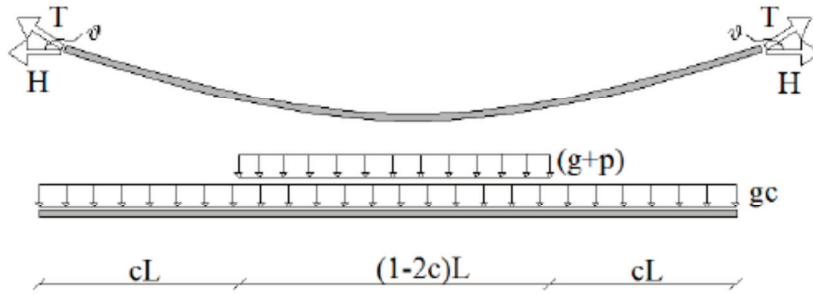


**Figure 1.14** Structural scheme for maximum main cable force

$$y(z) = -\frac{M(z)}{H_{t0}} \quad (1.19)$$

$$H_{t0} = \left[ \frac{g_c + (g+p)(1-4c^2)}{8\lambda} \right] L \quad \text{with } \lambda = \frac{f}{L}$$

where ,  $g_c$  and  $g$ , are respectively, main cable and girder self-weights, while  $p$  is the live load (Gimsing & Georgakis, 2012).  $M(z)$  is a fictitious bending moment due to distributed self-weight loads taken by the suspension system calculated as for a simply supported beam.

Similarly to the suspended scheme, the main cable cross-section area can be expressed in terms of maximum main cable axial force, allowable tension, and slope of main cable profile, as (Gimsing & Georgakis, 2012):

$$A_c = \frac{H_{t0}}{\sigma_a \cos(\phi)_{\max}} \quad (1.20)$$

where  $\cos(\phi)_{\max} = \min\{\cos\phi_1, \cos\phi_2\}$ :

$$\begin{aligned}\cos\phi_1 &= \frac{1}{\sqrt{1+16\lambda^2}} \\ \cos\phi_2 &= \frac{1}{\sqrt{1+16\mu^2}}\end{aligned}\quad (1.21)$$

Assuming,  $\cos\phi_1 < \cos\phi_2$ , the main cable cross-section area can be defined by the following expression:

$$A_c = \frac{(g+p)(1-4c^2)L\sqrt{1+16\lambda^2}}{\sigma_a - \gamma_c L\sqrt{1+16\lambda^2}} \quad (1.22)$$

The main cable configuration is described by the following parabola expression:

$$y(x) : \begin{cases} 4f \frac{L[A_c\gamma_c + (1-2c)(g+p)] - A_c\gamma_c x}{L^2[A_c\gamma_c + (1-4c^2)(g+p)]} & 0 \leq x \leq cL \\ 4f \frac{x(L-x)(A_c\gamma_c + g+p) - c^2L^2(g+p)}{L^2[A_c\gamma_c + (1-4c^2)(g+p)]} & cL \leq x \leq 0.5L \end{cases} \quad (1.23)$$

where  $A_c$  and  $\gamma_c$  are the main cable cross-section and specific weight.

A generic stay or hanger initial cross-section area can be dimensioned, respectively, by means of the Eq.s (1.10) and (1.9). It is worth nothing that, in the case of self-anchored cable-stayed suspension bridge scheme, the initial stress design for hangers and stays can be expressed, as:

$$\sigma_{gs} = \sigma_{gh} = \frac{g}{g+p} \sigma_a \quad (1.24)$$

### **1.3 The longest suspension and cable-stayed bridges built to date**

The length of the main span is the most common way to rank cable supported bridges, often correlating with the height of the pylons.

Suspension bridges have the longest spans of any type of bridge and they can span length about 2000 meters, whereas, cable-stayed bridge are practical for spans up to around 1 kilometer. It is worth nothing that, The Strait of Messina Bridge, with a total length of 3.1 km, should have been the longest suspension bridge in the world.

As the span length increases, the height of the pylon increases in a cable-stayed bridge making it difficult to build the entire structure.

However, in the last years cable-stayed bridges were used more than suspension bridge as they offer all the advantages of a suspension bridge but at a lesser cost for spans of 152 to 853 meters. They require less steel cable and are faster to build. Moreover, cable-stayed bridges allow the construction of the individual segments of the bridge at remote locations. The suspension bridge requires the building of suspension cables across the entire span before the deck installation begins. A cable-stayed system is stiffer than a suspension one for the same midspan length which imply better structural performances. Also generally the deflections are less, therefore the girder can be made lighter and more slender. Structurally this improves wind resistance and aesthetically the appearance.

Lists of the first five longest suspension and cable-stayed bridges which only includes bridges that carry automobiles or trains are reported in Tab.s 1.3 and 1.4. Such bridge types have been widely used in the past.

Unfortunately, few cases of combined bridges are available, although some new project of long-span cable supported bridges is based on hybrid schemes, as the proposal for the Portland-Milwaukie Light Rail Bridge (Fig. 1.15). The hope is that the use of cable supported bridges based on hybrid configurations of cable system may grow in the next future.

Name	Main span metres	Image
<b>Akashi Kaikyō Bridge</b>	<b>1991</b>	
<b>Xihoumen Bridge</b>	<b>1650</b>	
<b>Great Belt Bridge</b>	<b>1624</b>	
<b>Yi Sun-sin Bridge</b>	<b>1545</b>	
<b>Runyang Bridge</b>	<b>1490</b>	

Table 1.3 List of longest suspension bridge spans

Name	Main span metres	Image
Russky Bridge	1104	 A photograph of the Russky Bridge, a cable-stayed bridge with a tall, slender pylon and multiple stay cables, set against a blue sky with light clouds.
Sutong Bridge	1088	 A photograph of the Sutong Bridge, a cable-stayed bridge with a tall, slender pylon and multiple stay cables, viewed from a low angle.
Stonecutters Bridge	1018	 An aerial photograph of the Stonecutters Bridge, a cable-stayed bridge with two tall, slender pylons, spanning a large body of water with a city and harbor in the background.
Tatara Bridge	890	 A photograph of the Tatara Bridge, a cable-stayed bridge with two tall, slender pylons, spanning a body of water with a green hill in the background.
Pont de Normandie	856	 An aerial photograph of the Pont de Normandie, a cable-stayed bridge with a tall, slender pylon and multiple stay cables, spanning a large body of water.

**Table 1.4** List of longest cable-stayed bridge spans





**Figure 1.15** The design proposal for the Portland-Milwaukie Light Rail Bridge

## 1.4 Literature review

### 1.4.1 Design methodologies

In the framework of the design methodologies, most of the existing studies are based on the use of simple design rules obtained by the experience and expertise of the designers, in which relationships typically adopted in the framework of pure cable-stayed or suspension configurations are utilized (Gimsing & Georgakis, 2012; Troitsky, 1988; Walther, Houriet, Isler, Moia, & Klein, 1999). However, during the last decades, many research efforts are carried out with the aim to propose proper procedures to calculate the optimum configuration of the bridge. In particular, zero displacement methods (ZDMs) are based on the use of explicit constraint equations, which enforce the bridge structure under dead loading to remain practically undeformed (Wang, Tseng, & Yang, 1993; Wang, Tang, & Zheng, 2004). The governing equations, expressed as a function of the internal forces of the cable system, introduce a determinate equation system, in which the unknown quantities are obtained, prescribing, at

discrete points of the structure, zero displacement conditions. Furthermore, force equilibrium method (FEMs) consider as control variables to be solved, the internal forces of the cable system, which are calculated to reduce bending moments and displacements of the girder, achieving a structural scheme of the girder approximately equivalent to a simply supported continuous beam (Chen, Au, Tham, & Lee, 2000; Kim & Lee, 2001; Janjic, Pircher, & Pircher, 2003).

Alternatively to direct methods, models, developed in the framework of structural optimization (OMs), are frequently adopted in the literature (Wickert, Canfield, & Reddy, 2010). In particular, post-tensioning forces are determined by solving constrained minimization problems as a function of performance or objective scalar valued functions, constraint equations and control variables.

For cable-stayed bridges, existing models based on optimization method utilize an objective scalar function, which is typically expressed in terms of norm of displacements (Wang, Vlahinos, & Shu, 1997; Hassan, Nassef, & El Damatty, 2012). From the minimization of the objective function, such methods are able to calculate the optimum set of post-tensioning forces, which achieves minimum deflections and a uniform bending moment distribution under the effect of dead loading.

Advanced techniques for cable-stayed bridges, proposed by Simões and Negrão (Simões & Negrão, 2000), are based on a multicriterion optimization procedure, in which in the minimization procedure also the characteristics of the girder cross-section are included. Moreover, refined formulations based on robust optimization algorithms can be recovered in a study proposed by Barbero and Makkapati (Barbero & Makkapati, 2000), in which models based on the neural-network concepts are able to obtain the optimum structural configuration.

In the framework of suspension bridges, the procedure to calculate the initial configuration under dead loads is relatively simple, because the main cable extremities are fixed at earth constrains. As a consequence, optimization techniques are, frequently, employed with the purpose to identify the structural behavior of the bridge with respect more complex external loads, such as aeroelastic (Nieto, Hernández, & Jurado, 2009) or seismic (Ferreira & Simões, 2011) phenomena. It is worth noting that, models described above, developed in

the framework of ZDM, FQM or SO, evaluate the initial cable forces directly on the final configuration. However, in the literature, several approaches can be recovered, in which target stress state is predicted by means of step by step procedures based on the actual construction process going from the initial to the final configuration. In particular, computational procedures for the shape finding analysis based on a forward and a backward process are proposed (Behin & Murray, 1992; Wang, Tang, & Zheng, 2004), in which different erection stages are investigated in the framework of the free cantilever method. In this framework, the unit load model (ULM) developed by Janjic et al. (Janjic, Pircher, & Pircher, 2003) evaluate the desired moment distribution in the final configuration, computing the post-tensioning strategy of the construction method by using additional constraint conditions. An extended and reviewed version of the ULM is proposed by Lee et al. (Lee, Kim, & Kang, 2008) also for asymmetric cable-stayed bridges, in which a two-step scheme is proposed for the optimum evaluation of the initial cable forces.

#### **1.4.2 Moving loads and damage mechanisms problems**

In the literature, many investigations have been developed to analyze the influence of the moving loads on the dynamic behavior of cable supported bridges, mainly, for undamaged bridge structures.

Actually, many models are devoted to predicting dynamic bridge behavior by using refined structural schematizations as well as accurate descriptions of the moving loads (Cheng, Au, & Cheung, 2001; Zhang & Xie, 2011; Yang & Fonder, 1998; Wang, Qin, Zhang, Huang, & Xu, 2010). In this framework, the bridge behavior is analyzed by means of analytical continuum approaches or finite element models, in which, the behavior of the cable suspension system is typically described by means of linear equations expressed in terms of tangent or secant Dischinger elastic moduli (Au, Wang, & Cheung, 2001; Au, Wang, & Cheung, 2002; Bruno, Greco, & Lonetti, 2008). This assumption is frequently supported by experimental evidence for static analyses (Gimsing & Georgakis, 2012; Troitsky, 1988). However, in order to reproduce

the dynamic behavior correctly, especially when the bridge is subjected to extreme loading conditions, local vibration effects of the cable elements should be, properly, taken into account (Zhang & Xie, 2011; Chatterjee, Datta, & Surana, 1994). Additional complexities in the prediction of the dynamic behavior of long span bridges arise from the description of the interaction behavior between moving loads and bridge vibrations. At this aim, many papers have been developed to analyze the influence of the external mass and its motion on the bridge behavior, introducing an accurate description of the inertial forces between bridge deformation and moving load kinematic (Bruno, Greco, & Lonetti, 2008; Bruno, Greco, & Lonetti, 2009; Konstantakopoulos & Michaltsos, 2010). Cable supported bridges are frequently exposed to severe environmental conditions such as marine environment, rain, pollution, etc. Such phenomena lead to degradation effects which may cause a reduction of the stiffness properties of the structural components. In particular, with reference to the cable system, which usually consists of high tensile galvanized steel wires, damage mechanisms can lead, in extreme cases, the complete failure of a single or multiple cable elements. For this reason, the evaluation of the structural behavior of cable structures, subjected to unexpected damage mechanisms, is considered to be an important tasks, in health monitoring for the maintenance and rehabilitation of older structures or in the design procedure for the analysis of new ones. In the literature, damage analyses are mainly developed on a single cable or simplified cable systems involving a preexisting inelastic region in the cable development. In particular damage behavior of elastic suspended cables or cable-stayed beams is analyzed by means of closed form expressions or numerical approaches, in which the effects of diffused inelastic damage modes are investigated in terms of intensity and location along the cable development (Lepidi, Gattulli, & Vestroni, 2007; Zhu, Ye, Xiang, & Chen, 2011). The results proposed by these papers show how damage phenomena induce notable tension loss and sag augmentation with respect to the cable profile of the undamaged configuration.

Only few comprehensive investigations have been carried out with the purpose of analyzing the influence of damage phenomena on cable supported bridges (Bruno, Greco, Lonetti, & Nevone Blasi, 2012; Zhang & Au, 2013).

In the framework of cable-stayed bridges, behavior under damage phenomena in the cable system is typically investigated by means of standard linear analyses, in which the allowable stresses in the bridge components are obtained by means of proper factored loading combinations, involving self-weight and accidental loads (Post-Tensioning Institute, 2007; Service d'Etudes Techniques des Routes et Autoroutes, 2001). In the framework of suspension bridges, the influence on bridge behavior of damage mechanisms in the cable system has been scarcely analyzed in the literature. Typically, analyses are carried out with the purpose of investigating the fatigue assessment of the bridge under traffic or wind loads, in which the performance of the structure is evaluated at critical locations of the cable system (Petrini & Bontempi, 2011; Xu, Chen, & Xia, 2012). To the Author knowledge, only in (Materazzi & Ubertini, 2011) the influence of damage phenomena is considered for the case of a single span suspension bridge scheme, in which the relationships between vertical vibrations and damage characteristics of the cable system are discussed from an analytical viewpoint.

Finally, in the framework of hybrid cable supported bridges, the literature dealing with such bridge schemes was mainly devoted to investigating undamaged configurations under static and dynamic loading conditions by means of analytical or numerical approaches (Bruno, Greco, & Lonetti, 2009; Konstantakopoulos & Michaltsos, 2010).

### **1.4.3 Nonlinear behavior of cable supported bridges**

The sources of nonlinearity affect the structural behavior and as a consequence the maximum load carrying capacity.

Typically, the maximum load carrying capacity can be evaluated by two different approaches, known as limit-point stability approach and bifurcation-point stability approach, which, respectively, employ a nonlinear static analysis and an eigenvalue analysis. In particular, the former is more suitable than the latter for structures characterized by a remarkable nonlinear behavior as cable supported bridges since it can accurately account for both geometric and

material nonlinearities (Yoo & Choi, 2008). However, a good approximation of bearing capacity of steel cable-stayed bridges was obtained by a modified bifurcation-point stability methodology based on an iterative eigenvalue problem combined with the tangent stiffness theory (Yoo & Choi, 2009; Yoo & Choi, 2012). The limit point stability procedures present in literature were developed mainly for pure cable-stayed and suspension bridges and, to the Author's knowledge, there aren't works on hybrid typologies. Such methodologies differ from each other depending on assumptions and formulations adopted for reproducing the inelastic material behavior and geometric nonlinearities of each structural element. Most of the work offer accurate description of structural behavior of girder and pylons reproducing geometric nonlinearities by stability functions or refined finite element formulations and material nonlinearities by fiber models or plastic hinge models (Thai & Kim, 2011; Thai & Kim, 2012).

Nevertheless, no accurate formulations have been assumed for cable elements in all cases. As a matter of fact, with reference to the geometric nonlinearities, if a catenary formulation for the main cable of suspended bridges was adopted, in the case of cable-stayed bridges the stays nonlinear behavior was modeled widely by approximate approach according to Ernst's theory (Adeli & Zhang, 1995; Thai & Kim, 2012). By this theory, any inclined cable is considered as a straight element with uniform properties from end to end incorporating the sag effect by means of the equivalent elasticity modulus under the hypothesis that the change in tension in the cable during a load increment is not large.

## **1.5 Objectives and motivations of the thesis**

The present thesis aims to achieve three main goals in agreement with the current issues on cable supported bridges introduced in the previous paragraph 1.1. For each one a brief motivation is provided:

- i) *Develop a design methodology to predict optimum post-tensioning forces and dimensioning for each typologies of cable supported bridge. The optimum design is defined with respect to both dead and live load configurations, taking into account design constrains concerning serviceability and ultimate limit states.*

Previous models based on the zero displacement method or force equilibrium method, are mainly developed in the frameworks of cable-stayed or suspension systems, in which typically, the initial configuration is derived by solving a determinate system of equations.

As a matter of fact, in the cases of hybrid cable-stayed suspension bridges, the presence of the two cable systems introduces additional variables in the solving procedure and thus further equations are required to impose the constraint equations on the bridge configuration (Konstantakopoulos & Michaltsos, 2010). On the other hand, models developed in the framework of optimization methods, especially in the cases of long span bridges, due to the presence of a large number of variables are affected by convergence problems in the solving procedure, which may lead to a local minimum of the objective function and unpractical results in the bridge definition.

However, most of the previous methodologies are typically concerned to evaluate only the initial stress state and the corresponding cable forces under dead loads, without verifying if the cable dimensioning is consistent with the design code prescriptions on both stress or deflections, produced by the live load application. Such tasks were investigated only recently by few methodologies, mainly developed in the framework of cable-stayed bridge schemes. In particular, Hassan (Hassan, 2013) introduced a generalized formulation by means of a combined approach based on the finite element method and an optimization genetic algorithm, in which the distribution of the cable cross-sections is expressed by means of B-spline curves.

Moreover, Baldomir et al. (Baldomir, Hernández, Nieto, & Jurado, 2010) have proposed an iterative approach, in which, initially, the post-tensioning cable forces in the dead load configuration are determined by solving

compatibility conditions arising from flexibility matrix of the structure. Subsequently, the optimization procedure is utilized to minimize the cross-sections of the cable system, on the basis of the maximum effects on stress and displacement variables evaluated on the live load configurations.

Finally, as far as hybrid scheme cable supported bridges are concerned, no works on the optimal design of hybrid cable-stayed suspension bridges or self-anchored cable-stayed suspension bridges are available from the literature.

The proposed methodology want to overcome these limitations and ensure a better design of the bridge which meets the structural requirements under the action of dead and live load. In particular, under dead loads, the analysis is developed with the purpose to calculate the post-tensioning cable forces to achieve minimum deflections for both girder and pylons.

Moreover, under live loads, for each cable elements, the lowest required cross-section area is determined, which verifies prescriptions, under ultimate or serviceability limit states, on maximum allowable stresses and bridge deflections. The final configuration is obtained by means of an iterative procedure, which leads to a progressive definition of the stay, hanger and main cable characteristics, concerning both post-tensioning cable stresses and cross-sections. The design procedure is developed in the framework of a finite element (FE) modeling, by using a refined formulation of the bridge components, taking into account of the geometric nonlinearities involved in the bridge components.

- ii) Investigate the structural behavior of cable supported bridges due to the presence of damage mechanisms in the cable system under the action of moving load.*

The behavior of cable supported bridges under the action of moving load is mainly analyzed for undamaged structures, whereas the influence of cable failure mechanisms produced by loss of stiffness due to cable degradation or due to an accidental failure is rarely analyzed.



Existing codes on cable-stayed bridges, that is, P.T.I. (Post-Tensioning Institute, 2007) and S.E.T.R.A. (Service d'Etudes Techniques des Routes et Autoroutes, 2001), in order to identify the amplification effects provided by the failure mechanism in the cable system, recommend to amplify the results obtained in the framework of quasi-static analyses by using fictitious amplification factors suggested in the range between 1.5 and 2.0. In particular, the codes identify the dynamic characteristics of the failure mode of a generic element of the cable system, introducing a static loading configuration, in which the cable failure is reproduced by means of compression forces to simulate cable release. The stress distribution arising from such a loading scheme is combined with the effects of other existing loading schemes by means of proper factored loading combinations.

However, recent papers have demonstrated that such a simplified approach becomes unsafe in many cases, leading to dynamic amplification factors higher than those suggested by existing recommendations (Bruno, Greco, Lonetti, & Nevone Blasi, 2012; Starossek, 2009). In particular, some parametric studies have been developed for bridge typologies subjected to accidental cable failure by using a numerical approach based on classical standard linear dynamic framework (Wolff & Starossek, 2009; Starossek, 2009). Such analyses denote that the results obtained by using such code prescriptions are affected by high underestimations in the prediction of typical design bridge variables related to the girder and pylons.

Moreover, codes on cable supported bridges, typically, do not consider non-standard inertial contributions arising from the inertial description of the moving loads in the definition of the moving load forces. Such effects, taken only by using coupled dynamic analyses, combined with those introduced by the presence of damage mechanisms in the cable system, can cause notable underestimations in the prediction of the actual bridge deformability and internal stress distribution. However, additional developments are required to be simulate the effect produced by the nonlinearities and damage mechanisms involved cable system and by the inertial coupling between girder and moving loads deformations. Furthermore, the future design requirement of heavy traffic bridges should consider the application of the “fail-safe” concept (Sih, Tang,

Li, Li, & Tang, 2008; Sih & Tang, 2008; Zhang Y. , 2003). This should be distinguished from the use of safety factor and redundant structural members. In general, fail-safe applies to local failure while the structure remains intact globally and can still support load.

Comprehensive analyses that include nonlinear dynamic effects are quite rare and thus further investigations to verify code prescriptions and to quantify the influence on the bridge behavior of the dynamic excitation produced by the failure mode characteristics of the cable system are much required. Furthermore, as far as hybrid cable supported bridges are concerned, the structural behavior has been mostly analyzed in the context of undamaged configuration and, to the best of the Author knowledge, no work on dynamic bridge behavior of combined bridges affected by damage mechanisms is available in the literature. As a consequence, the influence on bridge structures damage mechanisms is in need of investigation, in order to reach a better understanding of bridge vulnerability behavior subjected to both long term and sudden failure mechanisms due to unpredictable events.

The inertial description of the moving loads is reproduced by means of a refined schematization of the inertial forces produced by the moving system and girder bridge interaction. Comparisons between cable-stayed, suspension and combined cable-stayed suspension bridge schemes are proposed to quantify the vulnerability index of the structure and to point out the enhanced properties of the hybrid bridges, also in the light of existing codes on cable supported bridges. In particular, as far as cable-stayed bridge typology, a parametric study to investigate the influence on the bridge behavior of the dynamic excitation produced by damage mechanisms in the cable system and the transit of moving loads is proposed.

*iii) Propose an efficient numerical model for predicting the ultimate strength and behavior capacity of self-anchored cable-stayed suspension bridges considering both geometric and material nonlinearities of each structural element.*

As far as geometric nonlinear of cable elements, most refined formulation of stays nonlinear behavior have been developed by finite element procedure where the response of a single stay has been modeled combining finite strain formulation with multiple truss element approach.

In such a way, one can reproduce the stays nonlinear behavior more accurately than the factious elasticity model approach, and although it has been adopted in several works on cable-stayed bridges, it has been taken into account only in few studies on the nonlinear behavior of cable supported bridges (Bruno, Greco, Nevone Blasi, & Bianchi, 2013).

Similarly, only in rare cases the inelastic behavior of cables material was considered, although several studies have shown how it greatly affects the maximum load-bearing capacity of a cable supported bridge (Ren, 1999; Nagai, Iwasaki, & Nogami, 2003). As a matter of fact, in most studies it was assumed a cable post-elastic behavior in such a way that each element vanish when it reach yield stress. Such a disadvantageous approach could be too cautionary since neglects the cable mechanical properties leading to an over-sizing structure.

## 1.6 Thesis Structure

The three topics introduced in the previous section are analyzed in three distinct chapters of this thesis.

Chapter 2 treats the optimum design methodology. After a brief description of the various design methodologies available from the literature, the formulation of the proposed design methodology is presented. In particular, many efforts are devoted to illustrate the application of such methodology with reference to the hybrid cable-stayed suspension bridge since it is the most complex case. The extension to the other bridge configurations as pure cable-stayed and suspension scheme or self-anchored cable-stayed suspension scheme is obtained as simplification of the formulation of the previous case. Subsequently, the numerical implementation is presented, which is based on a combination of an finite element approach and an iterative optimization procedure. In order to prove the effectiveness and the robustness of the

proposed design methodology, comparisons with existing formulations available from the literature and application to a fictitious case of a self-anchored cable-stayed suspension bridge with noticeably reduced number of design variables are performed. Furthermore, the long-span bridge cases, which are composed by a high number of elements which have to be designed, are treated. In this framework, parametric studies in terms of cable system configurations are proposed.

Chapter 3 is devoted to the analysis of the dynamic behavior of cable supported bridges subjected to moving loads and affected by damage mechanisms in the cable system is given. The main aim of the study is to investigate the vulnerability behavior of cable supported bridges in the presence of damage mechanisms, which are simulated by using a damage formulation to reproduce static or time dependent evolution laws. Furthermore, the purpose of this investigation is to analyze the amplification effects of the bridge structure produced by the moving load application and damage mechanisms in the cable system. In the first part of the chapter, the damage law and moving load problem coupled with the bridge structure formulation are presented. Afterwards, the numerical implementation of such problems as well as the evaluation of the initial configuration of the bridge structure under self-weight loads are illustrated.

In the last part of the chapter, numerical results are proposed. At first, results are proposed to investigate the behavior of cable-stayed bridge subjected to an accidental failure in the cable system. To this end, parametric studies in terms of bridge and moving loads characteristics and failure mode typology in the cable system are reported. In the last part, comparisons between cable-stayed, suspension and hybrid cable-stayed suspension bridge schemes are proposed to quantify the vulnerability index of the structure and to point out the enhanced properties of the hybrid cable-stayed suspension bridges, also in the light of existing codes on cable supported bridges.

In Chapter 4, the numerical model for analyzing the nonlinear behavior of self-anchored cable-stayed suspension bridges considering both geometric and material nonlinearities of each structural element is reported. In particular, the proposed model is employed for predicting the ultimate strength and

behavior capacity of such cable supported bridge typology pointing out the influence of materials nonlinear behavior. At first, the formulations of geometric and material nonlinearities for cables, girder and pylons are presented. Subsequently, the numerical implementation is explained. In this framework, a detailed description of the nonlinear analysis employed is given.

In the last part of the chapter, numerical results are reported which are devoted to analyze the influence of the nonlinear material behavior as well as the geometrical and structural parameters of the bridge on the maximum load capacity of the structure.

Finally, Chapter 5 presents a number of conclusions that may be formulated from the topics treated in the present thesis and includes recommendations for future research works.

# 2

## OPTIMUM DESIGN METHODOLOGY

### 2.1 Introduction

In the framework of cable supported bridges most of the existing design methodologies are devoted to evaluate the post-tensioning cable forces distribution to achieve the initial configuration of the bridge under the effect of the self-weight of the structure. In particular, post-tensioning cable forces are determined so that girder and pylon displacements are eliminated or at least reduced as much as possible. In such a way, girder and pylons would be mainly compressed.

Recently, new methodologies were proposed to evaluate both post-tensioning forces and cross-section areas of the cable system. As the previous approaches, such methods determine the post-tensioning cable forces distribution under dead load and, in addition, they regulate cable cross-sections in order to improve the structural performances under the effect of live loads.

The methodologies which find just the post-tensioning cable forces distribution under the action of dead loads are known as *direct methods* and

they are characterized by a slender mathematical problem which requires less computational efforts. Such methods was mainly developed for standard geometries based on cable-stayed and suspension bridge schemes in which the minimization of the material utilized in the construction were not considered.

The direct methods are:

- *The Unit Load Method (ULM);*
- *The Zero Displacement Method (ZDM);*
- *The Force Equilibrium Method (FEM);*

On the other hand, methodologies allows to design cross-section dimension and post-tensioning cable forces have been defined in the framework of *optimization methods (OMs)*.

The optimization methods are based on more complicated mathematical models than direct methods. Such a feature can lead to several problem in the definition of the design of the cable system as convergence problems. Moreover, in the case of high number of variables, unphysical results in the definition of the structural elements could be obtained.

It is worth nothing that, models introduced above evaluate the initial cable forces directly on the final configuration.

Briefly, the main features of the previous design methods are presented in the following.

### **2.1.1 The Unit Load Method (ULM)**

The Unit Load Method is a procedure to determine post-tensioning cable forces in order to obtain a desired bending moments or displacements distribution at specific degrees of freedom (cable-girder and cable-pylons connections). It was developed mainly in the framework of cable-stayed bridges and takes into account all relevant effects in the design of the structure, including construction sequence, second-order behavior, large displacements, sag effect as well as time-dependent factors. Due to its simplicity and easy hand

calculation, such method is usually used by designers in the tender and preliminary design.

From a practical point of view, the unit load method works as follows:

Bending moments or displacements at specific DOFs are first calculated due to unit forces applied successively along each cable of the system. Subsequently, the bridge is analyzed under the action of the dead load.

From these data, a system of linear equations can be established with one equation for each DOFs. This system of equations can be directly solved for the unknown cable forces that are used to achieve the desired bending moment or displacement distribution.

With respect to the case of the cable-stayed bridge represented in Fig. 2.1, the system of equations to get the desired bending moment distribution can be obtained starting from the maximum bending moment in the stiffening girder due to dead load  $M_r$ .

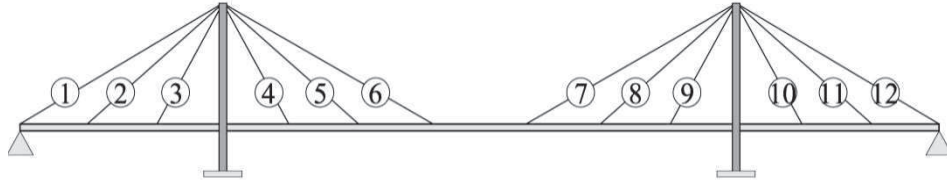


**Fig. 2.1** Post-tensioning forces in cables. Basic system

To reduce such a bending moment to  $C_0 M_r$ , where  $C_0$  is a reduction factor less than unity, the basic linear equation is

$$M_r^1 X_1 + \dots + M_r^{12} X_{12} = M_r (C_0 - 1) \quad (2.1)$$

In Eq. (2.1),  $M_r^i$  is the bending moment at location  $r$  due to the action of a unit load applied along  $i$ -th cable and  $X_i$  is the post-tensioning force to be applied in  $i$ -th cable to reduce bending moment from  $M_r$  to  $C_0 M_r$ .

On the other hand, the procedure to obtain the desired displacements consists of determining first the matrix of displacements  $D$  at  $n$  selected



locations, where  $n$  is the number of cables. The displacements are due to a unit force applied successively along each cable to the bridge.

For this reason the size of this matrix is  $n \times n$  and as far as the cable-stayed system of Fig. 2.1, the size is  $12 \times 12$ .

Further, the vector  $\underline{d}$  of displacements due to dead load at the points selected is determined. Also in this case, considering a reduction factor  $C_0$ , the system of equations is

$$\underline{d} + \underline{D}\underline{X} = C_0 \underline{d} \quad (2.2)$$

where  $\underline{X}$  is the vector of post-tensioning cable forces which can be determined easily.

### 2.1.2 The Zero Displacement Method (ZDM)

The Zero-Displacement Method identifies girder and pylons profile under permanent loading by adjusting the initial cable forces to give zero-displacements at the cable anchorages. The method takes into account nonlinearities due to large displacement ( $P-\Delta$  effect) and cable sag effects.

The zero displacement method is based on the use of a set of explicit constraint equations and it can be employed for cable-stayed, suspension and self-anchored cable-stayed suspension schemes.

With reference to the scheme reported in Fig. 2.2, which is a self-anchored cable-stayed suspension scheme, the unknown quantities are represented by the post-tensioning stresses in the cables ( $S_i^S, S_i^H, S^M$ ), which are designed by means of the following relationships:

$$\underline{S}_C = \{S_1^S, \dots, S_{N^S}^S, S_1^H, \dots, S_{N^H}^H, S^M\} \quad (2.3)$$

where  $N^S$  is the number of stays,  $N^H$  is the number of hangers and the superscripts  $S, H$  and  $M$  refer to the stays, hangers and main cable, respectively.

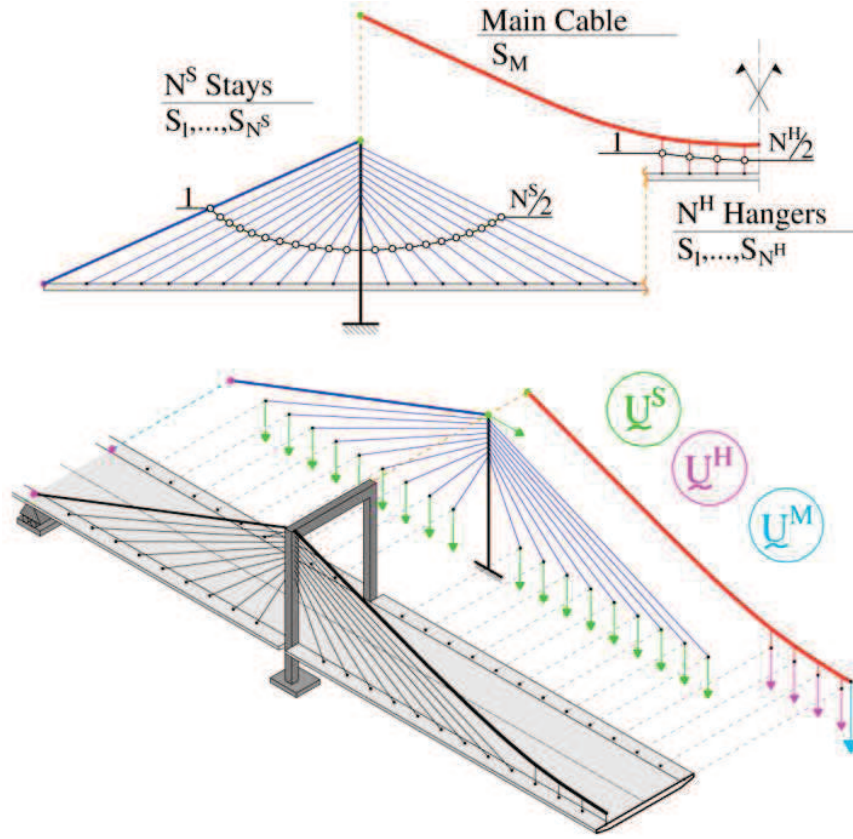


Fig. 2.2 Displacements and control variables for “zero configuration”

The displacement conditions to achieve zero displacement at the cable anchorage, are expressed as follows:

$$\begin{aligned}
 \underline{L}_S \left[ (\bar{S}_1^S + \Delta S_1^S, \dots, \bar{S}_{N^S}^S + \Delta S_{N^S}^S), \underline{U}^S \right] &= 0 \\
 \underline{L}_H \left[ (\bar{S}_1^H + \Delta S_1^H, \dots, \bar{S}_{N^H}^H + \Delta S_{N^H}^H), \underline{U}^H \right] &= 0 \\
 \underline{L}_M \left[ (\bar{S}^M + \Delta S^M), \underline{U}^M \right] &= 0
 \end{aligned} \tag{2.4}$$

where  $\underline{L}_S$ ,  $\underline{L}_H$  and  $\underline{L}_M$  are the constraint operators referred to the stays, hangers and main cable variables, respectively. In the constrain equations (2.4),

$\underline{U}^S$  and  $\underline{U}^H$  are the vector containing, respectively, the horizontal displacements of the top pylon left ( $L$ ) and right ( $R$ ) cross-sections and the vertical displacements of the stays at the girder connections ( $U_{3(1)}^G, \dots, U_{3(N^S)}^G$ ) and the vertical displacement of the hangers at the girder connections ( $U_{3(1)}^G, \dots, U_{3(N^H)}^G$ ):

$$\underline{U}^S = [U_1^{P_L}, U_1^{P_R}, U_{3(1)}^G, \dots, U_{3(N^S)}^G] \quad (2.5)$$

$$\underline{U}^H = [U_{3(1)}^G, \dots, U_{3(N^H)}^G] \quad (2.6)$$

Finally,  $U^M$  is the vertical displacement of the main cable at the midspan cross-section. It is worth noting that, in previous equations (2.4) the total initial stress is expressed as the sum of a constant quantity  $(\bar{S}_i)^{S,H,M}$  and an incremental one  $(\Delta S_i)^{S,H,M}$ . The former is a set of trial initial post-tensioning cable forces which are estimated by means of simple design rules commonly adopted in the context of long-span bridges, whereas the last are the additional amounts which are the unknowns of the problem. The problem is resolved iteratively.

### 2.1.3 The Force Equilibrium Method (FEM)

The Force Equilibrium Method searches for a set of cable forces which will give rise to achieve target bending moments at selected locations along the stiffening girder. As the method works only on the equilibrium of forces rather than deformation, there is no need to deal with nonlinearity caused by cable sag and other effects.

With respect to the cable-stayed bridge reported in Fig. 2.3, in which it is only necessary to consider one half of the bridge with appropriate boundary conditions at the middle section to account for symmetry, the target bending moments (dead load condition) are determined by replacing all supports from the cables and tower by rigid simple supports, as shown in Fig. 2.4.

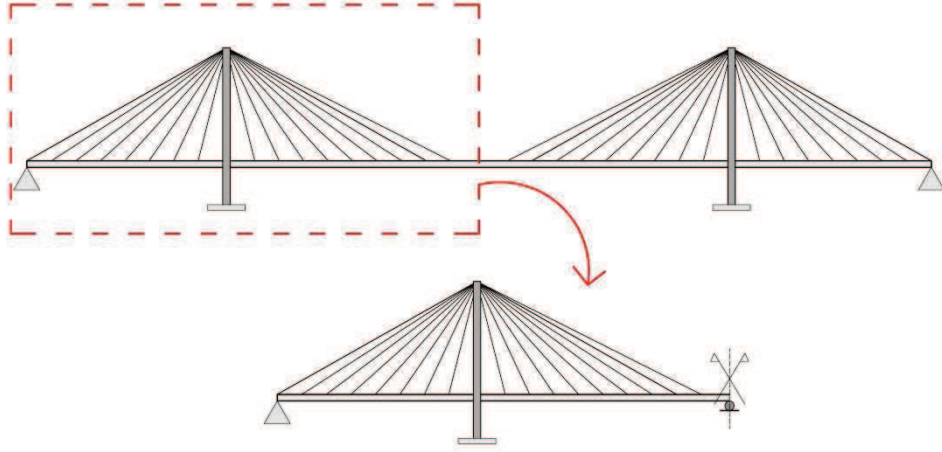


Fig. 2.3 Model of a cable-stayed bridge

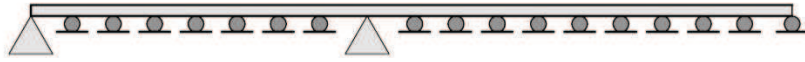


Fig. 2.4 Rigid simple supports model

The conditions to achieve target bending moments at the selected locations (cable anchorages) can be obtained by imposing at the entire structure expressions as follows:

$$\underline{L}_s \left[ \left( \bar{S}_1^S + \Delta S_1^S, \dots, \bar{S}_{N^S}^S + \Delta S_{N^S}^S \right), \underline{M}_i^G - \underline{M}_i^{G^{DL}} \right] = 0 \quad (2.7)$$

In Eq. (2.7),  $\left( \bar{S}_1^S + \Delta S_1^S, \dots, \bar{S}_{N^S}^S + \Delta S_{N^S}^S \right)$  represents the vector containing the initial post-tensioning cable forces expressed as the sum of a trial value and an incremental one, which is the unknown of the problem. Further,  $\underline{M}_i^G$  is the  $i$ -th bending moment of the  $i$ -th control section, refer to the entire structure and  $\underline{M}_i^{G^{DL}}$  is the bending moment obtained by rigid simple support model under the action of dead load. The constrain operator  $\underline{L}_s$  finds the post-tensioning cable forces distribution which ensures that the bending moments ( $\underline{M}_i^G$ ) are equal to the target bending moment ( $\underline{M}_i^{G^{DL}}$ ). In the force equilibrium method it is

difficult to control bending moments at girder-pylon junctions and pylon sections. In addition, incorrect selections of the target moments can lead to singularities in the system of equations. The method can easily account for the effect of prestressing and the vertical profile of the bridge deck.

#### 2.1.4 The Optimization method (OM)

In general, an optimization problem is composed by three fundamental parts: the *control variables*, the *objective function* and the *constraint equations*.

The optimization problem finds the value of the control variables that minimizes (or maximizes) the objective function, subject to a number of constraints. The constraints collectively define a set, the feasible set, of permissible values for the control variables. The typical formulation of an optimization problem can be written as:

$$\begin{cases} \min Q(x) \\ x \in C \end{cases} \quad (2.8)$$

where  $x$  denotes the control variable,  $Q(x)$  the scalar-valued objective function and  $C$  the feasible set. Such a feasible set can be expressed as a set of inequality constraints under the hypothesis of sufficient continuity:

$$C = \{x : lb \leq F(x) \leq ub\} \quad (2.9)$$

where  $F(x)$  is a vector-valued function or a scalar-valued function depending on the possibility to have multiple or single constraints. In the first case, the inequality defining  $C$  is to be interpreted component-wise and lb and ub are the corresponding vectors containing, respectively, the upper and lower bounds. As far as cable supported bridges, the design of cable system is based on the optimization of certain objective functions which may either be related to structural performances or economic efficiency, such as the total strain energy or the construction cost. In the optimization method of determining the stresses

of the stay cables under permanent loads, the objective function are chosen so the material used in girders and pylons is minimized. When the internal forces, mainly the bending moments, are evenly distributed and small, the quantity of material reaches a minimum value. Also the stresses in the structure and the deflections of the deck are limited to prescribed tolerances. With reference to a cable-stayed bridge, since the shear deformations in the girder and pylons are neglected, the strain energy can be represented by

$$U = \frac{1}{2} \int_0^L \frac{M^2}{2EI} dx + \frac{1}{2} \int_0^L \frac{N^2}{2EA} dx \quad (2.10)$$

where  $EI$  is the bending stiffness of girder and pylons and  $EA$  is the axial stiffness. It can be given in a discrete form when the structure is simulated by a finite element model as

$$U = \sum_{k=1}^n \frac{L_k}{4E_k} \left( \frac{M_i^2 + M_j^2}{I_k} + \frac{N_i^2 + N_j^2}{A_k} \right) \quad (2.11)$$

where  $n$  is the total number of the girder and pylon elements,  $L_k$  is the length of the  $k$ -th element,  $E_k$  is the modulus of elasticity,  $I_k$  and  $A_k$  are the moment of inertia and the sections area, respectively.  $M_i, M_j, N_i, N_j$  are the ends moments and the ends normal forces of the  $i$ -th element. Under the application of dead loads and cable forces the bending moments and normal forces of the deck and pylon are given by

$$\{M\} = \{M_D\} + \{M_P\} = \{M_D\} + [S_M] \cdot \{P_0\} \quad (2.12)$$

$$\{N\} = \{N_D\} + \{N_P\} = \{N_D\} + [S_N] \cdot \{P_0\} \quad (2.13)$$

where  $\{M_D\}$  and  $\{M_P\}$  are the bending moment vectors induced by dead loads and the cable forces, respectively;  $[S_M]$  is the moment influence matrix;  $[S_N]$  is the normal force influence matrix, the component  $S_{ij}$  of influence matrix represents changes of the moment or the normal force in the  $i$ -

th element induced by the  $j$ -th unit cable force.  $\{N_D\}, \{N_P\}$  are the normal force vectors induced by dead loads and cable forces, respectively.  $\{P_0\}$  is the vector of cable forces. The corresponding displacements in deck and pylon are given as:

$$\{F\} = \{F_D\} + \{F_P\} = \{F_D\} + [S_F] \cdot \{P_0\} \quad (2.14)$$

where  $\{F\}$  is the displacement vector,  $[S_F]$  is the displacement influence matrix,  $\{F_D\}$  and  $\{F_P\}$  are the displacement vectors induced by dead loads and by cable forces respectively. Substitute Eq.s (2.12) and (2.13) into Eq. (2.11), the shear deformations is expressed as a function of the cable forces.

In the optimization problem the minimization of the strain energy of the structure will be expressed as follows:

$$\frac{\partial U}{\partial P_0} = 0 \quad (2.15)$$

Under the following constraint conditions:

- a) The stress range in girders and pylons must satisfy

$$\{\sigma\}_L \leq \{\sigma\} \leq \{\sigma\}_U \quad (2.16)$$

in which  $\{\sigma\}$  is the maximum stress value vector. And  $\{\sigma\}_L, \{\sigma\}_U$  are vectors of the lower and upper bounds.

- b) The stresses in stay cables are limited so that the stays can work normally

$$\{\sigma\}_{LC} \leq \left\{ \frac{P_{0c}}{A_c} \right\} \leq \{\sigma\}_{UC} \quad (2.17)$$

in which  $A_c$  is the area of a stay,  $P_{0c}$  is the cable force and  $\{\sigma\}_{LC}, \{\sigma\}_{UC}$  represent the lower and upper bounds, respectively.

c) The displacements in the deck and pylon satisfy

$$\{|D_i|\} \leq \{\Delta\} \quad (2.18)$$

in which the left hand side of Eq. (2.18) is the absolute value of maximum displacement vector and the right-hand side is the allowable displacement vector.

It is worth nothing that, it is necessary to impose the constraints for optimization very carefully, or else the resulting schemes may sometimes become impractical.

## 2.2 The proposed design methodology

An efficient methodology to design the cable system of cable supported bridges should be based on the following features:

- *Easy to implement;*
- *Wide applicability;*
- *Provide consistent results from a structural point of view;*
- *No require excessive computational efforts.*

The proposed design method evaluate post-tensioning forces and optimum cross-section areas of the cable system to satisfy structural and design requirements in either dead and live configurations. In particular, under the action of dead loads (DL), the post-tensioning cable forces are calculated in such a way that the bridge structure should behave as a simply supported continuous beam, thus presenting reduced displacements of the girder and pylons. Moreover, from the design point of view, the cross-sections of the cable system elements should be designed consistently to the "*maximum performance criterion*", which, basically, consists to verify, under the worst live load (LL) combinations, the equality condition between the maximum absolute or



incremental applied stresses and the corresponding allowable strength values. Such task is developed by means of an iterative procedure defined by a two-step algorithm, based on the results arising from both dead load and live load configurations. In the first step, the structure is analyzed under the action of dead loading and the design variable of the cable system are defined (**STEP 1 – Optimization Phase**). In the second step, starting from the structure designed in the previous step, the structure is analyzed under the action of live loading and displacement and stresses variables are calculated and checks are carried out (**STEP 2 – Correction Phase**). In the following, the proposed design method is presented for the cable supported bridge typology described in chapter 1.

### 2.2.1 Hybrid cable-stayed suspension bridge scheme

With reference to the hybrid cable-stayed suspension bridge scheme reported in Fig. 2.5, the design variables, are represented by the cross-sections  $(A_i^S, A_i^H, A^M)$  and the post-tensioning forces of the cable system  $(S_i^S, S_i^H, S^M)$  and are designed by means of the following relationships:

$$\begin{aligned} \underline{S}_C &= \{S_1^S, \dots, S_{N^S}^S, S_1^H, \dots, S_{N^H}^H, S^M\} \\ \underline{A} &= \{A_1^S, \dots, A_{N^S}^S, A_1^H, \dots, A_{N^H}^H, A^M\} \end{aligned} \quad (2.19)$$

where  $N^S$  is the number of stays,  $N^H$  is the number of hangers and the superscripts  $S$ ,  $H$  and  $M$  refer to the stays, hangers and main cable, respectively. Such design variables are derived in the dead load configuration by solving an optimization modeling of the bridge aimed to reduce the steel quantity involved in the cable system. The design variables relative to stays and main cable are assumed to be expressed in terms of the optimization factors  $(\xi_i, \psi_i) \in \Xi^S$  and  $(\xi^M, \psi^M) \in \Xi^M$  for a better convergence of the problem

$$\begin{aligned} A_i^S &= \xi_i \bar{A}_i^S, \quad S_i^S = \psi_i \bar{S}_i^S \\ A^M &= \xi^M \bar{A}^M, \quad S^M = \psi^M \bar{S}^M \end{aligned} \quad (2.20)$$

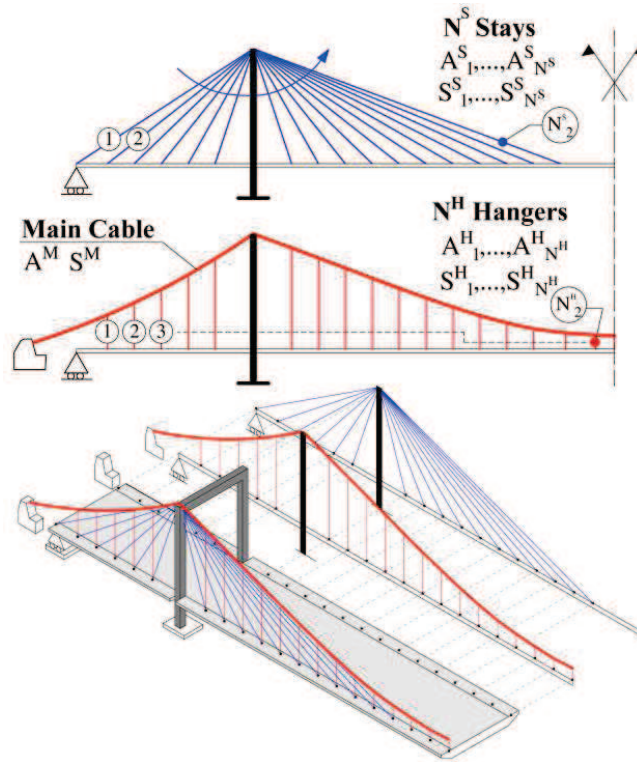


**Fig.2.5** Design and control variables to be determined in hybrid cable-stayed suspension bridge scheme

where  $i = 1..N^S$ ,  $\Xi^S$  and  $\Xi^M$  are the domain spaces of the optimization variables associated to the cable-stayed system ( $S$ ) and the main cable ( $M$ ) and the quantities reported with the superscript  $(\bar{\bullet})$  refer here and in the following to the values arising from previous iteration step or, in the case of the first step, assumed by trial variables obtained by preliminary dimensioning rules reported in chapter 1. As a consequence, the factors  $(\xi_i, \psi_i)$  and  $(\xi^M, \psi^M)$  should be considered as a variable to be changed during the optimization procedure. Moreover, the cross-sections of the suspension system elements, i.e.  $A_i^H$ , are changed from their previous estimated values, i.e.  $\bar{A}_i^H$ , introducing additive incremental variables, i.e.  $\Delta A_i^H$ , as a function of explicit constraint equations, which enforce the stresses in the hangers to be equal to the design quantity  $S_{gi}^H$ :

$$L_{S_i} \left[ (\bar{A}_i^H + \Delta A_i^H), S_i^H(\xi, \psi) - S_{gi}^H \right] = 0, \quad \text{with } i = 1..N^H, \Delta A_i^H \in \Xi^H \quad (2.21)$$

where  $L_{S_i}$ , with  $L_{S_i} : \Xi^H \rightarrow \Xi$ , is the constrain operator, which ensures that the stress variables are equal to the design value, i.e.  $S_{gi}^H$  (discussed subsequently),  $\Xi^H$  and  $\Xi$  are the domain of the hanger cross-sections or the global bridge solution, respectively, and  $(\xi, \psi)$  are the vectors collecting the optimization factors of the stays and main cable, i.e.  $(\xi_i, \psi_i)$  and  $(\xi^M, \psi^M)$ , respectively. The displacement conditions to achieve the “zero configuration” are expressed by the operator  $L_U$ , with  $L_U : \Xi^S \times \Xi^H \times \Xi^M \rightarrow \Xi$ , which reproduces the undeformed configuration on the basis of a proper set of post-tensioning stresses in the suspension system  $S_i^H$ , with  $i = 1..N^H$ , in the main cable  $S^M$  and the anchor stays as follows:

$$L_U \left[ (\bar{S}_j^H + \Delta S_j^H, \bar{S}_1^S + \Delta S_1^S, \bar{S}_{N^S}^S + \Delta S_{N^S}^S, \bar{S}^M + \Delta S^M), U(\xi, \psi, \xi^M, \psi^M) \right] = 0 \quad (2.22)$$

where  $j = 1..N^H$ ,  $U$  with  $U^T = [U_{3(1..N^H)}^G, U_1^{P_L}, U_1^{P_R}, U_1^{M-P_L}, U_1^{M-P_R}]$  is the vector containing the vertical displacements at the hangers/girder connections ( $N^H$ ) and the horizontal displacements at the top pylon left ( $L$ ) and right ( $R$ ) cross-sections ( $U_1^{P_L}, U_1^{P_R}$ ) and at the intersection points of the left and right top pylon cross-sections with the main cable ( $U_1^{M-P_L}, U_1^{M-P_R}$ ). The objective function, which is minimized during the optimization procedure, is represented by the scalar valued function  $Q$ , which describes the total steel quantity involved in the cable system:

$$\underset{(\xi, \psi)}{\text{Min}} Q(\xi, \psi) = \underset{(\xi, \psi)}{\text{Min}} \left( \sum_{i=1}^{N^S} L_i^S A_i^S + \sum_{i=1}^{N^H} L_i^H A_i^H + A^M L^M \right) \gamma \quad (2.23)$$

where  $\gamma$  is the specific weight of the cables and  $(L_i^S, L_i^H, L^M)$  are the lengths of the  $i$ -th stay, hanger or main cable, respectively. Additional conditions on the stress distribution in the cable system are imposed by explicit

constraint equations, ensuring that the stresses in the stays and main cable under dead loading are fixed to a design quantity, i.e.  $(S_{gi}^S, S_g^M)$

$$L_{S_2} \left[ S_i^S(\xi, \psi) - S_{gi}^S \right] = 0, \quad \text{with } i = 1, N_S \quad (2.24)$$

$$L_{S_3} \left[ \max(S^M(\xi, \psi)) - S_g^M \right] = 0 \quad (2.25)$$

It is worth noting that the optimization procedure, defined by Eq.s (2.21)-(2.25), is concerned to determine the optimum bridge configuration, which involves the lowest steel quantity in the cable system and verifies constrain equations on design displacement and stress variables of the bridges. However, the initial post-tensioning stresses in the cable systems, namely  $(S_{gi}^H, S_{gj}^S, S_g^M)$  with  $i=1..N^S, j=1..N^H$ , should be considered as known variables when the optimization problem is solved. To this aim, in order to calculate such quantities an iterative procedure, namely two-step algorithm, is required, going between the optimization and the correction steps, iteratively. In the former the optimization problem is considered by solving Eq.s (2.21)-(2.25), whereas in the latter the initial post-tensioning stresses are quantified on the basis of the live load results. In particular, in the framework of live load combinations, based on ultimate, fatigue and serviceability, i.e. ULS, FLS and SLS, the following conditions, concerning maximum and relative stresses and maximum absolute displacements should be verified:

$$\begin{aligned} \max \left[ S_i^H(\xi, \psi) \right]_{ULS} &\leq S_A, \quad \max \left[ \Delta S_i^H(\xi, \psi) \right]_{FLS} \leq \Delta S_A \quad \text{with } i = 1, N^H \\ \max \left[ S_i^S(\xi, \psi) \right]_{ULS} &\leq S_A, \quad \max \left[ \Delta S_i^S(\xi, \psi) \right]_{FLS} \leq \Delta S_A \quad \text{with } i = 1, N^S \end{aligned} \quad (2.26)$$

$$\begin{aligned} \max \left[ S^M(\xi, \psi) \right]_{ULS} &\leq S_A, \quad \max \left[ \Delta S^M(\xi, \psi) \right]_{FLS} \leq \Delta S_A \\ \max \left[ \left[ U_3^G \right] \right]_{SLS} &\leq \delta_{3A}^G, \quad \max \left[ \left[ U_1^P \right] \right]_{SLS} \leq \delta_{1A}^P \end{aligned} \quad (2.27)$$

where  $S_A$  and  $\Delta S_A$  are the maximum or incremental allowable values in the cables,  $\delta_{3A}^G$  is the maximum vertical displacement of the girder and  $\delta_{1A}^P$  is

the maximum displacement of the pylon. It is worth noting that the maximum value of the internal stresses can be associated to the effects of live loads or produced by seismic or aeroelastic loading schemes. Similarly, proposed formulation can be generalized in such a way to be consistent with respect to enhanced reliability formulations such as the one reported for instance in (Barbero, Sosa, Martínez, & Gutiérrez, 2013). The initial stresses for the cable elements  $(\tilde{S}_g^S, \tilde{S}_g^H, \tilde{S}_g^M)$  are evaluated as a function of two sets of factors associated to stays, hangers and main cable, namely  $\Phi_i$  and  $\Omega_i$ , which are introduced to verify code prescriptions defined by Eq.s (2.26) and (2.27), ensuring that the predicted values should be equal in the worst loading combination to the corresponding permissible values, leading to the optimum utilization of the bridge components and thus the lowest steel quantity involved in the cable system. Such quantities must be considered as variables, which are solved for during the iteration procedure by using as secant approach as a function of the values arising from the previous iteration steps. The main purpose of the optimization factors is to modify the stiffness or the stress distribution of the cable elements, in such a way to verify prescriptions on bridge deformability, reducing the material volume involved in the cable system. In particular, the performance factors  $\Phi_i$  optimize the stress distribution in the cable system, in such a way that the maximum value should be close to the strength of the material, reaching the optimum solution in terms of material utilization and volume involved in the cable system. On the contrary, variables  $\Omega_i$  define the allowable level of strength and stiffness for each cable element, enforcing the pylons and girder to have lower displacements than the maximum permissible values. In the proposed modeling, the stiffness of the stays in the lateral or in the central spans are designed to reduce horizontal and vertical displacements of the girder and pylon, respectively, whereas that of hangers is designed to reduce vertical displacements of the girder. Moreover, the stiffness of the main cable is utilized to reduce maximum vertical displacements of the girder. Such choices can be considered reasonable, from the physical point of view, especially in the cases of long span bridges, in which girder deformability is mostly influenced by the stiffness of the cable system in relationship to the prevailing truss behavior of

the bridge structures. Therefore, in order to satisfy prescriptions on allowable displacements and stresses, the evaluation of the performance factors  $\Omega_i$  and  $\Phi_i$  is defined by the following assumptions:

- the performance factors for the cable-stayed system elements, lateral and central stays, i.e.  $\Omega_i^S$ , are defined to reduce the horizontal displacements of the pylons and vertical deflections of the girder, whereas for the hanger members the variables  $\Omega_i^H$  are associated to reduce the vertical displacements of the girder (see Fig. 2.6);
- the factor  $\Omega^M$  concerning the main cable dimensioning is modified to verify prescriptions on girder displacements with respect to the maximum absolute value observed in the girder deflections;
- for all cable elements  $(\Phi_i^S, \Phi_i^H, \Phi^M)$  factors are defined enforcing that the maximum stresses should be equal to the allowable quantity;
- the definition of the performance factors is based on a linear approximation of the displacement and stresses, based on the secant description, whose path can be thought defined by the line connecting two states, represented by the final, i.e. the maximum allowable status, and the current solution arising from the last converged configuration, i.e. at  $k - 1$ .

Therefore, on the basis of the previous remarks, introducing the following limit functions concerning the horizontal and vertical displacements of the pylon and girder and allowable stresses

$$\begin{aligned}
 g_{U_{1i}^k}^P &= \frac{\delta_{1A}^P}{\max(U_{1LL}^P)_i^k} - 1 \\
 g_{U_{3i}^k}^G &= \frac{\delta_{3A}^G}{\max(U_{3LL}^G)_i^k} - 1 \quad j = S, H, M \\
 g_{S_{Ai}^k} &= \frac{(S_A^J)_i^{k-1}}{S_A} - 1
 \end{aligned} \tag{2.28}$$

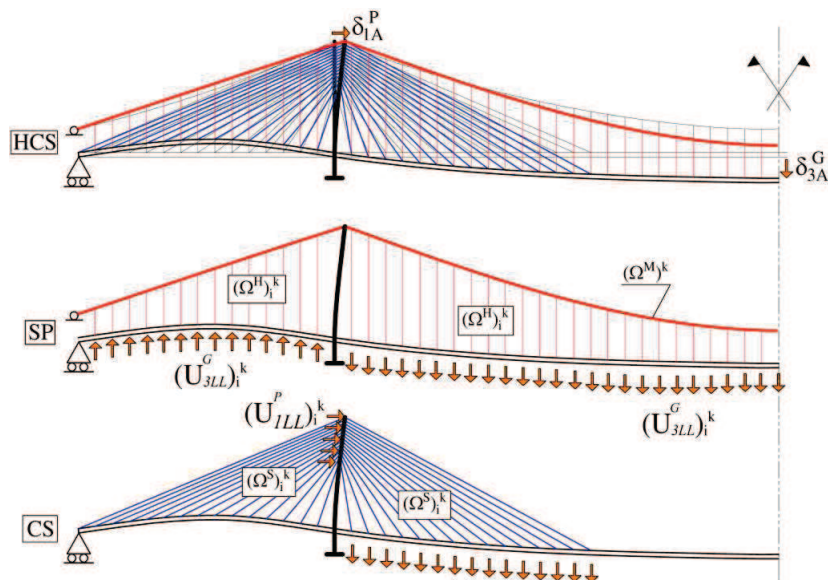


Fig.2.6 Identification of the performance factors and design variables on the bridge scheme

the relationships, which quantify the performance factors  $\Omega_i$  for the cable-stayed system, are defined by the following expressions:

$$(\Omega)_i^k = \begin{cases} \frac{|\Delta_{\max}|}{\max_{LL} [ (|\Delta|)_i^k ]} \frac{(S_A)_i^{k-1}}{S_A} & \text{if } g_{\Delta_i}^k \leq 0 \\ \frac{|\Delta_{\max}|}{\max_{LL} [ (|\Delta|)_{i-1}^k, (|\Delta|)_{i+1}^k ]} \frac{(S_A)_i^{k-1}}{S_A} & \text{if } g_{S_{A_i}}^k < 0 \text{ and } g_{\Delta_i}^k > 0 \\ 1 & \text{if } g_{S_{A_i}}^k \geq 0 \text{ and } g_{\Delta_i}^k > 0 \end{cases} \quad (2.29)$$

with:

$$\begin{aligned} \Delta = U_1^P, \quad \Delta_{\max} = \delta_{1A}^P, \quad g_{\Delta} = g_{U_{1i}}^P & \quad (\text{Stays - lateral span}) \\ \Delta = U_3^G, \quad \Delta_{\max} = \delta_{3A}^G, \quad g_{\Delta} = g_{U_{3i}}^G & \quad (\text{Stays - main span}) \\ \Delta = U_3^G, \quad \Delta_{\max} = \delta_{3A}^G, \quad g_{\Delta} = g_{U_{3i}}^G & \quad (\text{Hangers}) \\ \Delta = \max(U_3^G), \quad \Delta_{\max} = \delta_{3A}^G, \quad g_{\Delta} = \max(g_{U_{3i}}^G) & \quad (\text{Main cable}) \end{aligned} \quad (2.30)$$

where  $k$  represents the number of iterations during the solving procedure. It is worth noting that in Eqs. (2.29) and (2.30), the expressions utilized in the case of negative values of the displacement functions, i.e.  $g_{U_{3i}}^k \leq 0$  or  $g_{U_{1i}}^k \leq 0$ , indicate the need to increase the stiffness of the cable system, since the displacements do not verify girder and pylon displacement prescriptions. Contrarily, when the displacement functions are strictly positive the cable stiffness is released enforcing the equality with maximum permissible value, which is achieved only for positive values of the allowable stress function, i.e.  $g_{S_{Ai}}^k \geq 0$ . The factors concerning the stresses, namely  $\Phi_i$ , can be derived by the ratios between the allowable stress and the maximum value observed in the live load combinations:

$$\left(\Phi^S\right)_i^k = \frac{\left(S_A\right)}{\max_{LL}\left(S_{LL}^S\right)_i^k}, \quad \left(\Phi^H\right)_i^k = \frac{\left(S_A\right)}{\max_{LL}\left(S_{LL}^H\right)_i^k}, \quad \left(\Phi^M\right)_i^k = \frac{\left(S_A\right)}{\max_{LL}\left(S_{LL}^M\right)_i^k} \quad (2.31)$$

A synoptic representation of the variables reported in Eq.s (2.29)–(2.31) are reported in Fig. 3. Starting from Eq.s (2.29)–(2.31), the estimate the design initial stresses on the basis of the following relationships:

$$\begin{aligned} \left(S_{gi}^S\right)^k &= \left[\Phi^S \Omega^S\right]_i^k \left(S_g^S\right)_i^{k-1}, \\ \left(S_{gi}^H\right)^k &= \left[\Phi^H \Omega^H\right]_i^k \left(S_g^H\right)_i^{k-1}, \\ \left(S_g^M\right)^k &= \left[\Phi^M \Omega^M\right]_i^k \left(S_g^M\right)_i^{k-1} \end{aligned} \quad (2.32)$$

It is worth noting that Eq. (2.32) predict, by means of the factors  $\Phi_i^{S,H,C}$ , the initial stresses on the basis of a linear approximation of the stress and displacement increments between dead and live load configurations, enforcing the maximum stresses, reached in all cable-system elements or the displacements on the girder and pylon cross-sections, to be equal approximately to the corresponding allowable values. Moreover, the piecewise functions defined by Eq.s (2.29) and (2.30) modify the allowable stress levels, increasing



the stiffness of the cable system and verifying prescriptions on maximum displacements on both girder and pylons. Finally, once the new values of the stress levels in the dead load configuration are evaluated by means of Eq.s (2.32), the procedure goes back to find the new cross-sections of the cables and the post-tensioning forces on the basis of the optimization method by means of Eq.s (2.29)–(2.30). This procedure is repeated until achieving the convergence conditions of the algorithm defined on the basis of the following expression:

$$\max \left\{ \begin{array}{l} \sum_{i=1}^{N_S} \left[ \frac{(S_{gi}^S)^k - (S_{gi}^S)^{k-1}}{(S_{gi}^S)^{k-1}} \right], \\ \sum_{i=1}^{N_H} \left[ \frac{(S_{gi}^H)^k - (S_{gi}^H)^{k-1}}{(S_{gi}^H)^{k-1}} \right], \\ \frac{(S_g^M)^k - (S_g^M)^{k-1}}{(S_g^M)^{k-1}} \end{array} \right\} \leq toll. \quad (2.33)$$

A synoptic representation of the optimization procedure is reported in Fig. 2.7. It is worth noting that the previous procedure can be easily specialized for the cases of pure cable-stayed and suspension bridge schemes. It is worth nothing that, the design method, is quite general to be applied to several schemes based on small, medium or long spans and can be, easily, specialized for pure cable-stayed, suspension and self-anchored cable-stayed suspension schemes since they can be easily derived as particular cases. Moreover, the description of the model is presented with reference to the final configuration, but can be easily specialized also for the different steps involved in the bridge construction. As a matter of fact, in the loading scheme concerning the erection procedure, only the service prescriptions should be verified, which are less restrictive than the ones required by the ULS combinations. Moreover, in such analyses, the variables concerning the cable dimensioning can be considered as known quantities, which are identified on the basis of the design prescriptions defined on the final bridge configuration and with respect to ultimate loading conditions.

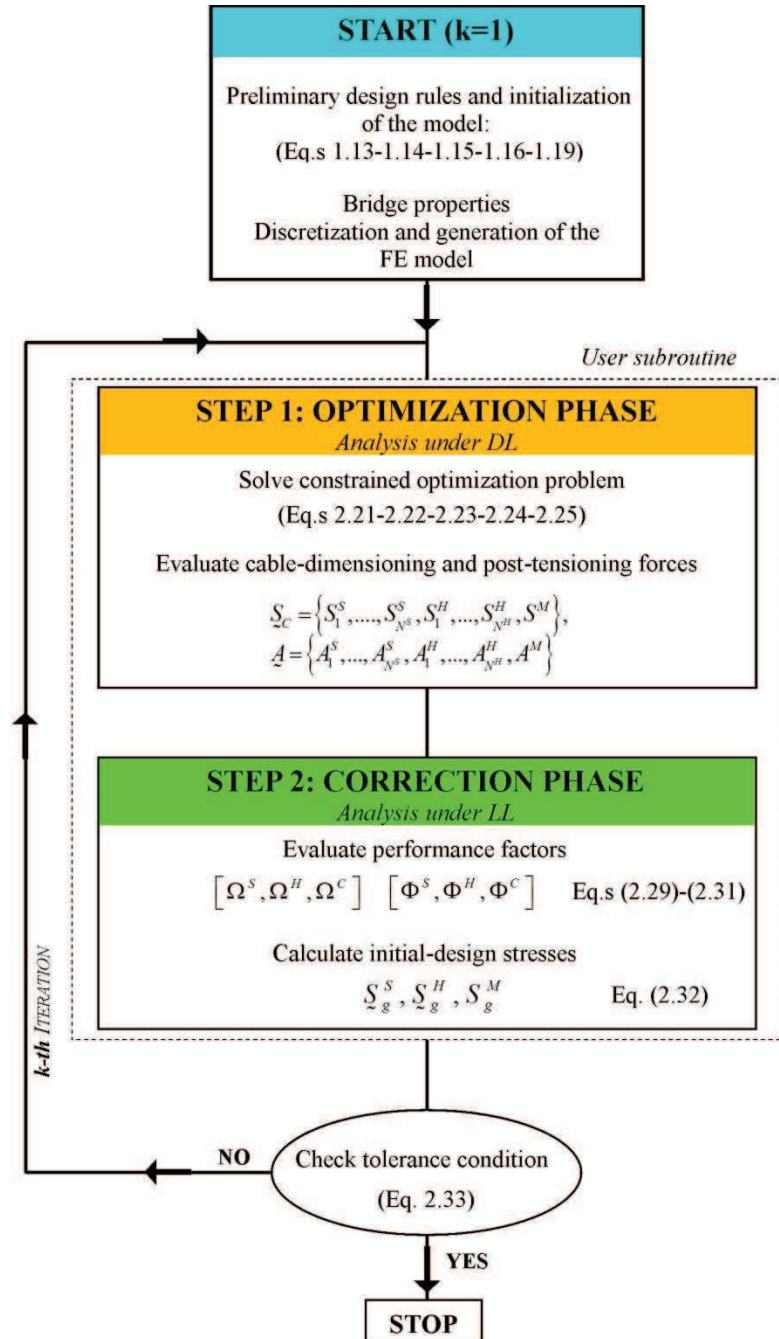
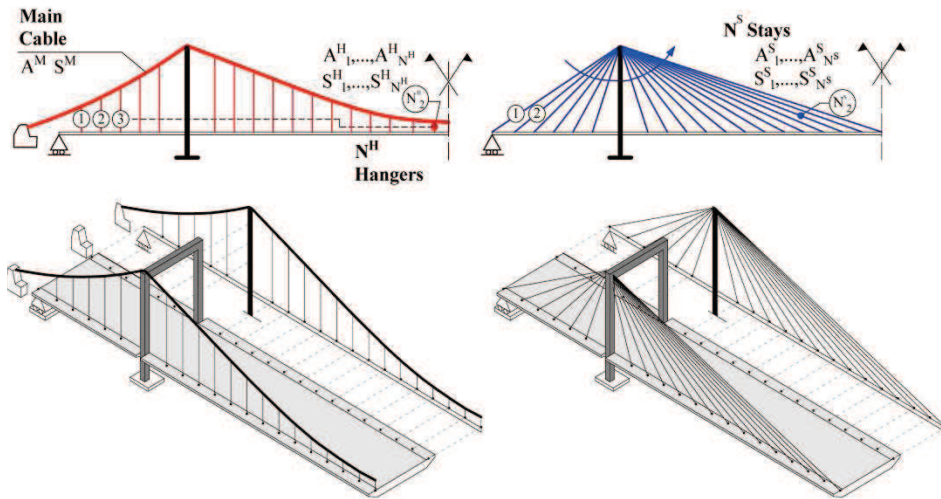


Fig.2.7 Flowchart of the optimization procedure

### 2.2.2 Cable-stayed and suspension schemes – Pure systems



**Fig.2.4** Design and control variables to be determined in cable-stayed and suspension schemes

The optimization model presented for hybrid cable-stayed suspension bridges is specialized here for the cases concerning pure cable-stayed and suspension schemes. In such cases, since the number of variables is equal to the number of equations, the optimization problem is transformed in terms of a determinate system equation formed by explicit relationships defined in terms of initial post-tensioning stresses, cross-sections of the cable system elements and design stresses under dead load. In particular for the cable-stayed bridge scheme the control variables are expressed by the post-tensioning stress and cable cross-section vectors, as follows:

$$\begin{aligned} \mathcal{S}_C &= \{S_1^S, \dots, S_{N_s}^S\} \\ \mathcal{A} &= \{A_1^S, \dots, A_{N_s}^S\} \end{aligned} \quad (2.34)$$

The unknown quantities are derived in the dead load configuration by solving the set of constraint equations concerned to enforce displacements of

girder and pylons to be zero and the internal stresses to be equal to the initial design values, namely  $S_{gi}^S$ :

$$L_v \left[ \left( \bar{S}_i^S + \Delta S_i^S, \bar{S}_1^S + \Delta S_1^S, \bar{S}_{N_s}^S + \Delta S_{N_s}^S \right), \underline{U} \right] = 0 \quad (2.35)$$

$$L_{S_3} \left[ \left( \bar{A}_i^S + \Delta A_i^S \right), S_i^S \left( \underline{\xi}, \underline{\psi} \right) - S_{gi}^S \right] = 0 \quad (2.36)$$

with  $i=1..N_s$ ,  $\underline{U}^T = \left[ U_{3(2..N_s-1)}^G, U_1^{P_L}, U_1^{P_R} \right]$  is the vector containing vertical displacements of the stays except for the anchor ones ( $U_{3,i}^G$ ) and the horizontal displacements at the top pylon right and left cross-sections ( $U_1^{P_L}, U_1^{P_R}$ ). Finally, at the  $k$ -th iteration, optimization factors  $(\Omega^S)_i^k$  and  $(\Phi^S)_i^k$  are calculated in the live load combinations by using Eq.s (2.29) and (2.31). Similarly, the control variables for the suspension bridge are defined by the following vectors:

$$\begin{aligned} \underline{S}_C &= \{ S_1^H, \dots, S_{N^H}^H, S^M \} \\ \underline{A} &= \{ A_1^H, \dots, A_{N^H}^H, A^M \} \end{aligned} \quad (2.37)$$

whereas the constrain equations to impose zero vertical and horizontal displacements on the girder and pylons and, horizontal and internal stresses equal to the initial design value,  $S_{gi}^H$ :

$$L_{S_1} \left[ \left( \bar{A}_i^H + \Delta A_i^H \right), S_i^H \left( \underline{\xi}, \underline{\psi} \right) - S_{gi}^H \right] = 0 \quad (2.38)$$

$$L_U \left[ \left( \bar{S}_j^H + \Delta S_j^H, \bar{S}^M + \Delta S^M \right), \underline{U} \right] = 0 \quad (2.39)$$

with  $i=1..N^H$ , and  $\underline{U}^T = \left[ U_{3(1..N^H)}^G, U_1^{M-P_{L,R}} \right]$ .

Finally, at the  $k$ -th iteration, optimization factors  $(\Omega^S)_i^k$  and  $(\Phi^S)_i^k$  are calculated in the live load combinations by using Eq.s (2.29) and (2.31).

### 2.2.3 Self-anchored cable-stayed suspension bridge scheme

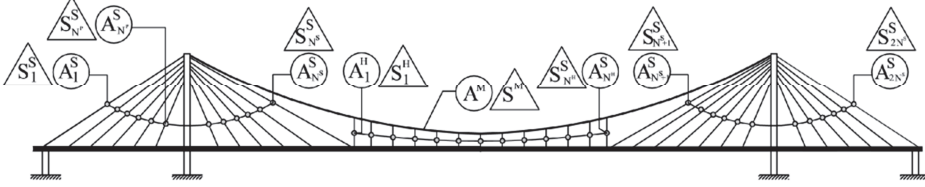


Fig. 2.9 Identification of the variables involved in the design procedure

With reference to the bridge scheme reported in Fig. 2.9, the design variables are represented by the cross-sections  $(A_i^S, A_i^H, A^M)$  and the post-tensioning forces of the cable system  $(S_i^S, S_i^H, S^M)$ , which are designed by means of the following relationships:

$$\begin{aligned} \underline{S}_C &= \{S_1^S, \dots, S_{2N^S}^S, S_1^H, \dots, S_{N^H}^H, S^M\} \\ \underline{A} &= \{A_1^S, \dots, A_{2N^S}^S, A_1^H, \dots, A_{N^H}^H, A^M\} \end{aligned} \quad (2.40)$$

where  $N^S$  is the number of stays of the left or right pylons,  $N^H$  is the number of hangers and the superscripts  $S$ ,  $H$  and  $M$  refer to the stays, hangers and main cable, respectively. The constraint equations are formulated to enforce zero the following displacement conditions :

- horizontal displacements of the pylons and vertical displacements of the stays in the main cable at the girder connections, i.e.  $\underline{U}^{S(T)} = [U_1^S, U_2^S, \dots, U_{N_1^S}^S, V_{N_1^S+1}^S, \dots, V_{N^S}^S]$ ;
- vertical displacements of the hangers at the girder connections, i.e.  $\underline{U}^{H(T)} = [V_1^H, V_2^H, \dots, V_{N^H}^H]$ ;
- vertical displacement of the main cable at the midspan cross section, i.e.  $U^M$ .

Therefore, the required equations to verify the kinematic prescriptions are defined as:

$$\begin{aligned} \underline{L}_S \left[ (\bar{S}_1^S + \Delta S_1^S, \dots, \bar{S}_{2N_S}^S + \Delta S_{2N_S}^S), \underline{U}^S \right] &= 0, \\ \underline{L}_H \left[ (\bar{S}_1^H + \Delta S_1^H, \dots, \bar{S}_{N^H}^H + \Delta S_{N^H}^H), \underline{U}^H \right] &= 0, \\ \underline{L}_M \left[ (\bar{S}^M + \Delta S^M), U^M \right] &= 0, \end{aligned} \quad (2.41)$$

where  $\underline{L}_S$ ,  $\underline{L}_H$  and  $\underline{L}_M$  are multi freedom constraint operators referred to the stays, hangers and main cable variables, respectively. Similarly, additional constraint equations, which enforce the stresses in the cables to be equal to the initial design quantity are introduced:

$$\begin{aligned} \underline{C}_S \left[ (\bar{A}_i^S + \Delta A_i^S), S_i^S - S_{gi}^S \right] &= 0, \quad i = 1, \dots, 2N^S, \\ \underline{C}_H \left[ (\bar{A}_i^H + \Delta A_i^H), S_i^H - S_{gi}^H \right] &= 0, \quad j = 1, \dots, N^H, \\ C_M \left[ (\bar{A}^M + \Delta A^M), S^M - S_g^M \right] &= 0, \end{aligned} \quad (2.42)$$

where  $\underline{C}_S$ ,  $\underline{C}_H$  and  $C_M$  are the constrain operators, which ensures that the stress variables of the cable elements, i.e.  $(S_i^S, S_j^H$  and  $S^M)$ , are equal to the prescribed values  $(S_{gi}^S, S_{gi}^H$  and  $S_g^M)$ .

#### 2.2.4 Application on intermediate erection stages

In the case of hybrid cable-stayed suspension bridges, during the erection procedure, at the  $k$ -th construction step, the unknown quantities are represented by the post-tensioning forces of the cable system elements:

$$\underline{S}_C = \{ S_1^S, \dots, S_k^S, S_1^H, \dots, S_k^H, S^M \}, \quad (2.43)$$

Moreover, the objective function  $D$  to be minimized during the optimization procedure consists of a scalar valued function defined by the

square root of the vertical and horizontal displacements of girder and pylons, evaluated at the corresponding nodal points:

$$\underset{(\psi)}{\text{Min}} D(\psi) = \underset{(\psi)}{\text{Min}} (\|U\|) \quad (2.44)$$

where,  $\|\bullet\|$  is the Euclidean norm of the  $(\bullet)$  vector,  $U$  with  $U^T = [U_{3(1..k)}^G, U_1^{P_L}, U_1^{P_R}, U_1^{M-P_L}, U_1^{M-P_R}]$  is the vector containing the vertical displacements at the hangers/girder connections at the  $k$ -th step erected element, horizontal displacements at the top pylon left ( $L$ ) and right ( $R$ ) cross-sections ( $U_1^{P_L}, U_1^{P_R}$ ) and at the intersection points of the left and right top pylon cross-sections with the main cable ( $U_1^{M-P_L}, U_1^{M-P_R}$ ).

In addition, to Eq.s (2.43)-(2.44), constrain equations are necessary to guide the optimization procedure through a reasonable solution:

$$\begin{aligned} \max [S_i^H(\psi)]_k &\leq S_A \\ \max [S_i^S(\xi, \psi)]_k &\leq S_A \\ \max [S^M(\xi, \psi)]_k &\leq S_A \end{aligned} \quad (2.45)$$

For the pure suspension and cable-stayed bridge schemes, the solution during the erection procedure is derived by solving a determinate equation system. In particular, the unknown quantities are represented by the post-tensioning forces, which are evaluated reproducing the undeformed configuration on the basis of the following constrain relationships:

$$\begin{aligned} L_U^H [S_k^H, U] &= 0 \\ L_U^S [S_k^S, U] &= 0, \end{aligned} \quad (2.46)$$

where  $(S_k^H, S_k^S)$  are the vectors containing the stresses of the hangers or the stays elements and  $U^{H(T)} = [U_{3(1)}^G, U_{3(2)}^G, \dots, U_{3(k)}^G, U_1^{M-P}]$  contains the

vertical displacements of the girder and the horizontal displacement of the pylon.

## 2.3 Bridge formulation

In this section the governing equations for the bridge constituents are discussed. Such governing equations represent the basis for the theoretical formulation of the model, whose numerical implementation is presented in the next paragraph.

### 2.3.1 Girder and pylons formulation

Girder and towers are described by tridimensional geometric nonlinear beam elements by means of a formulation based on Euler-Bernoulli kinematic assumptions and a Green-Lagrange strain measure. The constitutive relationships are defined on the basis of moderately large rotations in which only the square of the terms  $U_{i,X_1}^{2G}$  representing the rotations of the transverse normal line in the beam are considered. Starting from the status concerning the initial configuration in which only dead loading are considered, the following relationships between generalized strain and stress variables are obtained:

$$\begin{aligned}
 N_1^G &= N_1^{0(G)} + E^G A^G \varepsilon_1^G \\
 &= N_1^{0(G)} + E^G A^G \left\{ U_{1,X_1}^G + \frac{1}{2} \left[ U_{1,X_1}^{2(G)} + U_{2,X_1}^{2(G)} + U_{3,X_1}^{2(G)} \right] \right\} \\
 M_2^G &= M_2^{0(G)} + E^G I_2^G \chi_2^G \\
 &= M_2^{0(G)} + E^G I_2^G \Psi_{2,X_1}^G \\
 &= M_2^{0(G)} - E^G I_2^G U_{3,X_1 X_1}^G \\
 M_3^G &= M_3^{0(G)} + E^G I_3^G \chi_3^G \\
 &= M_3^{0(G)} + E^G I_3^G \Psi_{3,X_1}^G \\
 &= M_3^{0(G)} + E^G I_3^G U_{2,X_1 X_1}^G \\
 M_1^G &= G^G J_t^G \Theta^G = G^G J_t^G \Psi_{1,X_1}^G
 \end{aligned} \tag{2.47}$$



where  $E^G A^G$  and  $\varepsilon_1^G$  are the axial stiffness and strain,  $\chi_2^G$  and  $\chi_3^G$  or  $E^G I_2^G$  and  $E^G I_3^G$  are the curvatures or the bending stiffnesses with respect to the  $X_2$  and  $X_3$  axes, respectively,  $\Theta^G$  and  $G^G J_t^G$  are the torsional curvature and stiffness, respectively,  $N_1^G$  is the axial stress resultant,  $M_2^G$  and  $M_3^G$  are the bending moments with respect to the  $X_2$  and  $X_3$  axes, respectively,  $M_1^G$  and  $G^G J_t^G$  are torsional moment and girder stiffness, respectively, and  $(\cdot)^0$  represents the superscript concerning the variables associated with the "zero configuration". Since the optimum design is defined by Ultimate limit state (ULS) and Service load state (SLS), only the application of live loads is considered. The external loads are expressed by a vector:

$$\underline{p} = [p_{X_1}, p_{X_2}, p_{X_3}] \quad (2.48)$$

In particular, for the component  $p_{X_3}$ , an eccentricity  $e$  with respect to the geometric axis can be considered. On the basis of Eq.s (2.47) and (2.48), taking into account notation reported in Fig. 2.10, the governing equations are derived by means of the local form of static equilibrium equations as:

$$\begin{aligned} \frac{d}{dX_1} \left\{ N_1^G \left( 1 + \frac{dU_1^G}{dX_1} \right) \right\} + p_{X_1} &= 0 \\ -E^G I_2^G \frac{d^4 U_3^G}{dX_1^4} - p_{X_3} &= 0 \\ E^G I_3^G \frac{d^4 U_2^G}{dX_1^4} + p_{X_2} &= 0 \\ G^G J_t^G \frac{d^2 \Psi_1^G}{dX_1^2} - p_{X_3} e &= 0 \end{aligned} \quad (2.49)$$

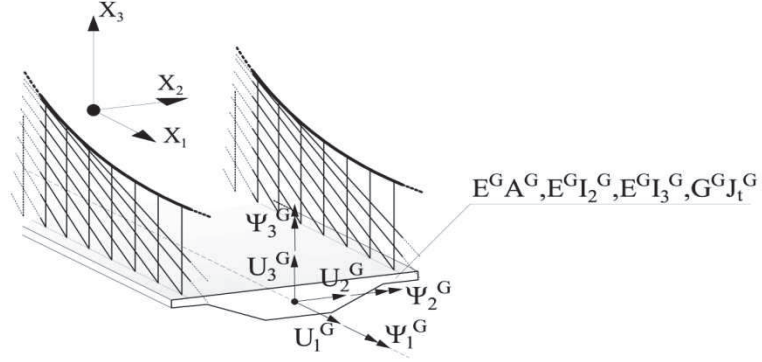


Fig. 2.10 Girder cross-section notations

The pylon governing equations can be easily obtained from Eq.(2.49) by removing all the terms related to the external loads and changing the relative variables from with the superscript  $(\cdot)^G$  to  $(\cdot)^P$  and the parameters concerning the mechanical and material characteristics:

$$\begin{aligned} \frac{d}{dX_1} \left\{ N_1^P \left( 1 + \frac{dU_1^P}{dX_1} \right) \right\} &= 0 \\ -E^P I_2^P \frac{d^4 U_3^P}{dX_1^4} &= 0 \\ E^P I_3^P \frac{d^4 U_2^P}{dX_1^4} &= 0 \\ G^P J_t^P \frac{d^2 \Psi_1^P}{dX_1^2} &= 0 \end{aligned} \quad (2.50)$$

### 2.3.2 Cable formulation

The constitutive laws of the cable are defined by the second Piola-Kirchhoff stress  $(S_1^C)$  and Green-Lagrange strain  $(E_1^C)$  as:

$$S_1^C(\underline{X}) = S_0^C + C^C E_1^C(\underline{X}) \quad (2.51)$$

with

$$E_1^C(\underline{X}) = U_{1,X_1}^C(\underline{X}) + \frac{1}{2} \left[ U_{1,X_1}^2(\underline{X}) + U_{2,X_1}^2(\underline{X}) + U_{3,X_1}^2(\underline{X}) \right] \quad (2.52)$$

where  $C^C$  is the elastic modulus,  $S_0^C$  is the stress referred to the initial configuration. The governing equations of a single cable are expressed by means of the following partial differential equations:

$$\begin{aligned} \frac{d}{dX_1} \left[ N_1^C + N_1^C \frac{dU_1^C}{dX_1} \right] - b_1 &= 0, \\ \frac{d}{dX_1} \left[ N_1^C \frac{dU_2^C}{dX_1} \right] &= 0, \\ \frac{d}{dX_1} \left[ N_1^C \frac{dU_3^C}{dX_1} \right] - b_2 &= 0 \end{aligned} \quad (2.53)$$

where  $N_1^C$  is the axial force defined as  $N_1^C = S_1^C A^C$  with the area of generic  $i$ -th cable element,  $\varphi_1$  and  $\varphi_2$  are the slope angles of the cable along the  $X_1X_2$  and  $X_1X_3$ , respectively,  $b_1$  and  $b_2$  are the body load projections in the  $X_1X_2$  and  $X_1X_3$ , respectively.

## 2.4 Finite element implementation

The governing equations reported in the previous section introduce a nonlinear partial differential system, whose analytical solution is quite complex to be extracted. As a consequence, a numerical approach based on the finite element formulation is utilized. In particular, starting from Eq. (2.49) and Eq. (2.53), the corresponding weak forms for the  $i$ -th finite element related to the girder (G), pylon (P) and the cable system (C), respectively, are defined by the following expressions:

Girder

$$\begin{aligned}
& \int_{l_e^i} N_1^G (1 + U_{1,X_1}^G) w_{1,X_1} dX_1 - \sum_{j=1}^2 N_{1j}^G U_{1j}^G = 0, \\
& \int_{l_e^i} -M_2^G w_{2,X_1 X_1} dX_1 - \sum_{j=1}^2 T_{3j}^G U_{3j}^G - \sum_{j=1}^2 M_{2j}^G \Psi_{3j}^G = 0, \\
& \int_{l_e^i} M_3^G w_{3,X_1 X_1} dX_1 - \sum_{j=1}^2 T_{2j}^G U_{2j}^G - \sum_{j=1}^2 M_{3j}^G \Psi_{2j}^G = 0, \\
& \int_{l_e^i} M_1^G w_{4,X_1} dX_1 - \sum_{j=1}^2 M_{1j}^G \Psi_{1j}^G = 0,
\end{aligned} \tag{2.54}$$

### Pylon

$$\begin{aligned}
& \int_{l_e^i} N_1^P (1 + U_{1,X_1}^P) w_{1,X_1} dX_1 - \sum_{j=1}^2 N_{1j}^P U_{1j}^P = 0 \\
& \int_{l_e^i} -M_2^P w_{2,X_1 X_1} dX_1 - \sum_{j=1}^2 T_{3j}^P U_{3j}^P - \sum_{j=1}^2 M_{2j}^P \Psi_{3j}^P = 0 \\
& \int_{l_e^i} M_3^P w_{3,X_1 X_1} dX_1 - \sum_{j=1}^2 T_{2j}^P U_{2j}^P - \sum_{j=1}^2 M_{3j}^P \Psi_{2j}^P = 0 \\
& \int_{l_e^i} M_1^P w_{4,X_1} dX_1 - \sum_{j=1}^2 M_{1j}^P \Psi_{1j}^P = 0
\end{aligned} \tag{2.55}$$

### Cable System

$$\begin{aligned}
& \int_{l_e^i} N_1^C (1 + U_{1,X_1}^C) w_{1,X_1} dX_1 - \int_{l_e^i} b_1 w_1 dX_1 - \sum_{j=1}^2 N_{1j} U_{1j}^C = 0 \\
& \int_{l_e^i} N_1^C w_{2,X_1} dX_1 - \sum_{j=1}^2 T_{2j}^C U_{2j}^C = 0 \\
& \int_{l_e^i} N_1^C w_{3,X_1} dX_1 - \int_{l_e^i} b_3 w_3 dX_1 - \sum_{j=1}^2 T_{3j}^C U_{3j}^C = 0
\end{aligned} \tag{2.56}$$

where  $(N_{1i}, T_{2i}, T_{3i}, M_{2i}, M_{3i})^k$  with  $k=C, G, P$  and  $i=1, 2$  represents the internal forces applied at the end node  $i$  of the generic cable (C), girder (G) or pylon (P) element. Finite element expressions are written starting from the weak forms previously reported, introducing Hermit cubic interpolation functions  $(\xi_i)$  for the girder and pylon flexures in the  $X_1 X_2$  and  $X_2 X_3$  deformation planes

and Lagrange linear interpolation functions ( $\zeta_i$ ) for the cable system variables and the remaining variables of the girder and the pylons:

$$\begin{aligned} \underline{U}^C(\underline{r}, t) &= \underline{N}^C(\underline{r}) \underline{q}^C(t) \\ \underline{U}^G(\underline{r}, t) &= \underline{N}^G \underline{q}^G(t) \\ \underline{U}^P(\underline{r}, t) &= \underline{N}^P \underline{q}^P(t) \end{aligned} \quad (2.57)$$

where  $\underline{q}^C, \underline{q}^G, \underline{q}^P$  are the vectors collecting the nodal degrees of freedom of the cable, girder and pylon respectively,  $\underline{N}^C, \underline{N}^G, \underline{N}^P$  are the matrixes containing the displacement interpolation function for cable element (C), girder (G) and pylons (P),  $\underline{r}$  is the local coordinate vector of the  $i$ -th finite element. The discrete equations in the local reference system of the  $i$ -th element are derived substituting Eq. (2.57) into Eq.s (2.54)-(2.56), leading to the following equations in matrix notation:

$$\underline{K}^G \underline{U}^G = \underline{P}^G + \underline{Q}^G \quad (2.58)$$

$$\underline{K}^P \underline{U}^P = \underline{P}^P + \underline{Q}^P \quad (2.59)$$

$$\underline{K}^C \underline{U}^C = \underline{P}^C + \underline{Q}^C \quad (2.60)$$

where  $\underline{K}^i$  is the stiffness matrix,  $\underline{P}^i$  is the load vector produced by the dead and live loading,  $\underline{Q}^i$  is the unknown force vector collecting the point source. In order to reproduce the bridge kinematic correctly, additional relationships to define the connections between girder, pylon and cable system are necessary. In particular, the cable system displacements should be equal to those of the girder and the pylons at the corresponding intersection points; thus, the bridge kinematic is restricted by means of the following constrain equations (Fig. 2.11):

$$\begin{aligned} U_3^G(\underline{X}_{C_i}, t) + \Psi_1^G(\underline{X}_{C_i}, t) b &= U_3^C(\underline{X}_{C_i}, t) \\ U_1^G(\underline{X}_{C_i}, t) - \Psi_3^G(\underline{X}_{C_i}, t) b &= U_1^C(\underline{X}_{C_i}, t) \end{aligned} \quad (2.61)$$

$$\begin{aligned}
U_1^P(\underline{X}_P, t) &= U_1^C(\underline{X}_P, t) \\
U_2^P(\underline{X}_P, t) &= U_2^C(\underline{X}_P, t) \\
U_3^P(\underline{X}_P, t) &= U_3^C(\underline{X}_P, t)
\end{aligned} \tag{2.62}$$

where  $\underline{X}_{C_i}$  and  $\underline{X}_P$  represent the vectors containing the intersection positions of the  $i$ -th cable element and the pylon top cross section, respectively, and  $(U_1^G, U_2^G, U_3^G)$  and  $(\Psi_1^G, \Psi_2^G, \Psi_3^G)$  are the displacement and rotation fields of the centroid axis of the girder with respect to the global reference system, respectively. It is worth nothing that, Eq. (2.61) are constraint equation imposed between the off-set nodes of the girder and those associated to the cable elements. Finally, starting from Eq.s (2.58)-(2.60), taking into account of Eq.s (2.61)-(2.62) as well as the balance of secondary variables at the interelement boundaries, the resulting equations of the finite element model are:

$$\underline{K}\underline{Q} = \underline{P} \tag{2.63}$$

where  $\underline{Q}$  with  $\underline{Q} = \underline{U}_C \cup \underline{U}_G \cup \underline{U}_P$  is the generalized coordinate vector containing the kinematic variables associated with the girder, the pylons and the

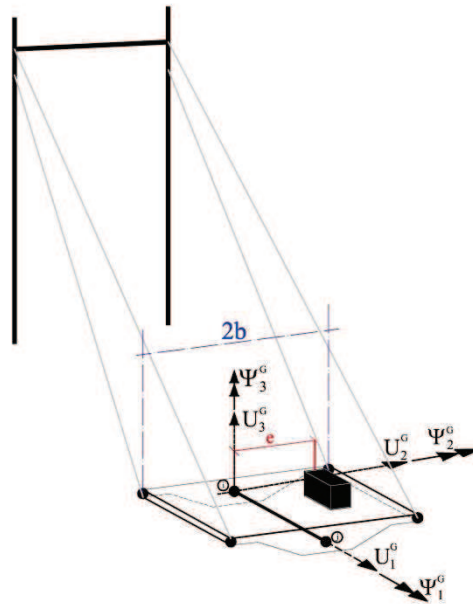


**Fig.2.11** Cable connection

cable system,  $\underline{K}$  is the global stiffness matrix and  $\underline{P}$  is the loading vector. Since the structural behavior of each element depends on the deformation state of the members, the governing equations defined by Eq.(2.63) will change continuously as the structure deforms.

The governing equations are solved numerically, using a user customized finite element program, i.e. COMSOL Multiphysics TM version 4.4 (COMSOL, 2012). Despite existing bridge modeling available from the literature, the importance of the proposed bridge formulation can be summarized by the following points:

- from a practical point of view, the proposed formulation, based on one dimensional beam or truss descriptions, is able to avoid complexities and large computational costs arising when shell and continuum finite elements are adopted, whose improvements in terms of global dynamical parameters (midspan vertical displacement, bending moment and torsional rotation, for instance), can be neglected, especially in the case of long span bridges.

- The cable system is modeled according to the multi element cable system (MECS) approach, where each cable is discretized using multiple truss element. Such modeling is suitable in the case of reduced values of bending stiffness and small sag at equilibrium. The stiffness reduction caused by sagging is accounted for by allowing the cable to deform under applied loads. Large deformations are reproduced by using Green Lagrange formulation and the axial strain is calculated by expressing the global strains in tangential derivatives and projecting the global strains on the cable edge:

$$\varepsilon_n = \underline{t}^T \underline{E} \underline{t} \quad (2.64)$$

In the equation (2.64),  $\underline{E}$  and  $\underline{t}$  are, respectively, the Green-Lagrange strain tensor and the tangent element versor.

## 2.5 Numerical implementation of the design methodology

The numerical algorithm was implemented by using an external subroutine, which combines Comsol Multiphysics and Livelink™ for Excel package (COMSOL, 2012). The former is required to calculate the current solution on the basis of the FE method, whereas, the latter is employed to evaluate the design factor  $\Phi_i$  and  $\Omega_i$ . Therefore, both steps can be easily developed by using several computational frameworks, since it is based on data, which can be easily extracted and handled from quite standard commercial FE software. The numerical algorithm is based on the following different steps, which are executed, iteratively:

- generation of the finite element model (Fig. 2.12), evaluation of the initial post-tensioning forces and the cable cross-sections in the cable system by means of the optimizations procedure;
- calculation of the maximum stresses and displacements under live loads and prediction of the new set of the initial stress quantities on the basis of the performance factors.



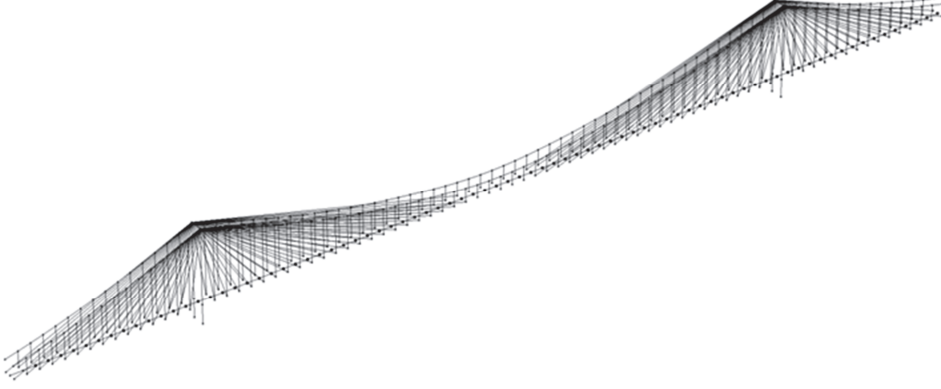


**Fig. 2.12** FE model of an hybrid cable-stayed suspension bridge

At first, the generation of the FE model is defined on a 3D description, whose initial configuration, only for the first iteration, is designed on the basis of practical design rules, typically, accepted in the framework of cable-supported bridges and defined in paragraph 1.2. In particular, the configuration of the main cable can be expressed by expression (1.17). Moreover, only for first iteration, i.e. for  $k = 1$ , the initial cable cross-sections for stays ( $\bar{A}_i^S$ ), hangers ( $\bar{A}_i^H$ ), main cable ( $A^M$ ) and the initial stresses ( $S_g^S, S_g^H$ ) are estimated from Eq.s (1.13)-(1.15). The evaluation of the post-tensioning forces and the optimum cable cross-sections is developed by solving the governing equations concerning equilibrium (EQ), optimization (OBJ) and constrain equations, (CE) defined by Eq.s (2.21)-(2.25) and (2.63), whose compact form can be expressed as follows:

$$\begin{aligned}
 OBJ &\rightarrow \underset{(\xi, \psi)}{Min} Q(\xi, \psi, U), \\
 EQ &\rightarrow \underline{K}(\xi, \psi, U) \underline{U} = \underline{F}(\xi, \psi), \\
 CE, L_U = 0 &\rightarrow \underline{S}_0^H(\xi, \psi) + \underline{C}(\xi, \psi, U) \Delta \underline{S} = 0, \\
 CE, L_{S_1} = 0 &\rightarrow \underline{K}^H(\xi, \psi, U) \underline{U}^H - \Delta \underline{A}^H \underline{S}_g^H = 0, \\
 CE, L_{S_2} = 0 &\rightarrow \underline{K}^S(\xi, \psi, U) \underline{U}^S - \Delta \underline{A}^S \underline{S}_g^S = 0, \\
 CE, L_{S_3} = 0 &\rightarrow \max_{i=1..N^{Mc}} \left[ \underline{K}^M(\xi, \psi, U) \underline{U}^M(\xi, \psi) \right]_i - \Delta \underline{A}^M \underline{S}_g^M = 0.
 \end{aligned} \tag{2.65}$$

where  $\Delta \underline{S}^T = [\Delta S_1^H, \Delta S_2^H, \dots, \Delta S_{N^s}^H, \Delta S_1^S, \Delta S_{N^s}^S, \Delta S^M]$ ,  $\underline{K}$  is the global stiffness of the structure,  $\underline{U}$  is the global displacement vector,  $\underline{F}$  is the external force vector associated to the dead loading configuration,  $\underline{S}_0^H$  and  $\Delta \underline{S}^H$  are the initial and incremental stress vectors of the hanger elements,  $\underline{C}$  is the corresponding flexibility matrix,  $(\underline{K}^H, \underline{K}^S, \underline{K}^M)$  are the matrixes collecting the stiffness coefficients of the hangers, cable-stayed and main cable, respectively,  $\Delta \underline{A}^H$  and  $\Delta \underline{A}^S$  are the vectors containing the cross-sections of the hangers and the stays and  $\Delta \underline{A}^M$  is the cross-section of the main cable element. It is worth noting that Eq. (2.65) introduce a nonlinear constrained optimization problem, in which the unknown quantities are represented by displacements and cable dimensioning of the cable systems. However, since the structural behavior is essentially nonlinear an iterative integration procedure must be performed. At this aim, the solving procedure is defined in the framework of gradient-based solver algorithms based on SNOPT solver, in which the optimal solution is computed by the evaluation of the gradients of both the objective function and all constraints by using numerical differentiation (Ohsaki, 2011).

The objective function and constrain conditions are interpolated by means quadratic and linear polynomial approximations, respectively. Once the configuration under dead loads is evaluated, the analysis is developed to determine maximum effects on the bridge components produced by the live loads in terms of stresses and displacements. However, since the bridge behavior is essentially nonlinear, the analysis under live loads should be considered as a continuation from the previously converged configuration under the dead load, taking into account also the construction steps involved in the erection procedure. In particular, all the variables involved in the solving procedure or in the definition of the structural elements of the bridge are taken from the last converged solution, i.e. under dead loads. At this point, the solving procedure is defined by a restarting analysis, in which the initial values are scaled as a function of the current solution. The solution is performed for a fixed number of loading conditions, i.e.  $N^{LL}$ , which collect, for all bridge components, maximum stress and displacement effects:

$$\tilde{K}(\tilde{\xi}, \tilde{\psi}, \tilde{U}_i) \Delta \tilde{U} = G_i(\tilde{\xi}, \tilde{\psi}) - P_0(\tilde{\xi}, \tilde{\psi}) \quad i=1, \dots, N^{LL} \quad (2.66)$$

with

$$\begin{aligned} \tilde{\xi} &= \xi^{DL}, \\ \tilde{\psi} &= \psi^{DL}, \\ \tilde{S}^{S,H} &= \bar{S}^{S,H} + \Delta S^{S,H}, \\ \tilde{S}^M &= \bar{S}^M + \Delta S^M \end{aligned} \quad (2.67)$$

where  $P_0$  is the vector of nodal point forces corresponding to the increment in element displacements and stresses from the dead load to the live load configurations,  $\Delta \tilde{U}$  are the incremental displacement vector,  $(\Delta \tilde{S}^{S,H}, \Delta S^M)$  are the variable associated to the incremental value of internal stress evaluated starting from the last converged values, i.e.  $(\bar{S}^{S,H}, \bar{S}^M)$ , and  $G_i$  is the live load vector force of the  $i$ -th loading configuration. From the loading combinations defined by Eq. (2.66), the new estimates of initial stresses are derived on the basis of Eq.s (2.29)–(2.32). Subsequently, convergence conditions defined by Eq.(2.33) are checked and if they are not satisfied, the analysis goes back to evaluate the configuration of the bridge under dead loading with the new values of the initial stresses.

## 2.6 Results

At first, results are presented in order to validate the proposed model in terms of convergence of the solution during the iterations steps and efficiency of the formulation to predict the cable system dimensioning and post-tensioning stresses of the cable elements. In this framework, the analysis is developed with respect to two different cases: in the first case a cable-stayed bridge is considered and the proposed model is validated by comparisons with existing optimization techniques on cable-stayed bridges available from the literature.

The second case refers to the optimum design of a self-anchored cable-stayed suspension bridge with a small central span and a reduced number of elements, which is useful to verify the consistency and robustness of the

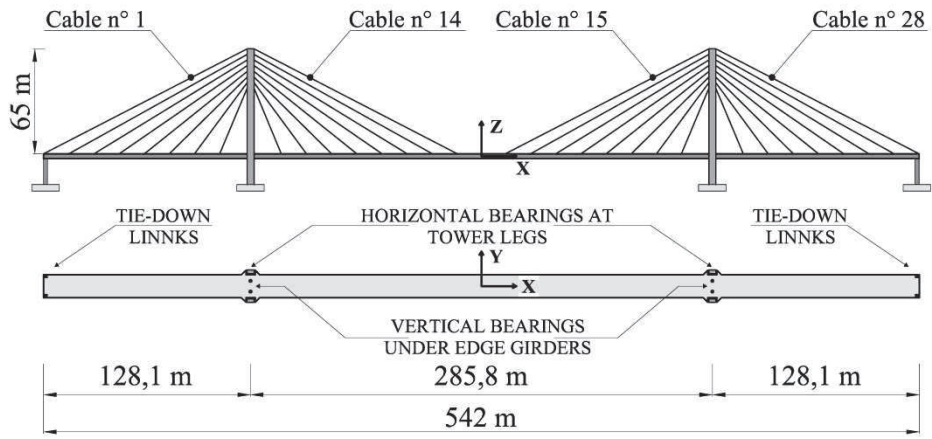
proposed design methodology. Subsequently, further results are developed for more complex structures involving several configurations of the cable system and a large number of variables such as those involved in long span bridges. This to prove the wide applicability of the proposed methodology.

### **2.5.1 Validation of the proposed design method based on design methodologies available from literature**

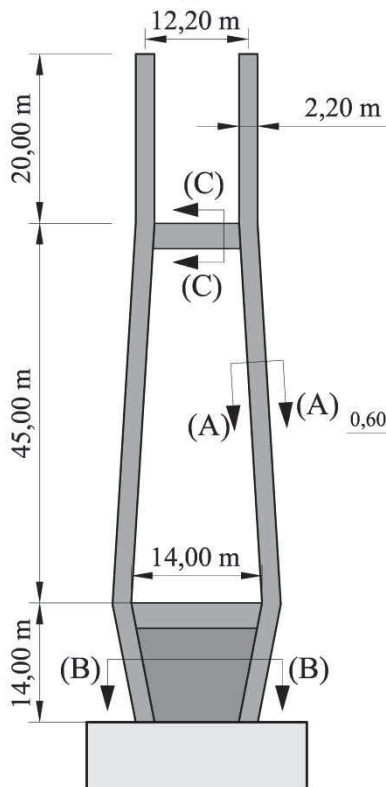
The cable-stayed bridge considered is the Quincy Bayview Bridge, located in Illinois (USA) (Fig. 2.13). The bridge is based on H-shaped concrete towers, 79 m high from the foundation structure, a double layer of cable system formed by 80 cables and a composite precast concrete-steel deck. The central and lateral spans are equal to 285.6 m and 128.1 m, respectively, as depicted in Fig. 2.14 (a). The precast concrete deck has a thickness of 0.23 m and a width of 14.2 m as illustrated in Fig.2.14 (b). It also has two steel main girders that are located at the outer edge of the deck. These girders are internally attached by a set of equally spaced floor beams. The pylons have two concrete legs as they are connected internally with a pair of struts. The lower legs of the pylon are connected by a 1.12 m thick wall (Wilson & Gravelle, 1991).



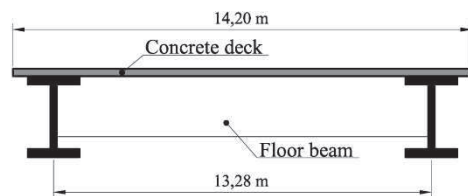
**Fig.2.13** Quincy Bayview Bridge Wilson and Gravelle (1991)



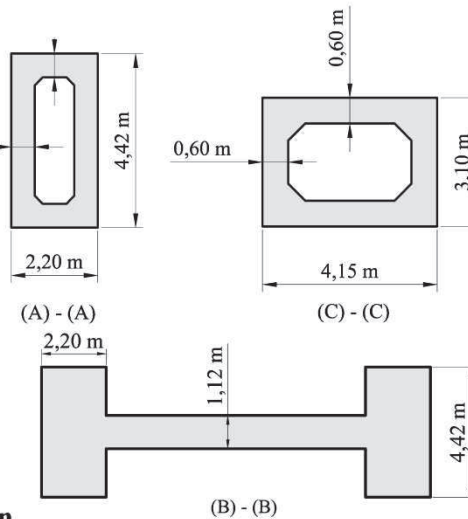
(a) Cable numbers and geometry of the bridge



(c) Elevation view of the bridge pylon



(b) Cross section of the bridge deck



(d) Cross section of the bridge pylon

Fig.2.14 Geometry of the Quincy Bayview Bridge

<i>Stiffening Girder</i>			<i>Pylon</i>			<i>Cable and Loads</i>		
$A^G$	0.602	$m^2$	$A^P$	6.50 ÷ 15.10	$m^2$	$S_A$	1.60	GPa
$I_2^G$	0.704	$m^4$	$I_2^P$	6.50 ÷ 15.10	$m^4$	$\gamma^{SH,M}$	84	$kN/m^3$
$I_3^G$	14.2	$m^4$	$I_3^P$	3.65 ÷ 383.70	$m^4$	$E^{SH,M}$	205	GPa
$E^G$	200	GPa	$E^P$	24.87	GPa	$p$	9	$kN/m/lane$
$\gamma^G$	77	$kN/m^3$	$\gamma^P$	24	$kN/m^3$	$p/g^G$	0.10 ÷ 0.12	-

**Tab. 2.1** Mechanical and geometric properties of Quincy Bayview Bridge

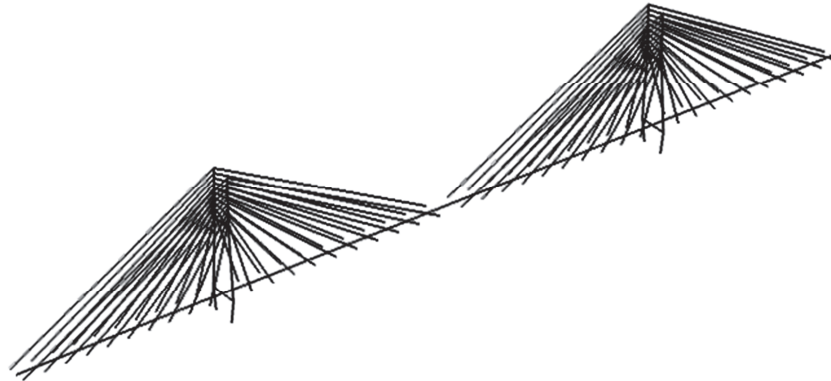


**Fig.2.15** Finite element modeling of the structural scheme of the Quincy Bayview Bridge

The elevation view of this bridge is depicted in Fig. 2.14 (c). As one can see, the pylon has a H-shape with two concrete legs. The cross-section of the pylons is also given in Fig. 2.14 (d). The data utilized for the simulations are presented in table 2.1, whereas the FE model utilized in the results is reported in Fig. 2.15. It is worth nothing that nine possible live load cases have been considered (Fig. 2.16). The entire model has been discretized by a regular mesh. In particular, each stay and each hanger are divided, respectively, in fifteen and in three linear truss elements, whereas the stiffening girder and pylons are meshed by a maximum element length approach so that five and ten meters are the size of the girder and pylons elements, respectively.

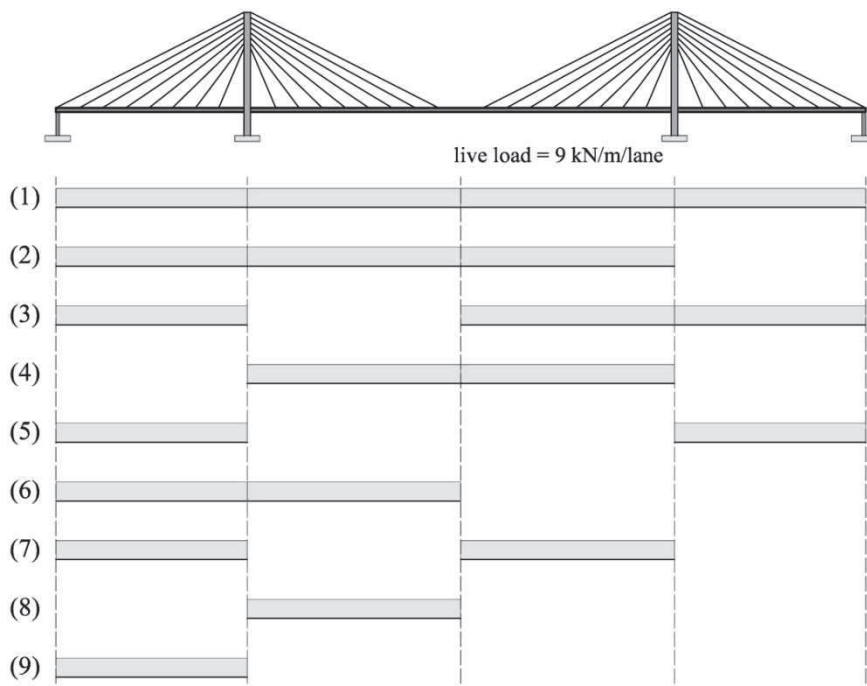


**Fig. 2.16** Live load cases used in the optimization design technique

At first, results in terms of distribution of optimized cable cross-sections are presented in Fig. 2.17, in which comparisons between the data predicted by proposed model and those obtained in (Hassan, 2013) are analyzed. Moreover, in the same figure, the evolution of the total steel quantity as a function of the percentage number of iterations is also reported. The analyses show that the distribution of cable cross-sections determined by the proposed formulation is always below the cross-section values obtained in (Hassan, 2013) and the corresponding percentage reduction of the total steel quantity is almost equal to 26%. The proposed formulation appears to be quite stable in reaching the optimum configuration, since a low number of iterations is required to obtain the convergence of the solution. The comparison in terms of cross-section distribution denotes, that, despite results obtained in (Hassan, 2013), the proposed modeling finds the largest values of the cable areas in proximity of the anchor stays, in which, typically, maximum transferring stresses arising from stays of the central span are observed.

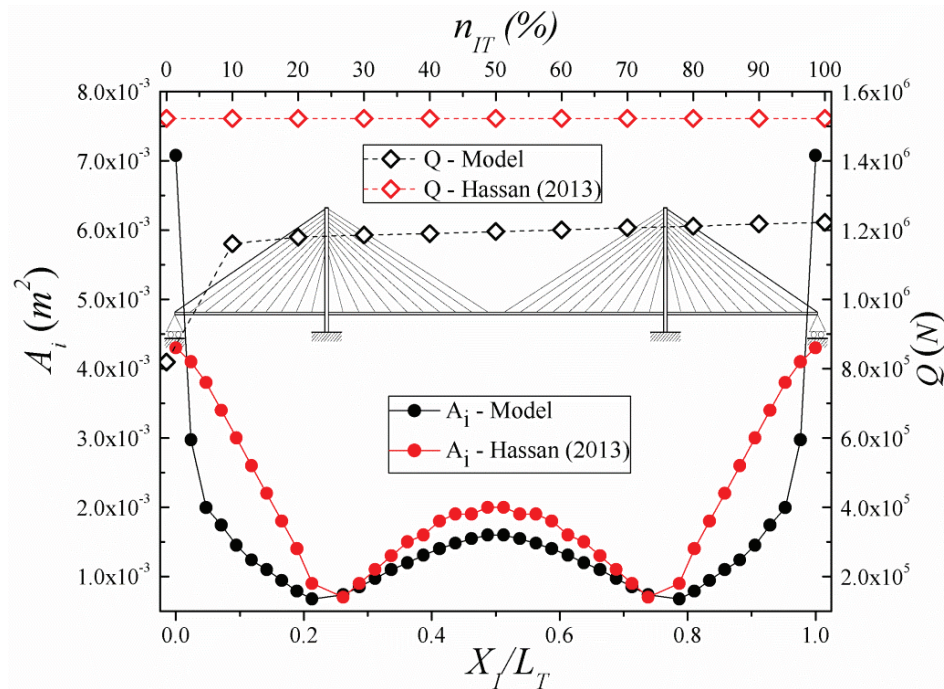


**Fig.2.17** Comparisons with results obtained in (Hassan, 2013) in terms of cross-section distribution of the cables ( $A_i$ ), total steel quantity ( $Q$ ) as a function of the number of iterations.

Such results can be considered reasonable also with common design procedures and experimental evidences on cable-stayed bridges, since the anchor cables are responsible of both pylon and girder deformability, much more than adjoining elements.

Additional analyses, reported in Fig. 2.18, are developed with the purpose to investigate the stress distribution observed in the cable system produced by the application of live loads. In particular, the envelope of maximum internal stresses for each element of the cable system is reported as function of the position of the cable along girder profile.

A synoptic representation of the stress distribution also in relationship to the assumed loading combination is reported in Fig. 2.19.

The results denote that the optimum solution, obtained by the proposed model, presents values of the stresses in the cables equal or mostly close to the



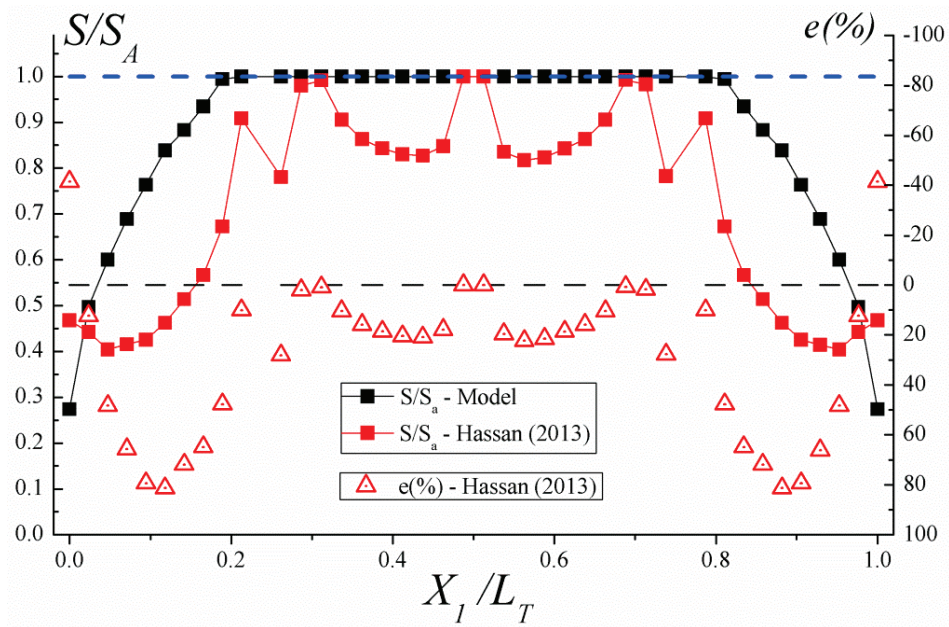


Fig.2.18 Comparisons in terms of maximum stresses produced by live loads and percentage error (e) with the values determined in (Hassan, 2013).

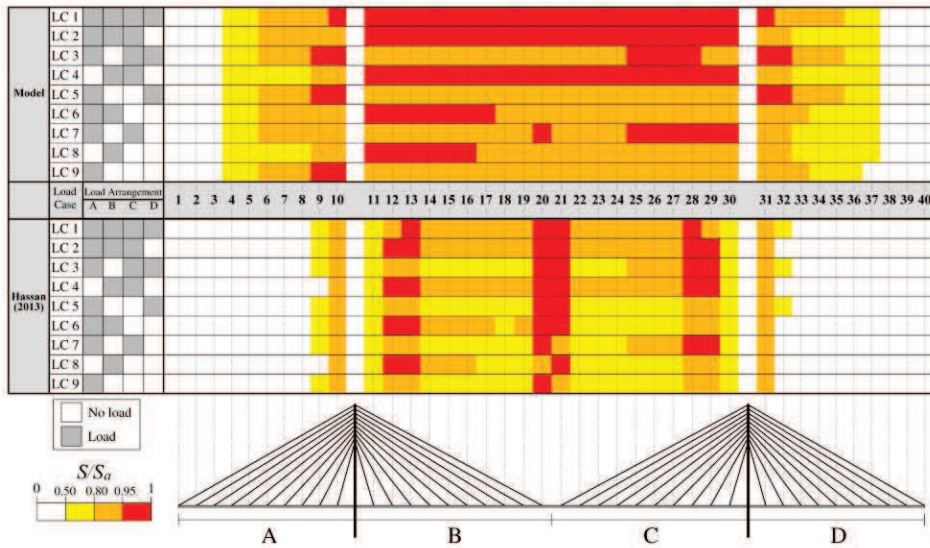
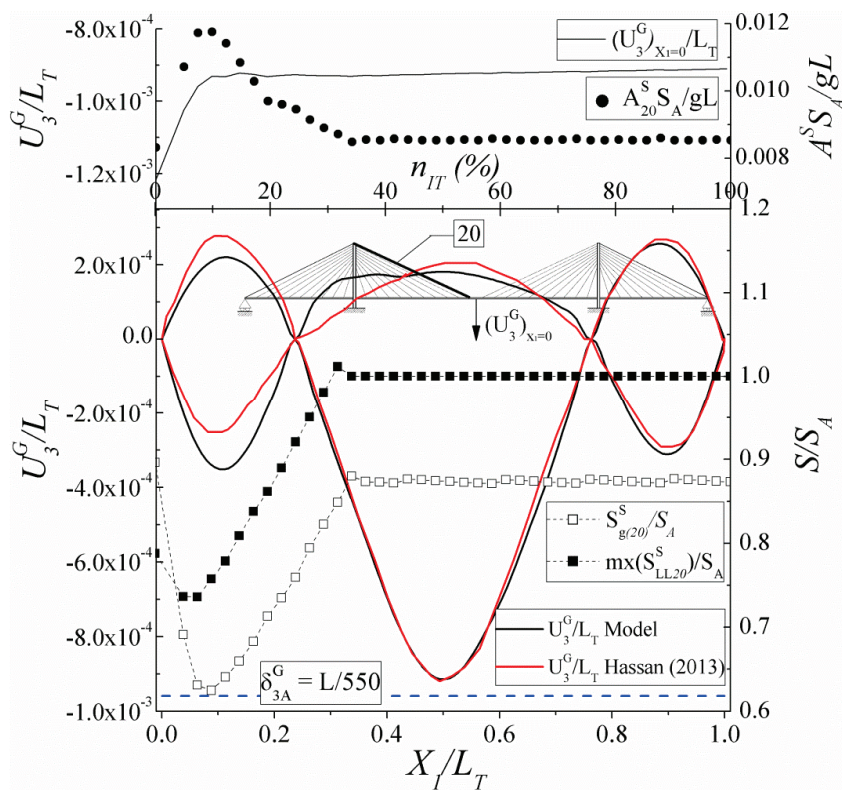


Fig.2.19 Synoptic representation of the live load configurations, maximum stresses and comparison with data obtained in (Hassan, 2013).

allowable quantity; the comparison with respect to values obtained in (Hassan, 2013) denote percentage errors ranging from -41.37 to 81.31 with an average value of 28.88. The equality to the permissible value is not verified for all the cables in the lateral span, whereas those of the central span under live load are designed to reach a value exactly equal to their strength. Such condition determines the best optimization of the cable-system cross-sections, which leads to strong reductions of the total steel quantity involved in the cable system.

However, for those elements of the lateral span, including also the anchor stays, the stress rate is lower than the allowable value, since more a stiffness amount in such elements is required in order to verify prescriptions on maximum girder deflections.



**Fig.2.20** Comparisons in terms of girder displacements produced by live loads with values determined in (Hassan, 2013), convergence behavior of the cross-sections, maximum and initial post-tensioning stresses as a function of the percentage value of the iteration steps ( $n_{IT}\%$ ).

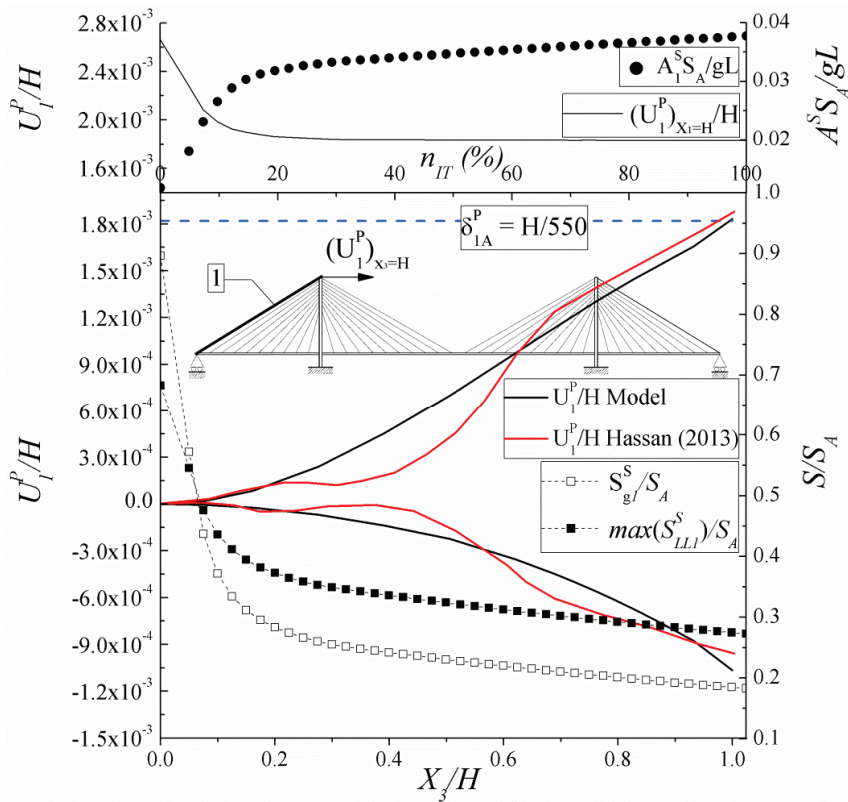


**Fig.2.21** Comparisons in terms of pylon displacements produced by live loads with values determined in (Hassan, 2013), convergence behavior of the cross-sections, maximum and initial post-tensioning stresses as a function of the percentage value of the iteration steps (nIT%).

Finally, in Figs. 2.20 and 2.21, comparisons with results developed in (Hassan, 2013) are proposed in terms of envelope of vertical and horizontal displacements of girder and pylons, respectively.

The analyses show how prescriptions on maximum deflections for both girder and pylons are below the permissible values. Moreover, in the same figures the evolution of the midspan vertical displacement (Fig. 2.20) the top pylon horizontal displacement (Fig. 2.21) and the cross-sections of the cables as well as the stress ratios between maximum stress and allowable value are reported as a function of the number of iteration steps. The analyses show how from the initial value the displacements are modified to verify bridge

deformability; such task is performed reducing the maximum working stresses of the cables much below the allowable value and thus increasing the stiffness or the area of the elements of the cable system.

Finally, the results show that the solutions present a convergent behavior toward the final optimum configuration.

### **2.5.2 Robustness test: The self-anchored cable-stayed suspension scheme with reduced number of cable element**

Results are developed with reference to a bridge structure with central span (L) and total length (LT) equal to 100 m and 180 m (Fig.5), whose aspect ratios  $f/L$  and  $H/cL$  are equal to 0.12 and 0.45, respectively. Without loss of generality, as before, in analyses only live loads concerning traffic loads are considered, which are combined with dead loading by using factored or unfactored loading combinations equal to  $1.2DL + 1.7LL$  or to  $DL + LL$  in cases of ULS or SLS, respectively. The main purpose is to present a benchmark analysis, involving a low number of the stays and hangers having a large spacing step. In such configuration, it is quite difficult to verify prescriptions on girder and pylon deformability or in terms of maximum or incremental cable strength. The cable system consists of a double layer formed by only 10 stays and 3 hangers and the main cable, whose elements present an allowable stress ( $S_a$ ) equal to  $6.4 \times 10^8$  Pa.

The displacement limits of both girder and pylons are assumed to be equal to  $1/600$  of the corresponding lengths. The girder and pylons present steel rectangular single box sections, whose data are reported in Tab. 2.2. Moreover, the dead loads on the girder include contributions arising from the weight of structural and non-structural elements, which are equal to 44.15 kN/m and 60 kN/m, respectively. Moreover, the ratio between live and dead loads, i.e.  $\lambda$ , is equal to 0.57. Such value is consistent with specification reported in (American Association of State Highway and Transportation Officials, 2007; Yoo & Choi, 2009) in which approximately a number of six uniform traffic lanes are considered.

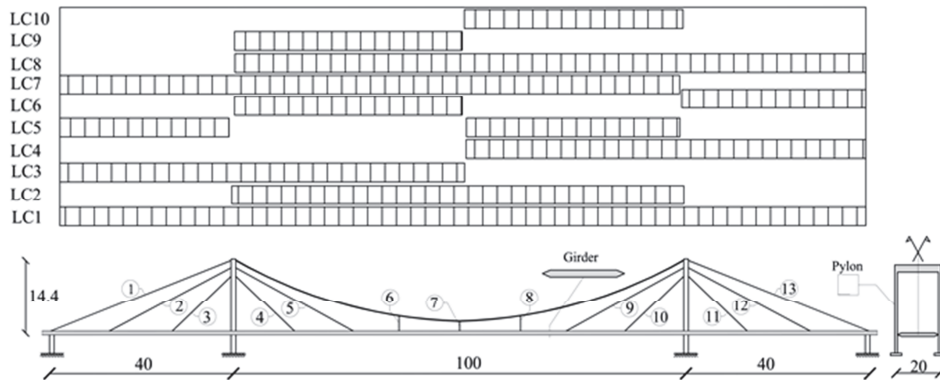


Fig.2.22 Synoptic representation of the self-anchored cable-stayed suspension scheme

	Cross sectional area [m <sup>2</sup> ]	Second moment of cross section [m <sup>4</sup> ]
Girder	0.57	0.024
Pylon (vertical strut)	0.30	0.24

Tab. 2.2 Bridge parameters of the girder and pylons

Finally live loads are applied on the structure to produce maximum effects in terms stresses or displacements by using the loading combinations reported synoptically in Fig. 2.22.

Results concerning the cross-section area distribution of all cable elements are reported in Fig. 2.23, whereas the convergence behavior of the predicted solution is reported in Fig. 2.24. The analysis denotes that with respect to the initial values, essentially based on preliminary design rules reported in the paragraph 1.2, the cross-section areas are strongly modified. In particular, in the cable-system, the anchor stays and the main cable are dimensioned with larger values than the remaining elements. The convergence of the solution toward the optimum solution is reached with a relatively low number of iterations especially for the internal cable elements, i.e. from cable 2 to 5, whereas for the anchors stays and the main cable a larger number of iterations is required to verify prescriptions on maximum displacements.

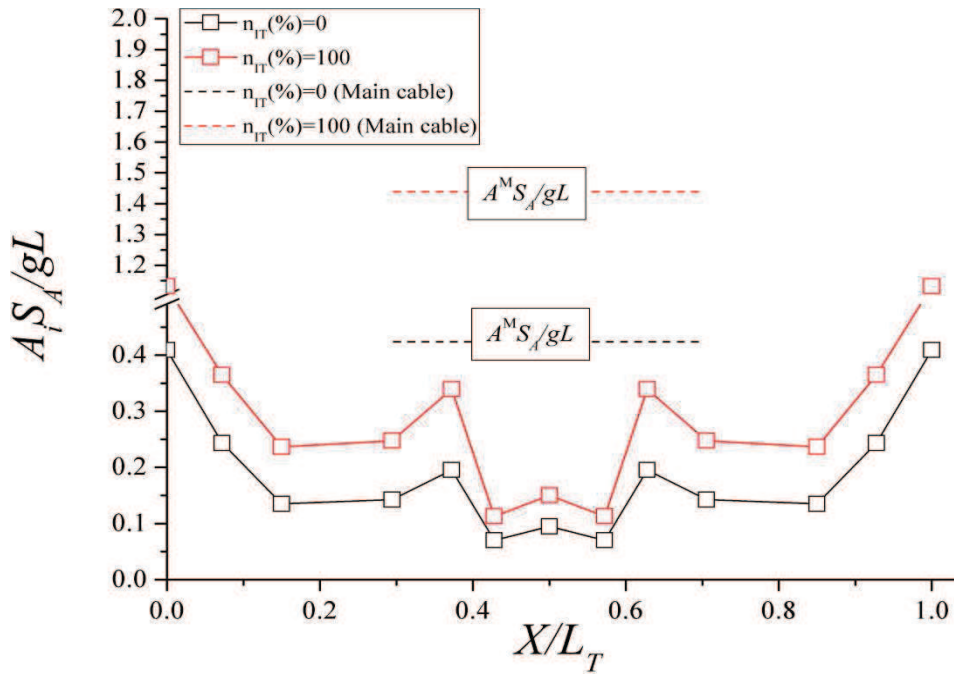


Fig.2.23 Cross-section distribution: initial and final evaluations

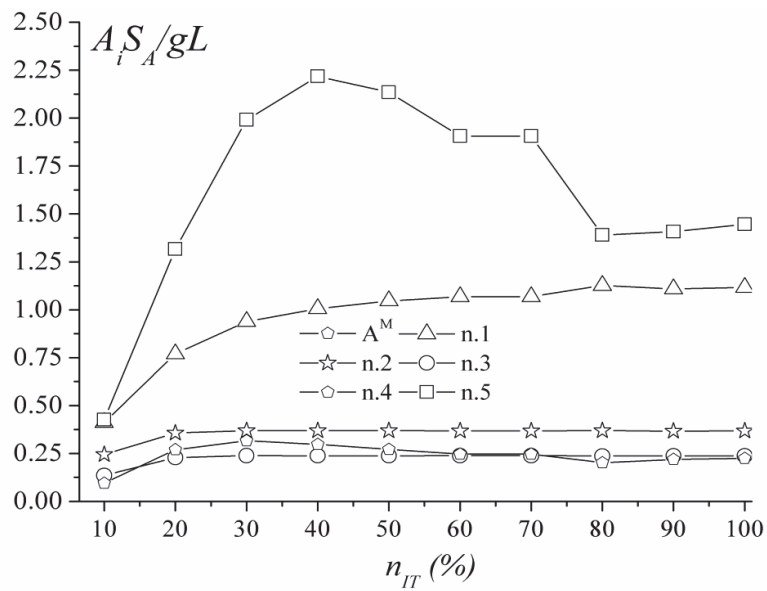


Fig.2.24 Convergence behavior of the cross-sections as a function of the iteration number

In Figs. 2.25, 2.26 results in terms of bridge deformability under dead load and live load are presented for both girder and pylons. In particular, in Fig. 2.25, the analysis shows that under dead load the deflections of the girder are practically negligible in comparisons to those observed in the case of live load.

The initial configuration, predicted by the proposed model in terms of the cable forces, is able to constraint to zero the displacements of the girder at the connections with the cables. Moreover, in Fig.2.26, the bridge deformability is presented in terms of convergence behavior to evaluate the optimum solution. Such results show how the maximum value of the normalized girder displacements, which is equal to -0.003 in the initial configuration, is reduced to a value almost close to its half and thus in agreement with design prescriptions on girder deflections. Moreover, the analysis denotes that the iterative procedure is based on a quite convergent and stable behavior, without jumps or singularities of the solution toward the final configuration.

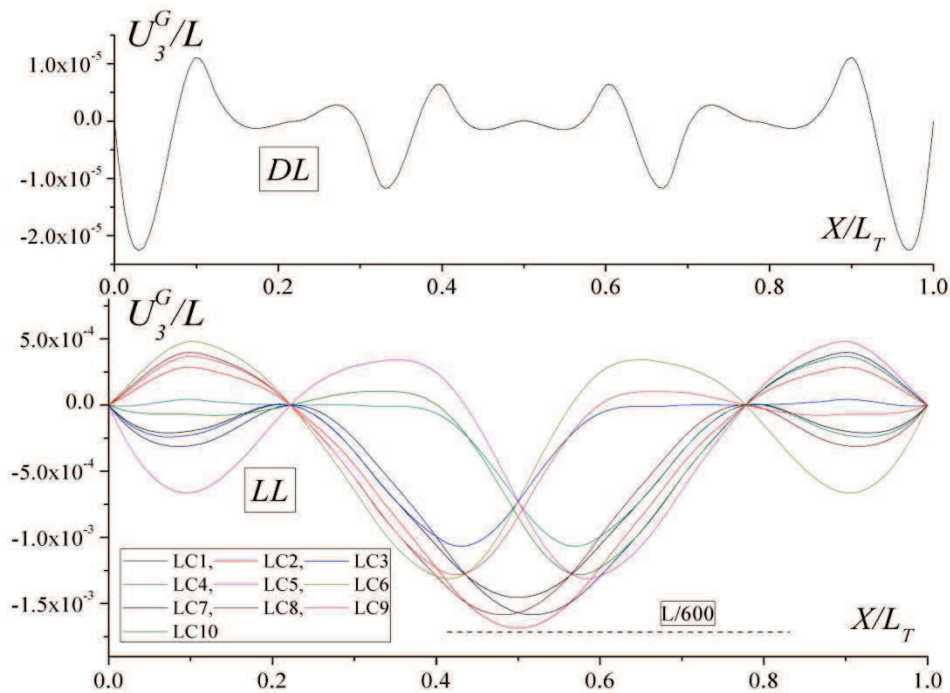
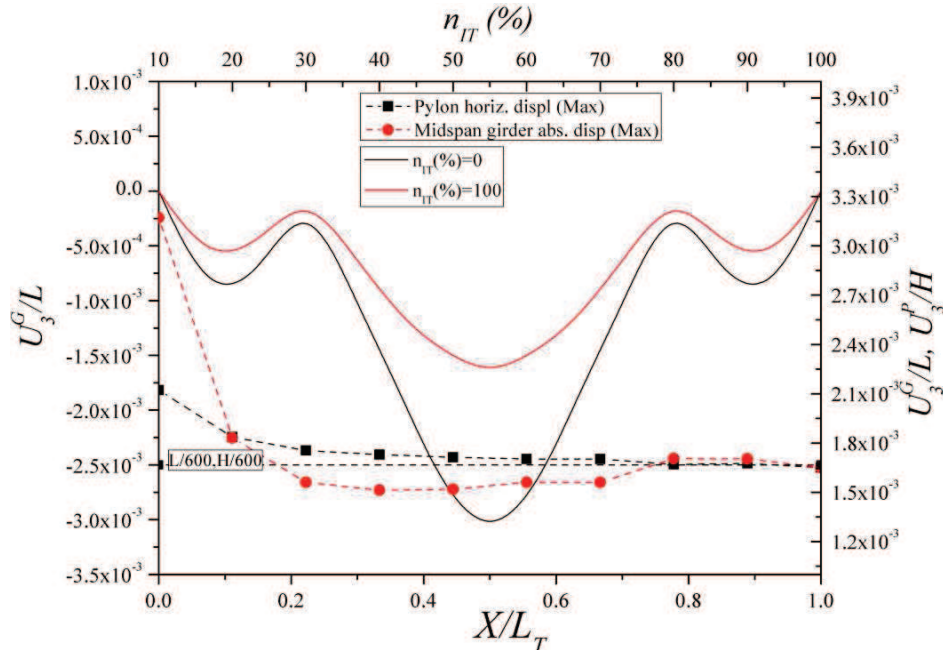


Fig.2.25 Envelope of the girder deflections under DL and LL



**Fig.2.26** Comparisons between initial and final evaluations of the girder deflections, convergence behavior of the top pylon horizontal displacement and midspan vertical deflections

The distribution of the optimization factors  $\Omega_i$  and  $\Phi_i$  for all elements of the cable system from the initial to the final configurations is reported in Fig. 2.27, whereas the initial stresses under dead load for each cable element are analyzed in Fig. 2.28. It is worth noting that factors  $\Phi_i$  have the role to constrain the equality of the stresses with the allowable quantity, whereas the factors  $\Omega_i$  are responsible of the prescriptions regarding bridge deformability. Both of them during the iterations, modify the stiffness of the cables, reducing or increasing the quantity of material involved in the cable system. During the iterative procedure, the internal cables, namely from 2 to 6, present increasing values of the factors  $\Phi_i$  and  $\Omega_i$ , except for the anchor stays and the main cable, since both of them are directly responsible of the midspan girder deflections and the horizontal top pylon displacements. Therefore, in order to verify prescriptions on bridge deformability, in such elements lower values than the unity of  $\Omega_i$  are predicted by the iterative procedure.



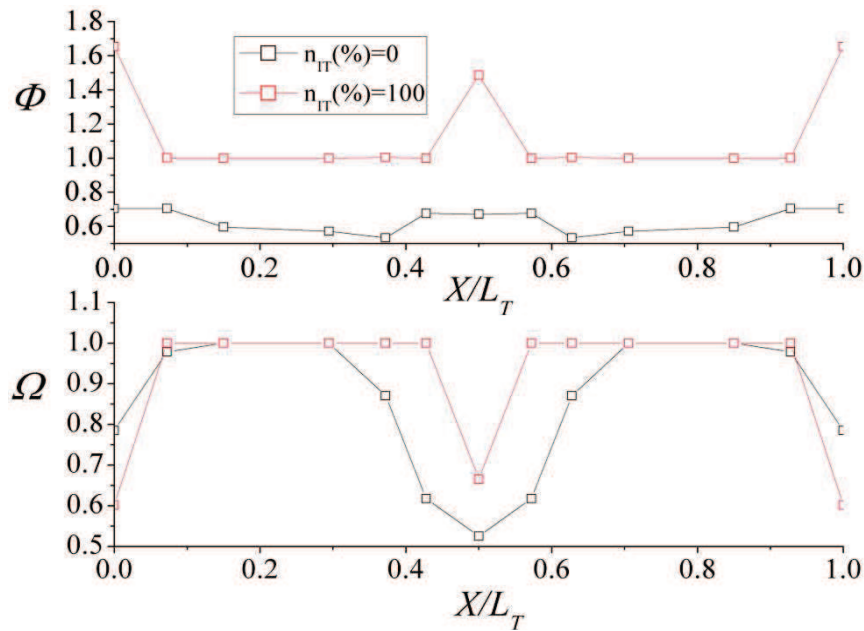


Fig.2.27 Stress and displacement optimization factors: initial and final prediction

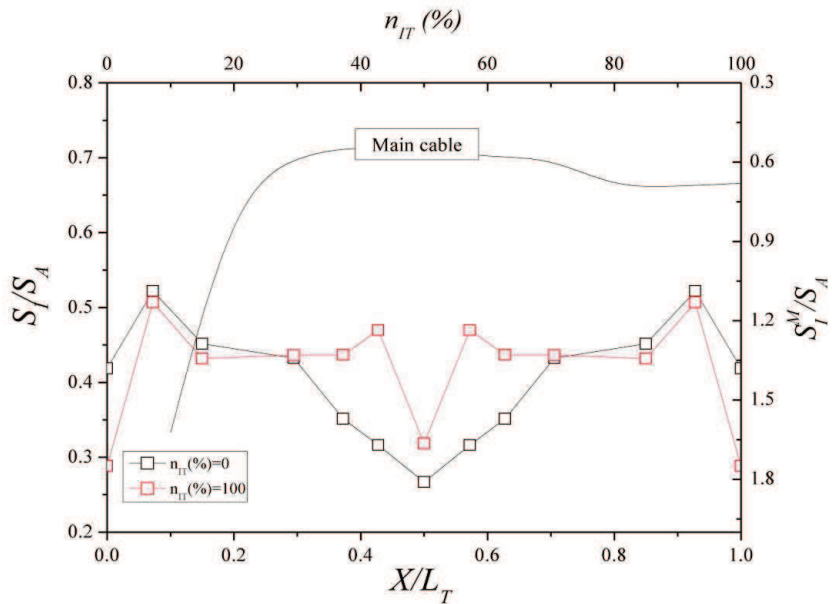
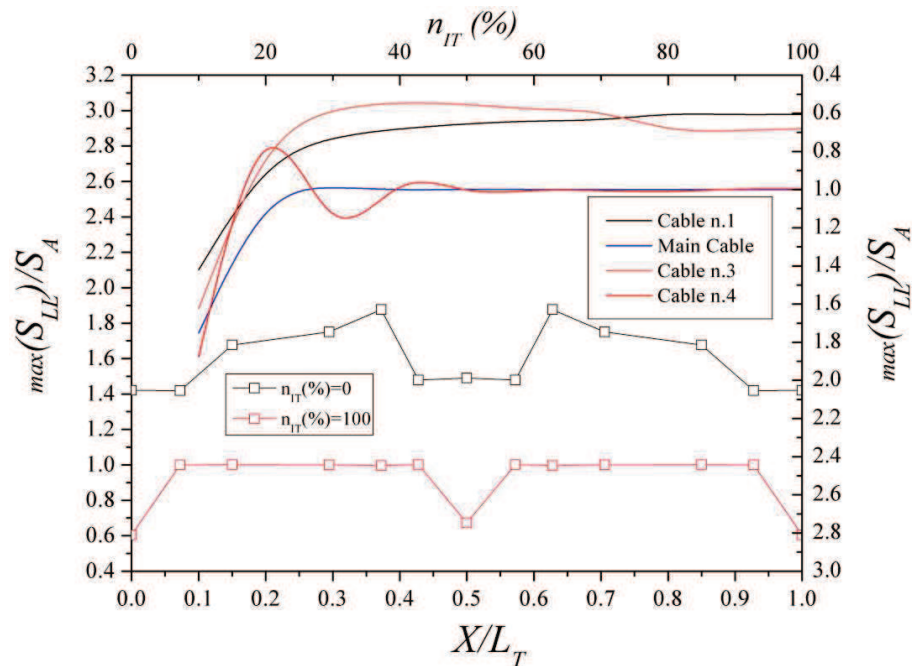


Fig.2.28 Distribution of the initial stresses (SI) under DL and convergence behavior of the values observed in the main cable as a function of the percentage value of the iteration steps (nIT%)

Similarly, the initial stresses presented in Fig. 2.28, are modified from the initial distribution, in such a way that the anchor stays and main cable during the iterations are forced to have lower post-tensioning forces, larger stiffness and cross-section than the remaining elements. In particular, in such cables, the maximum allowable stresses are modified from the standard value arising from the material characteristics, i.e.  $S_A$ , introducing lower thresholds under live loads. Such behavior can be also discussed on the basis of the results presented in Fig. 2.29, in which the distribution of the maximum stresses under live load for all cable elements is considered. In particular, during the iterations the most of the elements of the cable system are designed consistently with P.B.A., since the ratio between actual and allowable stresses, i.e.  $\max(S_{LL})/S_A$ , is close to the unity; contrarily for that elements with values lower than one, in order to verify design constrains on bridge deformability, larger values of cross-sections than the remaining elements are predicted.



**Fig.2.29** – Distribution of the maximum stresses under LL and convergence behavior of the maximum stresses as a function of the iteration percentage number ( $n_{IT}\%$ ).

### 2.5.3 The long span bridges case: comparisons between hybrid and pure systems

The analysis is developed for three different bridge schemes based on hybrid cable-stayed suspension, pure cable-stayed or suspension systems, whose main span is equal for all cases to 1000 m. The deck is made of steel with aerodynamic cross-section, 4 m depth and 20 m wide; the vertical moment of inertia ( $I_2^G$ ), the transverse moment of inertia ( $I_3^G$ ), the cross-section area ( $A^G$ ) and the torsional constant ( $J^G$ ), the modulus of elasticity of steel ( $E^G$ ) for the bridge deck are  $3.41 \text{ m}^4$ ,  $31 \text{ m}^4$ ,  $2.1 \text{ m}^2$ ,  $15 \text{ m}^4$ ,  $2.1 \times 10^8 \text{ kN/m}^2$ , respectively.

The towers are formed by *H*-shaped steel components, whose elements present vertical moment of inertia ( $I_2^P$ ), transverse moment of inertia ( $I_3^P$ ), cross-section area ( $A^P$ ), torsional constant ( $J^P$ ), modulus of elasticity ( $E^P$ ) and in plane flexural top pylon stiffness ( $K^P$ ) are  $20.57 \text{ m}^4$ ,  $9.78 \text{ m}^4$ ,  $1.97 \text{ m}^2$ ,  $21.13 \text{ m}^4$ ,  $2.1 \times 10^8 \text{ kN/m}^2$  and  $50 \text{ g}^G$  respectively.

Moreover, the aspect ratio ( $H/l$ ) between pylon height and lateral span is equal to 0.4 for the hybrid cable-stayed suspension and pure suspension bridges or equal to 0.66 for the pure cable-stayed bridge.

The stays and the hangers present a distance equal to 20 m and an allowable stress ( $S_a$ ) equal to  $1.6 \times 10^6 \text{ MPa}$  and a minimum fatigue strength stress variation equal to 200 MPa (Strand). Dead loading of the girder including also permanent loads ( $g^G$ ) are equal to  $3.0 \times 10^5 \text{ N/m}$ , whereas the ratio between live and dead loads, defined consistently to the code prescriptions established in (Eurocode 1, 2003), is equal to 0.18 for ULS.

In particular, results concerning the valuation of stress distribution are analyzed under ULS (factored) or FLS (unfactored), whereas results concerning displacements are considered under SLS (unfactored). The data utilized for the simulations are summarized in Tab. 2.3.

Stiffening Girder			Pylon			Cable and Loads		
b	10	m	$A^P$	1.97	$m^2$	$S_A$	1.60	GPa
d	4	m	$I_2^P$	20.57	$m^4$	$\Delta S_A$	200	MPa
$A^G$	2.1	$m^2$	$I_3^P$	9.78	$m^4$	$\gamma^{S,H,M}$	77	$kN/m^3$
$I_2^G$	3.41	$m^4$	$E^P$	210	GPa	$E^{S,H,M}$	205	GPa
$I_3^G$	31	$m^4$	(H/D) <sub>HCS,SP</sub>	0.4	-	$g^G$	300	$kN/m$
$J^G$	15	$m^4$	(H/D) <sub>CS</sub>	0.66	-	$p/g^G$	0.18	-
$E^G$	210	GPa	$K^P$	50 $g^G$	-			

Tab.2.3 Parametric study: mechanical and geometric properties of bridge

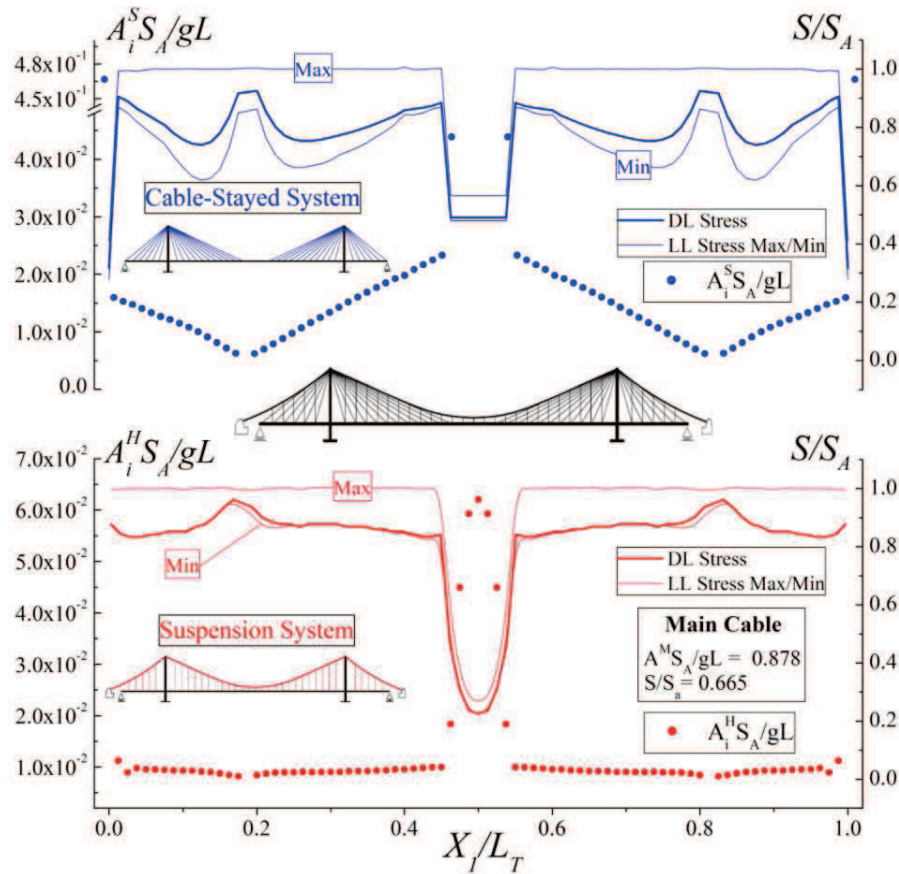


Fig. 2.30 HCS bridges: distribution of the cable cross-sections and envelope of the stresses in the cable-system in the stays, hangers and main cable.

At first, results concerning hybrid cable-stayed suspension bridges are presented in Fig. 2.30, in which the variability of the cross-sections of the cable system elements and their stress ranges observed under dead and live loads are reported. The cross-section distribution in the cable stayed-system presents its largest values in the anchor stays and in the longest stays of the main span, which, mostly, influence the deformability of the bridge. The hanger dimensioning presents a constant distribution of the cross-sections in the lateral and in the main spans, except in the midspan region, in which the cable-system of the HCS bridge behaves as a pure suspension scheme.

As a matter of fact, in such region, the absence of the stays, produces a reduction of stiffness against vertical displacements, which are, mostly, influenced by the main cable characteristics. Such concept can be highlighted also analyzing the envelope of stresses, presented in the same figure.

The results shows how most of the cable system elements, i.e. hangers and stays, are designed in such a way that under the application of live load, worst observed stress reaches the allowable value. However, for the anchor stays or in the midspan region, the design methodology predicts values of the cross sections, which produce maximum working stresses, locally, lower than the corresponding allowable value. Such predictions in terms of both stress or cross-sections can be explained due to the fact that the optimization procedure, in order to verify prescriptions on maximum displacements automatically modifies the cable stiffness of the most active elements, which produce the optimum stiffness effects and distribution on girder and pylon deflections.

Stress and displacement distributions as a function of the iteration steps to reach the optimum solution are presented in Figs. 2.31 and 2.32, respectively.

Results concerning bridge deformability or stress distribution denote that from the initial configuration, girder displacements and maximum stresses in the cable system present a convergent behavior toward the final solution.

In particular, such configuration is obtained by means of 25 iterations, in which the cross-sections of the cables as well as their initial stresses under dead load are modified to verify code prescriptions on bridge deformability and cable strength. However, most of the optimization process is performed in the initial substeps, i.e. before 12 iterations, in which both displacements and

stresses present values equal approximately to the corresponding design quantities, whose maximum error with respect to the final optimized values is lower than 7%. Moreover, maximum stresses in the cable system are strongly modified from the initial trial values, namely from  $k = 1$ , which, basically, correspond to the application of preliminary dimensioning rules available from the literature. From such values, the optimization method modifies the cable cross-sections according to stress and displacement requirements provided by the code prescriptions, leading to a reduced steel quantity involved in the cable system.

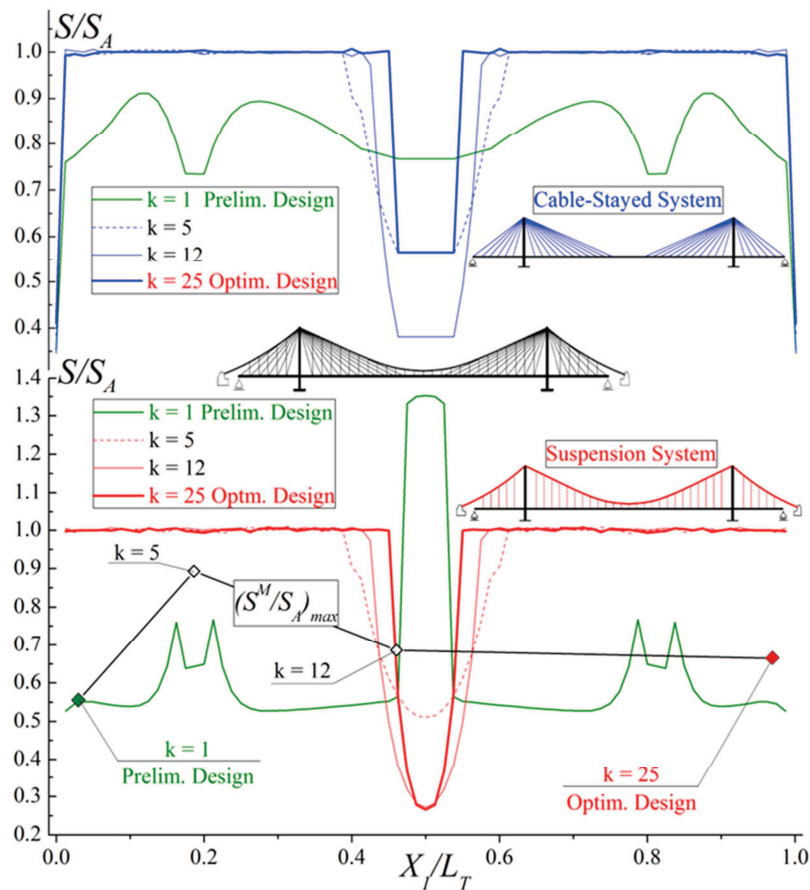


**Fig. 2.31** HCS bridges: convergence behavior of the predicted maximum stresses in the cable system as a function of the iteration steps

Such behavior can be observed from the results presented in Fig. 2.33, in which the evolution of cable stresses and girder displacements at discrete points of the bridge are presented as a function of the number of iterations obtained in the solving procedure.

The results show how the proposed method adjusts the maximum working stresses and thus the cross-sections of the cable system, providing improvements in the bridge deformability, which is reduced to verify prescription on maximum displacements.

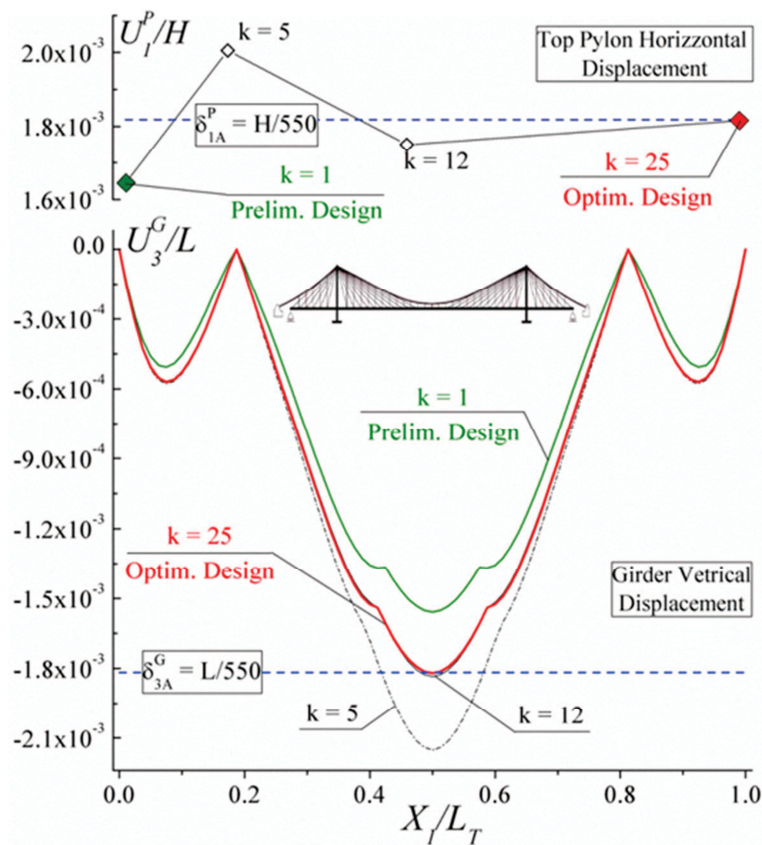


**Fig. 2.32** HCS bridges: convergence behavior of the girder and pylon displacements in the cable systems as a function of the iteration steps.

Finally, a comparison in terms of cable-system configurations is developed, in which results obtained by the proposed methodology are analyzed with respect to long span bridge configurations based on hybrid cable-stayed suspension bridge or pure cable-stayed (CS) or suspension (SP) cable systems.

The key of these results is to analyze the applicability, in terms of convergence and stability, of the proposed formulation for different bridge schemes and to investigate the differences in terms of cable dimensioning between the bridge configurations. Results in terms of cross-section distribution and dead load and live load stresses are reported in Figs. 2.34 and 2.35, respectively.

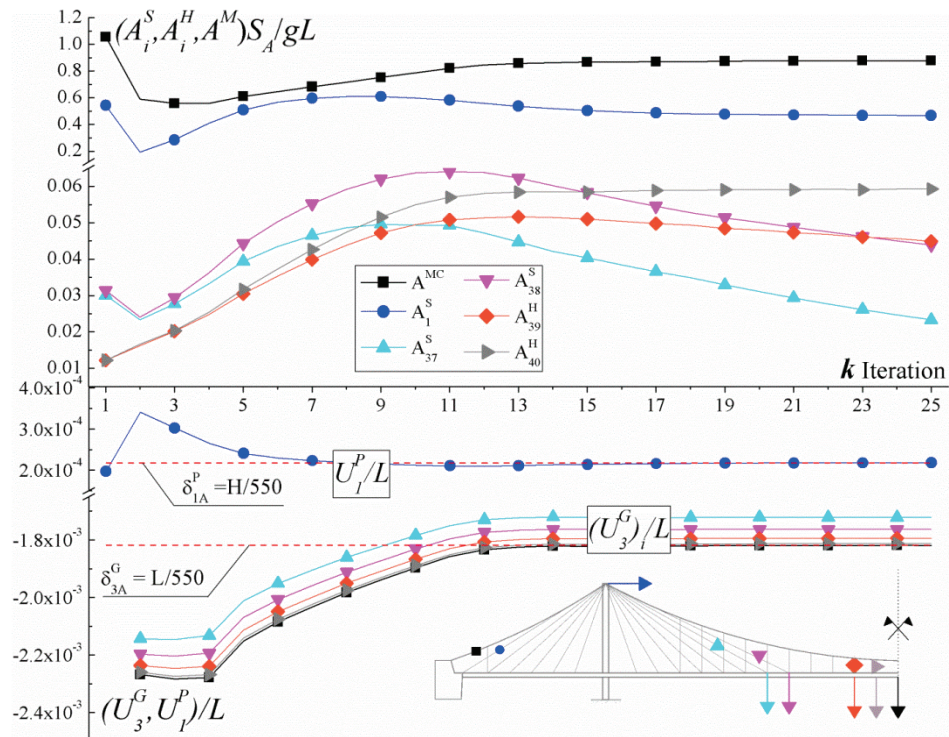


**Fig. 2.33** – HCS bridges: comparisons between maximum stresses in the cable system and vertical displacements in the girder at discrete points of the bridges as a function of the iteration steps.



The analyses denote that the cable cross sections of the HCS bridge scheme are always below the corresponding ones obtained from the configurations based on pure CS and SP schemes.

For pure CS configuration, the distribution of the cross-sections is similar to that of the HCS bridge, since the largest values are predicted in proximity of the anchor stays and the longest stays of the central span.

Analogous conclusions can be drawn for the distribution of the stresses in the cable elements, which are in both cases, under live load, equal or lower than the corresponding allowable value.

Contrarily, the suspension system dimensioning presents larger value of required steel quantity than those observed in the case of HCS bridge for both main cable and hangers cross-sections, i.e. larger than 3.45 and 3.89 times, respectively. Moreover, the distribution of the hanger cross-sections is not constant as in the case of HCS bridge, since it presents a maximum value at a position on the girder profile equal to  $X1/LT = 0.35$ .

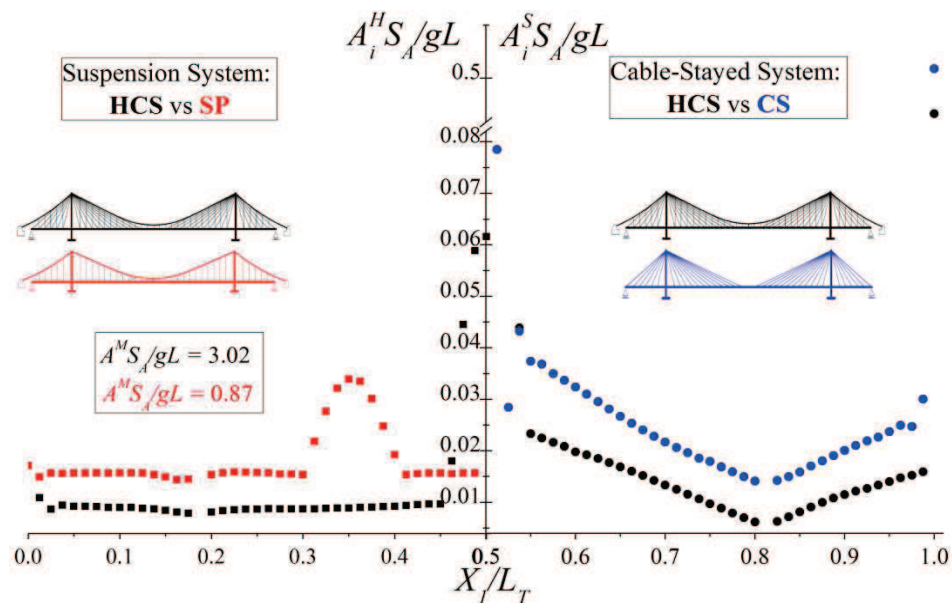
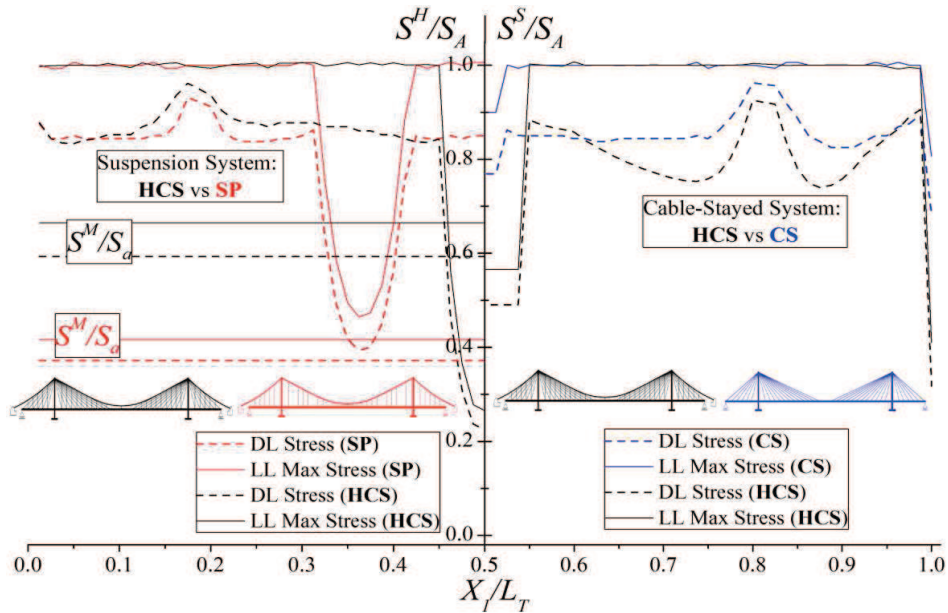


Fig. 2.34 Comparisons between predicted values of the cross-sections in the cable-system between hybrid cable-suspension (HCS), cable-stayed (CS) and suspension (SP) bridges.



**Fig. 2.35** Comparisons between predicted values of the maximum stresses in the cable-system between hybrid cable-suspension (HCS), cable-stayed (CS) and suspension (SP) bridges.

Such prediction can be explained by the fact that SP bridges are mostly influenced by the characteristics of the main cable, which is typically affected by large displacements in the case of unsymmetrical loading distributions on the girder main span length.

Similarly, results concerning SP system denote that the stress distribution presents at  $X_1/L_T = 0.35$  a reduction of the maximum allowable stresses, since in that region, the bridge scheme is affected by large deformability and thus the cable dimensioning requires important contributions to verify prescriptions on maximum displacements. The analyses on HCS configurations do not denote such behavior, because of the presence of the cable-stayed system, which partially balances the reduced stiffness of the main cable, producing a regular distribution of cross-sections in the hanger cable-system.

Finally, the working rate of the main cable cross-section is much larger than that observed in the case of SP dimensioning, since HCS bridges are

characterized by an improved stiffness behavior because of the presence of the stays in the cable system. As a matter of fact, the stiffness behavior of the SP system is mainly influenced by main cable dimensioning, which is increased during the design procedure to verify deformability and stress prescriptions, leading to low values of the working stress rates and thus large amount of steel quantity involved in such bridge component.

Finally, the evolution of the total required steel quantity involved in the cable system for each bridge scheme as a function of the number of iteration steps to obtain the optimum solution is reported in Fig. 2.35.

Results denote for all bridge schemes a convergent behavior, since a limited number of iterations are required to derive the design configuration.

The SP system presents the maximum steel quantity, which is mainly given by the contribution of the main cable, whereas the lowest configuration in terms of steel quantity is achieved by using CS system.

The optimum solution of HCS bridge presents lower cross-sections of the main cable and stays than those observed in SP or in the CS systems. In particular, the main cable cross-section, which produces the most relevant contribution in the total steel quantity, from the pure SP system is reduced almost of 62%. Contrarily, the contribution arising from the hangers can be considered comparable, even if the corresponding steel quantity is much less of the one observed in the main cable.

Finally, the configuration, which is characterized by the lowest steel quantity involved in the cable system is the one associated to the CS system.

However, such results should be considered also in relationship to the geometry of the bridge scheme, which presents, typically, larger ratios between pylon and lateral span than those observed in SP or HCS bridge configurations.

Therefore, the reduced values of total steel quantity in the cable-system are partially compensated by the costs involved in the pylon construction.

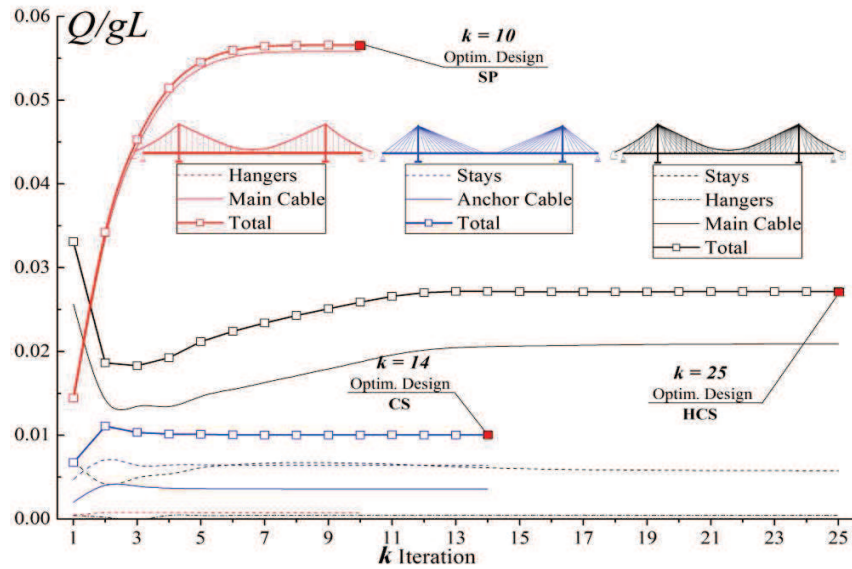


**Fig. 2.35** Comparisons between predicted values of the maximum stresses in the cable-system between hybrid cable-suspension (HCS), cable-stayed (CS) and suspension (SP) bridges.

### 2.5.4 The long span bridges case: the self-anchored cable-stayed suspension scheme

Additional results are presented for a long span self-anchored cable-stayed suspension bridge structure, similar to the one proposed in (Wang et al., 2013), whose main span length ( $L$ ) and total length ( $L_T$ ) are equal to 800 m and 1337 m, respectively (Fig.2.36). Moreover, the aspect ratios  $f/L$  and  $H/cL$  are equal to 0.12 and 0.46. The stays and the hangers present a distance equal to 12.5 m and an allowable stress ( $S_a$ ) equal to  $6.4 \times 10^8 \text{ Pa}$ , whereas the geometrical properties of girder and pylons are reported in Tab. 2.4.

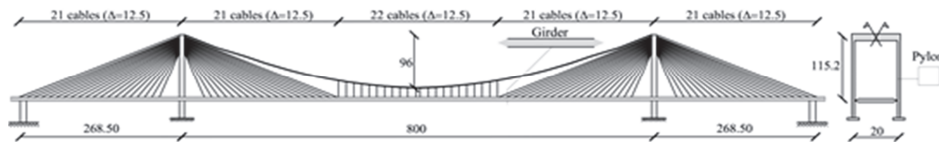


**Fig.2.36** Structural model of the long span self-anchored cable-stayed suspension bridge

	Cross sectional area [m <sup>2</sup> ]	Second moment of cross section [m <sup>4</sup> ]
Girder	1.60	4.96
Pylon (vertical strut)	2.72	49.64

Tab. 2.4 Bridge parameters of the girder and pylons

Dead loads of the girder including also the permanent contributions are equal to  $Q_{DL} = \gamma_s A_s + 60 = 2.06E5kN/m$ , whereas live loads, according to bridge design specifications reported in (American Association of State Highway and Transportation Officials, 2007; Yoo & Choi, 2009) consist of eight uniform traffic lanes with a value equal to  $Q_{LL} = 76.2kN/m$ .

In the analysis, the displacement limits of both girder and pylons are assumed equal to  $1/800$  and  $1/600$  of the corresponding lengths. From the mechanical and geometric characteristics defined above, dimensionless parameter concerning the ratio between stiffness of the girder ( $G$ ) and the cable system, i.e.  $\bar{\alpha}^2 = EI^G/H_t L^2$  and  $\bar{\lambda}^2 = (8f/L)^2 \times (L/L_e) \times (E^C A^C/H_t)$ , are equal to  $\bar{\alpha}^2 = 0.092$  and  $\bar{\lambda}^2 = 223$ , where  $EI^G$  is the bending stiffness of the girder and  $H_t$  is the dead load horizontal component of the cable tension.

Such values are consistent with data available from the literature, whose range, obtained on existing cable-supported bridge structures are equal to  $\bar{\alpha}^2 = [0.5 - 10] \times 10^{-3}$  and  $\bar{\lambda}^2 = [170 - 800]$  (Enrique Luco & Turmo, 2010).

Results in terms of cross-sections of the cable and post-tensioning stresses as a function of the normalized positions on the girder projection are reported in Fig.2.37 and Fig.2.38, respectively.

The analysis denotes that the design procedure defines a cross section distribution, whose maximum values are observed in the main cable and anchor stays. Moreover, the remaining stays present their largest values at the extremities of the cable-stayed system. Finally, the hangers are affected essentially by a constant distribution of the cross-sections. Such dimensioning predicted by the proposed modeling can be assumed quite reasonable from the structural and physical viewpoints.

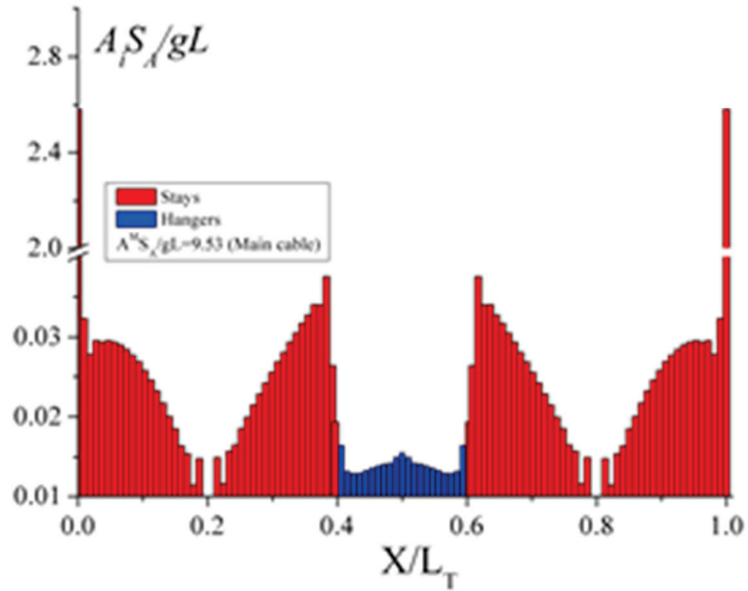


Fig. 2.37 Normalized cross-sections distribution ( $A_i S_i / gL$ ) in the cable-system as a function of the normalized position on the girder projection ( $X/L_T$ ).

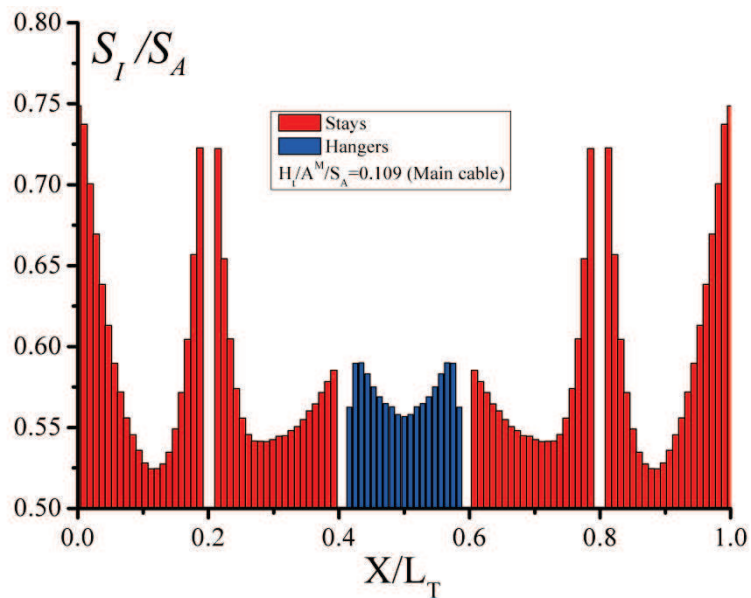


Fig. 2.38 Initial stresses ( $S_i / S_A$ ) in the cable-system as a function of the normalized position on the girder projection ( $X/L_T$ ).

In particular, the high values of the cross-section in the anchor stays are due to the development of the internal force arising from the main cable, which carries out most of the loading contributions arising from the central span. For this reason, in self-anchored schemes, the cross-sections of both anchor stays and main cable should be comparable. Moreover, the reduced values of the cross-sections of the stays located close to the pylons can be explained by the fact that in such regions the elements present their maximum efficiency in terms of loss stiffness due to sag effects. In addition, the prescriptions on girder or pylon displacements are not restrictive as the ones at the mid-span girder cross-section, because such cables are placed in proximity to the girder support. As a consequence, a low cable dimensioning is required.

In Figs. 2.39-2.40, results concerning bridge deformability are presented. In particular, girder deflections or horizontal displacements of the pylons are reported as function of the percentage number of iterations to obtain the final configuration. Moreover, in the same figure the evolution of the cross-sections of the main cable and the anchor stays are analyzed. The results denote that the anchor stays are mostly responsible of the horizontal displacements of the pylons, which is reduced as far as the cross-sections of such cable elements increase. Moreover, the girder deformability of the central span at the midspan cross-section is mostly affected by the stiffness of the main cable.

Actually, the hangers have the role to transfer the loads from the girder to the main cable, without providing any important contributions in terms of stiffness improvement; the stays, which are the most stiffness elements in combined cable-stayed suspension bridge schemes, are far from the midspan and thus their effect on the girder deformability is negligible.

In both cases, the results show that during the iterations the solutions are strongly modified from the initial trial solution. In particular, the cross-sections of the cable elements are increased to verify prescriptions on bridge deformability. Such behavior can be also analyzed by the envelope of maximum displacements reported in the same figures, which show how all the displacements at the final step are below the corresponding allowable limits typically adopted for design purposes.

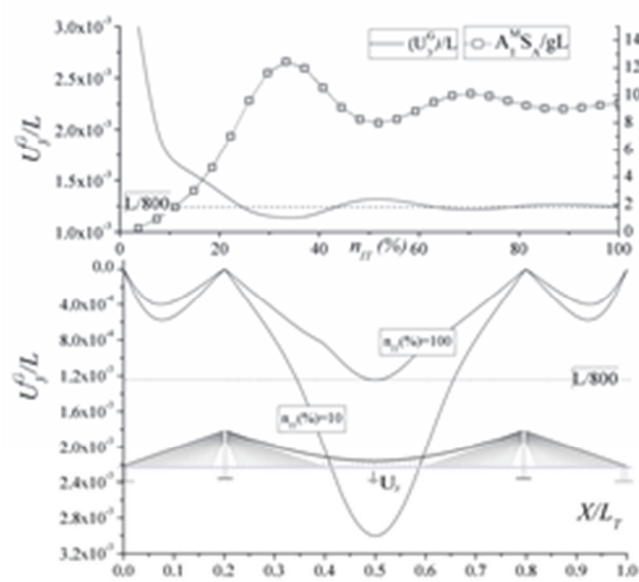


**Fig. 2.39** Normalized girder ( $U_3^G/L$ ) displacements produced by live loads; convergence behavior of the cross-sections and the displacements as a function of the percentage value of the iteration steps ( $n_{IT}\%$ ).

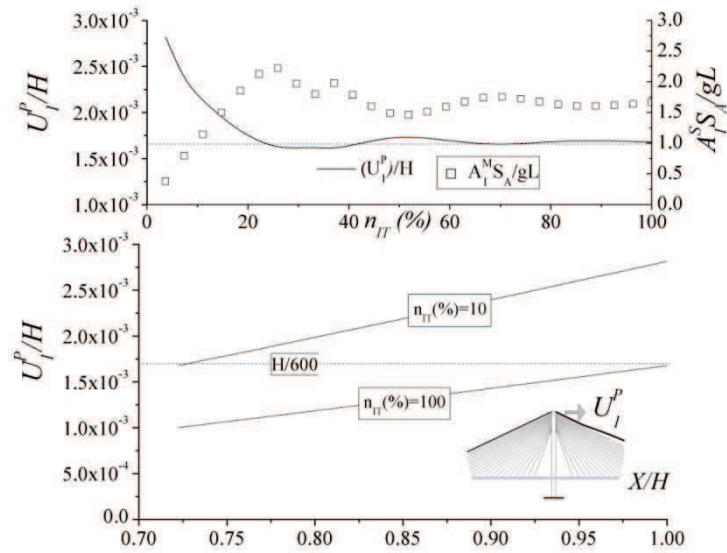


**Fig. 2.40** Normalized pylon ( $U_1^G/L$ ) displacements produced by live loads; convergence behavior of the cross-sections and the displacements as a function of the percentage value of the iteration steps ( $n_{IT}\%$ ).



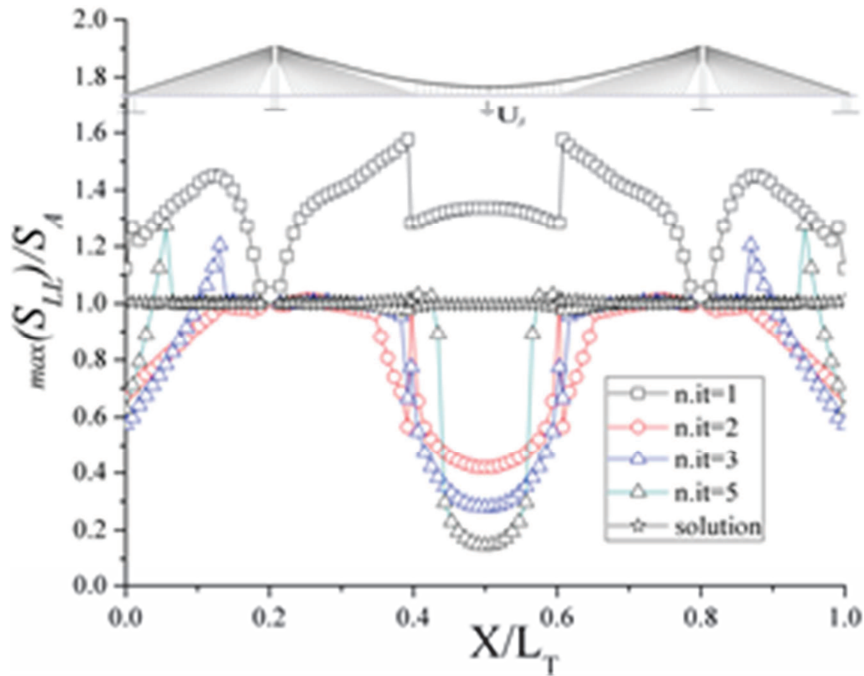


Fig. 2.41 Normalized maximum tensile stresses ( $\max(S_{LL})/S_A$ ) under live loads

Additional results are presented in Fig.2.41, in which tensile stresses in the cables resulting from the ULS combinations are reported as function of the iteration steps. In particular, consistently with the PBA, during the iterations, maximum cable stresses are forced to reach the equality with the allowable strength value. Such condition cannot be reached in the first iterations since initially the conditions regarding the bridge deformability are more restrictive than the ones related to the cable strength. However, once a number of iterations is developed, the cable dimensioning as well as the post-tensioning forces are calibrated to verify such proscriptions.

Finally, in Fig.2.42, the convergence behavior of the solution is investigated, by means of the relationships between the maximum stresses of some cable elements and percentage number of iterations developed by the iterative procedure.

Except for the main cable, whose dimensioning is quite constrained by the displacements prescriptions on bridge deformability, all the cables after a low number of iterations present a stress rate equal to the allowable strength value, reaching, consistently with the PBA, the optimum design.

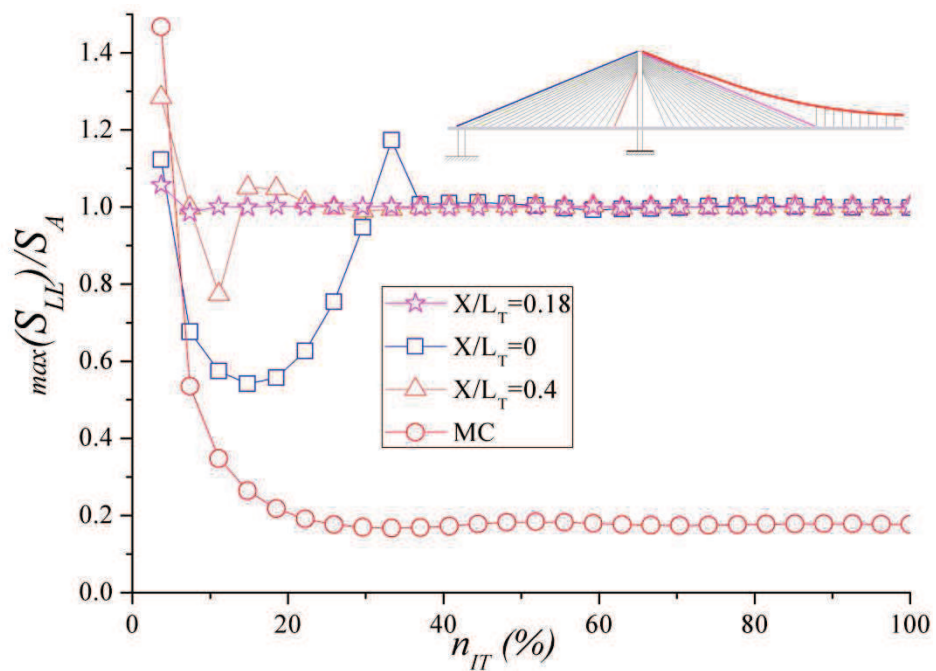


Fig. 2.42 Normalized maximum tensile stresses ( $\max(S_{LL})/S_A$ ) evolution as a function of the percentage value of the iteration steps ( $n_{IT}\%$ )

# 3

## **VULNERABILITY AND FAILURE ANALYSIS OF CABLE SUPPORTED BRIDGES SUBJECTED TO DAMAGE MECHANISMS UNDER THE ACTION OF MOVING LOADS**

### **3.1 Introduction**

Cable supported bridges are affected by several actions, which can be distinguished mainly in direct and induced type ones.

The most frequent direct actions are moving loads, which induced dynamic structural vibrations. Vehicles such as trucks and trains passing bridges at certain speeds will cause dynamic effects, among them global vibration and local hammer effects. The dynamic loads for moving vehicles are considered “impact” in bridge engineering because of the relatively short duration.

The magnitude of the dynamic response depends on the bridge span, stiffness and surface roughness, and vehicle dynamic characteristics such as moving speed. Cable supported bridges are frequently employed in the context of long spans, leading to slender structures. As a results, such external loads are comparable with those involved by the bridge self-weight ones and an accurate description of the effects of the moving loads is needed to properly evaluate dynamic bridge behavior.

At the same time, new developments in rapid transportation systems make it possible to increase the allowable speed range and traffic load capacity. As a matter of fact, during the last years the maximum speed range of train vehicles has grown significantly (Tab 3.1). Consequently, the moving system can greatly influence the dynamic bridge vibration, by means of non-standard excitation modes.











As far as induced actions, damage mechanisms are the most dangerous. As a matter of fact, during their life, cable supported bridges are affected by several damage phenomena, which produce a reduction of the mechanical properties of the bridge constituents. In particular, the cable system is the main structural component which can be subjected to potential damage.

The basic element for all cables to be found in modern cable supported bridges is the steel wire characterized by a considerably larger tensile strength than that of ordinary structural steel. Those wires are cylindrical with a diameter ranging between 3 mm and 7 mm and they have a high-grade of carbon (about 0.8%) and are obtained by cold drawing.

Although the single wire forms the basic element for cables, several wires are often shop-assembled to form pre-fabricated strands, subsequently used in the shop or at the site as basic elements for the construction of the final cable. Cable damage mechanisms are the consequence of the deterioration of the steel wire. Wires of civil engineering cables are submitted to two main damage mechanisms: fretting-fatigue, corrosion or a combination of them.

Such phenomena lead to degradation effects, which may cause a reduction of the stiffness properties or, in extreme cases, the complete failure of a single or multiple cable elements.

Fretting-fatigue is generally observed near the anchorage where the cable is submitted to free bending deformations. Vibrations induced by climatic loads (wind, rain, etc.) and traffic loads can lead to small relative displacements between wires. On the other hand, the possibility of corrosion phenomena is due to the fact that cables are frequently exposed to severe environmental conditions such as marine environment, rain and pollution.

Name	Max Speed	Operator	Image
CRH380A	486 km/h	 <i>Ministry of Railways</i>	
TGV Reseau	379 km/h	 <i>SNCF</i>	
KTX 2	350 km/h	 <i>Korail</i>	
Eurostar	320 km/h	 <i>SNCF</i>	
ETR-500	305 km/h	 <i>Trenitalia</i>	

Tab. 3.1 – High speed train

Although wires are protected against corrosion in several ways such as lubrication and zinc coating, during the cable life such a protection disappear and corrosive solution can penetrate inside the cable. Corrosion deterioration of cable wires takes different forms: stress corrosion cracking, pitting and hydrogen embrittlement.

**Hydrogen embrittlement** is the process by which various metals, most importantly high-strength steel, become brittle and fracture following exposure to hydrogen. Hydrogen embrittlement is often the result of unintentional introduction of hydrogen into susceptible metals during forming or finishing operations and increases cracking in the material (Fig. 3.1). Reduced ductility combined with non-reduced cross-section are suggestive of a brittle regime of fracture. The effect of hydrogenation is mirrored in the reduced ductility of the wire material and not in the effective cross-section area. Hydrogen embrittlement mechanisms involve the ingress of hydrogen into the metal, reducing its ductility and load bearing capacity. Stress below the yield stress of the susceptible material then causes subsequent cracking and catastrophic brittle failures.

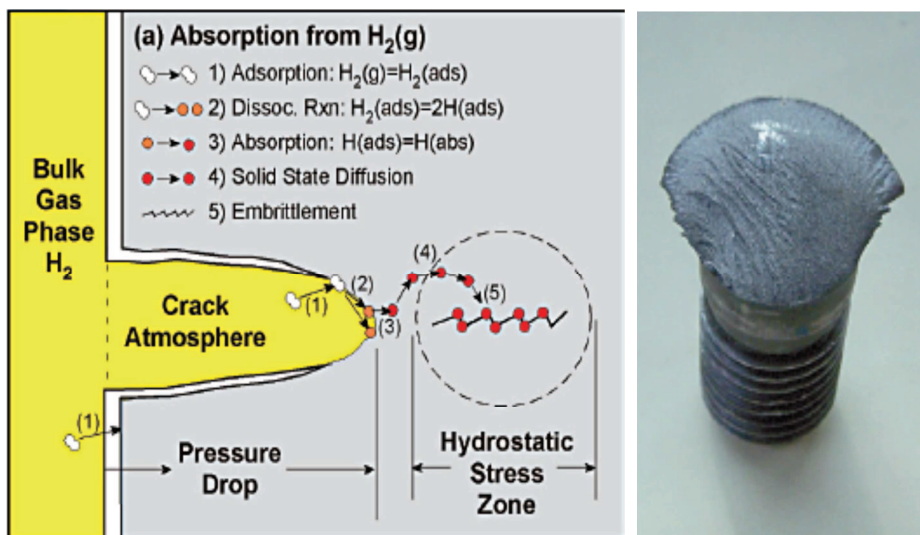
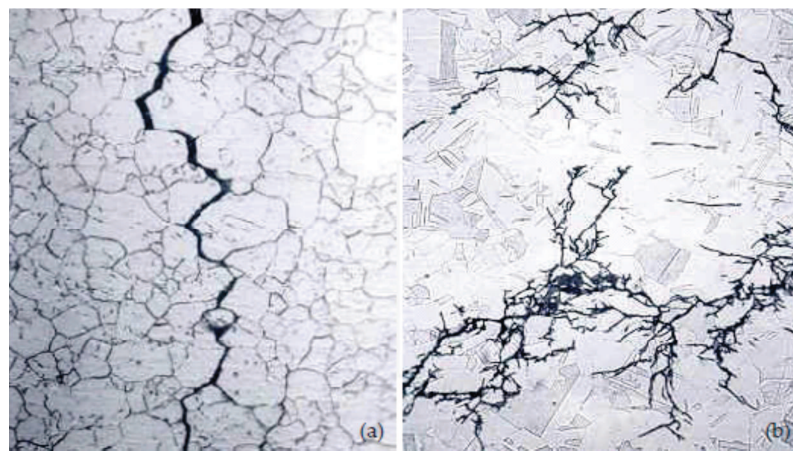


Fig. 3.1 Hydrogen embrittlement mechanisms and failure of a hard chromium-plated chain conveyor bolt

**Stress corrosion cracking** is brittle, practically without material loss, and visible corrosion products. It is normally “river branched” (the crack on the material is similar to a river – the primary crack, and its tributaries – the multibranched secondary ones. The cracks which occur just below the yield strength of the material, and could be intergranular or intergranular as showed in Fig. 3.2.



**Fig.3.2** Stress corrosion cracking propagation: (a) intergranular SCC of an Inconel heat exchanger tube (X500 micrograph); (b) transgranular: the micrograph (X300) illustrates SCC in a 316 stainless steel chemical processing piping system

The chemical environment that causes stress corrosion cracking for a given alloy is often one which is only mildly corrosive to the metal otherwise. Hence, metal parts with severe stress corrosion cracking can appear bright and shiny, while being filled with microscopic cracks. This factor makes it common for stress corrosion cracking to go undetected prior to failure. Stress corrosion cracking often progresses rapidly, and is more common among alloys than pure metals. The specific environment is of crucial importance, and only very small concentrations of certain highly active chemicals are needed to produce catastrophic cracking, often leading to devastating and unexpected failure. Stress corrosion cracking mechanisms begin when materials protecting prestressing strands are inflected (concrete carbonation, chloride ions penetration.).

**Pitting corrosion**, or pitting, is a form of extremely localized corrosion that leads to the creation of small holes in the metal. The driving power for pitting corrosion is the depassivation of a small area, which becomes anodic while an unknown but potentially vast area becomes cathodic, leading to very localized galvanic corrosion (Fig. 3.3). The corrosion penetrates the mass of the metal, with limited diffusion of ions. The mechanism of pitting corrosion is probably the same as crevice corrosion.

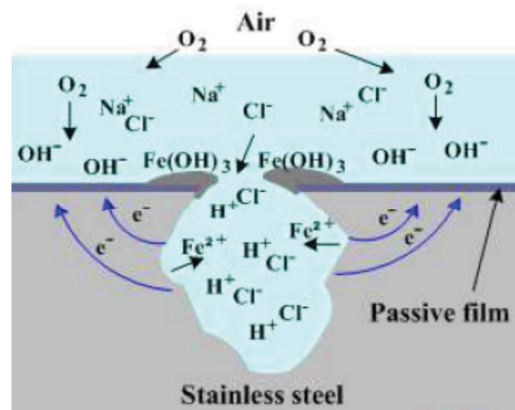


**Fig. 3.3** Pitting corrosion

Inspections on existing cable supported bridges confirms that steel wire had an evolution of the mechanical properties. An example is the Mid-Hudson Bridge which across the Hudson River between Poughkeepsie and Highland in the state of New York (Fig. 3.4).

The Mid-Hudson Bridge, based on a suspension cable system, has a total bridge length of 914.4 meters, with a main span of 455.7 m and side spans of 228.6 m.





**Fig. 3.4** The Mid-Hudson Bridge

Each main cable is composed of 6,080 parallel galvanized cold drawn wires. The individual cable wires were constructed into 19 strands; each containing 320 continuous, endless wires looped around strand shoes at each anchorage. After the wires in each strand were spun and adjusted, the 320 parts were compacted by special hand tongs and seized with tin bands at 1.5 meter intervals. The compacted cables, excluding the protective wire wrapping, are 425 mm in diameter and about 1,000 meters long between anchorages.

The wire was specified to have a modulus of elasticity of 186,000 MPa and a minimum ultimate strength of 1,480 MPa. The first limited inspections of the interior of the cables began in 1969 as part of a general condition inspection of the bridge. Similar inspections were also conducted in 1981 and 1982. These inspections were limited to the exterior wires of the cable and were accomplished by removing the wrapping wires over very short distances.

The 1969 openings indicated little if any corrosion. The areas unwrapped in 1981 and 1982 revealed indications of more active corrosion.

In November 1986, nine main cable locations were selected for unwrapping and examination. These locations were at the low points, near mid-length between low points and the pylons, and in the west anchorage adjacent to the splay castings. One or two plies of wrapping wire were removed over a length of 100 to 350 mm at the locations, to view the outer wires (Fig. 3.5).

White zinc corrosion residue and brown and black steel corrosion residue were found in varying degrees at eight of the nine locations.

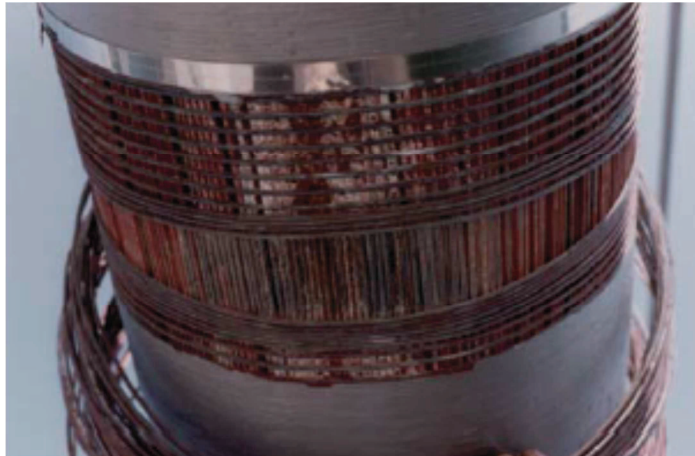


Fig. 3.5 Partial removal of wrapping wires

The exposed wires at the selected location near the mid-point of the south cable in the center span (low point) were observed to be more extensively corroded than the wires at the other locations. As shown in Fig. 3.6, a length of 2.0 m was unwrapped at this location and probed with wooden wedges. Extensive corrosion of the zinc coating was observed on the outer wires between the 2:00 o'clock and 9:00 o'clock positions on the cable perimeter.





**Fig. 3.6** Expanded Inspection area

The most significant wire section loss was observed on the underside of the cable at the location of the black residue formed by the corrosion process.

The visible surfaces of the outer wires on the upper portions of the cables appeared in good condition; however, the red lead coating on the wires was dry and brittle and could be easily brushed from the cable. White zinc oxidation residue from the galvanizing was noted on all visible interior wires at the four positions probed. Some brown steel corrosion residue was noted on interior wires at three of the four positions, but no significant loss of wire section or broken wires was visible.



**Fig. 3.7** – Pitting effect on a wire

There was some minor loss of wire section, in the form of flat spots or "pitting", noted on some of the outer wires Fig. 3.7.

These inspections revealed that corrosion had affected wires throughout the cable cross-section in a non-uniform manner. Deterioration ranged from minor oxidation of the zinc coating on the wires to local depletion of the zinc and steel corrosion causing uniform loss of section in the form of flat spots or local cavities, accompanied by a black corrosion product. Broken wires were discovered both internally and on the cable circumference while unwrapping or driving the wooden wedges.

### 3.1.1 Code prescriptions

Regarding design, existing codes on cable supported bridges recommend verifications of the robustness and the vulnerability of the bridge with respect to extreme and accidental loading conditions.

A moving vehicle on a bridge generates deflections and stresses in the structures that are generally greater than those caused by the same vehicle loads applied statically. The dynamic response is commonly presented in terms of Dynamic Amplification Factors (D.A.F.). These factors suggested to states how many times the static response, of a railway bridge due to moving traffic, must be magnified in order to cover the additional dynamic loads.

Many definitions are used in experimental and numerical studies.

Most frequently, the Dynamic Amplification Factor is defined as a dimensionless ratio of the absolute dynamic response to the absolute maximum static response.

$$\text{Dynamic Amplification Factor (D.A.F.)} = \frac{\text{Absolute Dynamic response}}{\text{Absolute Maximum Static response}}$$

In the American Association of State Highway and Transportation Officials (American Association of State Highway and Transportation Officials,

2007) specifications effects of moving vehicles on bridges are accounted for by a dynamic load allowance,  $IM$ , in addition to static live load (LL):

$$IM = \frac{D_{dyn}}{D_{st}} - 1$$

where  $D_{dyn}$  is the maximum dynamic response for deflection, moment, or shear of the structural members and  $D_{st}$  is the corresponding maximum static response. The total live load effect,  $LL$ , can then be expressed as

$$LL = AF \times D_{st}$$

and

$$AF = 1 + IM$$

where  $AF$  is the amplification factor representing the dynamic amplification of the static load effect and  $IM$  is the impact factor determined by empirical formulas in design codes. Such simplified approach in the design practice avoids any analysis of vehicle induced vibration.

However, the impact effect on bridges by moving vehicles is influenced by factors such as bridge span, stiffness, surface roughness, speed and suspension system of moving vehicles, which lead the impact factor to vary within a large range. In (American Association of State Highway and Transportation Officials, 2007) the impact factor is simply expressed as a function of bridge span

$$IM = \frac{50}{L + 125} \leq 0.30$$

where  $L$  (in ft) is the length of span loaded to create maximum stress.

For railway bridges the ratio of live load caused by moving vehicles such as locomotive and trains to the dead load is mostly higher than that in highway bridges. It can be two cases:

- Percentage of live load for rolling equipment without hammer blow, such as diesels and electric locomotives, etc.,

$$IM = RE + 40 - \frac{3L^2}{1600} \quad \text{if } L < 50 \text{ ft}$$

$$IM = RE + 16 - \frac{600}{L - 30} \quad \text{if } L \geq 80 \text{ ft}$$

- Percentage of live load for steam locomotives with hammer blow:

For beam spans and floor beams	$IM = RE + 40 - \frac{L^2}{500} \quad \text{if } L < 100 \text{ ft}$ $IM = RE + 10 - \frac{1600}{L - 40} \quad \text{if } L \geq 100 \text{ ft}$
For truss spans	$IM = RE + 10 - \frac{4000}{L + 25}$

where  $L$  is the effective span length. Because of the simplicity, the Dynamic Amplification Factor expressions specified in bridge design codes can't characterize the effect of all parameters that influence the dynamic response. However, in order to get a more exact behavior of the dynamic effects, the additional dynamic loads should be determined in a more accurate way. For this reason, the code allows to design high speed railway bridges by means of commercial software programs which take into account resonance effects and other vibration effects in the particular bridge structure.

Similarly, the analysis of the structural response of the bridge structure due to damage mechanisms in the cable system is based on the use of fictitious amplification factors. In particular, verifying the capacity to sustain accidental breakage of cables is an essential requirement within design of cable-supported structures. In order to verify this requirement, codes and guidelines for the design of cable supported structures have traditionally recommended the

analysis of the sudden breakage, or loss, of a cable, through static analysis amplified by a dynamic amplification factor in the range between 1.5 and 2.0. Such approach has been recommended by several associations (Post-Tensioning Institute, 2007; Service d'Etudes Techniques des Routes et Autoroutes, 2001) in their design guidelines for cable-stayed bridges, and that is also proposed implicitly in Eurocode 3 Part 1.11 (The European Committee for Standardisation, 1993) and explicitly in Eurocode 1 Part 1.7 (The European Committee for Standardisation, 2005). More in detail, such approach identifies the undamaged state of the structure which includes possible live loads. In this state, the cable force of the considered cable loss  $T_0$  is calculated. Subsequently, the failed cable is eliminated and it is replaced by corresponding cable force amplified by DAF.

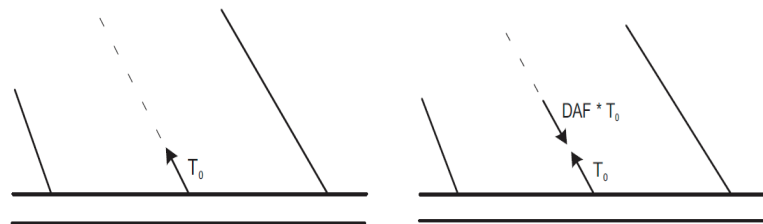


**Fig. 3.8** – The PTI and SETRA method

The stress distribution arising from such a loading scheme is combined with the effects of other existing loading schemes by means of proper factored loading combinations. It is worth nothing that, the PTI Recommendations (Post-Tensioning Institute, 2007) additionally allow the determination of a dynamic amplification factor in a nonlinear dynamic analysis, because it is assumed that, in general, smaller factors can be chosen for cable stayed-bridges. But how this factor is to be determined or which assumptions are to be made are not described.

### 3.2 The proposed analysis model

A numerical model for considering the damage and failure behavior on the cable system is proposed, which can be utilized for obtaining the response of cable supported bridges subjected to moving loads.

Damage and failure phenomena on the cable system elements, produced by preexisting corrosion phenomena or unexpected failure mechanisms, are analyzed by using stationary or time dependent explicit laws, developed in the framework of the Continuum Damage Mechanics theory.

The bridge analysis is developed by using a refined finite element nonlinear geometric formulation, in which the effects of local vibrations on the cable-stayed and suspension systems as well as the influence of large displacements in the girder and pylons are taken into account.

The main aim is to quantify, numerically, the dynamic amplification factors of typical kinematic and stress design variables taking into account the influence of the inertial characteristics of the moving loads, by accounting coupling effects arising from the interaction between girder and moving system. In particular, the effects produced by the moving system characteristics, the pylon typologies, and the failure mode characteristics involved in the cable system are investigated by means of comparisons between damaged and undamaged bridge configurations.

The analysis is performed by means of two different stages.

Initially, a preliminary analysis is devoted to calculating the initial configuration of the bridge structure. Since the loading condition refers to the application of dead loading only, the analysis is developed in the framework of a static analysis.

Once the initial configuration is determined in terms of the initial cable stress and strain distribution, a sequential dynamic analysis is developed starting with all dependent variables evaluated in the previously developed configuration.

In next paragraphs, theoretical formulations relative to damage, moving load and bridge structure will be discussed in detail. Subsequently, numerical implementation will be presented.



### 3.3 Damage formulation

In order to reproduce failure or damage phenomena in the cable system and to perform a dynamic analysis of the bridge structures, a time dependent damage modeling should be implemented.

Among the several approaches available from the literature, the one consistent to the Continuum Damage mechanics (CDM) theory (Sacco & Lebon, 2012; Lemaitre & Desmorat, 2005; Lemaitre & Chaboche, 1994; Wriggers, 2008) is adopted. In particular, the presence of damage mechanisms in the cable system involved by degradation phenomena are supposed to produce a reduction of the cross-section area, on the basis of the following expression (Sacco & Lebon, 2012; Barbero & Lonetti, 2001):

$$\xi_s(s,t) = \frac{C^c A^c(s,t) - \overline{C^c A^c}(s,t)}{C^c A^c(s,t)} \quad (3.1)$$

where  $\xi_s$  is the damage variable,  $S$  is the curvilinear coordinate used to describe the arc-length of the cable,  $C^c A^c$  and  $\overline{C^c A^c}$  are the actual and residual stiffnesses of the cable element, respectively.

In order to investigate not only the presence of preexisting damage produced by long-term effects, but also the influence produced by accidental failure mechanisms due to sudden loss of stiffness, such as the one occurring during a terroristic or vandalism attack and thus is not related to creep damage, Eq. (3.1) has been reviewed introducing the dependence of the time variable.

In particular, according to experimental evidence on the failure mechanisms of cable elements, a one dimensional time dependent formulation based on a Kachanov's law is utilized to describe the dynamic damage variable by the following expressions (Lemaitre & Desmorat, 2005):

$$\xi_d(s,t) = \left[ 1 - \frac{(t-t_0) \left[ 1 - (1-\xi_s)^{m+1} \right]}{t_f} \right]^{1/m+1} \quad (3.2)$$

where  $m$  is asymptotic parameter of the damage evolution and  $(t_0, t_f)$  are the initial and final times describing the failure mechanism (Fig.3.9a).

It is worth noting that Eq.(3.2) corresponds to a damage law whose degradation function from the undamaged state, i.e.  $t=t_0$ , evolves in a generalized way to include different evolutions of the damage curves.

The internal parameter  $m$  basically controls the evolution of the damage function, which is linear for  $m$  equal to zero and convex or concave for positive or negative values of the exponential parameter, respectively. From the practical point of view, the value of the parameter  $m$  in the damage definition is typically assumed close equal to 0.98. The region in which damage phenomena take place is defined in terms of the relative position and extent with respect to the element coordinate system as:

$$\alpha(s,t) = \frac{X_1^\xi + X_2^\xi}{2L_0}, \quad \beta(s,t) = \frac{X_1^\xi - X_2^\xi}{L_0} \quad \text{with } (\alpha, \beta) \in [0,1] \quad (3.3)$$

with  $(X_1^\xi, X_2^\xi)$  define the starting and the final region of the damage region in the damaged element of the cable system, i.e. main cable, hanger or stay, and  $L_0$  is the development of the cable in the initial configuration.

A synoptic representation of the damage constitutive laws and region affected by the damage mechanisms is reported in Fig.3.9 (b).

It is worth noting that the critical damage parameter represents the value corresponding to the occurrence of the complete failure of the cable element, in which the  $i$ -th generic cable element does not have the possibility of transferring any internal stresses from the girder and the pylon and thus can be considered not to produce any significant effects on the global behavior of the bridge.

Moreover, the above formulation cannot be considered in the creep damage framework, since the cable release phenomenon is produced in a short time step and it is concerned to simulate, essentially, an accidental failure in the cable system.

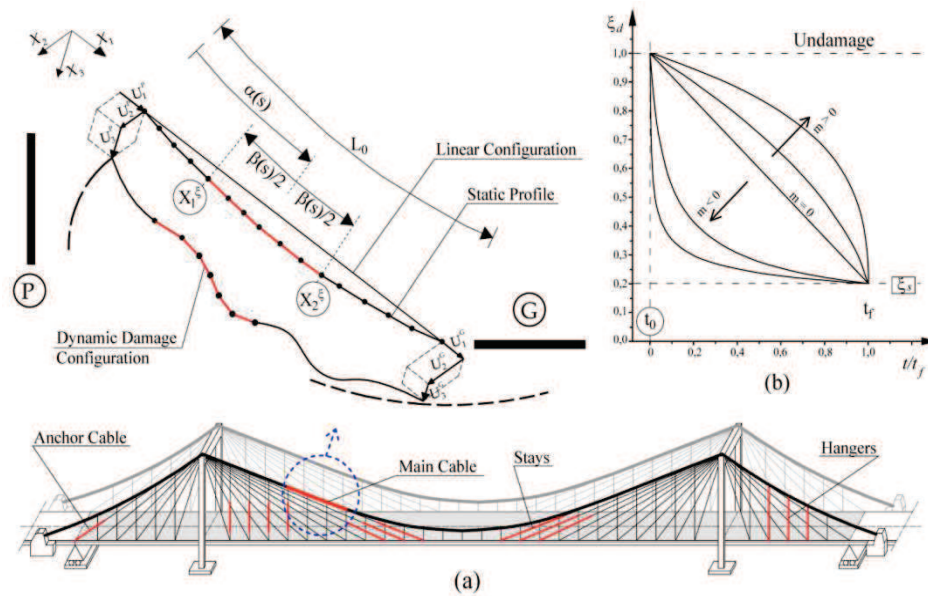


Fig.3.9 Damage definition and regions affected by the damage scenarios

### 3.4 Moving load formulation

The moving loads are described by a vehicle travelling with its own mass on the bridge at constant speed, namely ( $c$ ). In the proposed formulation, since the distance between the vehicle axles is small in comparison to the bridge length, the moving forces are defined by uniformly distributed vertical forces and masses acting on the girder profile at a fixed eccentricity ( $e$ ) with respect to the geometrical axis of the girder.

As a result, the kinematic parameters of the moving system coincide with the ones defined by the girder, neglecting frictional forces arising from the external loads, roughness effects of the girder profile, and local loading distribution produced by railway load components.

However, these assumptions are quite recurrent in the framework of cable supported bridges with long spans, in which, typically, such interaction forces produced by localized dynamic effects are negligible with respect to the global bridge vibration (Xia, Xü, & Chan, 2000).

Moreover, it is assumed that the damping energy is practically negligible. This hypothesis is verified in the context of long span bridges, where it has been proved that the bridge damping effects tend to decrease as span length increases (Kawashima, Unjoh, & Tunomoto, 1993; Yamaguchi & Ito, 1997). Detailed results about the influence of damping effects on DAFs have been presented in (Au, Wang, & Cheung, 2001; Au, Wang, & Cheung, 2002), from which it transpires that the assumption of an undamped bridge system leads to greater DAFs.

As a consequence, the analytic description of the moving mass function ( $\lambda$ ), acting on the girder profile, is defined as

$$\lambda = \lambda(s_1, t) = \lambda_{ML} \overline{H}(s_1 + L_p - ct) \overline{H}(ct - s_1) \quad (3.4)$$

where  $\overline{H}(\cdot)$  is the Heaviside step function,  $L_p$  is the length of the moving loads,  $s_1$  is the referential coordinate located at the left end of the girder cross section (Fig. 3.10) and  $\lambda_M$  is the mass linear density of the moving system.

Moreover, the expression of the moving loads, for a fixed inertial reference frame  $(0, \underline{n}_1, \underline{n}_2, \underline{n}_3)$ , is defined by the weight and the inertial forces produced by the inertial characteristics and the unsteady mass distribution of the moving loads, as follows:

$$p_{s_i} = \lambda g \underline{n}_i \times \underline{n}_3 + \frac{d}{dt} \left[ \lambda \frac{d\dot{\underline{U}}_i^m}{dt} \right] = \lambda g \underline{n}_i \times \underline{n}_3 + \frac{d\lambda}{dt} \frac{d\dot{\underline{U}}_i^m}{dt} + \lambda \frac{d^2\dot{\underline{U}}_i^m}{dt^2}, \quad (3.5)$$

where  $p_{s_i}$ , with  $i=1,3$ , is the  $i$ -th component of the external loads at contact points between moving loads and girder and  $\overline{\underline{U}}^m$  is the moving load kinematic.

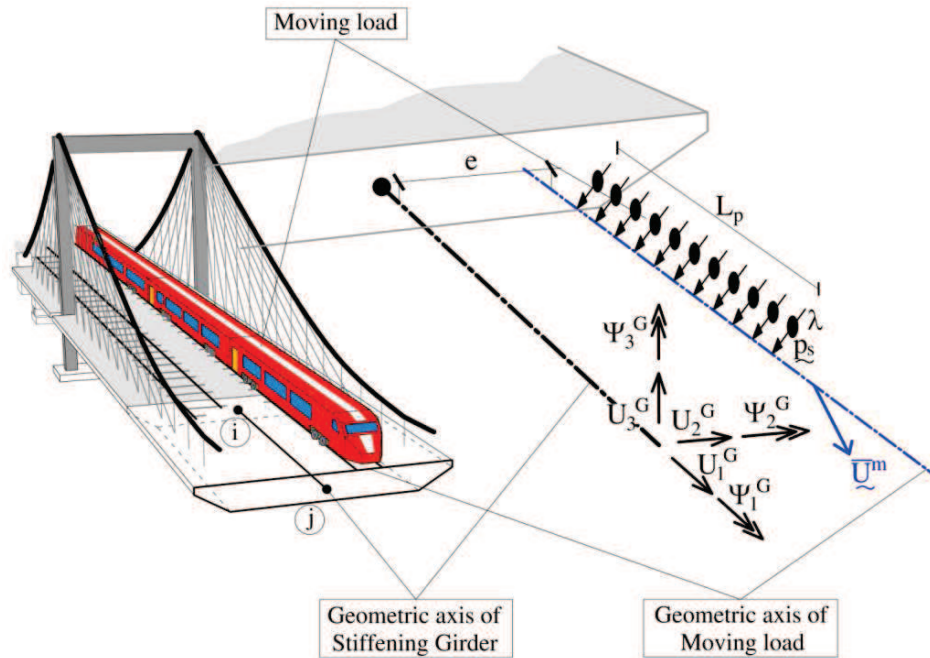


Fig. 3.10 Moving load description and girder kinematic

Since the external forces, defined by Eq.(3.5), are described in terms of a moving coordinate, the time dependent description introduces the following expressions for the velocity and the acceleration functions:

$$\begin{aligned} \frac{d \bar{U}_i^m}{dt} &= \frac{\partial \bar{U}_i^m}{\partial t} + \frac{\partial \bar{U}_i^m}{\partial t} \frac{\partial s(t)}{\partial t} \\ \frac{d^2 \bar{U}_i^m}{dt^2} &= \frac{\partial^2 \bar{U}_i^m}{\partial t^2} + 2c \frac{\partial^2 \bar{U}_i^m}{\partial t \partial s} + c^2 \frac{\partial^2 \bar{U}_i^m}{\partial s^2} \end{aligned} \tag{3.6}$$

where the second and the third terms in the acceleration function are known in the literature as the Coriolis and Centripetal accelerations, respectively (Kwaśniewski, Li, Wekezer, & Małachowski, 2006).

Finally, on the basis of Eq.s (3.4)-(3.5), assuming that the mass does not separate from the beam during its horizontal and vertical vibrations, the external load functions are defined by the following relationships:

$$\begin{aligned}
p_{X_1} &= \frac{d\lambda}{dt} \left[ \left( \frac{\partial U_1^G}{\partial t} - e \frac{\partial^2 U_2^G}{\partial t \partial X_1} \right) \right] + \lambda \frac{\partial^2 U_1^G}{\partial t^2} - \lambda \cdot e \frac{\partial^3 U_3^G}{\partial t^2 \partial X_1}, \\
p_{X_2} &= \frac{d\lambda}{dt} \frac{\partial U_2^G}{\partial t} + \lambda \frac{\partial^2 U_2^G}{\partial t^2}, \\
p_{X_3} &= \lambda g + \frac{d\lambda}{dt} \left[ \left( \frac{\partial U_3^G}{\partial t} + e \frac{\partial \Psi_1^G}{\partial t} \right) + c \left( \frac{\partial U_3^G}{\partial X_1} + e \frac{\partial \Psi_1^G}{\partial X_1} \right) \right] + \\
&+ \lambda \left[ \frac{\partial^2 U_3^G}{\partial t^2} + 2c \frac{\partial^2 U_3^G}{\partial t \partial X_1} + c \frac{\partial^2 U_3^G}{\partial X_1^2} \right] + \lambda \cdot e \left[ \frac{\partial^2 \Psi_1^G}{\partial t^2} + 2c \frac{\partial^2 \Psi_1^G}{\partial t \partial X_1} + c \frac{\partial^2 \Psi_1^G}{\partial X_1^2} \right].
\end{aligned} \tag{3.7}$$

### 3.5 Bridge formulation

In this section the governing equations for the bridge constituents are discussed. In particular, the same treatment will be carried out for girder and pylons.

#### 3.4.1 Girder and pylons

Girder and pylons are consistent with a beam model based on the Euler-Bernoulli formulation, in which large displacements are considered by using Green-Lagrange strain measure.

Moreover, the torsional behavior owing to eccentric loading is described by means of the classical De Saint Venant theory. With reference to Fig. 3.11, the displacements of the cross-section for a generic point located at the  $(X_1, X_2, X_3)$  coordinate along the girder, i.e.  $(\bar{U}_1^G, \bar{U}_2^G, \bar{U}_3^G)$ , are expressed by the following relationships:

$$\begin{aligned}
\bar{U}_1^G(X_1, X_2, X_3, t) &= U_1^G(X_1, t) + \Psi_2^G(X_1, t) X_3 - \Psi_3^G(X_1, t) X_2, \\
\bar{U}_2^G(X_1, t) &= U_2^G(X_1, t), \\
\bar{U}_3^G(X_1, X_2, X_3, t) &= U_3^G(X_1, t) + \Psi_1^G(X_1, t) X_2
\end{aligned} \tag{3.8}$$

where  $(U_1^G, U_2^G, U_3^G)$  and  $(\Psi_1^G, \Psi_2^G, \Psi_3^G)$  are the displacement and

rotation fields of the centroid axis of the girder with respect to the global reference system, respectively.

The constitutive relationships are defined on the basis of moderately large rotations in which only the square of the terms  $U_{i,X_1}^{2G}$  representing the rotations of the transverse normal line in the beam are considered.

Starting from the status concerning the initial configuration in which only dead loading are considered, the following relationships between generalized strain and stress variables are obtained:

$$\begin{aligned}
 N_1^G &= N_1^{0(G)} + C^G A^G \mathcal{E}_1^G \\
 &= N_1^{0(G)} + C^G A^G \left\{ U_{1,X_1}^G + \frac{1}{2} \left[ U_{1,X_1}^{2(G)} + U_{2,X_1}^{2(G)} + U_{3,X_1}^{2(G)} \right] \right\} \\
 M_2^G &= M_2^{0(G)} + C^G I_2^G \chi_2^G \\
 &= M_2^{0(G)} + C^G I_2^G \Psi_{2,X_1}^G \\
 &= M_2^{0(G)} - C^G I_2^G U_{3,X_1 X_1}^G \\
 M_3^G &= M_3^{0(G)} + C^G I_3^G \chi_3^G \\
 &= M_3^{0(G)} + C^G I_3^G \Psi_{3,X_1}^G \\
 &= M_3^{0(G)} + C^G I_3^G U_{2,X_1 X_1}^G \\
 M_1^G &= G^G J_t^G \Theta^G = G^G J_t^G \Psi_{1,X_1}^G,
 \end{aligned} \tag{3.9}$$

where  $C^G A^G$  and  $\mathcal{E}_1^G$  are the axial stiffness and strain,  $\chi_2^G$  and  $\chi_3^G$  or  $C^G I_2^G$  and  $C^G I_3^G$  are the curvatures or the bending stiffnesses with respect to the  $X_2$  and  $X_3$  axes, respectively,  $\Theta^G$  and  $G^G J_t^G$  are the torsional curvature and stiffness, respectively,  $N_1^G$  is the axial stress resultant,  $M_2^G$  and  $M_3^G$  are the bending moments with respect to the  $X_2$  and  $X_3$  axes, respectively,  $M_1^G$  and  $G^G J_t^G$  are torsional moment and girder stiffness, respectively.

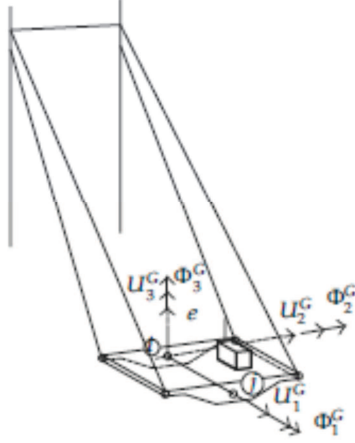


Fig. 3.11 Displacements of the cross-section

On the basis of Eq.(3.9), taking into account of Eq.s (3.4) and (3.7) notation reported in Fig. 3.11, the following governing equations are derived by means of the local form of dynamic equilibrium equations:

$$\begin{aligned}
 \frac{d}{dX_1} \left\{ N_1^G \left( 1 + \frac{dU_1^G}{dX_1} \right) \right\} - \mu_G \ddot{U}_1^G + p_{X_1} &= 0, \\
 -E^G I_2^G \frac{d^4 U_3^G}{dX_1^4} - \mu_G \ddot{U}_3^G - \ddot{\Phi}_{2,X_1}^G I_{02}^G - p_{X_3} &= 0, \\
 E^G I_3^G \frac{d^4 U_2^G}{dX_1^4} - \mu_G \ddot{U}_2^G - \ddot{\Phi}_{3,X_1}^G I_{03}^G + p_{X_2} &= 0, \\
 G^G J_t^G \frac{d^2 \Phi_1^G}{dX_1^2} - (I_{01}^G + \lambda_{ML}^0) \ddot{\Phi}_1^G - p_{X_3} e &= 0
 \end{aligned} \tag{3.10}$$

where  $\lambda_{ML}^0$  is the per unit length torsional girder mass,  $\mu_G$  is the girder mass per unit length.



Additional equations are required to take into account interelement continuity and initial conditions concerned with solving the dynamic problem, which can be expressed with reference to the i-th girder element as follows:

$$\begin{aligned} U_k^G(0) = 0, \dot{U}_k^G(0) = 0, U_k^{i(G)}(0) = U_k^{i-1(G)}(l_e^{i-1}), U_k^G(l_e^i) = U_k^{i+1}(0) \\ \Phi_k^G(0) = 0, \dot{\Phi}_k^G(0) = 0, \Phi_k^{i(G)}(0) = \Phi_k^{i-1(G)}(l_e^{i-1}), \Phi_k^G(l_e^i) = \Phi_k^{i+1}(0) \end{aligned} \quad (3.11)$$

where the superscripts i+1 and i-1 indicate the previous or the next girder elements and the subscript k, with k=1,2,3 define the displacement and rotation directions with respect to the coordinate reference system.

Moreover, the pylon governing equations can be easily obtained from Eq. (3.10), by removing all the terms related to the moving loads and changing the relative variables from with the superscript  $(\cdot)^G$  to  $(\cdot)^P$  and the parameters concerning the mechanical and material characteristics:

$$\begin{aligned} \frac{d}{dX_1} \left\{ N_1^P \left( 1 + \frac{dU_1^P}{dX_1} \right) \right\} - \mu_p \ddot{U}_1^P = 0 \\ -E^P I_2^P \frac{d^4 U_3^P}{dX_1^4} - \mu_p \ddot{U}_3^P - \ddot{\Phi}_{2,X1}^P I_{02}^P = 0 \\ E^P I_3^P \frac{d^4 U_2^P}{dX_1^4} - \mu_p \ddot{U}_2^P - \ddot{\Phi}_{3,X1}^P I_{03}^P = 0 \\ G^P J_t^P \frac{d^2 \Phi_1^P}{dX_1^2} - I_{01}^P \ddot{\Phi}_1^P = 0 \end{aligned} \quad (3.12)$$

### 3.4.2 Cable formulation

The formulation is presented assuming that the cable element is deformed in its initial cable configuration under dead loading, i.e.  $\Omega_c$ , and thus the deformed configuration of the cable due to the application of the live loads can be described by the following additive expression (Fig.3.12):

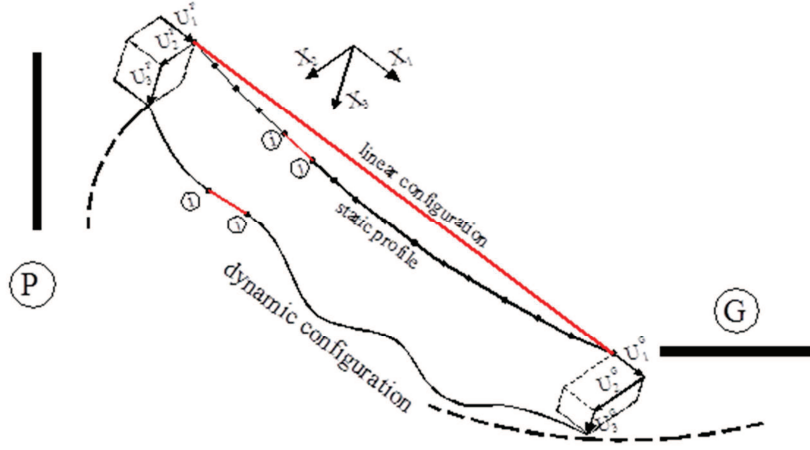


Fig.3.12 Initial and current configurations of the cable, support motion due to girder (G) and pylon (P) deformation.

$$\varphi(\underline{X}, t) = (X_1 + U_1^C(\underline{X}, t))n_1 + (X_2 + U_2^C(\underline{X}, t))n_2 + (X_3 + U_3^C(\underline{X}, t))n_3 \quad (3.13)$$

where the superscript  $(\cdot)^0$  represents, here and in the following, those variables associated to the initial configuration,  $\underline{X}$ , with  $\underline{X}^T = [X_1, X_2, X_3]$ , is the positional vector of the cable with respect to the reference system and  $U_i^C$ , with  $i = 1, 2, 3$ , are the displacement components in the local reference system  $X_i$  described by the basis  $n_i$  of the coordinate system (Thai & Kim, 2011).

Moreover, the constitutive laws of the cable are defined by the second Piola–Kirchhoff stress ( $S_1^C$ ) and Green-Lagrange strain ( $E_1^C$ ) on the basis of the damage description defined by Eq. or Eq., as follows:

$$S_1^C(\underline{X}, t) = S_0^C + C^C [1 - \xi_i(\underline{X}, t)] E_1^C(\underline{X}, t) \quad (3.14)$$

with

$$E_1^C(\underline{X}, t) = U_{1, X_1}^C(\underline{X}, t) + \frac{1}{2} \left[ U_{1, X_1}^2(\underline{X}, t) + U_{2, X_1}^2(\underline{X}, t) + U_{3, X_1}^2(\underline{X}, t) \right]^C \quad (3.15)$$

where  $C^C$  is the elastic modulus,  $S_0^C$  is the stress referred to the initial configuration and  $\xi_i$ , with  $i=d,s$ , refers to the static or dynamic description of damage variable. The governing equations of the motion of a single cable are expressed by means of the following partial differential equations (Warnitchai, Fujino, & Susumpow, 1995):

$$\begin{aligned} \frac{d}{dX_1} \left[ N_1^C + N_1^C \frac{dU_1^C}{dX_1} \right] - b_1 - \mu_c \ddot{U}_1^C &= 0, \\ \frac{d}{dX_1} \left[ N_1^C \frac{dU_2^C}{dX_1} \right] - \mu_c \ddot{U}_2^C &= 0, \\ \frac{d}{dX_1} \left[ N_1^C \frac{dU_3^C}{dX_1} \right] - b_2 - \mu_c \ddot{U}_3^C &= 0 \end{aligned} \quad (3.16)$$

$$\text{with } \begin{cases} b_1 = \mu_G g \cos(\varphi_1) \\ b_2 = \mu_G g \sin(\varphi_2) \end{cases}$$

where  $N_1^C$  is the axial force defined as  $N_1^C = S_1^C A^C$  with  $A^C$  the area of generic  $i$ -th cable element,  $\varphi_1$  and  $\varphi_2$  are the slope angles of the cable along the  $X_1X_2$  and  $X_1X_3$ , respectively,  $b_1$  and  $b_2$  are the body load projections in the  $X_1X_2$  and  $X_1X_3$ , respectively. In addition to Eq.s (3.16), boundary conditions on the cable kinematic are needed to describe the support motion produced by the girder and pylon motion at the corresponding intersection points with the cable development:

$$\begin{aligned} \underline{U}^C(\underline{X}_0) &= \underline{U}^P, \dot{\underline{U}}^C(\underline{X}_0) = \dot{\underline{U}}^P, \\ \underline{U}^C(\underline{X}_c) &= \underline{U}^G, \dot{\underline{U}}^C(\underline{X}_0) = \dot{\underline{U}}^G. \end{aligned} \quad (3.17)$$

where  $\underline{X}_0$  and  $\underline{X}_c$  correspond to the initial and final cross sections of the cable element,  $(\underline{U}^P, \dot{\underline{U}}^P)$  and  $(\underline{U}^G, \dot{\underline{U}}^G)$  are the displacement and speed of the pylon (P) and girder (G), respectively, at the corresponding intersections with the cable development.

### 3.6 Finite element implementation

As a consequence, a numerical approach based on the finite element formulation is utilized. In particular, starting from Eq.(3.10), Eq.(3.12) and Eq.(3.16), the corresponding weak forms for the  $i$ -th finite element related to the girder ( $G$ ), pylon ( $P$ ) and the cable system ( $C$ ), respectively, are defined by the following expressions:

#### Girder

$$\begin{aligned}
& \int_{l_e^i} N_1^G (1 + U_{1,X_1}^G) w_{1,X_1} dX_1 - \mu_g \int_{l_e^i} \dot{U}_1^G w_1 dX_1 - \lambda_{ML} \int_{l_e^i} [-\bar{\delta}_1 + \bar{\delta}_2] \dot{U}_1^G w_2 dX_1 \\
& - \lambda_{ML} \int_{l_e^i} \bar{H}_1 \bar{H}_2 \ddot{U}_1^G w_2 dX_1 - \sum_{j=1}^2 N_{1j}^G U_{1j}^G = 0 \\
& \int_{l_e^i} -M_2^G w_{2,X_1 X_1} dX_1 - \mu_g \int_{l_e^i} \dot{U}_3^G w_2 dX_1 \\
& + I_{02}^G \int_{l_e^i} \ddot{U}_{3,X_1}^G w_2 dX_1 - \lambda_{ML} \int_{l_e^i} [-\bar{\delta}_1 + \bar{\delta}_2] (\dot{U}_3^G + c U_{3,X_1}^G) w_2 dX_1 + \\
& - \lambda_{ML} \int_{l_e^i} \bar{H}_1 \bar{H}_2 \left[ (\ddot{U}_3^G + 2c \dot{U}_{3,X_1}^G + c^2 U_{3,X_1 X_1}^G) + g \right] w_2 dX_1 + \\
& - \sum_{j=1}^2 T_{3j}^G U_{3j}^G - \sum_{j=1}^2 M_{2j}^G \Phi_{3j}^G = 0 \\
& \int_{l_e^i} M_3^G w_{3,X_1 X_1} dX_1 - \mu_g \int_{l_e^i} \dot{U}_2^G w_3 dX_1 + \\
& - I_{03}^G \int_{l_e^i} \ddot{U}_{2,X_1}^G w_3 dX_1 - \lambda_{ML} \int_{l_e^i} [-\bar{\delta}_1 + \bar{\delta}_2] \dot{U}_2^G w_2 dX_1 + \\
& - \lambda_{ML} \int_{l_e^i} \bar{H}_1 \bar{H}_2 \left[ \ddot{U}_2^G + g - e \ddot{U}_{2,X_1}^G \right] w_2 dX_1 + \\
& + \lambda_{ML} e \int_{l_e^i} [-\bar{\delta}_1 + \bar{\delta}_2] \dot{U}_{2,X_1}^G w_2 dX_1 - \sum_{j=1}^2 T_{2j}^G U_{2j}^G - \sum_{j=1}^2 M_{3j}^G \Phi_{2j}^G = 0 \\
& \int_{l_e^i} M_1^G w_{4,X_1} dX_1 - I_{01} \int_{l_e^i} \ddot{\Phi}_1^G w_4 dX_1 + \\
& + \lambda_{ML} \left( e + \frac{\lambda_{ML}^0}{\lambda_{ML}} \right) \int_{l_e^i} \bar{H}_1 \bar{H}_2 \left( \ddot{\Phi}_1^G + 2c \dot{\Phi}_{1,X_1}^G + c^2 \Phi_{1,X_1 X_1}^G \right) w_4 dX_1 + \\
& + \lambda_{ML} \left( e + \frac{\lambda_{ML}^0}{\lambda_{ML}} \right) \int_{l_e^i} [-\bar{\delta}_1 + \bar{\delta}_2] \left( \dot{\Phi}_1^G + c \Phi_{1,X_1}^G \right) w_4 dX_1 - \sum_{j=1}^2 M_{1j}^G \Phi_{1j}^G = 0
\end{aligned} \tag{3.18}$$

Pylon

$$\begin{aligned}
& \int_{l'_e} N_1^P (1 + U_{1,X_1}^P) w_{1,X_1} dX_1 - \mu_p \int_{l'_e} \ddot{U}_1^P w_1 dX_1 - \sum_{j=1}^2 N_{1j}^P U_{1j}^P = 0 \\
& \int_{l'_e} -M_2^P w_{2,X_1 X_1} dX_1 - \mu_p \int_{l'_e} \ddot{U}_3^P w_2 dX_1 \\
& + I_{02}^P \int_{l'_e} \ddot{U}_{3,X_1}^P w_2 dX_1 - \sum_{j=1}^2 T_{3j}^P U_{3j}^P - \sum_{j=1}^2 M_{2j}^P \Phi_{3j}^P = 0 \\
& \int_{l'_e} M_3^P w_{3,X_1 X_1} dX_1 - \mu_p \int_{l'_e} \ddot{U}_2^P w_3 dX_1 - I_{03}^P \int_{l'_e} \ddot{U}_{2,X_1}^P w_3 dX_1 + \\
& - \sum_{j=1}^2 T_{2j}^P U_{2j}^P - \sum_{j=1}^2 M_{3j}^P \Phi_{2j}^P = 0 \\
& \int_{l'_e} M_1^P w_{4,X_1} dX_1 - I_{01}^P \int_{l'_e} \ddot{\Phi}_1^P w_4 dX_1 - \sum_{j=1}^2 M_{1j}^P \Phi_{1j}^P = 0
\end{aligned} \tag{3.19}$$

Cable system

$$\begin{aligned}
& \int_{l'_e} N_1^C (1 + U_{1,X_1}^C) w_{1,X_1} dX_1 - \mu_c \int_{l'_e} \ddot{U}_1^C w_1 dX_1 - \int_{l'_e} b_1 w_1 dX_1 - \sum_{j=1}^2 N_{1j}^C U_{1j}^C = 0 \\
& \int_{l'_e} N_1^C w_{2,X_1} dX_1 - \mu_c \int_{l'_e} \ddot{U}_2^C w_2 dX_1 - \sum_{j=1}^2 T_{2j}^C U_{2j}^C = 0 \\
& \int_{l'_e} N_1^C w_{3,X_1} dX_1 - \mu_c \int_{l'_e} \ddot{U}_3^C w_3 dX_1 - \int_{l'_e} b_3 w_3 dX_1 - \sum_{j=1}^2 T_{3j}^C U_{3j}^C = 0
\end{aligned} \tag{3.20}$$

where  $\bar{H}_1 = H(s_1 + L_p - ct)$ ,  $\bar{H}_2 = H(ct - s_1)$ ,  $\bar{\delta}_1 = \delta(s_1 + L_p - ct)$ ,  $\bar{\delta}_2 = \delta(ct - s_1)$ ,  $\delta(\cdot)$  represents the delta Dirac functions,  $(N_{1i}, T_{2i}, T_{3i}, M_{2i}, M_{3i})^k$  with  $k=C, G, P$  and  $i=1, 2$  represents the internal forces applied at the end node  $i$  of the generic cable (C), girder (G) or pylon (P) element.

Finite element expressions are written starting from the weak forms previously reported, introducing Hermit cubic interpolation functions  $(\xi_i)$  for

the girder and pylon flexures in the  $X_1X_2$  and  $X_2X_3$  deformation planes and Lagrange linear interpolation functions ( $\zeta_i$ ) for the cable system variables and the remaining variables of the girder and the pylons:

$$\begin{aligned}\underline{U}^C(\underline{r}, t) &= \underline{N}^C(\underline{r})\underline{q}^C(t) \\ \underline{U}^G(\underline{r}, t) &= \underline{N}^G\underline{q}^G(t) \\ \underline{U}^P(\underline{r}, t) &= \underline{N}^P\underline{q}^P(t)\end{aligned}\quad (3.21)$$

where  $\underline{q}^C$ ,  $\underline{q}^G$  and  $\underline{q}^P$  are the vectors collecting the nodal degrees of freedom of the cable, girder and pylon respectively,  $\underline{N}^C$ ,  $\underline{N}^G$  and  $\underline{N}^P$  are the matrixes containing the displacement interpolation function for cable element ( $C$ ), girder ( $G$ ) and pylons ( $P$ ),  $\underline{r}$  is the local coordinate vector of the  $i$ -th finite element. The discrete equations in the local reference system of the  $i$ -th element are derived substituting Eq.(3.21) into Eq.s (3.18)-(3.20), leading to the following equations in matrix notation:

$$(\underline{M}_S^G + \underline{M}_{NS}^G)\ddot{\underline{U}}^G + (\underline{C}_S^G + \underline{C}_{NS}^G)\dot{\underline{U}}^G + (\underline{K}_S^G + \underline{K}_{NS}^G)\underline{U}^G = \underline{P}^G + \underline{Q}^G \quad (3.22)$$

$$\underline{M}^P\ddot{\underline{U}}^P + \underline{C}^P\dot{\underline{U}}^P + \underline{K}^P\underline{U}^P = \underline{P}^P + \underline{Q}^P \quad (3.23)$$

$$\underline{M}^C\ddot{\underline{U}}^C + \underline{C}^C\dot{\underline{U}}^C + \underline{K}^C\underline{U}^C = \underline{P}^C + \underline{Q}^C \quad (3.24)$$

where  $\underline{M}_i$  is the mass matrix,  $\underline{C}_i$  is the damping matrix,  $\underline{K}_i$  is the stiffness matrix,  $\underline{P}_i$  is the load vector produced by the dead and live loading,  $\underline{Q}_i$  is the unknown force vector collecting the point sources and the subscripts  $(\cdot)_S$  or  $(\cdot)_{NS}$  refer to standard or nonstandard terms, respectively, introduced in the discrete equations. Most of the matrixes reported in Eq.s (3.22)-(3.24) can be easily recovered from the literature (Yamaguchi and Ito, 1997). Contrarily, the matrixes  $\underline{M}_{NS}$ ,  $\underline{C}_{NS}$  and  $\underline{K}_{NS}$  collect the nonstandard terms arising from the inertial description of the live loads and the interaction behavior between moving loads and bridge motion and are defined by the following expressions:

$$\begin{aligned}
 (M_{NS}^G) &= \int_{l_e} \overline{H_1} \overline{H_2} (N^{G(T)} \underline{\Lambda}_{M_1} N^G) dX_1, \\
 (C_{NS}^G)_{ij} &= \int_{l_e} \left[ (-\overline{\delta}_1 + \overline{\delta}_2) (N^{G(T)} \underline{\Lambda}_{C_1} N^G) + \overline{H_1} \overline{H_2} (N^{G(T)} \underline{\Lambda}_{C_2} N^G) \right] dX_1 \quad (3.25) \\
 (K_{NS}^G)_{ij} &= \int_{l_e} \left[ (-\overline{\delta}_1 + \overline{\delta}_2) (N^{G(T)} \underline{\Lambda}_{K_1} N^G) + \overline{H_1} \overline{H_2} (N^{G(T)} \underline{\Lambda}_{K_2} N^G) \right] dX_1,
 \end{aligned}$$

where the matrixes  $\underline{\Lambda}_{M_1}$ ,  $\underline{\Lambda}_{C_{1,2}}$  and  $\underline{\Lambda}_{K_{1,2}}$ , which assemble the coefficients associated with the inertial contribution arising from the moving loads and girder interaction, are defined as:

$$\begin{aligned}
 \underline{\Lambda}_{M_1} &= \text{diag} [\lambda_{ML}, \lambda_{ML}, \lambda_{ML}, \lambda_{ML} e + \lambda_{ML}^0, 0, 0] \\
 \underline{\Lambda}_{M_1} &= \text{diag} [0, -e\lambda_{ML}, 0, 0, 0, 0] \\
 \underline{\Lambda}_{C_1} &= \text{diag} [\lambda_{ML}, \lambda_{ML}, \lambda_{ML}, \lambda_{ML} e + \lambda_{ML}^0, 0, -\lambda_{ML} e] \\
 \underline{\Lambda}_{C_2} &= \text{diag} [0, 0, 2c\lambda_{ML}, 2c(\lambda_{ML} e + \lambda_{ML}^0), 0, 0] \\
 \underline{\Lambda}_{K_1} &= \text{diag} [0, 0, c\lambda_{ML}, c(\lambda_{ML} e + \lambda_{ML}^0), 0, 0] \\
 \underline{\Lambda}_{K_2} &= \text{diag} [0, 0, c^2\lambda_{ML}, c^2(\lambda_{ML} e + \lambda_{ML}^0), 0, 0]
 \end{aligned} \quad (3.26)$$

In order to reproduce the bridge kinematic correctly, additional relationships to define the connections between girder, pylon and cable system are necessary. In particular, the cable system displacements should be equal to those of the girder and the pylons at the corresponding intersection points; thus, the bridge kinematic is restricted by means of the following constrain equations:

$$U_3^G(X_{C_i}, t) + \Phi_1^G(X_{C_i}, t) b = U_3^C(X_{C_i}, t) \quad (3.27)$$

$$\begin{aligned}
 U_1^G(X_{C_i}, t) - \Phi_3^G(X_{C_i}, t) b &= U_1^C(X_{C_i}, t) \\
 U_1^P(X_P, t) &= U_1^C(X_P, t) \\
 U_2^P(X_P, t) &= U_2^C(X_P, t) \\
 U_3^P(X_P, t) &= U_3^C(X_P, t)
 \end{aligned} \quad (3.28)$$

where  $\underline{X}_{C_i}$  and  $\underline{X}_P$  represent the vectors containing the intersection positions of the  $i$ -th cable element and the pylon top cross section, respectively.

Finally, starting from Eq.s (3.22)-(3.24), taking into account of Eq.s (3.27)-(3.28) as well as the balance of secondary variables at the interelement boundaries, the resulting equations of the finite element model are:

$$\underline{M}\ddot{\underline{Q}} + \underline{C}\dot{\underline{Q}} + \underline{K}\underline{Q} = \underline{P} \quad (3.29)$$

where  $\underline{Q}$  with  $\underline{Q} = \underline{U}_B \cup \underline{U}_G \cup \underline{U}_P$  is the generalized coordinate vector containing the kinematic variables associated with the girder, the pylons and the cable system,  $\underline{M}$ ,  $\underline{C}$  and  $\underline{K}$  are the global mass, stiffness and damping matrixes and  $\underline{P}$  is the loading vector. Since the structural behavior of each element depends on the deformation state of the members, the governing equations defined by Eq.(3.29) will change continuously as the structure deforms. Moreover, the external loads owing to the presence of its own moving mass determine a time dependent mass distribution function on the girder profile. Consequently, the discrete equations are affected by nonlinearities in the stiffness matrix and time dependence in the mass matrix. The governing equations are solved numerically, using a user customized finite element program, i.e. COMSOL Multiphysics TM version 4.1 (COMSOL, 2012). The algebraic equations are solved by using an implicit time integration scheme based on a variable time step-size and backward differentiation formula (BDF). In order to guarantee accuracy in the predicted results, particular attention is devoted to the choice of the time integration step, which, assuming small vibrations about the non-linear equilibrium configuration under dead loads, can be defined as a function of the periods of those vibration mode shapes having a relevant participation on the response. However, in the case of moving load excitation, the dynamic solution strongly depends from the speed of the moving system, since different vibration frequencies are activated for low or large transit speeds (Xia, Xü, & Chan, 2000). In the present analyses, the initial integration time step, which is automatically reduced due to the time adaptation procedure, is assumed as at least 1/1000 of the observation period defined as the



time necessary for the moving train to cross the bridge. Considering the first natural period being the largest one, the integration step turns out to be always lower than 1/100 of the 50th natural period of the bridge structure and thus almost 1/20 of the time to reproduce cable release.

### 3.7 Dynamic amplification factors definition

The purpose of the analysis is to evaluate the amplification effects of the bridge structure produced by the moving load application and damage mechanisms in the cable system. As illustrated above, from the design point of view, existing codes on this argument, i.e. P.T.I. (Post-Tensioning Institute, 2007) and S.E.T.R.A. (Service d'Etudes Techniques des Routes et Autoroutes, 2001) recommend to reproduce the effects of such loading scheme by performing a quasi-static analysis and taking into account of the dynamic amplification effects by means of amplification factors in the range between 1.5–2.0. For this reason, the purpose of the following results is to identify the dynamic amplification effects produced by the cable failure by a using a refined dynamical formulation in place of a simplified quasi-static one.

In particular, in order to quantify the amplification effects produced by the moving loads over the static solution, numerical results are proposed in terms of dynamic amplification factors for undamaged (UD) and damaged (D) bridge structures in terms of the moving loads and the bridge characteristics. It is worth noting that UD configurations refer to a bridge structures, in which cables are not affected by any damage mechanisms. Contrarily, damaged (D) cable system corresponds to bridge configurations, in which one or more cable elements are subjected to the explicit damage mechanism defined on the basis of Eq. (3.2).

The dynamic amplification factors (DAFs) for the generic variable  $X$  under investigation related to damaged or undamaged structural configuration, namely  $\Phi_X^D$  and  $\Phi_X^{UD}$  are defined by the following relationships:

$$\Phi_X^D = \frac{\max(X^D, t=0..T)}{X_{ST}^D}, \quad \Phi_X^{UD} = \frac{\max(X^{UD}, t=0..T)}{X_{ST}^{UD}}, \quad (3.30)$$

where  $T$  is the observation period and the subscript  $(\bullet)_{ST}$  refers to the value of the variable determined in a static analysis. Moreover, an additional description of the DAF is proposed to quantify the relationship between damaged and undamaged configurations by means of the following expression:

$$\Phi_X^{D-UD} = \frac{\max(X^D, t=0..T)}{X_{ST}^{UD}} \quad (3.31)$$

It is worth noting that the formulation of the DAF defined by Eq.(3.31) characterizes the dynamical amplification effects of the investigated variable with respect to the static response in the undamaged structural configuration of the bridge. This parameter can be useful for design purpose, since when this kind of DAF is known in advance the designer is able to control the amplification effects of a generic bridge variable due to the combined action produced by the failure mechanism and the inertial forces, avoiding the analysis suggested by the existing codes on the argument (Post-Tensioning Institute, 2007; Service d'Etudes Techniques des Routes et Autoroutes, 2001). Moreover, an additional description of the DAFs is reported in the results is defined according to the relationship recommended by the PTI codes (Post-Tensioning Institute, 2007):

$$\Phi_\Gamma^{PTI} = \frac{\max(\Gamma^D, t=0..T) - \Gamma_{ST}^{UD}}{\Gamma_{ST}^D - \Gamma_{ST}^{UD}} \quad (3.32)$$

where  $\Gamma_{ST}^{UD}$  is the static value of the variable before its failure evaluated the combination of ALS. Finally, In order to quantify, numerically, the vulnerability of a bridge component, a dimensionless parameter, ranging from 0 to 1, is defined as the reduction ratio of the load multiplier from the undamaged to the damaged configurations:

$$V_I = \frac{\Gamma_{UD} - \Gamma_D}{\Gamma_{UD}} \quad (3.33)$$

where  $\Gamma_{UD}$  and  $\Gamma_D$  are the loading carrying capacities with respect to the allowable quantity before and after an unpredictable damage mechanism.

### 3.8 Results

The investigation is devoted to analyze the dynamic behavior of bridge structures subjected to moving load and affected by damage mechanisms in the cable system, which can consist in an accidental failure or an partial damage.

To this end, two sets of results are proposed: at first, results are proposed to investigate the behavior of cable-stayed bridge subjected to an accidental failure in the cable system. Sensitivity analyses of typical design bridge variables as well as effects produced by the moving system characteristics, pylon typologies and the failure mode characteristics involved in the cable system are investigated by means of comparisons between damaged and undamaged bridge configurations. The first set of results aims to reproduce damage cases treated by P.T.I. and S.E.T.R.A. (Post-Tensioning Institute, 2007; Service d'Etudes Techniques des Routes et Autoroutes, 2001) and, as a consequence, is useful to check the accuracy and effectiveness of the suggested simplified method. Subsequently, comparisons with bridge schemes based on hybrid cable-stayed suspension, pure cable-stayed and suspension cable system are proposed.

The study is conducted with the purpose of investigating the vulnerability of the structure against damage and complete failure phenomena produced in the cable system by means of comparisons between damaged and undamaged bridge configurations. In particular, the enhanced properties of the hybrid cable-stayed suspension bridges are point out, also in the light of existing codes on cable supported bridges.

### 3.7.1 Investigation on cable-stayed bridges subjected to an accidental failure in the cable system

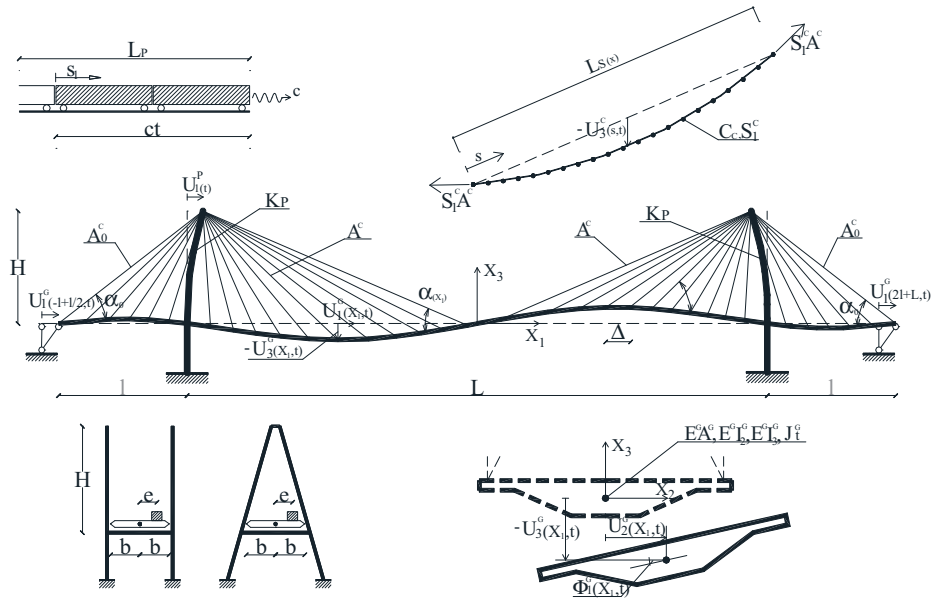


**Fig. 3.13** Cable-stayed bridge scheme: bridge kinematic, pylons, girder and cable system characteristics.

The study is developed by using dimensionless parameters, which are typically utilized to identify the structural and mechanical properties of a long-span bridge and moving loads. The bridge scheme reported in Fig. 3.13 is considered. It is consistent with a fan-shaped and a self-anchored cable-stayed bridge scheme in which pylons refer to A- or H-shaped typologies.

The bridge and moving load dimensioning is selected in accordance with the values utilized in practical applications and due, mainly, to both structural and economic reasons. The cross-section stay areas are designed according to Eq. (1.11) and Eq. (1.12) whereas, the post-tensioning cable forces are defined by the zero displacement method, illustrated in chapter 1. Moreover, aspect ratio, pylon stiffness, allowable cable stress and bridge and moving loads characteristics are assumed as equal to the following representative values

(Bruno, Greco, & Lonetti, 2008; Bruno, Greco, & Lonetti, 2009; Gimsing & Georgakis, 2012; Troitsky, 1988):

Bridge Geometry

$$\frac{L}{2H}=2.5, \frac{\ell}{H}=5/3, \frac{L}{\Delta}=\frac{1}{100}, a=\left(\frac{\gamma^2 H^2 E^C}{12\sigma_g^3}\right) \quad (3.34)$$

Girder and Pylon

$$\frac{I_2^G}{I_3^G}=\frac{1}{10}, \frac{I_{02}^G}{I_{03}^G}=\frac{1}{10}, \frac{J_t^G}{A^2}=100, \frac{I_2^P}{I_3^P}=\frac{1}{10}, \frac{E^{G,P}}{C^C}=1 \quad (3.35)$$

$$\varepsilon_F=\left(\frac{4I_2^G\sigma_g}{H^3g}\right)^{1/4} \quad \frac{K_P}{g}=50 \quad (3.36)$$

Moving Loads

$$\frac{\lambda_{ML}^0}{\mu_G b^2}=1, \frac{\lambda_{ML}}{\mu_G}=1, \frac{p}{g}=1, \frac{e}{b}=0.5 \quad (3.37)$$

Cable System

$$\frac{A_0^C E^C}{gL}=100, \tau_0=\frac{ct_0}{L}, m=1, \frac{\sigma_a}{C^C}=\frac{7.2E8}{2.1E11} \quad (3.38)$$

where  $H$  is the pylon height  $C^C$  is the modulus of elasticity of the cable,  $K_P$  is the in plane flexural top pylon stiffness,  $b$  is half girder cross section width,  $t_0$  is the initial time in which the damage mechanism starts the degradation effects,  $\tau_0$  is the normalized failure time and  $m$  is the parameter which controls the time evolution of the damage curve.

At first, the failure condition, located at the girder/cable intersection, is supposed to be produced in one anchor stay, located laterally to the longitudinal axis of the girder. The time of the failure mode is assumed to be consistent with values typically observed in experimental tests, whose representative value in

the computations is assumed to be 0.005 sec (Service d'Etudes Techniques des Routes et Autoroutes, 2001). It is worth noting that additional analyses, not reported for the sake of brevity, show that the influence of the failure time step on the dynamical amplification factors is practically negligible and within 8% up to very high moving load speeds, i.e.  $c = 160$  m/s. Moreover, in this preliminary analysis it is assumed that the failure of the stay starts when the moving load front reaches the midspan, i.e.  $t_R = c/l + L/2$ . This configuration can be considered as an average value with respect to the position which assumes the moving system on the bridge development, and will be taken as reference in the subsequent developments, in which different instants where failure starts are considered. The behavior of the bridge is analyzed to investigate the relationship between dynamic amplification factors (DAFs) and the normalized speed parameter of the moving system, i.e.

$$\Theta = c \left( \frac{\mu_G \sigma_g}{E^G gH} \right)^{1/2} \quad (3.39)$$

as a function of the pylon topology and the moving mass schematization.

Moreover, the dynamic response of the bridge is evaluated by means of comparisons between damaged (D) or undamaged bridge (UD) structures.

The results, reported in Figs 3.14, 3.15, 3.16 and 3.17, are defined through the relationships between moving system normalized speed and dynamic amplification factors for the midspan vertical displacement and bending moment. Nevertheless, the DAF evolution curves denote a tendency to increase with the speeds of the moving system. The results show that the DAFs developed for bridge structures affected by a failure mechanisms in the cable system are, typically, larger than those obtained assuming undamaged bridge configurations. Moreover, underestimations in the DAF predictions are observed in those cases, in which the inertial contributions arising from the external moving mass are completely neglected.

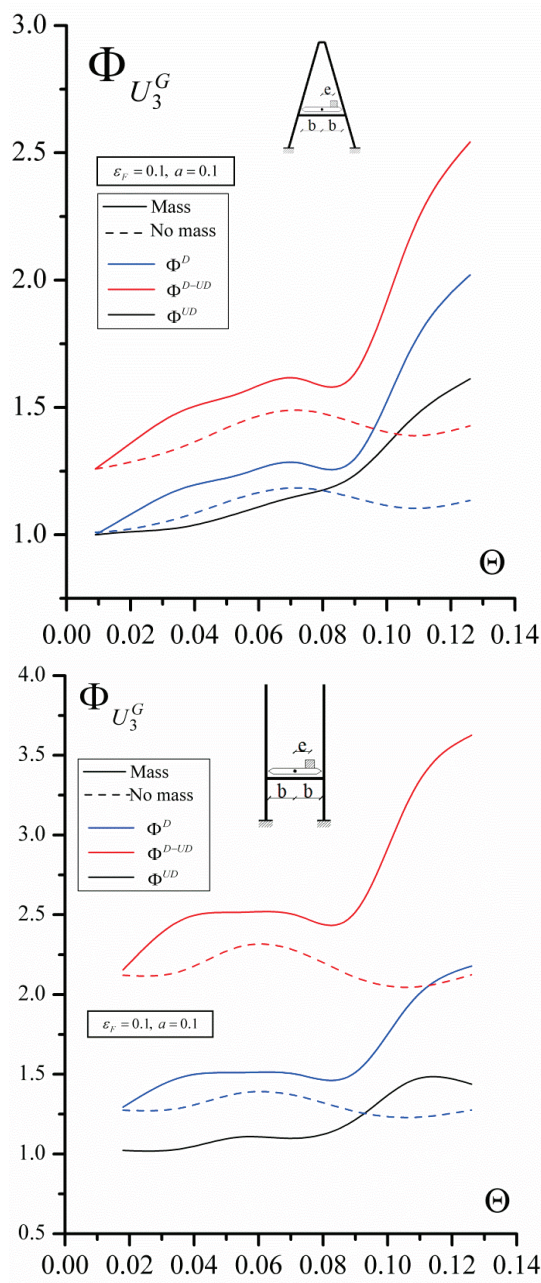


Fig.s 3.14-3.15: Dynamic amplification factors of the midspan vertical displacement as a function of the normalized speed parameter: effect of the failure mechanism, moving load schematization and pylon typology.

The analyses presented above in terms of the DAFs  $\Phi_X^{D-UD}$  for both the damaged and undamaged configurations, point out that bridge structures with A or H shaped typologies undergoing damage are characterized by large dynamic amplifications with respect to the undamaged case. As a matter of fact, the ranges of maximum value of the DAFs increase from [1.47-1.52] in the undamaged configuration to [2.5-3.6] in the damaged one for the midspan displacement, and similarly from [2.5-4.5] to [5.4-8.3] for the midspan bending moment. It is worth noting that the DAFs from the undamaged bridge configuration are affected by large amplifications, especially for the variables concerning the bending moments. This behavior can be explained in view of the prevailing truss behavior of the structure and the nonstandard inertial forces arising from the moving load application, which produce larger bending moments with respect to the ones obtained in the static configuration (Bruno, Greco, & Lonetti, 2009). For all investigated cases, the bridge structures based on H-shaped pylon topology are affected by larger dynamic amplifications than those structures based on A-shaped pylon.

This behavior can be explained in view of the differences in the cable stress distribution between undamaged and damaged structures. In particular, the H-shaped pylon bridges with respect to the A-shaped ones, owing to the failure of the lateral anchor stay, are affected by an unbalanced distribution of the internal stresses in the cable system, which produce larger torsional rotations and vertical displacements of the pylon and the girder, respectively.

To this aim, in Fig. 3.18(a), a comparison of A- and H-shaped pylons in terms of the DAFs  $\left(\Phi_{\Phi_1^G}\right)$  and maximum observed value of the torsional rotation  $\left(\overline{\Phi}_1\right)$  at the midspan cross section is reported.

These results show how the H-shaped pylons are much more affected by the investigated failure condition than the A-shaped pylons, since larger torsional rotations of the pylon and the girder are expected. In Fig. 3.18(b), a synoptic representation of this deformation scheme affecting H-shaped pylon bridges is reported.



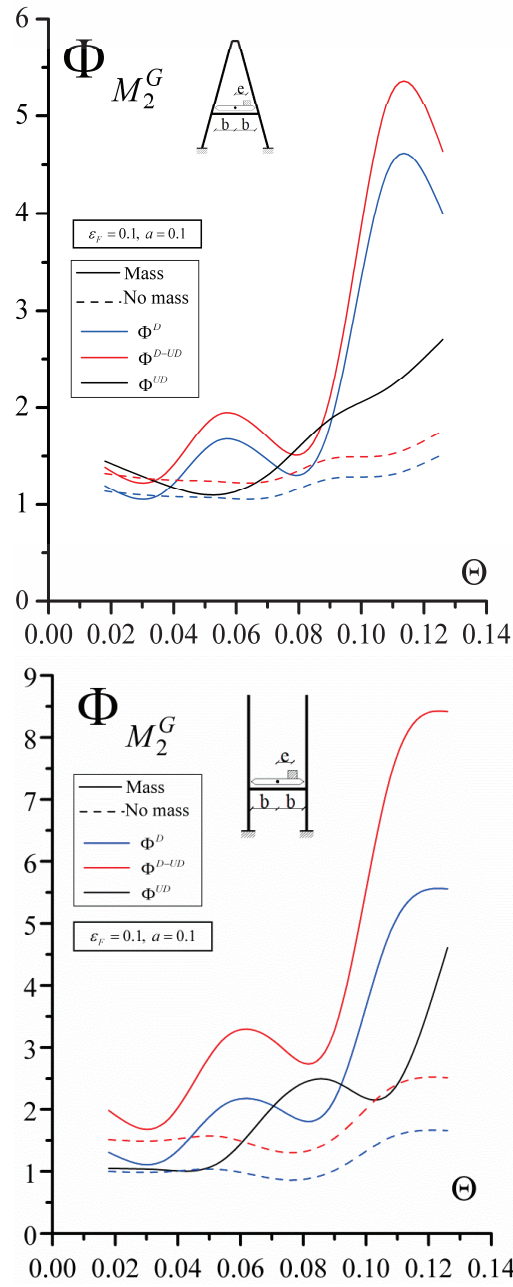


Fig.s 3.16-3.17: Dynamic amplification factors of the midspan bending moment as a function of the normalized speed parameter: effect of the failure mechanism, moving load schematization and pylon typology.

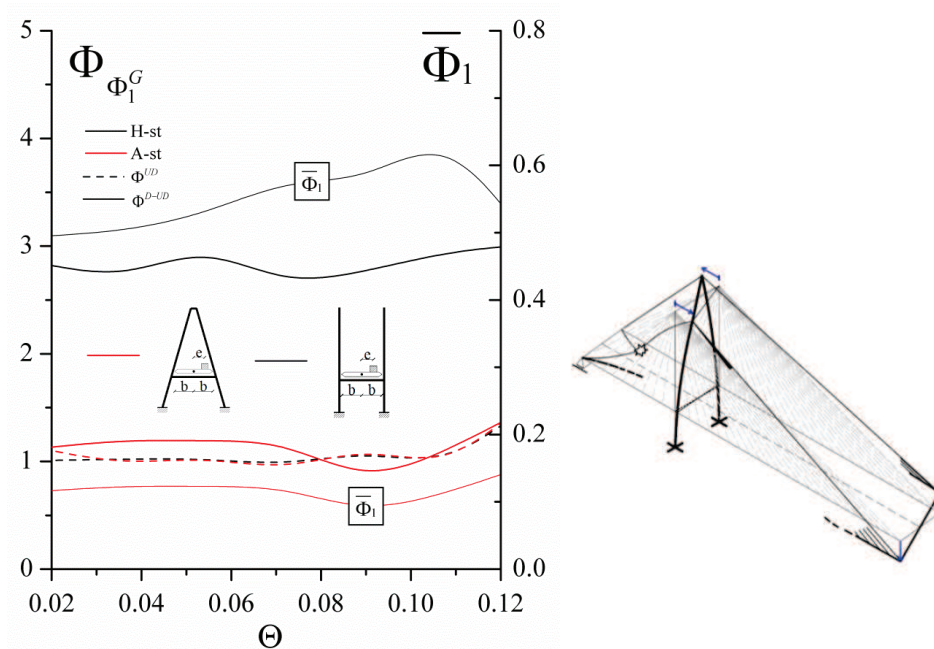


Fig.9: a) Dynamic amplification factors and maximum value of the midspan torsional rotation as a function of the normalized speed parameter  $\vartheta$ . b) Schematic deformation produced by the failure mechanism.

Finally, the influence of the failure mode characteristics on the DAFs, concerning the position which the moving system assumes on the bridge development is investigated. In particular, for a fixed value of the moving system speed, i.e.  $\vartheta=0.102$ , analyses are developed in terms of normalized failure time  $\tau_0$ . The analyzed cases correspond to failure modes in which the moving load front is located at the entrance, the exit configurations or at specified positions on the bridge development, i.e.:

$$\frac{X_1}{L} = \left[ \frac{l}{L}, \frac{l+L/2}{L}, \frac{l+L}{L}, \frac{2l+L}{L} \right]$$

The results are reported in Tab. 3.2 and Tab 3.3 in terms of DAFs of the midspan vertical displacement and bending moment, show how the dynamic

behavior is quite influenced by  $\tau_0$  variable, since from a numerical point of view the values of the DAFs change, significantly, in the investigated ranges.

Moreover, the results show that DAFs for damaged structures, much more for H-shaped pylon bridges, are typically larger than those evaluated for undamaged bridge cases.

$\tau_0$	H-shaped pylon			A-shaped pylon		
	$\Phi^D$	$\Phi^{D-UD}$	$\Phi^{UD}$	$\Phi^D$	$\Phi^{D-UD}$	$\Phi^{UD}$
0.00	6.26	9.48	2.81	5.85	6.84	3.24
0.50	5.89	8.92	2.81	5.49	6.42	3.24
0.87	7.52	11.39	2.81	6.10	7.13	3.24
1.25	6.45	9.77	2.81	6.20	7.25	3.24
1.62	4.82	7.30	2.81	5.84	6.82	3.24
2.00	5.67	8.58	2.81	5.33	6.23	3.24
2.50	1.38	2.09	2.81	3.26	3.81	3.24

**Tab. 3.2** DAFs of the midspan bending moments as a function of the normalized time of failure on the bridge development comparisons in terms of A and H shaped

$\tau_0$	H-shaped pylon			A-shaped pylon		
	$\Phi^D$	$\Phi^{D-UD}$	$\Phi^{UD}$	$\Phi^D$	$\Phi^{D-UD}$	$\Phi^{UD}$
0.00	1.973	3.046	1.451	1.62	2.03	1.60
0.50	1.890	2.918	1.451	1.58	1.98	1.60
0.87	2.032	3.137	1.451	1.75	2.20	1.60
1.25	2.096	3.237	1.451	1.72	2.15	1.60
1.62	2.264	3.495	1.451	1.61	2.02	1.60
2.00	2.238	3.456	1.451	1.65	2.07	1.60
2.50	0.940	1.451	1.451	1.26	1.59	1.60

**Tab 3.3** DAFs of the midspan vertical displacements as a function of the normalized time of failure on the bridge development comparisons in terms of A and H shaped

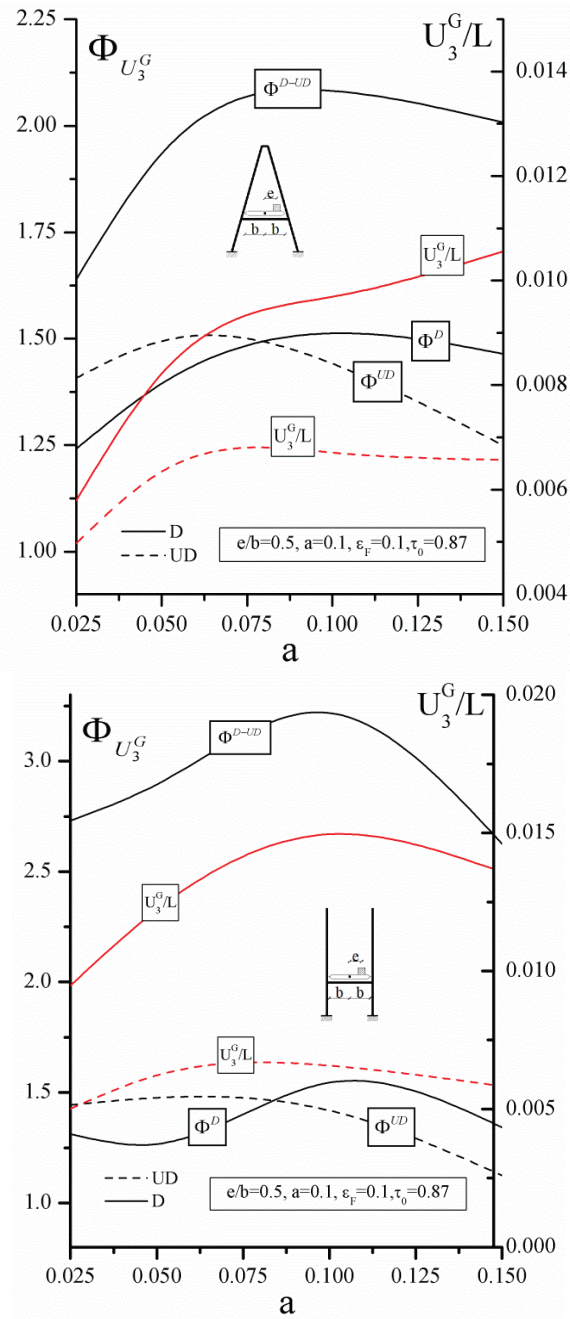


**Fig.s.3.19-3.20** Dynamic amplification factors of the midspan vertical displacement for damage and undamaged bridge structures as a function of the bridge size parameter  $a$ .

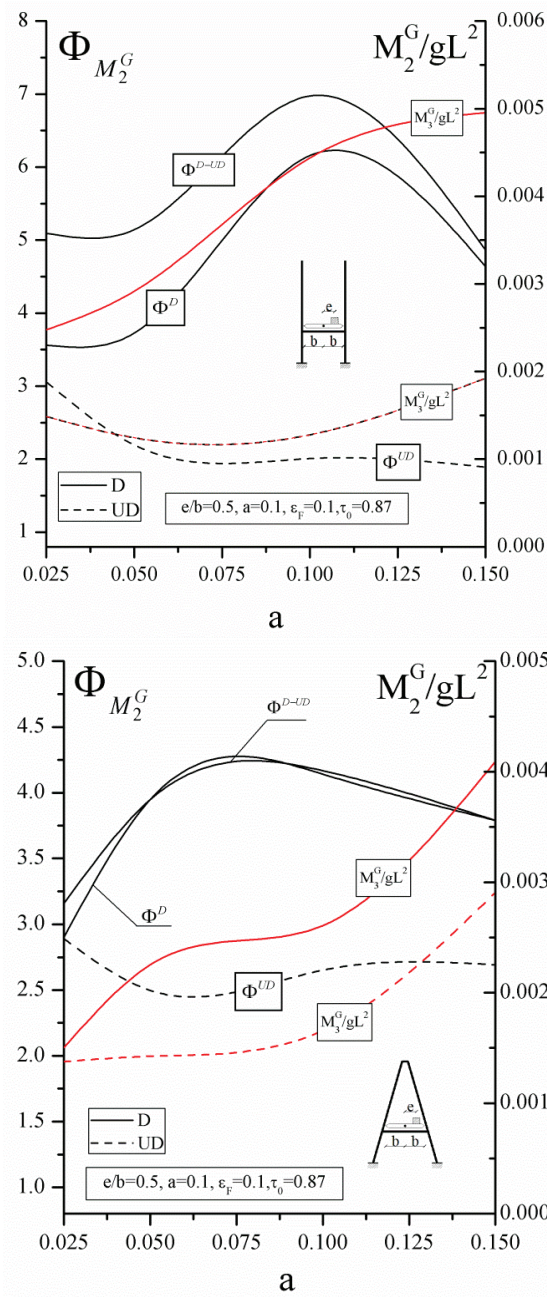


Fig.s 3.21-3.22 Dynamic amplification factors of the undamaged anchor stay axial stress: for damage and undamaged bridge structures as a function of the bridge size parameter a.

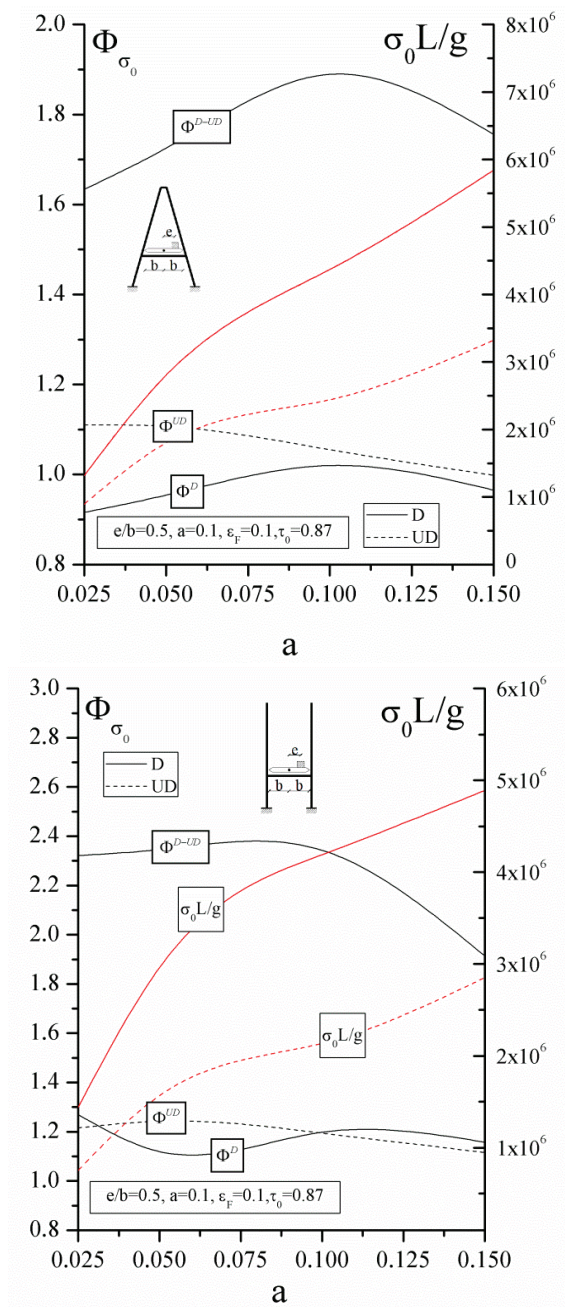


Fig.s 3.23-3.24 Dynamic amplification factors of the undamaged anchor stay axial stress: for damage and undamaged bridge structures as a function of the bridge size parameter a.

Additional results are developed to investigate the effects of the bridge geometry on the DAFs and on the maximum values of typical bridge design variables for both damaged and undamaged bridge configurations.

In particular, results are proposed in terms of the dimensionless parameter  $a$ , which describes the bridge size characteristics of the structure, and refer to a failure mechanism involving the complete failure of one lateral anchor stay of the cable system. The analyzed structures are consistent with a long-span bridge geometry, whose main span length varies from 500 to 1300 m and thus with a total length of the bridge between 900 m and 2100 m.

The results, reported in Figs. 3.19-3.24 concerning the undamaged configurations, show a tendency to decrease with increasing values of the bridge size variable. Contrarily, for damaged structures, the DAFs as well as the maximum values of the investigated kinematic and stress parameters display an oscillating behavior and some local peaks in curve development.

The comparisons between damaged or undamaged bridge structures in terms of the pylon typology show, essentially, that H-shaped pylon structures are much more affected by damage failure. As a matter of fact, the DAFs defined by the ratios between dynamic damage value and the corresponding undamaged static quantity, i.e.  $\Phi_X^{D-UD}$ , show that, for the analyzed cases regarding H-shaped pylon typology, the displacements or the bending moments are typically greater than the bridge structures based on A-shaped pylon typology.

Similar conclusions can be drawn in terms of the maximum values of the observed variables. In particular, the comparisons between damaged and undamaged bridge behavior indicate that the A-shaped pylon is able to reduce the increments produced by the failure mechanism, since the ratios defined in terms of displacements or bending moments are equal to 1.57 and to 1.66, respectively.

Contrarily, the results concerning H-shaped pylon denote that the undamaged variables are amplified with respect to factors equal to 2.2 and 2.5 for displacement and bending moments, respectively. A different behavior is observed with regard to the axial stresses of the undamaged anchor stay.

In particular, the results reported in Figs 3.23-3.24, show that the H-shaped pylon bridges are affected by higher DAFs but lower maximum stresses with respect to the bridge structures based on A-shaped pylons.

Finally, the behavior of the cable-stayed bridges is analyzed in terms of the failure mode, which affects the bridge structure. In particular, for both H or A-shaped pylon typologies, different damage mechanisms on the cable system are supposed on the cable system and the effects on the bridge structures is examined. The failure conditions, reported in Fig.3.25, are supposed to produce the complete collapse of the lateral anchor stay (Mode A) or the last three stays on both sides of the central part of the main span (Mode B).

Additional modes of failure, concerning the damage to a number of internal stays of the cable system, are also investigated. However, since they do not produce any relevant effect on the investigated variables, for the sake of brevity, they are not discussed. The analyses are developed involving a typical geometry of the bridge structure, which is consistent with a long-span bridge-based typology.

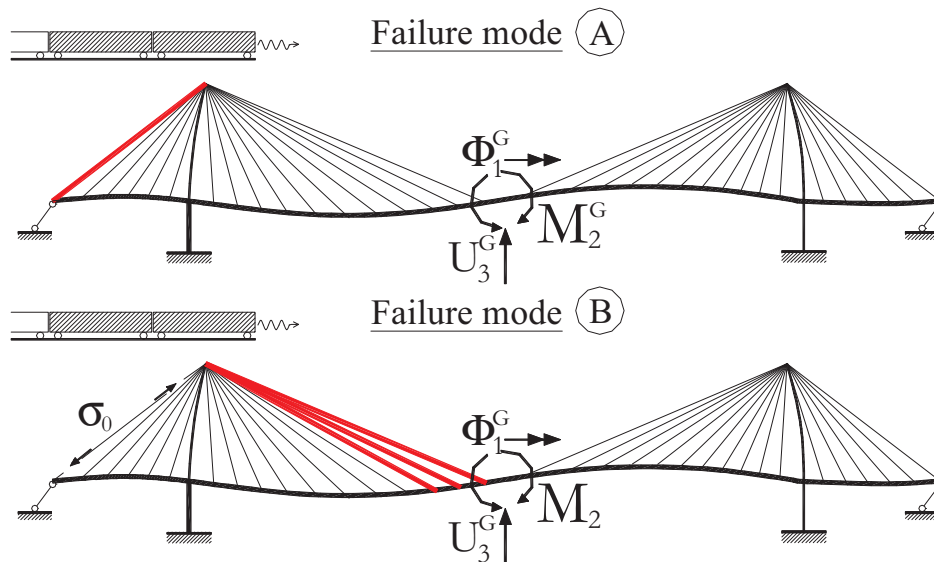


**Fig.3.25** Synoptic representation of the failure modes: A) failure in the lateral anchor stay, B) failure in the central part of the cable system.



The results, reported in Figs 3.26-3.31, are proposed by means of comparisons of damaged and undamaged behavior, in terms of time histories and DAFs of the following cinematic and stress quantities:

- midspan displacements along  $X_3$  axis of the girder, midspan torsional rotation of the girder;
- bending moment in the  $X_1X_3$  plane of the girder and undamaged anchor stay axial stress.

The analyses are developed for a fixed transit speed of the moving system, whereas the failure mechanism is supposed to begin when the moving system front reach the midspan of the bridge, i.e.  $\Theta = 0.102$  and  $\tau_0 = 0.87$ , respectively.

The results show that the larger amplification effects on the vertical midspan displacement are obtained for the case in which the mode of failure affects the lateral anchor stay of the cable system, i.e. mode A.

In this context, the vertical displacements from the undamaged bridge configuration are significantly amplified with respect to a multiplicative factor equal to 1.48 or to 2.28 for the A- or H-shaped pylon topologies, respectively.

Moreover, the DAFs for the investigated configurations are equal to 1.45 or 1.94, whereas the DAFs defined as the ratio between D on the UD quantities, i.e.  $\Phi_{U_3^G}^{D-UD}$ , are equal to 2.1 or to 3.2 for the respectively.

The results concerning the bending moments indicate that the greater effects are produced by the damage mechanism affecting the central part of the cable system, i.e. mode B. In this context, the increments of the bending moments with respect to the undamaged values are equal to 3.2 or 4.1 for bridge configurations based on H- or A-shaped pylon topology, respectively.

Moreover, the maximum DAFs are equal to 4.63 and 8.19 for A- and H-shaped pylon topologies, respectively, and both of them refer to a damage condition involving the failure of the anchor stay. It is worth noting that the results concerning the cases of undamaged bridge structures based on A- or H-shaped pylons denote, essentially, the same prediction on the investigated variables. Contrarily, when damage mechanisms affect the cable system, notable amplifications of the investigated parameters are observed.

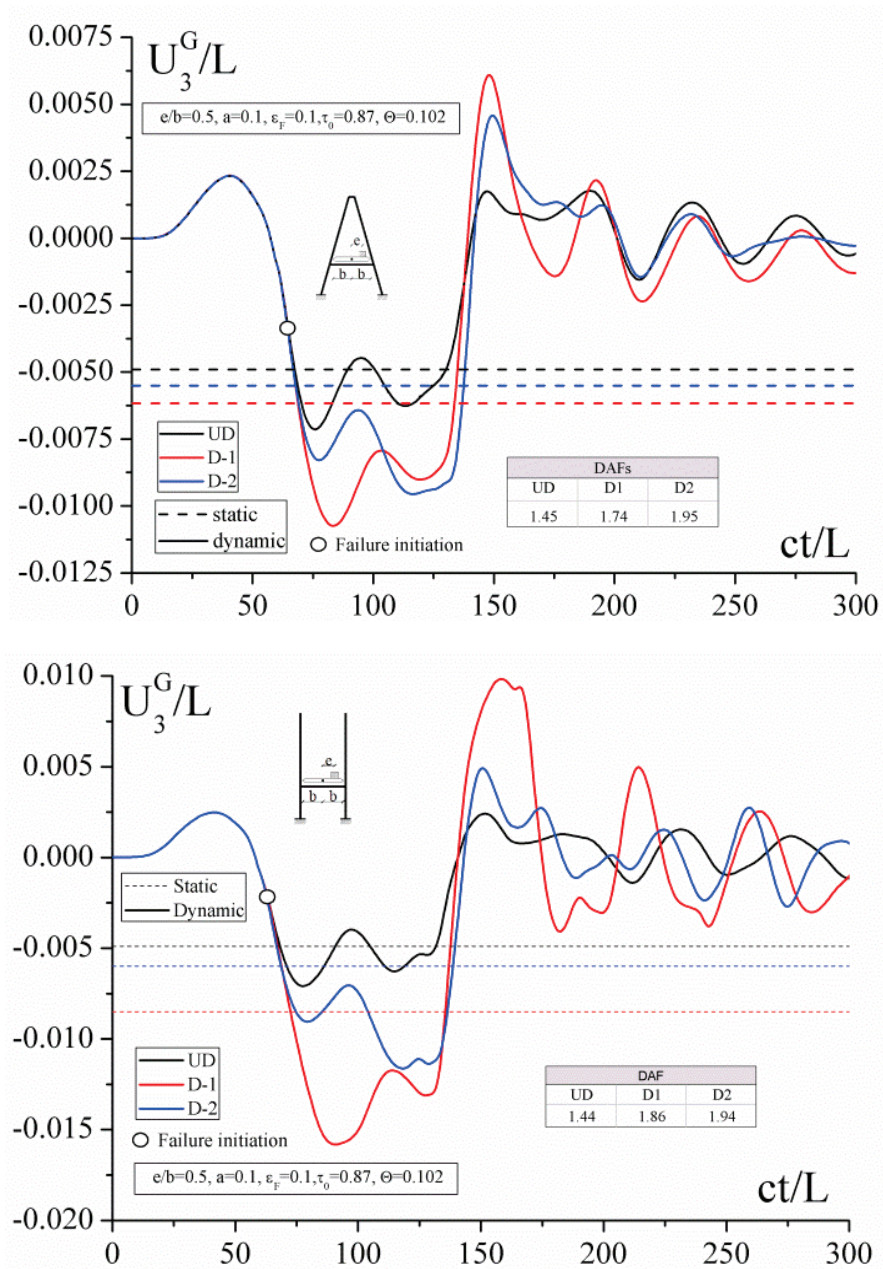


**Fig.s 3.26-3.27** Time history of the dimensionless midspan displacement and evaluation of the DAFs: comparisons between damage and undamaged bridge configuration.

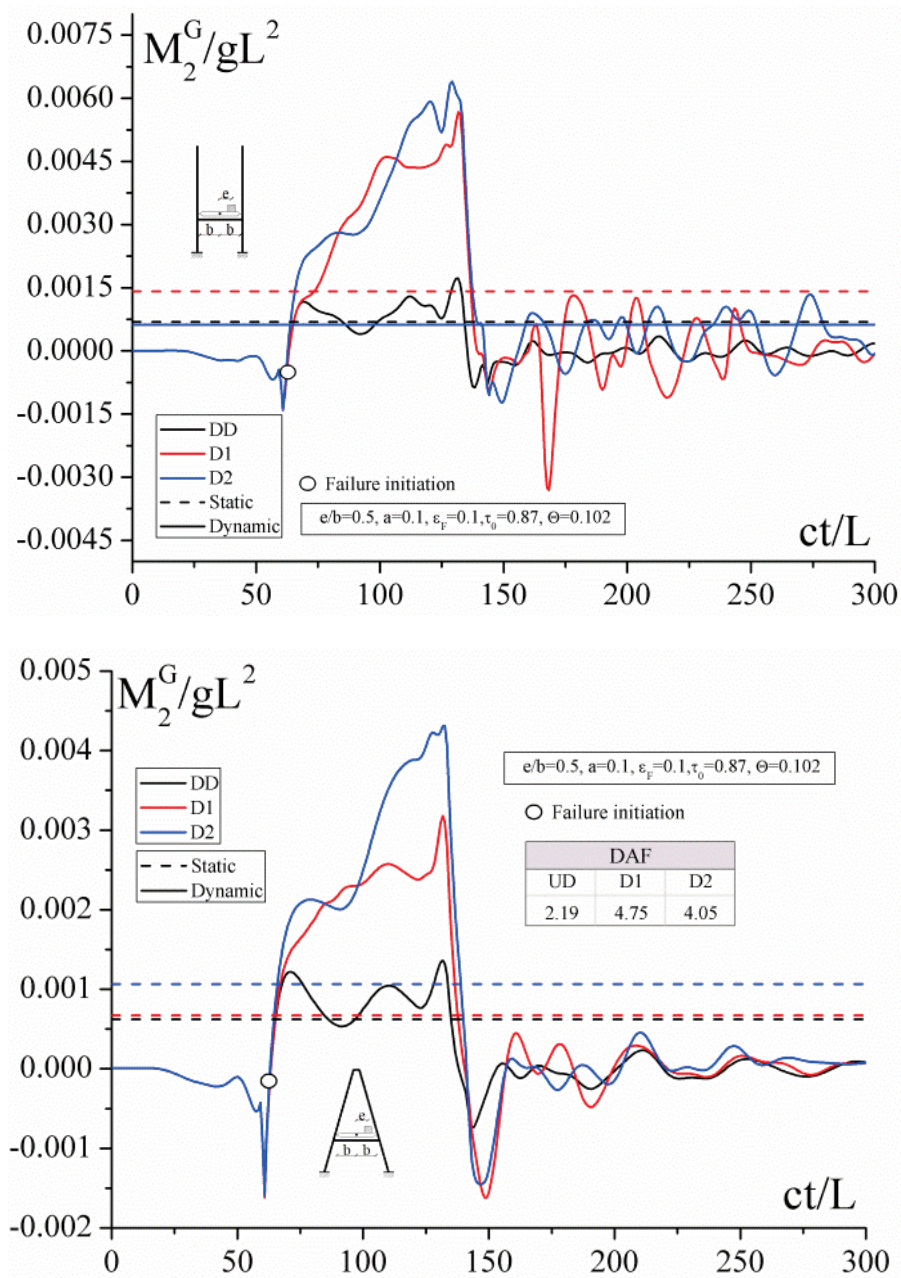


**Fig.s 3.28-3.29** Time history of the dimensionless midspan displacement and evaluation of the DAFs: comparisons between damage and undamaged bridge configuration.

In particular, the comparisons developed in terms of pylon typologies, indicate that H pylon-based structures are much more affected by the damage mechanisms of the cable system than the A-shaped ones. This behavior can be explained by the fact that the failure of the anchor stay (Mode A) or the stays in the central part (Mode B) produce unbalanced forces in the cable system and thus on the girder leading to high rotations of the pylons and the girder along vertical  $X_3$  and  $X_3$  axes, respectively.

This behavior is confirmed by the results reported in Figs. 3.30-3.31, in which time histories of the torsional rotation and anchor stay axial force in terms of the damage mechanism and pylon typology are reported. The analyses show that bridge structures based on A-shaped pylon are practically unaffected by the failure modes, since the same prediction on the maximum torsional rotations is observed.

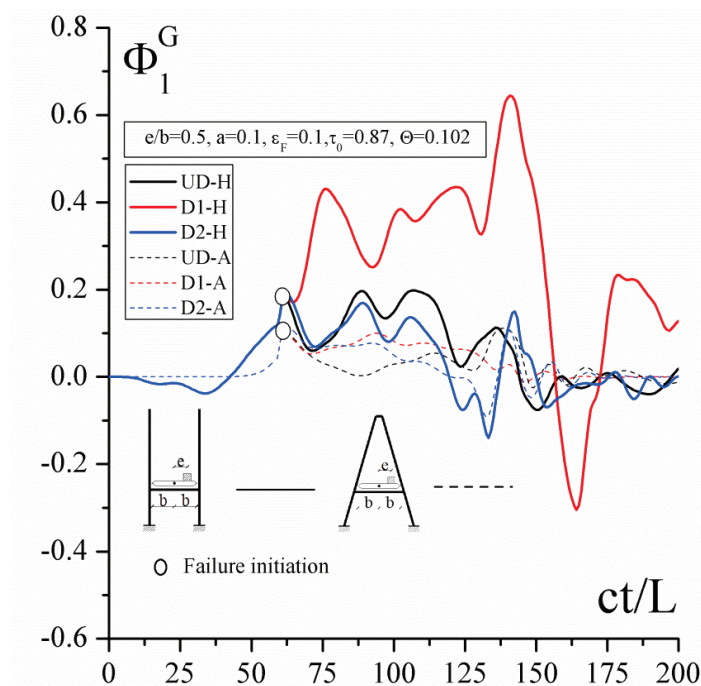


**Fig.3.30** Time history of the dimensionless midspan torsional rotation: comparisons in terms of the failure mode and pylon typology.

On the contrary, the H-shaped pylon bridges owing to the concurrent rotations of the girder and the pylons are affected by greater deformations and DAFs.

Moreover, the results shown in terms of the anchor stay axial stresses, reported in Fig. 3.31, denote that "mode A" failure mechanism produces high increments in the axial stress, mainly, for the A-shaped pylon typology.

This behavior can be explained by the geometric configuration of the A-shaped pylon and by its ability to redistribute the internal stresses from the damaged to the undamaged anchor stay.

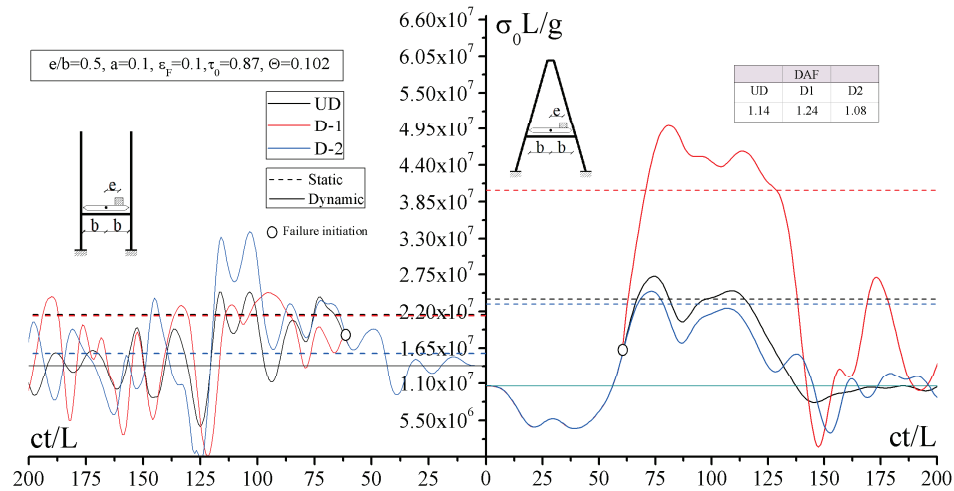


Fig.3.31 Time history of the dimensionless of the undamaged anchor stay axial force: comparisons in terms of the failure mode and pylon typology.

### 3.7.2 Comparisons between pure and hybrid cable system configurations

The investigation is developed on a long span bridge typology, with main span length ( $L$ ) equal to 1000 m. The deck is made of steel with aerodynamic cross section, 4 m depth and 20 m wide; the vertical moment of inertia ( $I_2^G$ ), the transverse moment of inertia ( $I_3^G$ ), the cross section area

( $A^G$ ) the torsional constant ( $J^G$ ) and the modulus of elasticity of steel  $E^G$  for the bridge deck are  $3.41 \text{ m}^4$ ,  $31 \text{ m}^4$ ,  $2.1 \text{ m}^2$ ,  $15 \text{ m}^4$ ,  $2.1 \times 10^8 \text{ kN/m}^2$ , respectively.

Moreover, the limit elastic bending moment ( $M_{20}^G$ ) for the upper and lower fibres and the normal stress resultant ( $N_{10}^G$ ) of the girder cross-section are equal to  $3.5 \times 10^8 \text{ Nm}$ ,  $2.45 \times 10^9 \text{ Nm}$  and  $7.56 \times 10^8 \text{ N}$ , respectively.

The pylons are formed by  $H$ -shaped steel elements, whose elements present vertical moment of inertia ( $I_2^P$ ), transverse moment of inertia ( $I_3^P$ ), cross-section area ( $A^P$ ), torsional constant ( $J^P$ ) and modulus of elasticity ( $E^G$ ) equal to  $20.57 \text{ m}^4$ ,  $9.78 \text{ m}^4$ ,  $1.97 \text{ m}^2$ ,  $21.13 \text{ m}^4$ ,  $2.10 \times 10^8 \text{ kN/m}^2$ , respectively.

Moreover, the limit elastic bending moment ( $M_{20}^P$ ) and the normal stress resultant ( $N_{10}^P$ ) are equal to  $1.85 \times 10^9 \text{ Nm}$  and  $6.84 \times 10^8 \text{ N}$ .

The stays and the hangers present a distance equal to  $20 \text{ m}$  and present allowable stress ( $S_a$ ) equal to  $7.2 \times 10^8 \text{ Pa}$ .

Finally, dead loading of the girder including also permanent loads are equal to  $3.0 \times 10^5 \text{ N/m}$ , whereas the ratio between live and dead loads is equal to  $0.5$ .

Cable-stayed and suspension bridges present the same mechanical characteristics of the hybrid cable-stayed suspension systems, except for the dimensioning of the cable-system elements, which are evaluated on the basis of the optimization procedure. From the mechanical and geometric characteristics defined above, dimensionless parameter concerning the ratio between stiffness of the girder and the cable system, i.e.  $\bar{\alpha}^2 = E^G I^G / H_t L^2$  and  $\bar{\lambda}^2 = (8f/L)^2 \times (L/L_e) \times (E^C A^C / H_t)$ , are equal to  $\bar{\alpha}^2 = 2.37 \times 10^{-3}$  and  $\bar{\lambda}^2 = 144$  for the hybrid cable-stayed suspension bridge scheme and  $\bar{\alpha}^2 = 1.99 \times 10^{-3}$  and  $\bar{\lambda}^2 = 153$  for the suspension system. Such values are consistent with data available from the literature, whose ranges, obtained on the basis of existing cable-supported bridge structures, are equal to  $\alpha^2 = [4 \times 10^{-4} - 11.4 \times 10^{-3}]$  and  $\lambda^2 = [90 - 231]$  (Enrique Luco & Turmo, 2010). The optimum design methodology described in chapter 2, utilized to calculate the initial configuration, is presented for the bridge scheme whose the mechanical and geometrical properties are defined in Tab. 3.4.

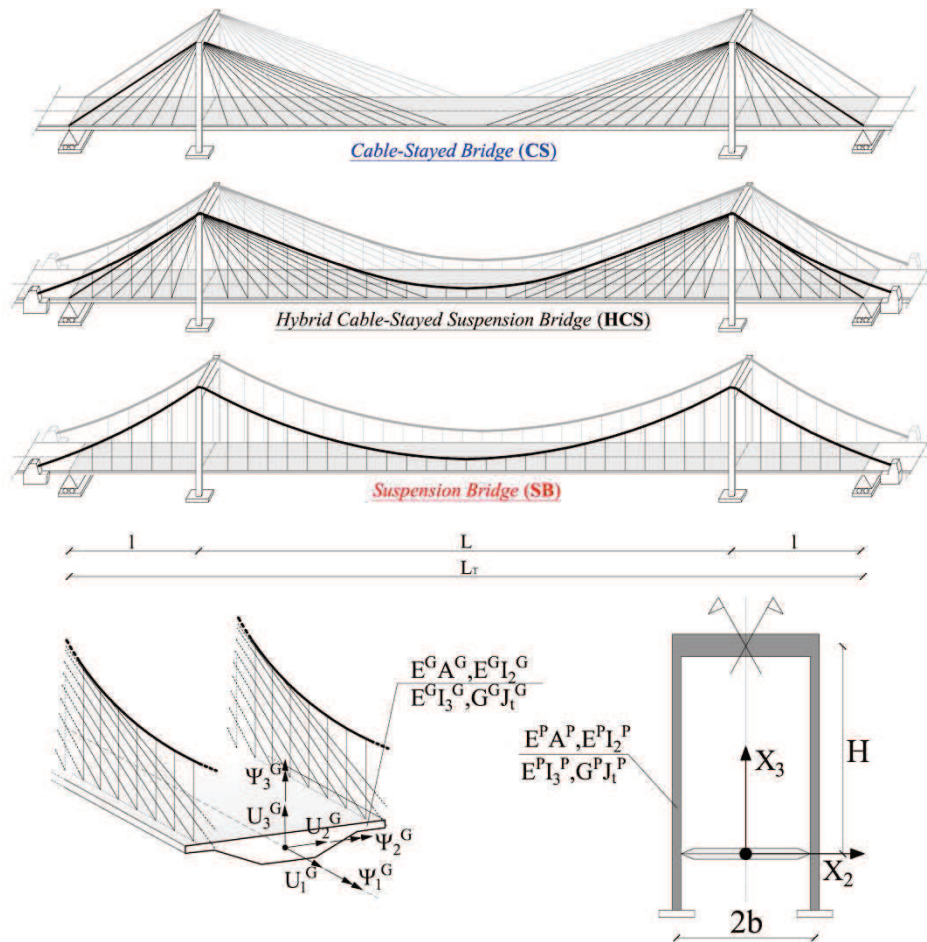


Fig.3.32 Cable supported bridge considered

Stiffening Girder			Pylon			Cable and Loads		
$b$	10	m	$A^P$	15	$m^2$	$S_A$	7.20	GPa
$d$	4	m	$I_2^P$	20.57	$m^4$	$\Delta S_A$	200	MPa
$A^G$	9.54	$m^2$	$I_3^P$	9.78	$m^4$	$\gamma^{S,H,M}$	77	$kN/m^3$
$I_2^G$	3	$m^4$	$E^P$	210	GPa	$E^{S,H,M}$	210	GPa
$I_3^G$	30	$m^4$	$H/l$	0.4	-	$g^G$	300	$kN/m$
$J^G$	15	$m^4$	$K^P$	50	$g^G$	$p/g^G$	0.5	-
$E^G$	210	GPa						

Tab. 3.4 Mechanical and geometric properties of bridges

The analyses are developed with the purpose of investigating the effect of the cable failure on the stress distribution in the bridge components and the corresponding dynamic influence produced by the cable release mechanisms.

To this aim four different damage scenarios, represented in Fig. 3.33, are considered, in which the damage mechanisms are assumed to affect the cable stayed system, at the anchor stay (SC1) or at the stays in the central span (SC2), or the suspension system, at the main cable (SC3) or at the hanger elements (SC4). In particular, the damage scenarios SC1 and SC2 consider the failure of the anchor stay and the longest three stays of the main span.

In the damage scenario SC3, the main cable at the central span is affected by a reduction of the 50% of its cross-section, i.e.  $\xi_s = 0.5$ ; the damage mechanism is located at  $1/4$  of the cable profile and it is distributed on a length equal to 0.25 of the cable development, i.e.  $\beta=0.25, \alpha=0.25$ .

The damage scenario SC4 affects a set of hanger elements, i.e.  $X_d/L=1/5$ , which are located on a length, measured on the girder development, equal to  $1/4$  of the girder main span.

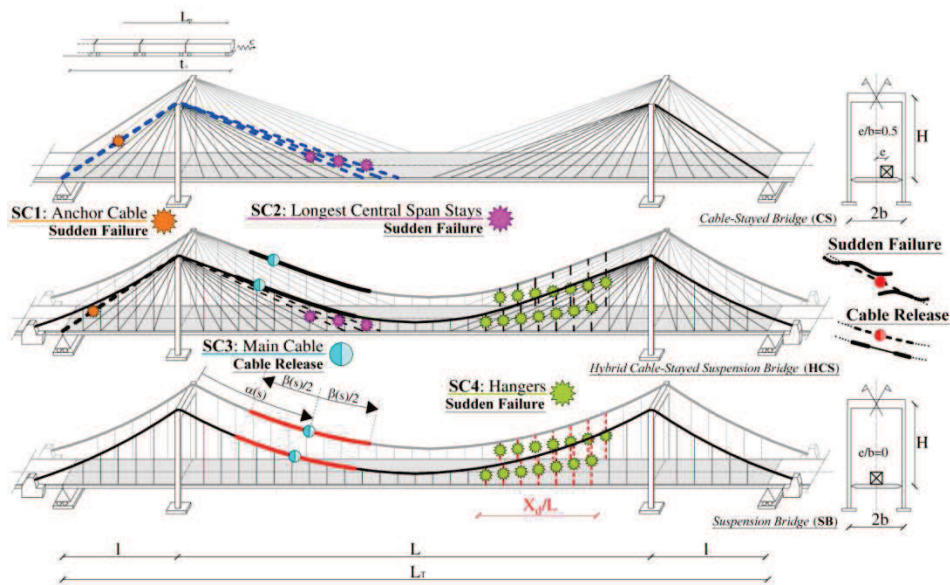


Fig. 3.33 Damage scenarios considered in the cable-system



Finally, in the damage scenarios SC1, SC2 and SC3, the damage element, affected by the cable release, is considered to be located at the connection between girder and cable element.

### 3.7.2.1 Initial configuration of bridges

A complete evaluation of the bridge behavior requires to correctly identify the cable dimensioning and the post-tensioning forces of the initial configuration, on the basis of displacements and stress conditions under dead and live loading schemes.

To this aim, the constrained optimization problem introduced in the previous chapter is employed. In particular, in this case, the analysis under live loads is performed in such a way to verify only prescriptions concerning ultimate and fatigue limit states Fig 3.34. As a consequence, the lowest possible steel quantity involved in the cable system is evaluated.

Results concerning cable dimensioning of the cable-stayed and suspension schemes of the hybrid cable-stayed suspension bridge in the final configuration are reported in Fig. 3.35.

Moreover, maximum stresses in the cable system due to accidental loads during the iteration steps and the total steel quantity involved in the cable systems are reported in Figs 3.36-3.37.

In particular, the assessment of the optimized values of the cable dimensioning requires five different iterations, in which a progressive reduction of the steel quantity involved in cable-stayed and suspension systems is achieved. The cable dimensioning and the post-tensioning forces, are modified from their initial values, obtained by preliminary design rules.

In particular, cable areas are reduced during the iterations developed in the optimization phased to involve a lower steel quantity in the cable systems, whereas the post-tensioning forces are modified to verify the stress criterion on the maximum stresses produced in live load configuration.

The distribution of the optimized steel areas in the cable-stayed and suspension systems presents large values in proximity to the midspan and left or right cross-section extremities, lower quantities at the girder/pylon connection.

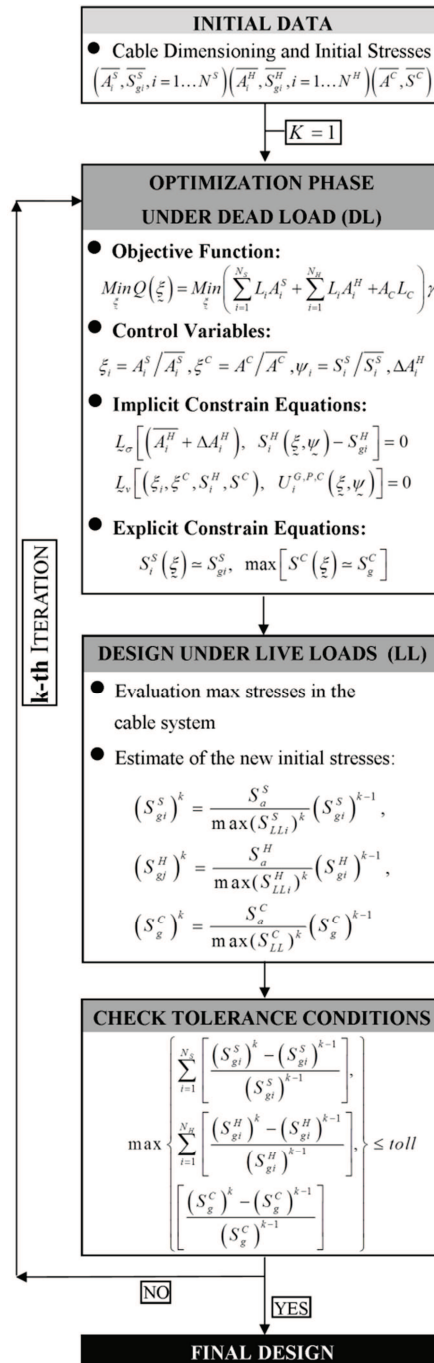


Fig. 3.34 Flow-chart of the optimization procedure for cable system dimensioning

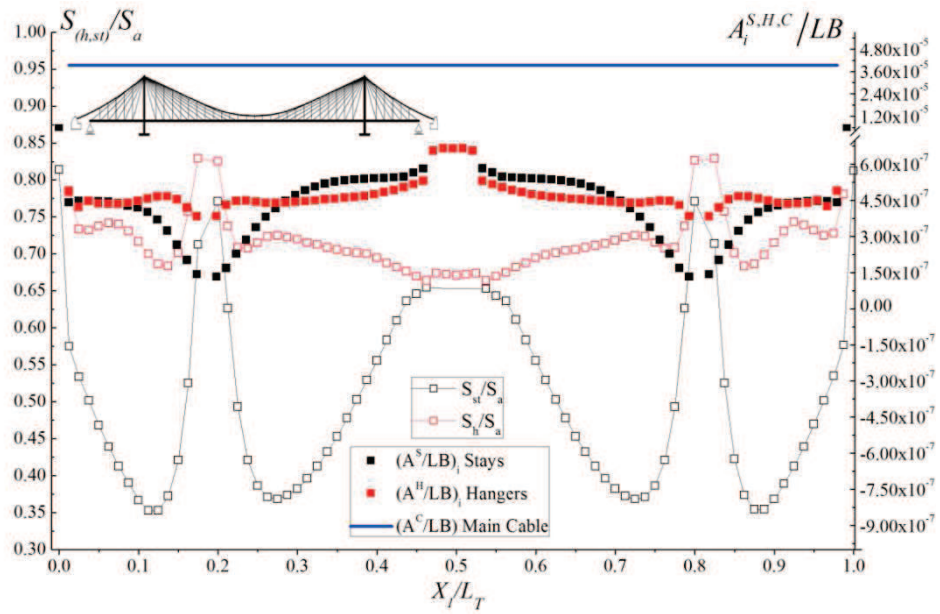


Fig. 3.35 Stress distribution and cable dimensioning in the initial configuration

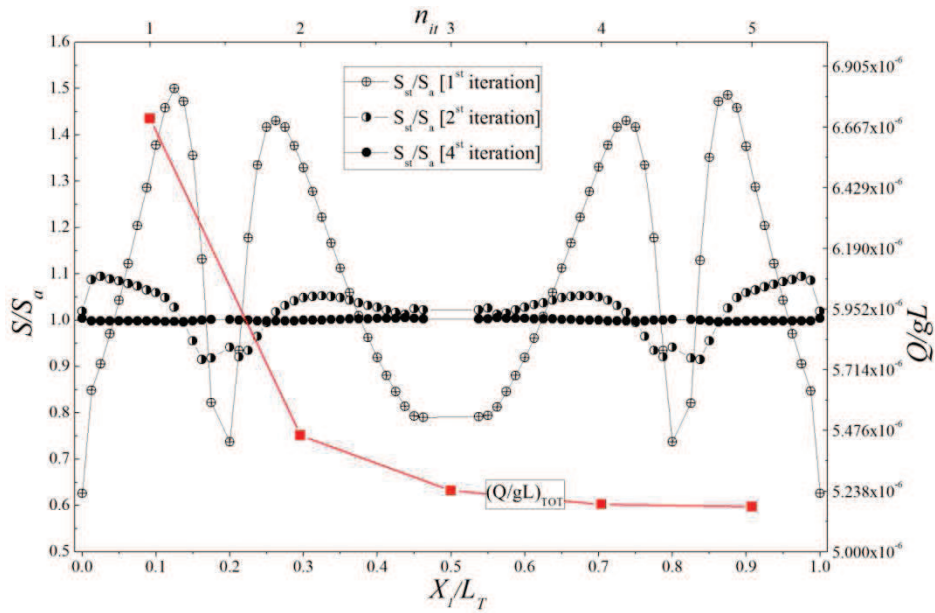


Fig. 3.36 Maximum stresses in the stays during the iteration steps and total steel quantity

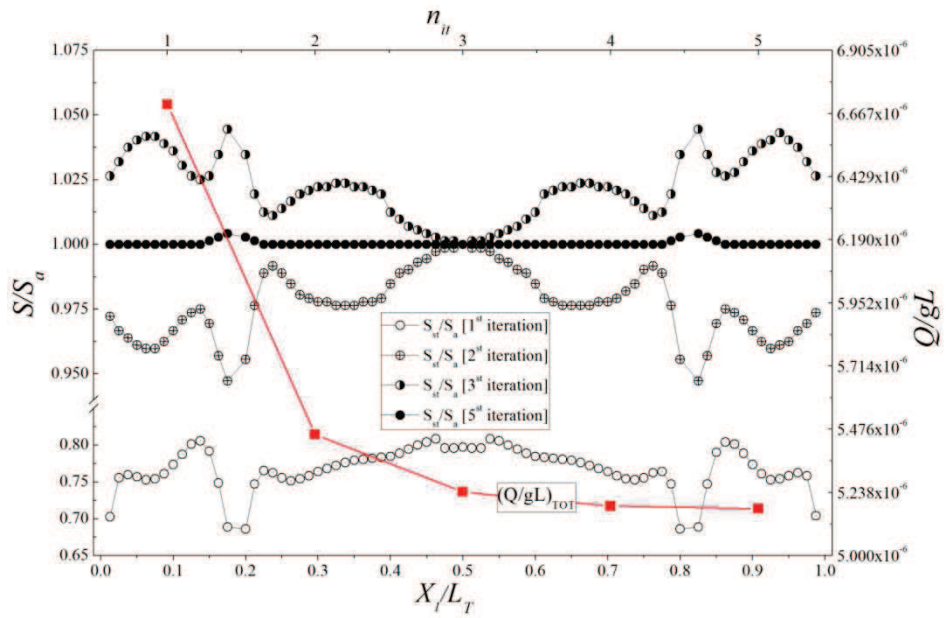


Fig. 3.37 Maximum stresses in the hangers during the iteration steps and total steel quantity

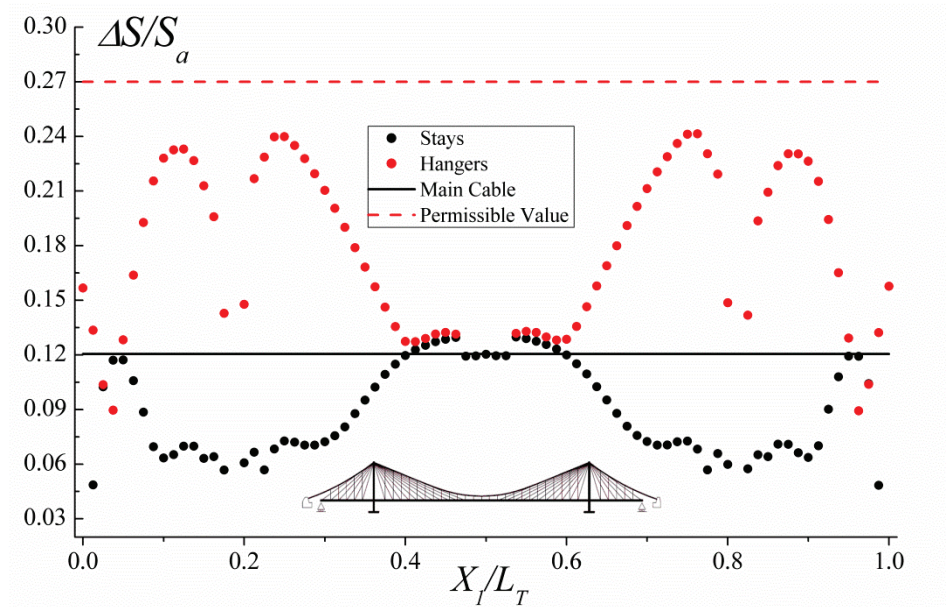


Fig. 3.38 Change of the stresses in the cable-system for the application of type 11 loading scheme (Eurocode 1, 2003) and comparison with maximum admissible value for fatigue requirement.

Moreover, the anchor cables, which basically control most of the loading transfer arising from the midspan, present the largest values of steel quantity in the cable system.

Finally, the area of the hangers on the region in which there are no stays is of typically greater than the area in which the two systems coexist.

In order to verify the validity of the proposed results and the consistency of the dimensioning procedure with fatigue criteria, additional results are expressed in terms of stress variations of the cable system elements.

In particular, the analyses are developed in the framework of SLS under every load combination with characteristic values based on Eurocode prescriptions (The European Committee for Standardisation, 2003)

Assuming a minimum fatigue strength stress variation equal to 200 MPa (Strand) for the cables, results in terms of stress variations produced by the fatigue loading schemes are developed. For the sake of brevity, only the worst loading scenario, corresponding to the application of type 11 locomotive-hauled freight train is reported, from which the stress variations of the cable system elements is lower than the permissible limit value (Fig. 3.38).

### 3.7.2.2 Damage analysis

At first, the effects of the cable failure are evaluated on the loading scheme, involving dead loads only. The main aim of such results is to investigate the effects of the cable release arising from an accidental cable failure and to quantify the corresponding dynamic amplification factors, also in the light of the actual recommendations provided by existing codes on cable supported bridges (Post-Tensioning Institute, 2007; Service d'Etudes Techniques des Routes et Autoroutes, 2001). For each bridge typology, static and dynamic damage definitions are considered, by using constitutive laws defined through Eq.(3.30) or Eq.(3.31). Moreover, results arising from the proposed formulation are analyzed in view of the recommendations provided by existing codes. In this framework, PTI codes (Post-Tensioning Institute, 2007) recommend to evaluate cable failure introducing static forces proportional to the

initial tension and multiplied by a two factor to reproduce the cable loss of stiffness. However, such prescription was not introduced in the latest guidance on stay cables (Federation International du beton, 2005) or in the new version of the P.T.I. codes (Post-Tensioning Institute, 2007), which suggest to verify the bridge behavior by means of a non-linear time history analysis

At first, results in terms of vertical displacements and torsional rotations of the girder, namely  $U_3^G/L$  and  $\Psi_1^G B/L$ , and normalized stresses ( $S/S_a$ ) of the cable system elements are investigated. The main purpose of the results is to evaluate the behavior of hybrid cable-stayed suspension bridges in comparison to bridge structures based on pure cable-stayed and suspension systems, when subjected to combined effects of moving loads and damage mechanisms. To this aim, results in terms of vertical displacements of the girder for different damage scenarios are proposed. Such results are able to provide an easy evaluation of the bridge behavior to better redistribute the overall stresses produced by the cable release, reducing the bridge deformations and the internal stresses of the bridge components. With reference to Figs 3.39-3.40, comparisons, concerning SC1 and SC2 damage scenarios, denote that the failure in the anchor cable or the stay elements affects the girder deformation, mainly in the cable-stayed bridge scheme, producing notable vertical displacements and torsional rotations. Such values are larger than the corresponding ones commonly recommended for the serviceability limit state by codes on cable-supported bridges. Moreover, the failure of the anchor stay seems to produce greater vulnerability than the damage mechanisms SC2, since larger deformations are observed. Contrarily, the combined system, owing to interaction of the cable systems, is able to reduce the effects produced by the cable release, leading to lower girder deformability.

Comparisons between static and dynamic damage modes denote that the dynamic characteristics of the cable release effect influence mainly vertical displacements for both SC1 and SC2 damage scenarios, whose maximum DAFs are equal to 1.9 for both bridge schemes. Results concerning girder torsional rotations denote that the DAFs are much lower than those observed for vertical displacements.

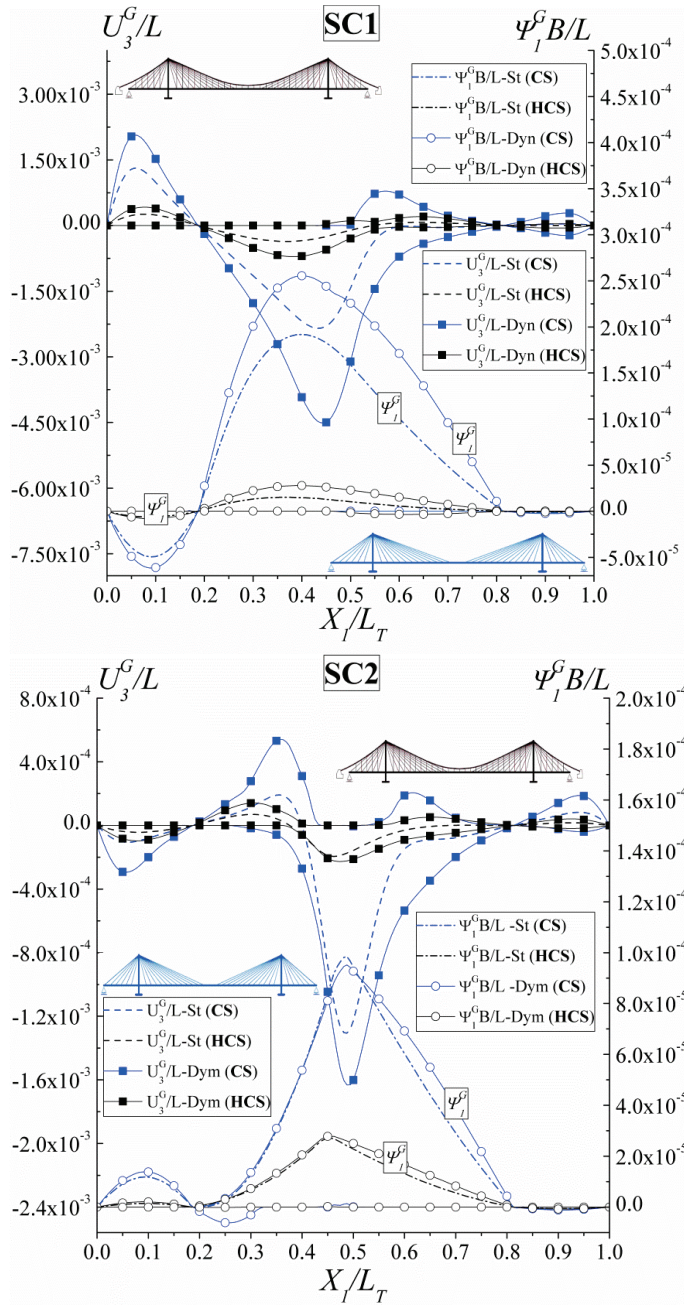


**Fig.s 3.39-3.40** Comparisons between Cable-Stayed bridge (CS) and Hybrid Cable-Stayed Suspension bridge (HCS) in terms of the girder deformability under the action of dead loads (DL) for the damage scenarios SC1(Fig. 3.39) and SC2(Fig. 3.40).

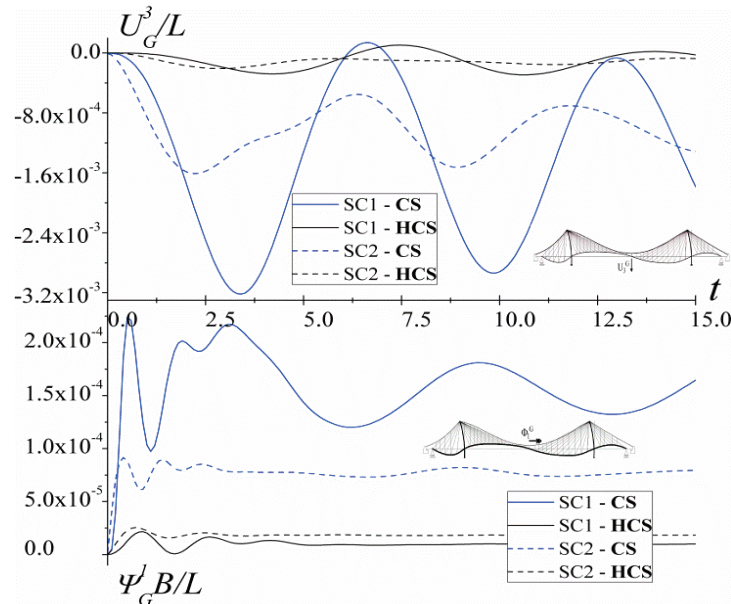


**Fig. 3.41** Comparisons between Cable-Stayed bridge (CS) and Hybrid Cable-Stayed Suspension bridge (HCS) in terms of time histories of dimensionless midspan vertical displacement and torsional rotation

In particular, the SC1 damage scenario produces a DAF equal to 1.31, whereas for the SC2 damage scenario the dynamic amplification effects are practically negligible and thus the corresponding DAF is close to the unity.

Such behavior can be explained in view of the characteristics of the damage scenario SC2, which produce vibrations with lower amplitudes than those observed for the damage scenario SC1. Moreover, the frequency contents, evaluated by the FFT approach (Meirovitch, 1986) are much larger than the fundamental frequencies of the bridges. As a consequence, in the SC2 damage scenarios, only localized effects with small amplifications with respect to the static damage condition are observed (Fig. 3.41).

The bridge behavior, reported in terms of stress distribution in the cable systems in Fig. 3.42, denotes that most dangerous damage condition is the one affecting the failure of the anchor stay in the cable-stayed system.

The initial stress distribution, obtained under “zero configuration”, is strongly modified with respect to the undamaged configuration.



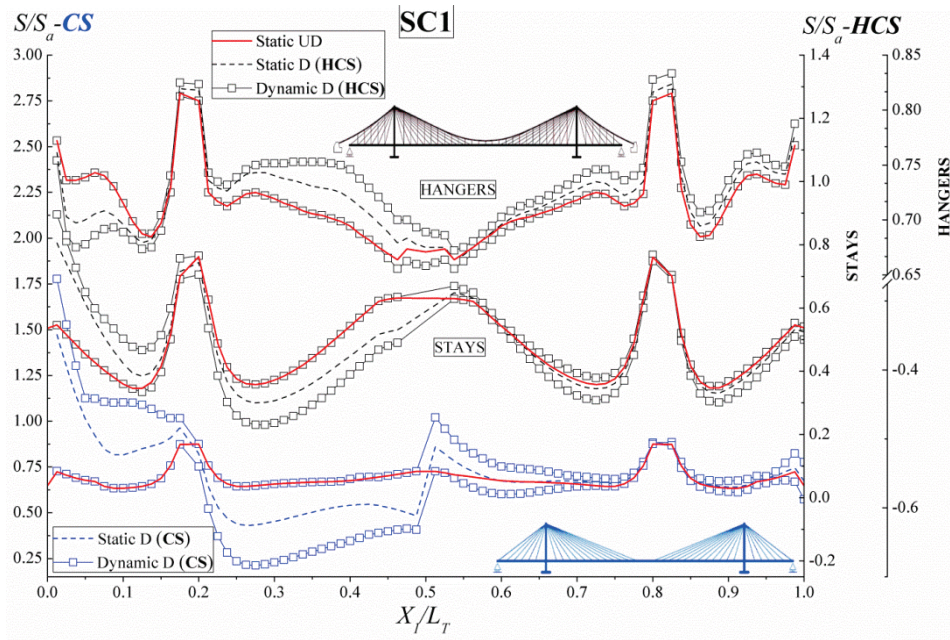


Fig. 3.42 Comparisons between Cable-Stayed bridge (CS) and Hybrid Cable-Stayed Suspension bridge (HCS) in terms of envelope of stress distribution in the cable systems under the action of dead loads (DL) for the damage scenario SC1.

In particular, the cable-stayed bridge is affected by stress amplifications mainly in the region close to the damaged anchor stay. The maximum value of the DAFs, namely  $\Phi_{S/S_a}^D$ , is equal to 1.21 whereas the maximum amplification from the UD configuration, namely  $\Phi_{S/S_a}^{D-UD}$ , is equal to 1.78. Moreover, results concerning the combined system denote that the presence of the additional hanger elements with respect to the pure cable-stayed bridge is able to reduce both maximum and the average values of stress levels, whose distribution is everywhere lower than the allowable stress. The analyses are extended to the loading combinations involving the presence of live loads (LL), taking into account, in those cases in which the calculation is developed in dynamics, the inertial effects produced by moving loads. At first, vulnerability behavior of the bridge structures is analyzed for all the damage scenarios in terms of girder displacements. The main purpose of the results is to provide an easy evaluation on the bridge capacity to better redistribute the overall stresses produced by the

cable release, reducing the bridge deformations and the internal stresses of the bridge components. In particular, the analyses collect results arising from static cases in the damaged (D) and undamaged (UD) configurations, or taking into account the dynamic effects produced by moving loads at high speed ranges, i. e.

$$v = c \left( \frac{\mu_G}{gH} \right)^{1/2} = 3.46.$$

The results, reported in Figs. 3.43-3.46 for the investigated scenarios, show how both bridge systems are affected by the presence of the damage mechanisms, since the prediction of vertical displacements is strongly modified from the UD cases. Moreover, girder deformability is much influenced by the inertial effects especially at high transit speeds, where notable amplifications of the vertical displacements are observed with respect to the static prediction. The comparisons between suspension and combined bridge typologies denote that the latter system is able to better redistribute stress release effects, leading to low displacement increments with respect to the UD configuration. In fact, the stayed and the suspension systems are affected by displacement increments measured from the UD analyses in ranges between  $2.04 \div 2.86$  and  $2.29 \div 2.96$ , respectively. Moreover, the HCS configuration presents DAFs between  $1.58$  and  $1.89$ , which are much lower than those observed in the cases of pure cable stayed or suspension bridge configurations.

Finally, the comparisons with maximum values of the DAFs based on PTI prescriptions, i.e.  $\Phi_{\Gamma}^{PTI}$ , denote that such definition typically overestimates the actual response in terms displacement effects. In order to quantify, numerically, the dynamic influence of cable release mechanisms on the bridge behavior, in Fig.s. 3.47-3.48 the effects of moving load characteristics as a function of the transit speeds, is investigated. For the sake of brevity the analyses are developed only for the damage scenarios SC1 and SC4 and are expressed in terms of DAFs, defined on the basis of Eq.s (3.30)-(3.31), and maximum values of the midspan girder displacements. Coupling effects between moving loads and cable release mechanisms are able to increase the DAFs distribution from the UD configuration.

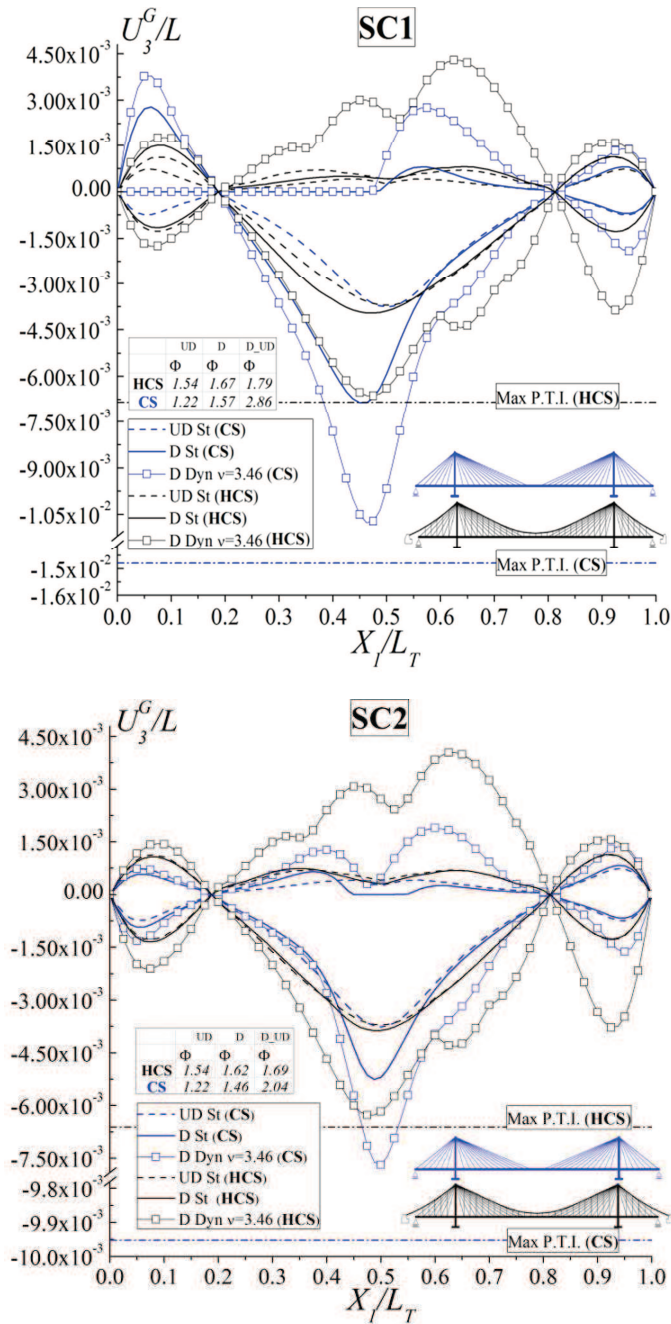


Fig.s 3.43-3.44 Comparisons between bridges typologies in terms of the girder deformability under the action of live loads (LL) for the damage scenarios SC1, SC2.

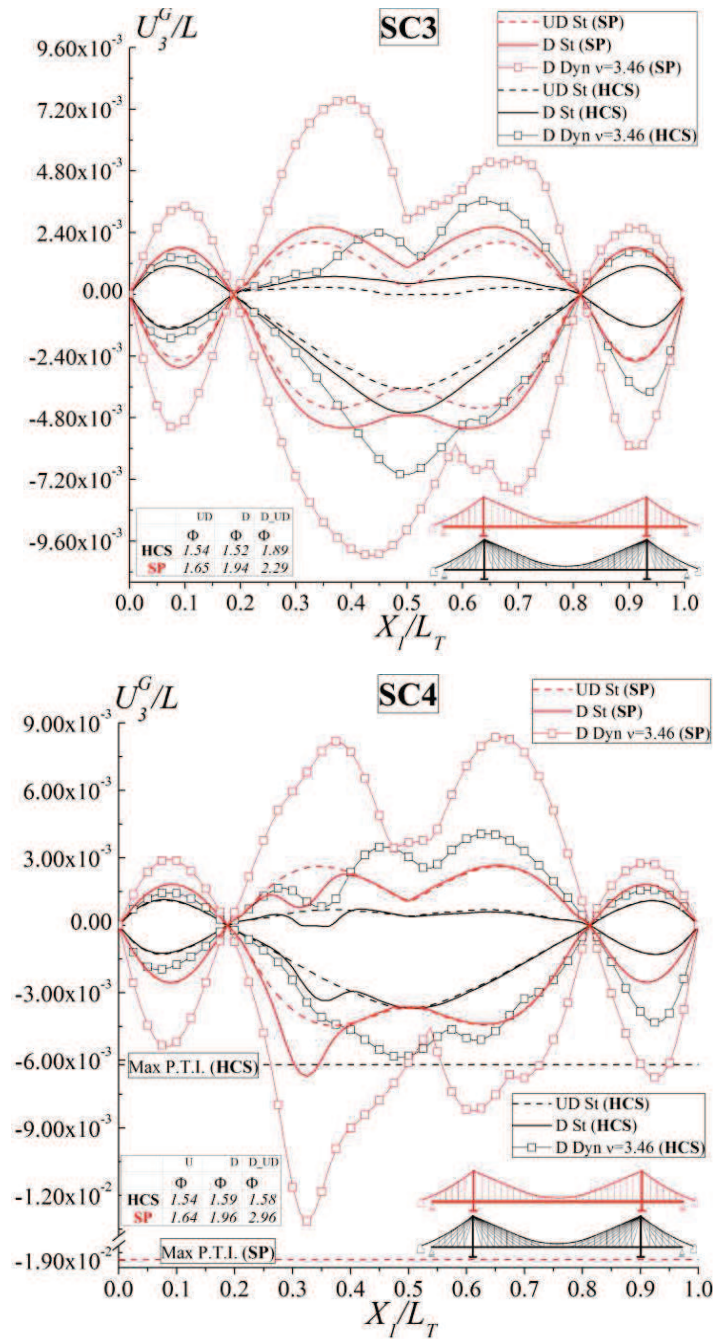
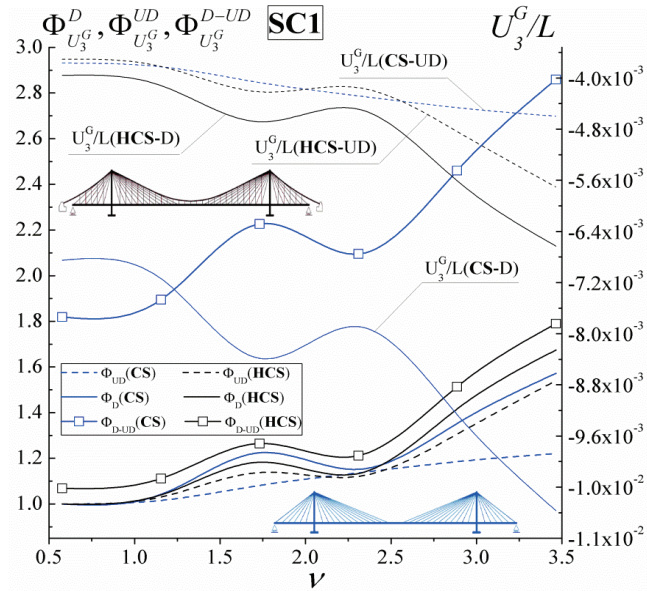
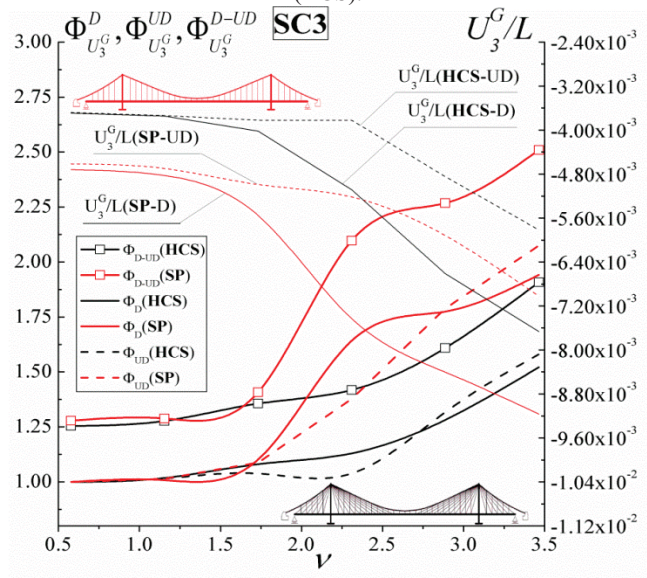


Fig.s 3.45-3.46 Comparisons between bridges typologies in terms of the girder deformability under the action of live loads (LL) for the damage scenario SC3, SC4.



**Fig. 3.47** Normalized vertical displacements and dynamic amplification factors of the maximum vertical displacement for damage scenario SC1 as a function of the normalized speed parameter: comparisons between Cable-Stayed bridge (CS) and Hybrid Cable-Stayed Suspension bridge (HCS).



**Fig. 3.48** Normalized vertical displacements and Dynamic amplification factors of the maximum vertical displacement for damage scenarios SC3 as a function of the normalized speed parameter: comparisons between Suspension Bridge (SP) and Hybrid Cable-Stayed Suspension Bridge (HCS).

Moreover, the damage mechanisms, except at low speeds of the moving system, are able to modify the results obtained in the UD configuration, producing increments to the bridge deformability.

In particular, the maximum vertical displacements observed in the time histories are amplified with respect to the UD configuration up to 2.51 and 2.84 for the pure suspension and cable-stayed bridge typologies, respectively.

Contrarily, the HCS bridge scheme, owing to a better performance of the cable-system, is able to reduce the girder deformability and the corresponding DAFs.

The cable-stayed bridge is affected by larger vulnerability than the combined system, since the presence of the damage mechanisms produce larger amplifications of the girder displacements with respect to the undamaged configuration.

Additional results are presented to analyze the influence of the damage scenarios on the stress distribution in the cable system. For the assumed damage scenarios, the envelope of the stress distribution normalized on the allowable stress is analyzed.

In particular, Fig. 3.49 and Fig.3.50 report results concerning SC1 damage scenario, which show how both cable-stayed and combined cable systems are affected by stresses amplifications, mainly in the region close to the cable failure.

However, cable-stayed bridge typologies are subjected to larger amplifications than those observed for the HCS bridge schemes, i.e. 2.4 against 1.81. Actually, the HCS bridge is able to better redistribute the additional stresses produced by the release of the anchor stay, leading to lower vulnerability indexes in the cable system.

Results in terms of bending moments of pylons and girder for the case of cable-stayed and HCS configurations are proposed, by means of comparisons between damaged, undamaged bridge schemes. In the present analyses, results are developed with the purpose to investigate the behavior of HCS bridges, emphasizing the enhanced behavior of such structural configurations in comparison to bridge schemes based on pure cable-stayed and suspension systems.

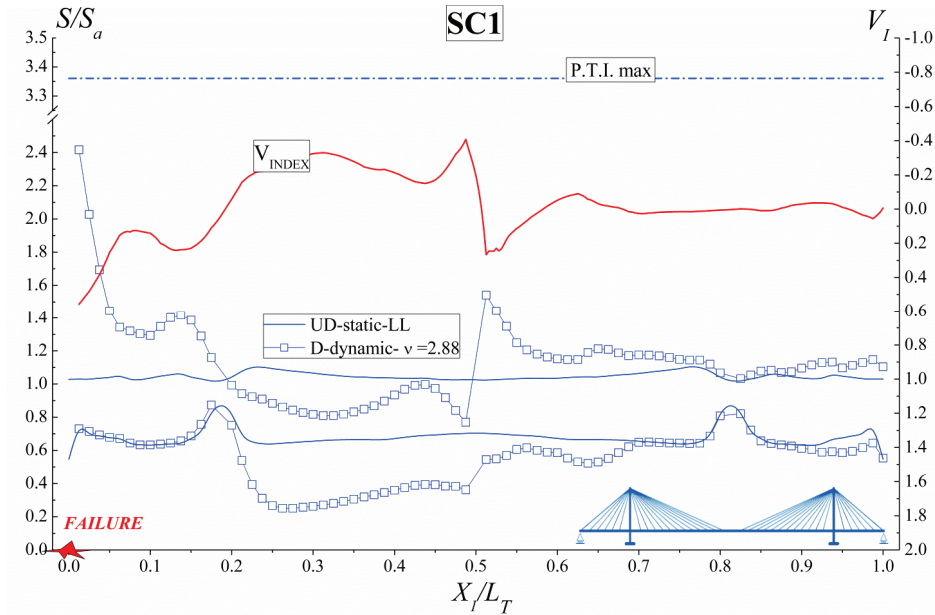


Fig. 3.49 Cable-Stayed Bridge: Envelope stress distribution in the cable systems under the action of live loads (LL) and vulnerability behavior for the damage scenario SC1

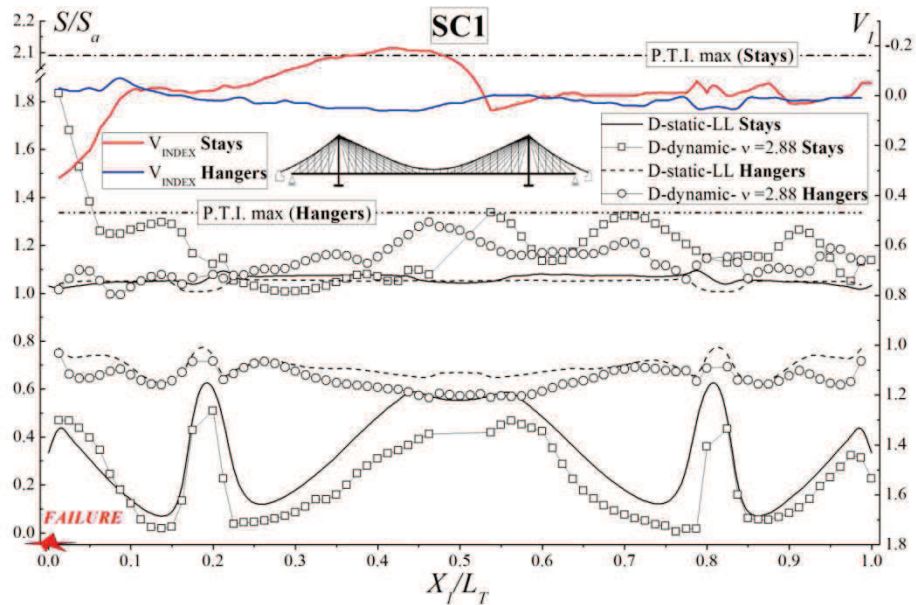
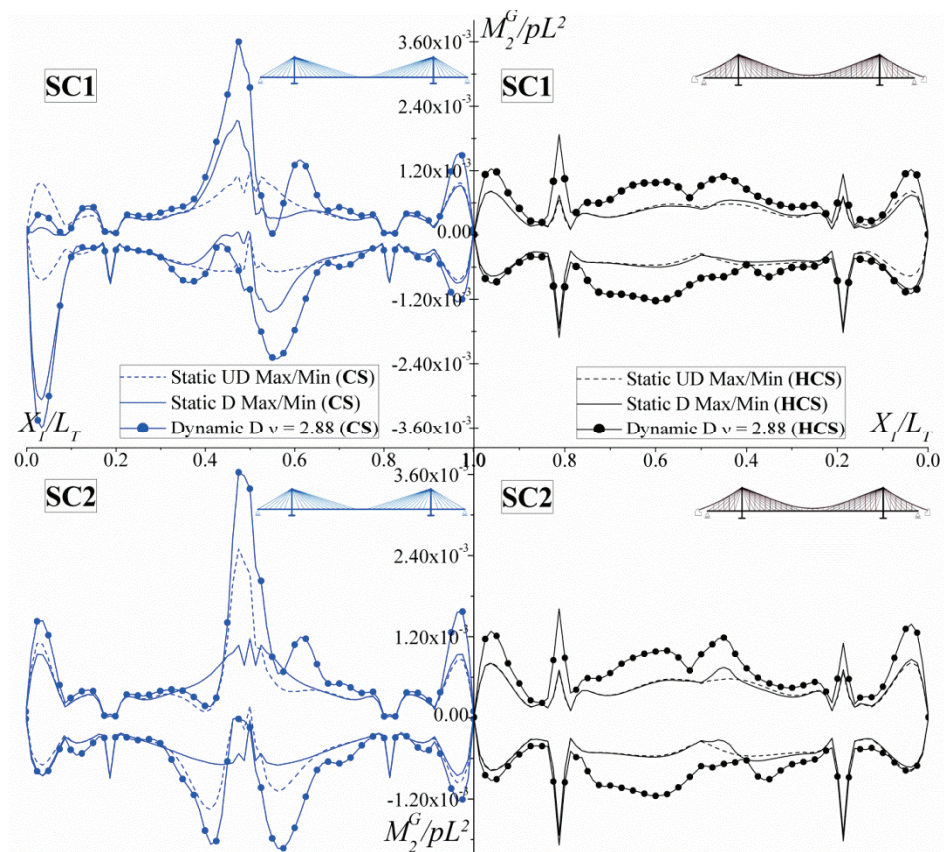


Fig. 3.50 Hybrid Cable-Stayed Suspension bridge: Stress distribution in the cable systems under the action of live loads (LL) and vulnerability behavior for the damage scenario SC1

In particular for the SC1 and SC2 damage scenarios, the envelope of bending moments for the cases of dynamic damaged, static damaged and static undamaged configurations are analyzed (Fig.3.51).

Moreover, the amplification effects produced by the damage mechanisms are quantified on the basis of different damage descriptions defined by Eq.(31)-(32) and the corresponding results are reported in Tables 3.5-3.7, in which bending moments at several cross sections of the girder and at base of the pylons are investigated.



**Fig. 3.51** Hybrid Cable-Stayed Suspension/Cable stayed bridges: envelope bending moments distribution of the stiffness girder under the action of live loads (LL) for the damage scenarios SC1 and SC2



The results denote that the cable stayed bridges are affected by important amplification effects, which are much larger than the allowable values defined by existing codes on ALS (Post-Tensioning Institute, 2007). On the contrary, HCS due to a better redistribution of the cable-system elements are able to strongly reduce the entity of such internal stresses. Contrarily, results concerning variables associated to the bending moments of the pylons, denote that both HCS and cable-stayed bridges are affected by the damage mechanisms, since large dynamic amplification factors are observed (Tab. 3.7).

SC1	Cable-Stayed Bridge (CS)						Hybrid Cable-Stayed Suspension Bridge (HCS)					
	$X_1/L_T$	$M_{ST}^{UD}/pL^2$ (x10 <sup>-3</sup> )	$M_{Sv}^D/pL^2$ (x10 <sup>-3</sup> )	$M_{Dyna}^D/pL^2$ (x10 <sup>-3</sup> )	$\Phi^{UD}$	$\Phi^D$	$\Phi^{D-UD}$	$M_{ST}^{UD}/pL^2$ (x10 <sup>-3</sup> )	$M_{Sv}^D/pL^2$ (x10 <sup>-3</sup> )	$M_{Dyna}^D/pL^2$ (x10 <sup>-3</sup> )	$\Phi^{UD}$	$\Phi^D$
0.038	-0.836	-3.016	-3.546	1.10	1.18	4.24	-0.765	-1.011	-1.094	1.07	1.08	1.43
0.263	0.281	0.294	0.348	1.15	1.18	1.24	0.374	0.382	0.549	1.44	1.42	1.47
0.425	0.737	1.356	1.738	1.27	1.28	2.36	0.574	0.647	1.006	1.55	1.60	1.75
0.500	1.182	1.384	2.754	1.31	1.99	2.33	-0.346	-0.377	-0.810	2.08	2.15	2.34
0.688	0.352	0.379	0.484	1.72	1.28	1.38	-0.525	-0.535	-1.103	1.91	2.06	2.10
0.963	-0.832	-0.895	-1.241	1.39	1.39	1.49	-0.766	-0.768	-0.900	1.21	1.17	1.17

Tab. 3.5 Dynamic amplification effects for the damage scenario SC1 in terms of bending moments at fixed cross-sections of the girder for the cable-stayed and HCS configurations

SC2	Cable-Stayed Bridge (CS)						Hybrid Cable-Stayed Suspension Bridge (HCS)					
	$X_1/L_T$	$M_{ST}^{UD}/pL^2$ (x10 <sup>-3</sup> )	$M_{Sv}^D/pL^2$ (x10 <sup>-3</sup> )	$M_{Dyna}^D/pL^2$ (x10 <sup>-3</sup> )	$\Phi^{UD}$	$\Phi^D$	$\Phi^{D-UD}$	$M_{ST}^{UD}/pL^2$ (x10 <sup>-3</sup> )	$M_{Sv}^D/pL^2$ (x10 <sup>-3</sup> )	$M_{Dyna}^D/pL^2$ (x10 <sup>-3</sup> )	$\Phi^{UD}$	$\Phi^D$
0.038	0.945	1.101	1.444	1.08	1.31	1.53	0.819	0.863	1.387	1.61	1.65	1.69
0.263	0.281	0.296	0.339	1.15	1.15	1.21	0.374	0.359	0.511	1.21	1.20	1.24
0.425	-0.668	-1.224	-1.803	1.06	1.47	2.70	0.574	0.608	0.950	1.56	1.60	1.66
0.500	1.182	2.133	3.394	1.31	1.59	2.87	0.509	0.519	0.940	1.81	1.79	1.84
0.688	0.352	0.366	0.504	1.72	1.38	1.43	-0.525	-0.530	-1.014	1.91	1.91	1.93
0.963	-0.832	-0.937	-1.213	1.39	1.29	1.46	-0.766	-0.777	-0.929	1.21	1.20	1.21

Tab. 3.6 Dynamic amplification effects for the damage scenario SC2 in terms of bending moments at fixed cross-sections of the girder for the cable-stayed and HCS configurations

SC1	Cable-Stayed Bridge (CS)						Hybrid Cable-Stayed Suspension Bridge (HCS)					
	Base (x,y)	$M_{ST}^{UD}/pL^2$ (x10 <sup>-3</sup> )	$M_{Sv}^D/pL^2$ (x10 <sup>-3</sup> )	$M_{Dyna}^D/pL^2$ (x10 <sup>-3</sup> )	$\Phi^{UD}$	$\Phi^D$	$\Phi^{D-UD}$	$M_{ST}^{UD}/pL^2$ (x10 <sup>-3</sup> )	$M_{Sv}^D/pL^2$ (x10 <sup>-3</sup> )	$M_{Dyna}^D/pL^2$ (x10 <sup>-3</sup> )	$\Phi^{UD}$	$\Phi^D$
(-L/2, -b)	3.236	10.685	12.829	1.24	1.20	3.96	5.860	9.184	14.253	1.94	1.55	2.43
(-L/2, b)	2.582	3.244	4.896	1.38	1.51	1.90	5.034	5.926	11.516	2.13	1.94	2.29
(L/2, -b)	-3.208	-7.516	-8.541	1.56	1.14	2.66	-5.879	-7.312	-14.084	1.99	1.93	2.40
(L/2, b)	-2.555	-6.642	-7.750	1.73	1.17	3.03	-5.053	-6.448	-13.327	2.17	2.07	2.64

Tab. 3.7 Dynamic amplification effects for the damage scenario SC1 in terms of bending moments at the lowest cross-sections of the pylons for the cable-stayed and HCS configurations

In order to verify the vulnerability of the structures against the observed bending moments, comparisons between applied stresses and elastic interaction domain of girder and pylon cross-sections are proposed.

To this end, in Fig. 3.52, the time histories of the internal forces, i.e. axial (N) and bending (M), for different damage scenarios are compared to the values of the limit elastic domain. Such results are important to verify if inelasticity phenomena in the beam elements occur during the damage mechanisms produced in the cable system.

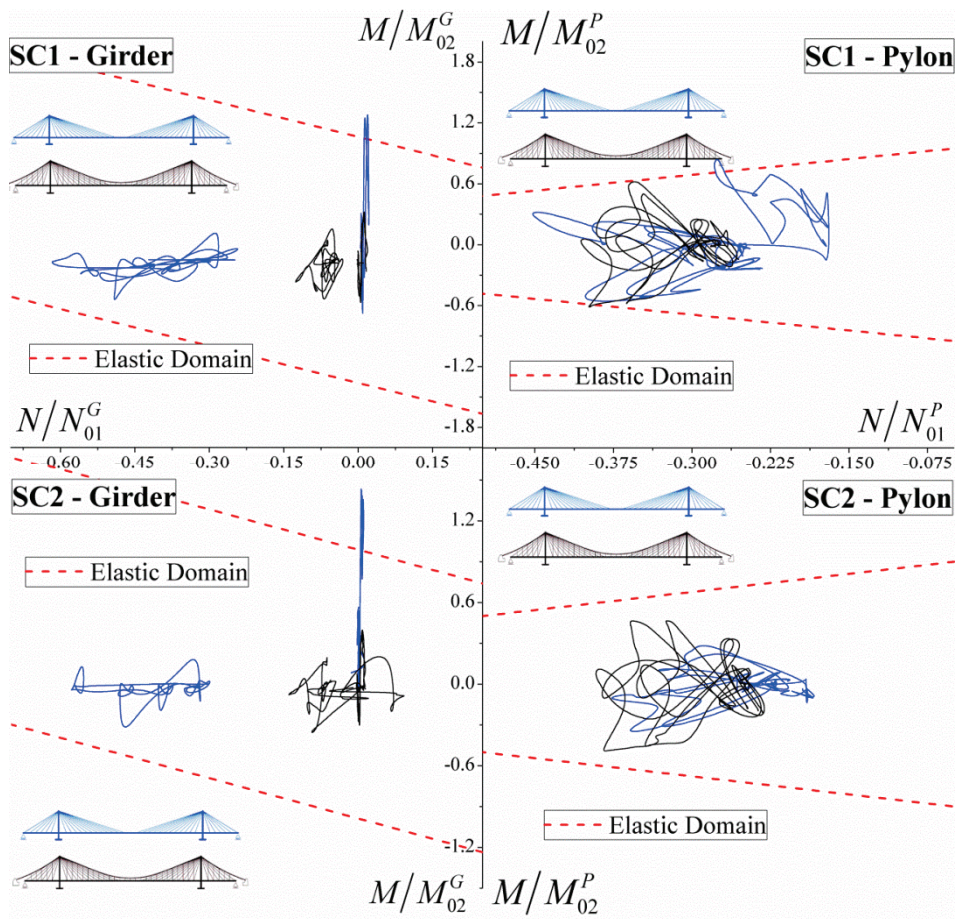


**Fig. 3.52** Hybrid Cable-Stayed Suspension/Cable stayed bridges: diagrams representing the path traced over time by the stress resultant (M,N) in the girder and pylons for SC1 and SC2 damage scenarios.

In particular, for several sections of the girder, i.e.  $X/LT=[1/2, 1+L/4, 1+L/2]$  and for the lowest ones of the pylons, the path traced over time by the values of internal forces (N,M) for SC1 and SC2 damage scenarios are presented in Fig. 3.52 (a-b) and Fig. 3.52 (c,d), respectively.

The analyses denote that the worst damage scenario for the cable-stayed is the one associated to the failure of the anchor-stay for which cable-stayed configuration is affected by internal stresses larger than those of the limit elastic domain. Results concerning HCS bridges denote the ability of such structures to reduce internal forces, which are always inside the elastic domain.

The behavior of the cable system is analyzed for the SC4 damage scenario with the purpose of investigating the effect produced by the failure in the hanger elements (Figs 3.53-3.54).

In particular, the influence of the damage description on the cable system stress distribution is analyzed as a function of the cable release dynamic characteristics, adopting for the damage description both static and dynamic damage definition. The analysis is developed for dead and live loads.

Moreover, PTI recommendations are reported to validate the applicability of such prescriptions in the framework of suspension and combined bridge systems. The results show that such damage scenario is able to produce the most dangerous amplifications in the cable stresses with respect to the previous ones.

The failure mode in both bridge configurations produces amplifications of the stresses, mainly, in proximity of the failure region, in which the hangers stresses reach values much larger than the allowable quantity, i.e. equal to 6 or 4 for the suspension and the combined bridge schemes, respectively.

Moreover, the dynamic characteristics of the moving loads are able to produce amplifications of such internal stresses, with a maximum factor, in comparison to the corresponding static quantities, equal to 1.7.

The comparisons between the proposed modeling and PTI recommendations denote that the code prescriptions produce overestimated predictions as opposed to those obtained by the proposed model, based on a fully coupled dynamic analysis.

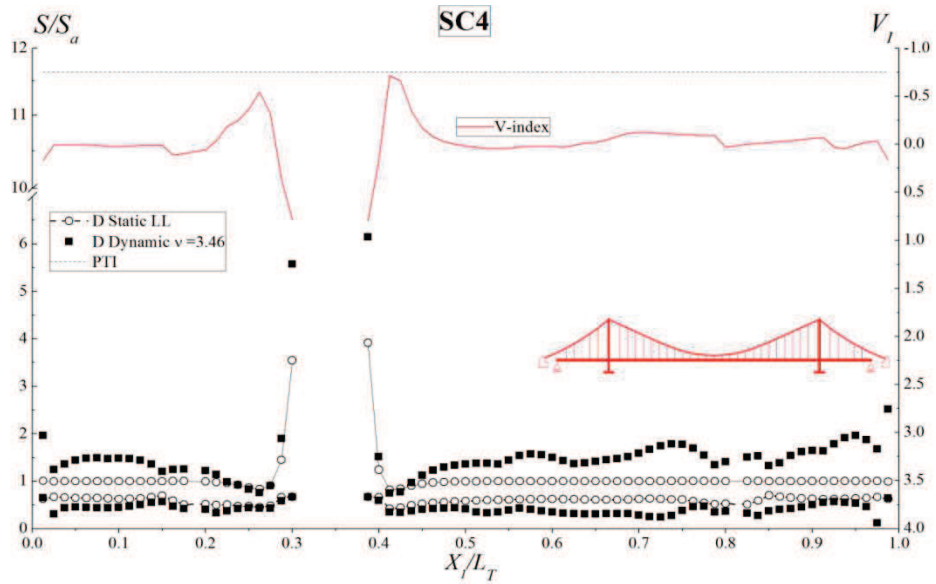


Fig. 3.53 Suspension Bridge: Envelope stress distribution in the cable systems under the action of live loads (LL) and vulnerability behavior for the damage scenario SC4

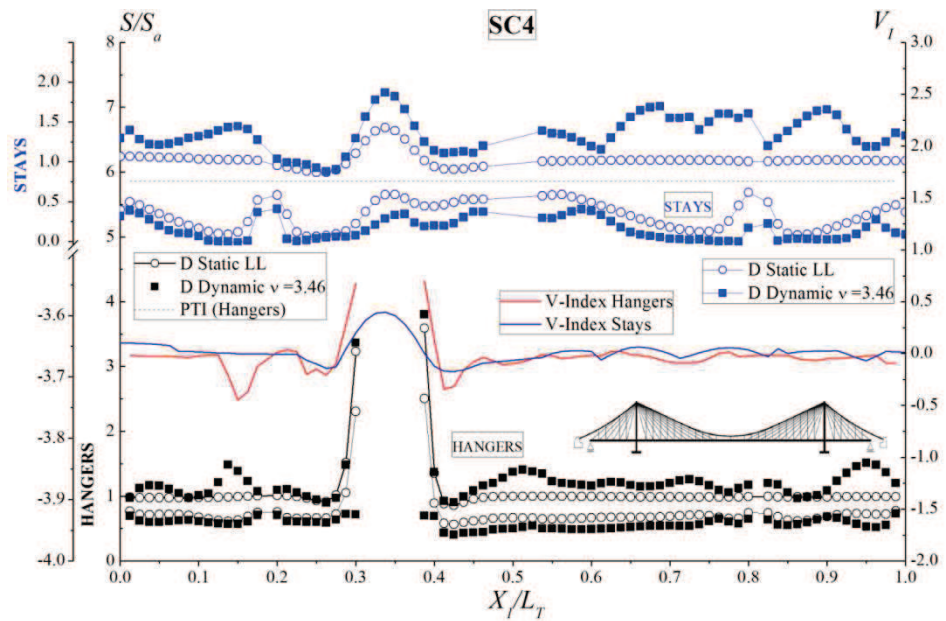
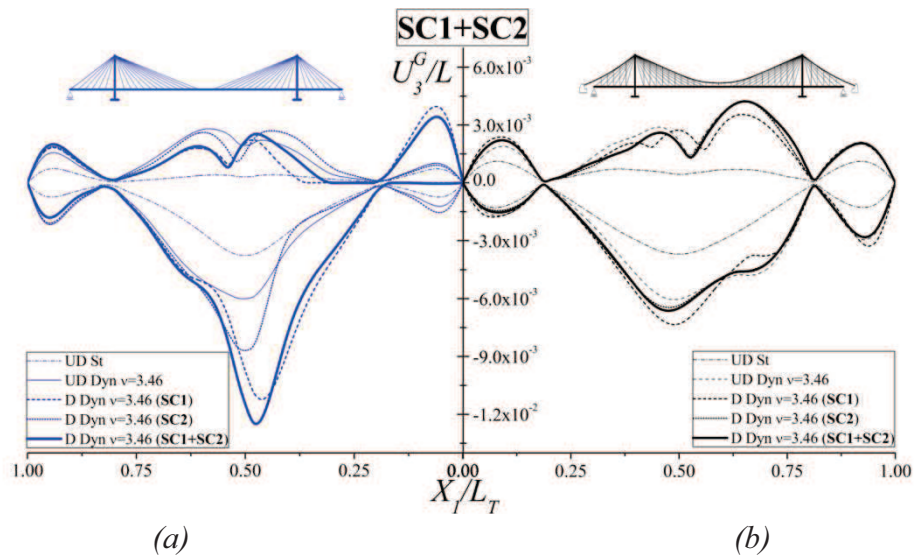


Fig. 3.54 Hybrid Cable-Stayed Suspension bridge: Envelope stress distribution in the cable systems under the action of live loads (LL) and vulnerability behavior for the damage scenario SC4

Results concerning the HCS bridge schemes reveal that the cable system based on both hanger and stay elements is able to reduce the effects of the failure mechanisms, since lower amplifications than those observed in the suspension bridge are noted (almost equal to a two factor).

This behavior can be explained in view of the presence of the stay elements, which are able to better redistribute the additional stresses produced by the cable release mechanisms, leading lower stress levels in the cable system.

Finally, additional results are developed to verify the interaction between different damage mechanisms considered in the analyses and their effects on the bridge behavior. In particular, the main aim of such investigations is to evaluate the ability of the bridge scheme to redistribute the over stresses involved in the cable system by the presence of more than one damage mechanism. The analyses are proposed by mean of comparisons between cable-stayed, suspension and HCS bridge typologies. In particular, in Fig. 3.55 (a-b), the envelope of vertical displacements of the girder produced by the presence of damage scenarios SC1 and SC2, considered individually or simultaneously, for both cable stayed and HCS bridge schemes is presented.



**Fig. 3.55** Envelope of vertical displacements of CS(a) and HCS (b) produced by damage scenarios SC1 and SC2, considered individually and simultaneously

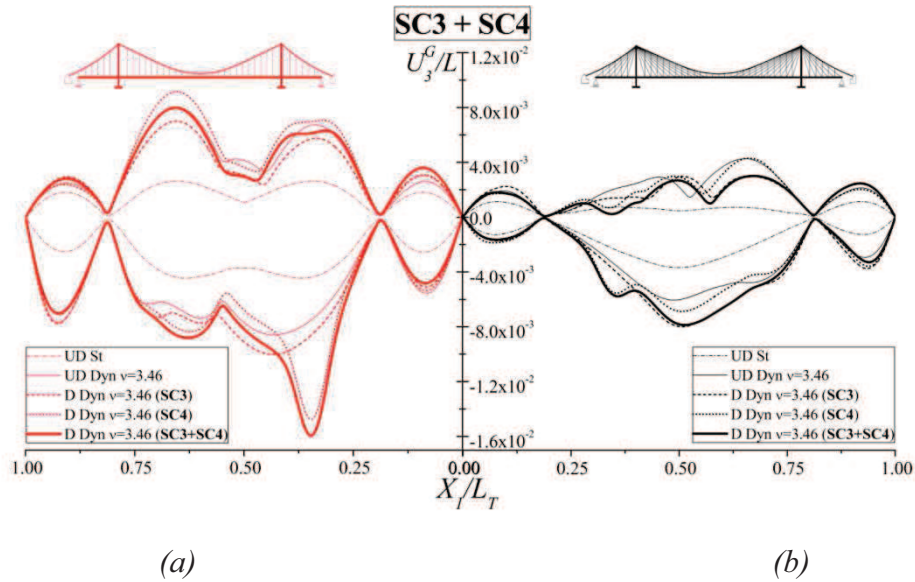


**Fig. 3.56** Envelope of vertical displacements of SP (c) and HCS (d) produced by damage scenarios SC3 and SC4, considered individually and simultaneously

Similarly, in Fig 3.56 (a-b), results concerning suspension and HCS bridge schemes are proposed in terms of damage scenarios SC3 and SC4.

The analyses denote that cable-stayed bridges are affected mostly by the failure mechanisms in the anchor stay, i.e. SC1. The concurrent presence of SC1 and SC2 produces an increment of maximum vertical displacement, measured from the SC1, equal to 11.52%. Such amplification of deformability is not observed in the case of HCS bridge schemes, whose maximum displacement is practically unaffected by the presence of the presence of more than one damage scenario.

Similar, results are obtained from the comparisons between the suspension and HCS systems. In particular, the worst damage scenario is the one involved by the failure of the hangers elements, i.e. SC4; results concerning HCS schemes denote that such bridges are practically unaffected by the combined effects of the damage scenarios, since the same displacements are observed. However, more refined analyses should be developed taking into

account different damage scenarios from the ones considered in the present analysis.

# 4

## **NONLINEAR BEHAVIOR OF SELF-ANCHORED CABLE-STAYED SUSPENSION BRIDGES (S.A.C.S.)**

### **4.1 Introduction**

Cable supported bridges have emerged as the dominant structural system for long span bridge crossing during the past thirty years.

That success is due to a combination of technical advancements and pleasing aesthetics attributes. The interaction of the various structural components results in an efficient structure which is continuously evolving and providing new methods to increase span lengths. As the span length increases more realistic analysis models are needed to improve the safety and reliability of these structures. In particular, more accurate and precise analysis techniques, which consider both material and geometric nonlinearities are required to predict the realistic behavior of structures. As a matter of fact, geometric and material nonlinearities affect cable supported bridges behavior significantly. Material nonlinearities come from the nonlinear stress–strain behavior of materials and they arise when one or more bridge elements exceed their individual elastic limits. Geometric nonlinearities may arise from different sources.



The cable system is affected by nonlinear behavior of single elements, since they exhibit a different response in loading and in unloading due to the cable “sag” effect induced by self-weight. For girder and pylons, the actual trend is to use more shallow or slender elements which are very flexible and undergo large displacements before attaining their equilibrium configuration (*P- $\Delta$  effect*). Moreover, nonlinear effects may arise owing to the so-called beam-column effect: beam-column effect can occur in cable supported bridges whose cable system configuration includes cable-stayed portions as pure cable-stayed, hybrid cable-stayed suspension and self-anchored cable-stayed suspension schemes. In these cases, since a high pretension force exists in stays, girder and pylons are subjected to a large axial compression and bending moment under the action of dead and live loads. Lateral deflection and axial force are interrelated such that the bending stiffness is dependent on the element axial force and the presence of bending moments will affect the axial stiffness. In particular the element bending stiffness decreases for compression axial force and increases for a tension force.

Since axial compression increases in proportion to the length of the central span, geometrical instabilizing effect can occur for girder and pylons. It is worth nothing that, the buckling instability of girder and pylons may be a fundamental problem that should be checked in the preliminary design of such bridge types because it directly controls the geometric dimensions of structural members and the practical limitation of the center span length.

However, the response of each element of cable system affects significantly the structural behavior regarding buckling. As a matter of fact, the axial stiffness of a cable will change with changing sag resulting in a stable or unstable effect regarding buckling. If the change in tension for a cable during a load increment is positive it will be a retaining effect and vice versa. This imply that the interaction between cable system and girder and pylons as well as the interaction between nonlinearity sources play a crucial role in the prediction of the nonlinear behavior of cable supported bridges. As a consequence, analysis models which not include all nonlinearity sources may lead to inappropriate predictions of structural behavior and, as a consequence, to notable

underestimation of the maximum load carrying capacity of the bridge structure for specific loading conditions.

However, the definition of the maximum load carrying capacity for a cable supported bridge has to be defined taking into account the evolution of the structure until the critical condition including effects related to nonlinearity sources, residual stresses and structural imperfections. For this reason, a conventional buckling analysis is not applicable. The most appropriate approach for analyzing the structural behavior of cable supported bridges is to employ a nonlinear inelastic analysis which allows to trace the equilibrium path and identify the ultimate strength of the structure. This approach, known as limit point instability approach, can account for all geometric and material nonlinearities. In this framework, several methodologies were developed, which differ from each other depending on the assumption made for reproduce the nonlinearity sources. As far as cable element, the material nonlinearity was taken into account simply excluding the presence of the element which reaches the yield stress, while the geometric nonlinearity due to sag effect was reproduced by three different possibilities: the elastic catenary formulation, the multiple-straight link discretisation and the modified modulus method, known as Ernst method. The elastic catenary formulation is consistent with the cable theory of Irvine whose geometrical compatibility equations and the expression of the cable tension along the curvilinear coordinate  $s$  in the three-dimensional space, with reference to Fig. 4.1, can be written as:

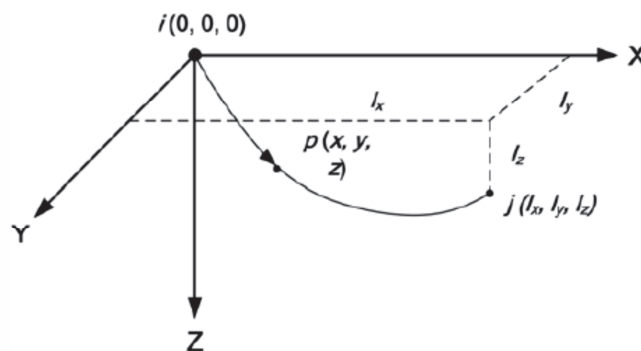


Fig. 4.1 Spatially suspended elastic catenary cable

$$T(s) = \left[ F_1^2 + F_2^2 + \left( F_3 + W \frac{s}{L_0} \right)^2 \right]^{1/2} \quad (4.1)$$

$$x(s) = \frac{F_1}{EA_0} s + \frac{F_1 L_0}{W} \left[ \sinh^{-1} \left( \frac{F_3}{H} \right) - \sinh^{-1} \left( \frac{F_3 - \frac{Ws}{L_0}}{H} \right) \right]$$

$$y(s) = \frac{F_1}{EA_0} s + \frac{F_2 L_0}{W} \left[ \sinh^{-1} \left( \frac{F_3}{H} \right) - \sinh^{-1} \left( \frac{F_3 - \frac{Ws}{L_0}}{H} \right) \right] \quad (4.2)$$

$$z(s) = \frac{F_3}{EA_0} s - \frac{F_1}{2EA_0} - \frac{HL_0}{W} \left\{ \left[ 1 + \left( \frac{F_3}{H} \right)^{1/2} \right] - \left[ 1 + \left( \frac{F_3 - \frac{Ws}{L_0}}{H} \right)^{1/2} \right] \right\}$$

$$\text{where } H = \sqrt{F_1^2 + F_2^2}$$

In the Eqs. (4.2),  $W$ ,  $A_0$  and  $E$  are, respectively, the self-weight, the cross-section and the elasticity modulus of the cable, whereas  $L_0$  is the cable length. The multiple-straight link approach is based on the use of multi truss elements. This approach divide each cable into several straight truss elements to adequately model both the sag effect due to the self-weight and the vibration modes of the cables. The Ernst method or modified elastic modulus method is often used in the analysis of cable-stayed bridges. In this approach each cable is replaced by one bar element and the sag effect is accounted for by an equivalent or fictitious elasticity modulus, which can be written as:

$$E_{eq}^{bar} = \frac{E^{cable}}{1 + \frac{(\rho g L_x)^2}{12 \sigma^3} E^{cable}} \quad (4.3)$$

where  $E^{cable}$  is the cable modulus of elasticity,  $\rho$  is the density of the cable material,  $g$  is the acceleration of gravity,  $L_x$  is the horizontal projected length of the cable, and  $\sigma$  the tensile stress in the cable. As far as girder and pylon geometrical nonlinearities, the beam-column effect was reproduced either through the use of stability functions or by considering a narrow mesh refinement with a finite element solver.

The stability functions reflect the stiffness degradation caused by the interaction effect between the axial force and bending moments. The force–displacement relationship of a beam–column can be written as:

$$[F]_{Local} = K[12 \times 12]_{Local} \times [U]_{Local} \tag{4.4}$$

where  $K[12 \times 12]_{Local}$  is the nonlinear tangent stiffness matrix for the beam–column reported in Fig. 4.2

$F_{10}$	$S_{1k_{1,1}}$													$u_0$
$F_{20}$	0	$S_{1k_{2,2}}$												$v_0$
$F_{30}$	0	0	$S_{1k_{3,3}}$											$w_0$
$M_{10}$	0	0	0	$k_{c,4}$					Symm -etric					$\theta_{10}$
$M_{20}$	0	0	$S_{1k_{5,3}}$	0	$S_{1k_{5,5}}$									$\theta_{20}$
$M_{30}$	0	$s_{1k_{6,2}}$	0	0	0	$s_{1k_{6,6}}$								$\theta_{30}$
$F_{50}$	$s_{1k_{7,1}}$	0	0	0	0	0	$S_{1k_{7,7}}$							$u_0$
$F_{70}$	0	$s_{1k_{8,2}}$	0	0	0	$s_{1k_{8,6}}$	0	$S_{1k_{8,8}}$						$v_0$
$F_{90}$	0	0	$s_{1k_{9,3}}$	0	$s_{1k_{9,5}}$	0	0	0	$S_{1k_{9,9}}$					$w_0$
$M_{60}$	0	0	0	$k_{10,4}$	0	0	0	0	0	$k_{10,10}$				$\theta_{60}$
$M_{70}$	0	0	$s_{1k_{11,3}}$	0	$s_{1k_{11,5}}$	0	0	0	$s_{1k_{11,9}}$	0	$s_{1k_{11,11}}$			$\theta_{70}$
$M_{80}$	0	$s_{1k_{12,2}}$	0	0	0	$s_{1k_{12,6}}$	0	$S_{1k_{12,8}}$	0	0	0	$s_{1k_{12,12}}$		$\theta_{80}$

Fig. 4.2 Nonlinear tangent stiffness matrix for a three-dimensional beam-column element

where the modification factors  $s_i$  with  $i = 1, \dots, 9$  are the stability function defined by the member length, cross-section properties, axial force and the end-moments. The stability functions assume different expression depending on the axial force is compression or tension. On the other hand, the material nonlinearities can be included by two approaches: plastic zone method or plastic hinge method. In the plastic zone method, a frame member is discretized into several elements, and the cross-section of each element is further subdivided into many fibers. The inelastic behavior of each fiber is accounted for by tracing the uniaxial stress-strain relationship. In the plastic hinge method material nonlinearity is considered by introducing plastic hinges at the element ends and within the element length. Plastic hinges are formed when the cross-section forces satisfy the plasticity criterion, which is expressed by a force-space interaction function. It is worth nothing that the plastic zone method is able to obtain the “exact solution”, although is too intensive in computation. Plastic hinge method is less expensive from a computational point of view, but over predicts the strength and stiffness of members.

## 4.2 The proposed analysis model

The nonlinear behavior of self-anchored cable-stayed suspension bridges is performed by a limit point instability approach based on a quasi-static transient analysis with increasing live loads.

Since the bridge behavior is mostly influenced by the post-tensioning force distributions in the cable system, a static analysis to identify the initial geometrical configuration of the bridge under the action of dead loads, that is the “zero configuration”, is performed in advance.

The initial configuration of the bridge has to satisfy both equilibrium and design requirements and it can be obtained by one of approaches described in chapter 2. Once the initial configuration is determined in terms of the post-tensioning cable forces distribution and cross-section dimensioning, it is set as initial condition for a new analysis in which the structure is loaded with increasing live load. In particular, the live load intensity is expressed as a

function of a scalar parameter  $\lambda$  which corresponds to the ratio between current and service load value. The scalar parameter  $\lambda$  is known as the load multiplier.

In the case of cable supported bridges, since the relationship between applied loads and displacements is highly nonlinear, a good approach to control the displacement amount is to use an algebraic equation that controls the value of  $\lambda$ , so that the generalized deflection of a selected control point reaches the prescribed values. Letting  $K$  and  $\Delta \underline{U}_K$ , respectively, the control point and the rate displacement vector resulting from the loading process, the control point displacement amount is controlled by the following explicit constraint equation:

$$\underline{L}_{CP} [\lambda, \Delta \underline{U}_K^G - C_L \Delta t] = 0 \quad (4.5)$$

where  $\underline{L}_{CP}$  is the constraint operators referred to the control point, whereas  $C_L$  and  $\Delta t$  are, respectively, the load increase speed and the time step analysis. At each time step, the previous condition (4.5) determines the value of the load multiplier  $\lambda$  such that the control point displacement  $\Delta \underline{U}_K^G$  is equal to the controlled displacement rate  $C_L \Delta t$ . Consequently, small values of the load increase speed imply small rate of control point displacement for a fixed time step. For each load increment, the nonlinear structural response of the bridge is calculated according to the material and geometric nonlinearities whose theoretical formulation is introduced in the next paragraph.

### 4.3 The formulation of nonlinear material behavior

#### 4.3.1 Girder and pylon

Girder and pylons are mainly subjected to axial force and bending moment. As a consequence, the nonlinear material behavior can be taken into account by a gradual yielding theory based on the combination of the Column Research Council (CRC) tangent modulus concept and a plastic hinge model (Chen, Kim and Choi, 2001). The first is suitable to account for gradual yielding along the length of an axially loaded element between plastic hinge,

while the latter, is used to represent the partial plasticization effect associate with the bending. The CRC tangent modulus can be expressed as:

$$\begin{aligned} E_t &= 1.0E & \text{for } N_l \leq 0.5P_y \\ E_t &= 4 \frac{N_l}{P_y} E \left( 1 - \frac{N_l}{P_y} \right) & \text{for } N_l > 0.5P_y \end{aligned} \quad (4.6)$$

where  $P_y$  is the full plastic axial load.

The gradual inelastic bending stiffness reduction is expressed by a dimensionless reduction parameter  $\eta$  which is assumed to vary according to the following parabolic functions Fig. 4.3:

$$\begin{aligned} \eta &= 1.0 & \text{for } \alpha \leq 0.5 \\ \eta &= 4\alpha(1-\alpha) & \text{for } \alpha > 0.5 \end{aligned} \quad (4.7)$$

where  $\alpha$  is a force-state parameter which measures the magnitude of axial force and bending moment at the element end.

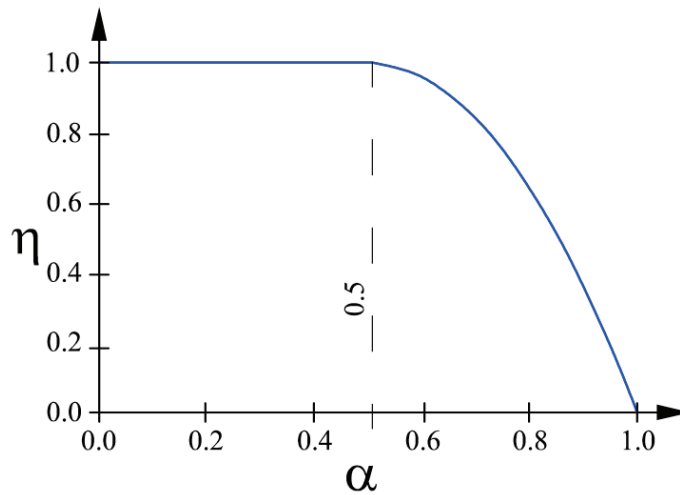


Fig. 4.3 Flexural stiffness reduction model for refined plastic hinge analysis

The term  $\alpha$  was expressed by AISC-LRFD interaction expression which express the cross-section plastic strength of the element as:

$$\alpha = \frac{N_l}{P_l} + \frac{8}{9} \frac{M_{l,y}}{M_{l,yp}} + \frac{8}{9} \frac{M_{l,z}}{M_{l,zp}} \quad \text{for} \quad \frac{N_l}{P_l} \geq \frac{2}{9} \frac{M_{l,y}}{M_{l,yp}} + \frac{2}{9} \frac{M_{l,z}}{M_{l,zp}} \quad (4.8)$$

$$\alpha = \frac{N_l}{2P_l} + \frac{M_{l,y}}{M_{l,yp}} + \frac{M_{l,z}}{M_{l,zp}} \quad \text{for} \quad \frac{N_l}{P_l} < \frac{2}{9} \frac{M_{l,y}}{M_{l,yp}} + \frac{2}{9} \frac{M_{l,z}}{M_{l,zp}}$$

where  $M_{py}$  and  $M_{pz}$  are the full plastic moments of the y- and z-axes for the element, respectively.

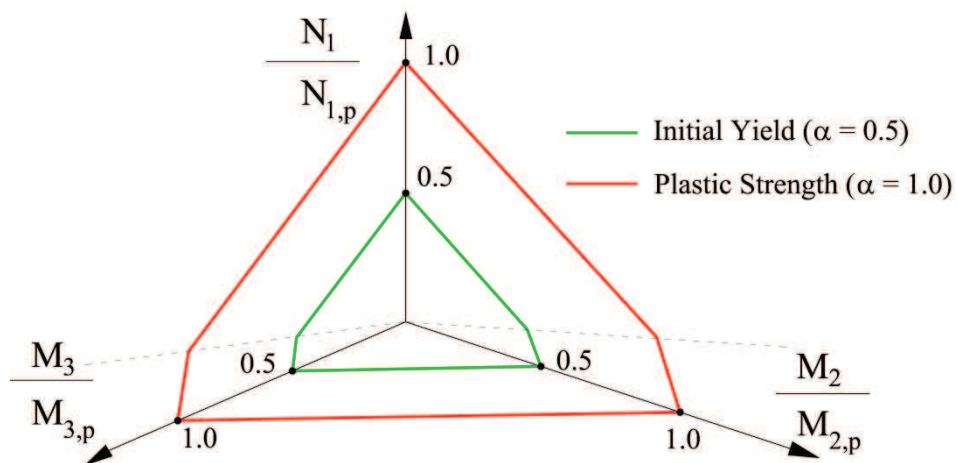


Fig. 4.4 Full plastification surface of AISC-LRFD

### 4.3.2 Cable elements

The nonlinear material behavior of cables is defined according to the finite plasticity theory of Green and Naghdi which forms the basis for modelling the behavior of a wide array of materials that exhibit elastic-plastic behavior at a macroscopic scale [Lu 1998 – Lu 2001].



The finite plasticity theory of Green and Naghdi is based on the following hypotheses:

- 1) The existence of a second-order tensor  $\underline{E}^P$  which serves as a measure of plastic strain as well as the existence of a symmetric Lagrangian tensor  $\underline{\alpha}$  and a scalar  $\kappa$  which characterize, respectively, kinematic and isotropic hardening;
- 2) The admittance of a stress response function  $\widehat{\underline{S}}$ , such that the constitutive law for the second Piola-Kirchhoff stress tensor  $\underline{S}$  may be written as:

$$\underline{S} = \widehat{\underline{S}}(\underline{E}, \underline{E}^P, \kappa, \underline{\alpha}) \quad (4.9)$$

or, equivalently,

$$\underline{S} = \widehat{\underline{S}}(\underline{E} - \underline{E}^P, \underline{E}^P, \kappa, \underline{\alpha}) \quad (4.10)$$

Furthermore, the function  $\widehat{\underline{S}}$  is taken to be invertible for fixed values of  $\underline{E}^P$ ,  $\kappa$ ,  $\underline{\alpha}$ , therefore one may equivalently write:

$$\underline{E} = \widehat{\underline{E}}(\underline{S}, \underline{E}^P, \kappa, \underline{\alpha}) \quad (4.11)$$

- 3) The existence of a convex, differentiable, yield function expresses in stress-space and strain-space, respectively, as  $f = f(\underline{S}, \underline{E}^P, \kappa, \underline{\alpha})$  and  $\bar{f} = \bar{f}(\underline{E}, \underline{E}^P, \kappa, \underline{\alpha})$ , so that the admissible state variable in stress-space belong to the set  $U := \{(\underline{S}, \underline{E}^P, \kappa, \underline{\alpha}) \mid f(\underline{S}, \underline{E}^P, \kappa, \underline{\alpha}) \leq 0\}$ .
- 4) The admittance of a symmetric second-order tensor function  $\underline{h} = \underline{h}(\underline{S}, \underline{E}^P, \kappa, \underline{\alpha})$ , a scalar function  $\sigma = \sigma(\underline{S}, \underline{E}^P, \kappa, \underline{\alpha})$  and a second-order tensor function  $\underline{\rho} = \underline{\rho}(\underline{S}, \underline{E}^P, \kappa, \underline{\alpha})$  in stress-space and their respective counterpart  $\bar{\underline{h}} = \bar{\underline{h}}(\underline{E}, \underline{E}^P, \kappa, \underline{\alpha})$ ,  $\bar{\sigma} = \bar{\sigma}(\underline{E}, \underline{E}^P, \kappa, \underline{\alpha})$  and  $\bar{\underline{\rho}} = \bar{\underline{\rho}}(\underline{E}, \underline{E}^P, \kappa, \underline{\alpha})$  in strain-space, so that the evolutions of plastic strain and hardening variables during plastic loading take the form:

$$\dot{\underline{E}}^P = \gamma \underline{h}(\underline{E}, \underline{E}^P, \kappa, \alpha) \quad (4.12)$$

$$\dot{\alpha} = \gamma \underline{\rho}(\underline{E}, \underline{E}^P, \kappa, \alpha) \quad (4.13)$$

$$\dot{\kappa} = \gamma \sigma(\underline{E}, \underline{E}^P, \kappa, \alpha) \quad (4.14)$$

where  $\gamma$  is the plastic consistency parameter.

An identification of the loading/unloading conditions can be obtained by the strain-space formulation. Indeed, letting

$$\hat{\bar{f}} = \frac{\partial \bar{f}}{\partial \underline{E}} \cdot \dot{\underline{E}} \quad (4.15)$$

the loading/unloading conditions are identified as follows:

$$\bar{f} < 0 \rightarrow \text{elastic state} \quad (4.16)$$

$$\bar{f} = 0 \rightarrow \text{plastic state} \begin{cases} \hat{\bar{f}} < 0: & \text{unloading} \\ \hat{\bar{f}} = 0: & \text{neutral loading} \\ \hat{\bar{f}} > 0: & \text{plastic loading} \end{cases} \quad (4.17)$$

The consistency condition  $\dot{\bar{f}} = 0$  imposed during loading ensures that the time evolution of the state variables is compatible with the current yield surface. Considering Eqs. (4.12)-(4.15) one may write:

$$\hat{\bar{f}} + \gamma \left( \frac{\partial \bar{f}}{\partial \underline{E}^P} \cdot \underline{h} + \frac{\partial \bar{f}}{\partial \alpha} \cdot \underline{\rho} + \frac{\partial \bar{f}}{\partial \kappa} \sigma \right) = 0 \quad (4.18)$$

The parameter  $\gamma$  is directly determined from Eq. (4.18), since the quantity inside the parenthesis necessarily attains non-zero values. A physically motivated work-based constitutive restriction can be postulated in order to simplify the structure of Eq.s (4.9) and (4.12), that is, the work done by the

external load in any temporally smooth, spatially homogeneous and closed strain cycle is nonnegative:

$$\int_{t_1}^{t_2} \underline{\underline{S}} \cdot \underline{\underline{\dot{E}}} \, d\tau \geq 0 \quad (4.19)$$

The above work inequality implies that exists a potential  $\psi = \psi(\underline{\underline{E}}, \underline{\underline{E}}^P, \kappa, \alpha)$ , such that

$$\underline{\underline{S}} = \frac{\partial \psi}{\partial \underline{\underline{E}}} \quad (4.20)$$

Moreover, it implies a generalized normality rule:

$$\frac{\partial \widehat{\underline{\underline{S}}}}{\partial \underline{\underline{E}}^P} \underline{\underline{\dot{E}}}^P + \frac{\partial \widehat{\underline{\underline{S}}}}{\partial \alpha} \dot{\alpha} + \frac{\partial \widehat{\underline{\underline{S}}}}{\partial \kappa} \dot{\kappa} = -\lambda^* \frac{\partial \bar{f}}{\partial \underline{\underline{E}}} \quad (4.21)$$

where,  $\lambda^*$  is a positive multiplier (also called plastic multiplier) which depends on the current state of stress and load history. A coherent assumption for purposes of the present work is that the stress response function  $\widehat{\underline{\underline{S}}}$  depends exclusively on  $\underline{\underline{E}} - \underline{\underline{E}}^P$ , so that the Second Piola-Kirchhoff stress can be expressed as following:

$$\underline{\underline{S}}_n = E(\underline{\underline{\varepsilon}}_n - \underline{\underline{\varepsilon}}_n^P) + \underline{\underline{S}}_{ni} \quad (4.22)$$

where  $\underline{\underline{\varepsilon}}_n$  is the total axial strain,  $\underline{\underline{\varepsilon}}_n^P$  is the axial plastic strain and  $\underline{\underline{S}}_{ni}$  is the initial stress. Moreover, such assumption imply that Eq. (4.21) reduces to the classical normality rule for the rate of plastic strain. This leads that plastic rate can be obtained by the Drucker-Prager conditions:

$$\lambda^* \geq 0, \bar{f} \leq 0 \text{ and } \lambda^* \bar{f} = \dot{\lambda}^* \bar{f} = 0 \quad (4.23)$$

## 4.4 Bridge and geometric nonlinear formulation

In this section the governing equations for the bridge constituents, including assumptions made to account for geometric nonlinearities of structural members are discussed. Such governing equations represent the basis for the theoretical formulation of the model, whose numerical implementation is presented in the next paragraph.

### 4.4.1 Girder and towers

Girder and towers are described by tridimensional geometric nonlinear beam elements by means of a formulation based on Euler-Bernoulli kinematic assumptions and a Green-Lagrange strain measure. The constitutive relationships are defined on the basis of moderately large rotations in which only the square of the terms  $U_{i,X_1}^{2G}$  representing the rotations of the transverse normal line in the beam are considered. Starting from the status concerning the initial configuration in which only dead loading are considered, the following relationships between generalized strain and stress variables are obtained:

$$\begin{aligned}
 N_1^G &= N_1^{0(G)} + E_t^G A^G \varepsilon_1^G \\
 &= N_1^{0(G)} + E_t^G A^G \left\{ U_{1,X_1}^G + \frac{1}{2} \left[ U_{1,X_1}^{2(G)} + U_{2,X_1}^{2(G)} + U_{3,X_1}^{2(G)} \right] \right\} \\
 M_2^G &= M_2^{0(G)} + \eta^G E_t^G I_2^G \chi_2^G \\
 &= M_2^{0(G)} + \eta^G E_t^G I_2^G \Psi_{2,X_1}^G \\
 &= M_2^{0(G)} - \eta^G E_t^G I_2^G U_{3,X_1 X_1}^G \\
 M_3^G &= M_3^{0(G)} + \eta^G E_t^G I_3^G \chi_3^G \\
 &= M_3^{0(G)} + \eta^G E_t^G I_3^G \Psi_{3,X_1}^G \\
 &= M_3^{0(G)} + \eta^G E_t^G I_3^G U_{2,X_1 X_1}^G \\
 M_1^G &= G^G J_t^G \Theta^G = G^G J_t^G \Psi_{1,X_1}^G
 \end{aligned} \tag{4.24}$$

where  $E_t^G A^G$  and  $\varepsilon_1^G$  are the axial stiffness and strain defined on the basis of Eq.(4.6),  $\chi_2^G$  and  $\chi_3^G$  or  $\eta E_t^G I_2^G$  and  $\eta E_t^G I_3^G$  are the curvatures or the bending stiffnesses with respect to the  $X_2$  and  $X_3$  axes, respectively. It is worth nothing that, previous bending stiffnesses are expressed as a function of Eqs. (4.6) and (4.7). Moreover,  $\Theta^G$  and  $G^G J_t^G$  are the torsional curvature and stiffness, respectively,  $N_1^G$  is the axial stress resultant,  $M_2^G$  and  $M_3^G$  are the bending moments with respect to the  $X_2$  and  $X_3$  axes, respectively,  $M_1^G$  and  $G^G J_t^G$  are torsional moment and girder stiffness, respectively, and  $(\cdot)^0$  represents the superscript concerning the variables associated with the "zero configuration". The external loads are expressed by a vector:

$$\underline{p} = [p_{X_1}, p_{X_2}, \lambda p_{X_3}] \tag{4.25}$$

In particular, the load component along vertical axis is expressed as a function of the load multiplier  $\lambda$ . Furthermore, an eccentricity  $e$  with respect to the geometric axis can be considered.

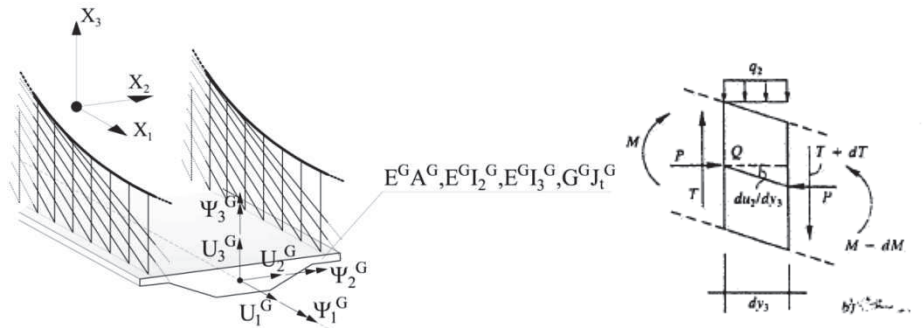


Fig. 4.5 Girder cross-section notations

On the basis of Eq.s (4.24) and (4.25), taking into account notation reported in Fig. 4.5, the governing equations are derived by means of the local form of static equilibrium equations as:

$$\begin{aligned}
& \frac{d}{dX_1} \left\{ N_1^G \left( 1 + \frac{dU_1^G}{dX_1} \right) \right\} + p_{x_1} = 0, \\
& -\eta^G E_t^G I_2^G \frac{d^4 U_3^G}{dX_1^4} - \frac{d}{dX_1} \left( N_1^G \frac{dU_3^G}{dX_1} \right) - \lambda p_{x_3} = 0, \\
& \eta^G E_t^G I_3^G \frac{d^4 U_2^G}{dX_1^4} - \frac{d}{dX_1} \left( N_1^G \frac{dU_2^G}{dX_1} \right) + p_{x_2} = 0, \\
& G^G J_t^G \frac{d^2 \Phi_1^G}{dX_1^2} - p_{x_3} e = 0
\end{aligned} \tag{4.26}$$

The pylon governing equations can be easily obtained from Eq.(4.26) by removing all the terms related to the external loads and changing the relative variables from with the superscript  $(\cdot)^G$  to  $(\cdot)^P$  and the parameters concerning the mechanical and material characteristics:

$$\begin{aligned}
& \frac{d}{dX_1} \left\{ N_1^P \left( 1 + \frac{dU_1^P}{dX_1} \right) \right\} = 0 \\
& -\eta^P E_t^P I_2^P \frac{d^4 U_3^P}{dX_1^4} - \frac{d}{dX_1} \left( N_1^P \frac{dU_3^P}{dX_1} \right) = 0 \\
& \eta^P E_t^P I_3^P \frac{d^4 U_2^P}{dX_1^4} - \frac{d}{dX_1} \left( N_1^P \frac{dU_2^P}{dX_1} \right) = 0 \\
& G^P J_t^P \frac{d^2 \Phi_1^P}{dX_1^2} = 0
\end{aligned} \tag{4.27}$$

#### 4.4.2 Cable element

The constitutive laws of the cable are defined by the second Piola-Kirchhoff stress  $(S_1^C)$  and Green-Lagrange strain  $(E_1^C)$  as:

$$S_1^C(X) = S_0^C + C^C [E_1^C(X) - E_{1,p}(X)] \tag{4.28}$$

where  $C^c$  is the elastic modulus,  $S_0^c$  is the stress referred to the initial configuration. The governing equations of a single cable are expressed by means of the following partial differential equations:

$$\begin{aligned} \frac{d}{dX_1} \left[ N_1^c + N_1^c \frac{dU_1^c}{dX_1} \right] - b_1 &= 0 \\ \frac{d}{dX_1} \left[ N_1^c \frac{dU_2^c}{dX_1} \right] &= 0 \\ \frac{d}{dX_1} \left[ N_1^c \frac{dU_3^c}{dX_1} \right] - b_2 &= 0 \end{aligned} \quad (4.29)$$

where  $N_1^c$  is the axial force defined as  $N_1^c = S_1^c A^c$  with the area of generic  $i$ -th cable element,  $\varphi_1$  and  $\varphi_2$  are the slope angles of the cable along the  $X_1X_2$  and  $X_1X_3$ , respectively,  $b_1$  and  $b_2$  are the body load projections in the  $X_1X_2$  and  $X_1X_3$ , respectively.

## 4.5 Finite element implementation

The governing equations reported in the previous section introduce a nonlinear partial differential system, whose analytical solution is quite complex to be extracted. As a consequence, a numerical approach based on the finite element formulation is utilized.

In particular, starting from Eq. (2.49) and Eq. (2.52), the corresponding weak forms for the  $i$ -th finite element related to the girder ( $G$ ), pylon ( $P$ ) and the cable system ( $C$ ), respectively, are defined by the following expressions:

Girder

$$\begin{aligned}
 & \int_{l_e^i} N_1^G (1 + U_{1,X_1}^G) w_{1,X_1} dX_1 - \sum_{j=1}^2 N_{1j}^G U_{1j}^G = 0 \\
 & \int_{l_e^i} \left\{ -M_2^G w_{2,X_1,X_1} + (N_1^G U_{3,X_1}^G) w_{2,X_1} \right\} dX_1 - \sum_{j=1}^2 T_{3j}^G U_{3j}^G - \sum_{j=1}^2 M_{2j}^G \Phi_{3j}^G = 0 \\
 & \int_{l_e^i} \left\{ M_3^G w_{3,X_1,X_1} + (N_1^G U_{2,X_1}^G) w_{3,X_1} \right\} dX_1 - \sum_{j=1}^2 T_{2j}^G U_{2j}^G - \sum_{j=1}^2 M_{3j}^G \Phi_{2j}^G = 0 \\
 & \int_{l_e^i} M_1^G w_{4,X_1} dX_1 - \sum_{j=1}^2 M_{1j}^G \Phi_{1j}^G = 0
 \end{aligned} \tag{4.30}$$

Pylon

$$\begin{aligned}
 & \int_{l_e^i} N_1^P (1 + U_{1,X_1}^P) w_{1,X_1} dX_1 - \sum_{j=1}^2 N_{1j}^P U_{1j}^P = 0 \\
 & \int_{l_e^i} \left\{ -M_2^P w_{2,X_1,X_1} + (N_1^P U_{3,X_1}^P) w_{2,X_1} \right\} dX_1 - \sum_{j=1}^2 T_{3j}^P U_{3j}^P - \sum_{j=1}^2 M_{2j}^P \Phi_{3j}^P = 0 \\
 & \int_{l_e^i} \left\{ M_3^P w_{3,X_1,X_1} + (N_1^P U_{2,X_1}^P) w_{3,X_1} \right\} dX_1 - \sum_{j=1}^2 T_{2j}^P U_{2j}^P - \sum_{j=1}^2 M_{3j}^P \Phi_{2j}^P = 0 \\
 & \int_{l_e^i} M_1^P w_{4,X_1} dX_1 - \sum_{j=1}^2 M_{1j}^P \Phi_{1j}^P = 0
 \end{aligned} \tag{4.31}$$

Cable System

$$\begin{aligned}
 & \int_{l_e^i} N_1^C (1 + U_{1,X_1}^C) w_{1,X_1} dX_1 - \int_{l_e^i} b_1 w_1 dX_1 - \sum_{j=1}^2 N_{1j}^C U_{1j}^C = 0 \\
 & \int_{l_e^i} N_1^C w_{2,X_1} dX_1 - \sum_{j=1}^2 T_{2j}^C U_{2j}^C = 0 \\
 & \int_{l_e^i} N_1^C w_{3,X_1} dX_1 - \int_{l_e^i} b_3 w_3 dX_1 - \sum_{j=1}^2 T_{3j}^C U_{3j}^C = 0
 \end{aligned} \tag{4.32}$$



where  $(N_{1i}, T_{2i}, T_{3i}, M_{2i}, M_{3i})^k$  with  $k=C, G, P$  and  $i=1, 2$  represents the internal forces applied at the end node  $i$  of the generic cable ( $C$ ), girder ( $G$ ) or pylon ( $P$ ) element. Finite element expressions are written starting from the weak forms previously reported, introducing Hermit cubic interpolation functions ( $\xi_i$ ) for the girder and pylon flexures in the  $X_1X_2$  and  $X_2X_3$  deformation planes and Lagrange linear interpolation functions ( $\zeta_i$ ) for the cable system variables and the remaining variables of the girder and the pylons:

$$\begin{aligned}\underline{U}^C(\underline{r}, t) &= \underline{N}^C(\underline{r})\underline{q}^C(t) \\ \underline{U}^G(\underline{r}, t) &= \underline{N}^G\underline{q}^G(t) \\ \underline{U}^P(\underline{r}, t) &= \underline{N}^P\underline{q}^P(t)\end{aligned}\quad (4.33)$$

where  $\underline{q}^C, \underline{q}^G, \underline{q}^P$  are the vectors collecting the nodal degrees of freedom of the cable, girder and pylon respectively,  $\underline{N}^C, \underline{N}^G, \underline{N}^P$  are the matrixes containing the displacement interpolation function for cable element ( $C$ ), girder ( $G$ ) and pylons ( $P$ ),  $\underline{r}$  is the local coordinate vector of the  $i$ -th finite element. The discrete equations in the local reference system of the  $i$ -th element are derived substituting Eq.(4.33) into Eqs. (4.30)-(4.32), leading to the following equations in matrix notation:

$$\underline{K}^G\underline{U}^G = \underline{P}^G + \underline{Q}^G \quad (4.34)$$

$$\underline{K}^P\underline{U}^P = \underline{P}^P + \underline{Q}^P \quad (4.35)$$

$$\underline{K}^C\underline{U}^C = \underline{P}^C + \underline{Q}^C \quad (4.36)$$

where  $\underline{K}^i$  is the stiffness matrix,  $\underline{P}^i$  is the load vector produced by the dead and live loading,  $\underline{Q}^i$  is the unknown force vector collecting the point source. In order to reproduce the bridge kinematic correctly, additional relationships to define the connections between girder, pylon and cable system are necessary. In particular, the cable system displacements should be equal to those of the girder and the pylons at the corresponding intersection points; thus, the bridge kinematic is restricted by means of the following constrain equations:

$$\begin{aligned} U_3^G(\underline{X}_{C_i}, t) + \Phi_1^G(\underline{X}_{C_i}, t)b &= U_3^C(\underline{X}_{C_i}, t) \\ U_1^G(\underline{X}_{C_i}, t) - \Phi_3^G(\underline{X}_{C_i}, t)b &= U_1^C(\underline{X}_{C_i}, t) \end{aligned} \quad (4.37)$$

$$\begin{aligned} U_1^P(\underline{X}_P, t) &= U_1^C(\underline{X}_P, t) \\ U_2^P(\underline{X}_P, t) &= U_2^C(\underline{X}_P, t) \\ U_3^P(\underline{X}_P, t) &= U_3^C(\underline{X}_P, t) \end{aligned} \quad (4.38)$$

where  $\underline{X}_{C_i}$  and  $\underline{X}_P$  represent the vectors containing the intersection positions of the  $i$ -th cable element and the pylon top cross section, respectively, and  $(U_1^G, U_2^G, U_3^G)$  and  $(\Psi_1^G, \Psi_2^G, \Psi_3^G)$  are the displacement and rotation fields of the centroid axis of the girder with respect to the global reference system, respectively. It is worth nothing that, eq.(4.37) are constraint equation imposed between the off-set nodes of the girder and those associated to the cable elements.

Finally, starting from Eq.s (4.34)-(4.36) taking into account of Eq.s (4.37)-(4.38) as well as the balance of secondary variables at the interelement boundaries, the resulting equations of the finite element model are:

$$\underline{K}\underline{Q} = \underline{P} \quad (4.39)$$

where  $\underline{Q}$  with  $\underline{Q} = \underline{U}_C \cup \underline{U}_G \cup \underline{U}_P$  is the generalized coordinate vector containing the kinematic variables associated with the girder, the pylons and the cable system,  $\underline{K}$  is the global stiffness matrix and  $\underline{P}$  is the loading vector.

Since the structural behavior of each element depends on the deformation state of the members, the governing equations defined by Eq.(4.39) will change continuously as the structure deforms.

The governing equations are solved numerically, using a user customized finite element program, i.e. COMSOL Multiphysics TM version 4.4 (Comsol, 2012).

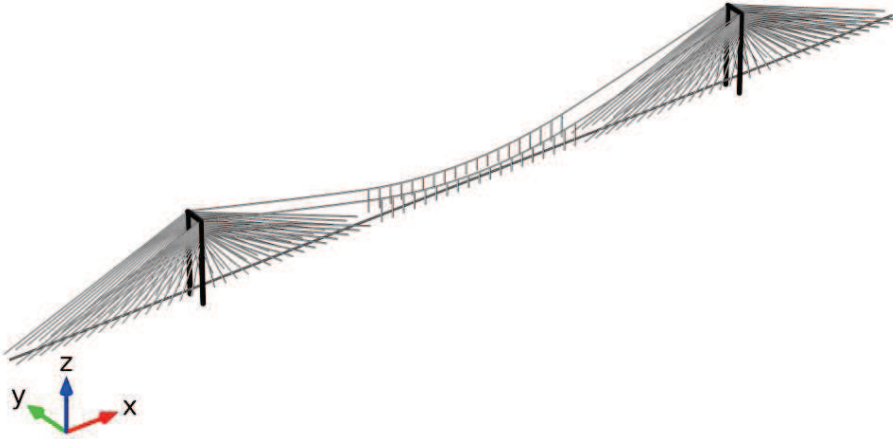


Fig. 4.6 Finite element modelling of the structural scheme

It is worth noting that the structural response at each time step is obtained by solving nonlinear and differential equations relates, respectively, to the structural response, which account for the geometric nonlinearities, and to the inelastic material behavior.

For this reason, the finite element model of the structure is coupled with several equation-based models, each of them related to definition of the inelastic properties of cables, pylons and girder.

For each load increment, plastic variable rate related to each structural element are carried out at each cross-section. In particular, for beam elements the rate of force-state parameter  $\dot{\alpha}$ , which correspond by Eq. (4.7) the dimensionless reduction parameters rate  $\dot{\eta}$ , and the tangent modulus rate  $\dot{E}_t$ , whereas for each truss element the axial plastic rate  $\dot{\epsilon}_{p,i}^C$ .

To this end, the following further equations, with relative consistence restrictions, are added to the equations model:

*Girder and Pylon:*

$$\dot{\alpha}^* \left\{ \begin{array}{l} 0 \quad \text{for } f_{p,b}^* < 0 \text{ and } \dot{\eta}^* > 0 \\ \frac{d}{dt} \left( \frac{|N_1^*|}{N_{1p}^*} + \frac{8|M_2^*|}{9M_{2p}^*} + \frac{8|M_3^*|}{9M_{3p}^*} \right) \quad \text{for } f_{p,b}^* \geq 0 \text{ and } \dot{\eta}^* \leq 0 \text{ and } \frac{|N_1^*|}{N_{1p}^*} \geq \frac{2|M_2^*|}{9M_{2p}^*} + \frac{2|M_3^*|}{9M_{3p}^*} \\ \frac{d}{dt} \left( \frac{|N_1^*|}{2N_{1p}^*} + \frac{|M_2^*|}{M_{2p}^*} + \frac{|M_3^*|}{M_{3p}^*} \right) \quad \text{for } f_{p,b}^* \geq 0 \text{ and } \dot{\eta}^* \leq 0 \text{ and } \frac{|N_1^*|}{N_{1p}^*} < \frac{2|M_2^*|}{9M_{2p}^*} + \frac{2|M_3^*|}{9M_{3p}^*} \end{array} \right. \quad (4.40)$$

$$\dot{E}_t^* : \left\{ \begin{array}{l} 0 \quad \text{for } f_{p,a}^* < 0 \\ \frac{d}{dt} \left[ 4 \frac{|N_1^*|}{N_{1p}^*} E \left( 1 - \frac{|N_1^*|}{N_{1p}^*} \right) \right] \quad \text{for } f_{p,a}^* \geq 0 \text{ and } \dot{N}_1^* \geq 0 \end{array} \right. \quad (4.41)$$

where  $f_{p,b}^*$  and  $f_{p,a}^*$  are the yield functions, respectively, for bending and axial plastic state variable which are expresses as:

$$f_{p,b}^* : \left\{ \begin{array}{l} \frac{|N_1^*|}{N_{1p}^*} + \frac{8|M_2^*|}{9M_{2p}^*} + \frac{8|M_3^*|}{9M_{3p}^*} - \alpha^* \quad \text{for } \frac{|N_1^*|}{N_{1p}^*} \geq \frac{2|M_2^*|}{9M_{2p}^*} + \frac{2|M_3^*|}{9M_{3p}^*} \\ \frac{|N_l^*|}{2N_{1p}^*} + \frac{|M_{l,y}^*|}{M_{l,yp}^*} + \frac{|M_{l,z}^*|}{M_{l,zp}^*} - \alpha^* \quad \text{for } \frac{|N_1^*|}{N_{1p}^*} < \frac{2|M_2^*|}{9M_{2p}^*} + \frac{2|M_3^*|}{9M_{3p}^*} \end{array} \right. \quad (4.42)$$

$$f_{p,a}^* = |N_1^*| - N_{1p}^* \quad (4.43)$$

It is worth noting that, in the previous Eqs.(4.40)-(4.43) the superscript  $(\cdot)^*$  refers  $(\cdot)^G$  for the girder and  $(\cdot)^P$  for pylons.

*Cable:*

$$\dot{\epsilon}_{p,i}^C \cdot \begin{cases} 0 & \text{for } f_i^C \dot{\epsilon}_i^C \geq 0 \text{ and } f_i^C \geq 0 \\ \frac{E_i^C}{E_i^C + E_i^C k^h} \dot{\epsilon}_i^C & \text{for } f_i^C \dot{\epsilon}_i^C \leq 0 \text{ and } f_i^C \leq 0 \end{cases} \quad (4.44)$$

$$\text{with } i = [1, \dots, (1 + N^S + N^H)]$$

where  $f_i^C$  is the yield function for i-th element of the cable system expressed as follows:

$$f_i^C : S_{n,i}^C - E_i^C k^h \epsilon_p - S_y^C \quad \text{with } i = [1, \dots, (1 + N^S + N^H)] \quad (4.45)$$

where,  $S_{n,i}^C$  and  $S_y^C$  are, respectively, the value of actual cable force and the yield stress, while  $k^h$  is the hardening parameter related to the hardening properties of the material.

## 4.6 Results

In the present work several models of self-anchored cable-stayed suspension bridges were considered. Each of them was defined by dimensional parameters relatives to the bridge scheme, introduced in previous Par 1.1, as well as properties related to materials and cables, girder and pylons cross-sections. In particular, analyzes were developed considering three bridge midspan lengths ( $L$ ), that is 500, 1000 and 1500 meters, combined with values of dimensionless cable-stayed part length ( $c$ ), height-span ratio ( $\mu$ ) and rise span to main span length ratio ( $\zeta$ ), which vary in the following ranges:  $0.25 \leq c \leq 0.45$ ,  $0.05 \leq \zeta \leq 0.20$  and  $0.40 \leq \mu \leq 0.50$ . Both girder and pylons were idealized by rectangular single-box cross-sections. In particular, the girder cross-section has constant width ( $b^G$ ) and thickness ( $\delta^G$ ) equal, respectively, to 33 and 0.033 meters ( $b^G/1000$ ), and variable depth ( $h^G$ ). The variability of the girder depth is express as a function of the relative bending stiffness ratios between the girder and the cable system,  $\epsilon_F = (4I_3^G \sigma_G / H^3 g)^{1/4}$ , which usually,

in the field of cable supported bridge, takes values within the following range:  $0.25 \leq \varepsilon_F \leq 0.35$ . The pylons cross-section has constant depth to width ratio ( $h^P/b^P$ ) and thickness ( $\delta^P$ ) equal, respectively, to 1.5 and  $b^P/100$ . The depth ( $h^P$ ) and the width ( $b^P$ ) are defined by an implicit way once fixed the tower to girder bending stiffness ratio  $I_r = I_2^P / I_2^G$ , which takes values from 1 to 100.

Both girder and towers are made of steel whose elasticity modulus ( $E^{G,P}$ ), yield stress ( $S_y^{G,P}$ ) and specific weight ( $\gamma^{G,P}$ ), are assumed, respectively, equal to 2.1 GPa, 450 MPa and  $78.5 \text{ kN/m}^3$ . Stays and hangers are uniformly distributed along the girder by a 20 meters steps ( $\Delta^G$ ). The same value is assumed for the distance between the anchor points and the nearest stay ( $L^G$ ). Moreover, four type of cable-stayed configurations are considered: a fan, an harp and two semi-fan schemes, which the stays present a distance ( $\Delta^P$ ) equal to  $H/200$  and  $H/500$ . Cable cross-section areas are designed by classic expressions reported in the paragraph 1.2

### Loads and combinations

The dead load ( $g^G$ ) of the girder was calculated as  $1.4A^G\gamma^G + 60 \text{ kN/m}$ , where ( $A^G$ ) is the girder cross-section and 1.4 is a section magnification factor of the dead loads for considering diaphragms and other utilities installed in the section, and  $60 \text{ kN/m}$  represents the weight of other structural and nonstructural elements such as pavement, street lamps, and other attachments (Yoo, Na and Choi, 2012). Without loss of generality, in all analyses only live loads ( $p$ ) concerning traffic loads are considered, which are combined with dead loads by using unfactored loading combination. However, the generalization of the proposed model to consider also the effects of seismic or wind forces, can be easily developed just introducing additional loading combinations to the ones concerning live loads. Live loads was assumed to be  $9 \text{ kN/m/lane}$  as specified by code (AASHTOO, 2013). The live loads was arranged on the deck in two different ways: (1) on the center span only (LC1) and (2) on the center span and one side span (LC2) (Fig. 4.7). Furthermore, the live load is considered located at the center of the structure, so as no torsional effect are produced.

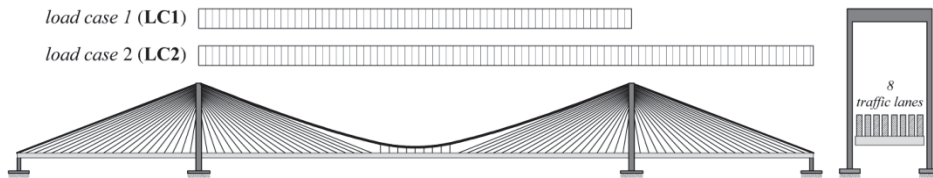


Fig. 4.7 Load cases

### Investigation on material nonlinear effects influence

The first part of the present study was devoted to analyze the influence of the nonlinear material behavior on the ultimate bearing capacity as well as the characterization of the ultimate configuration of a self-anchored cable-stayed suspension bridge.

The bridge structure considered was defined by properties reported in Tab. 4.1 and it has been analyzed by four different models, summarized in Tab. 4.2, which differ from each other depending on the possibility that cables and/or pylons and girder can assumed an elastic or an elastic plastic behavior.

$L$	1000	$m$	$l$	420	$m$	$\Delta^G$	20	$m$
$c$	0.4	-	$H$	160	$m$	$\Delta^P$	2	$m$
$\mu$	0.4	-	$f$	125	$m$	$L'$	20	$m$
$\delta$	0.125	-	$h^G$	3.1	$m$	$\sigma_A$	8	$GPa$
$\varepsilon_F$	0.3	-	$b^P$	11.24	$m$	$E^{G,P}$	2.1	$GPa$
$I_r$	50	-	$h^P$	16.86	$m$	$E^C$	2.05	$GPa$
$b^G$	33	$m$	$\delta^P$	0.1124	$m$	$S_y^{G,P}$	450	$MPa$
$\delta^P$	0.033	$m$	$p/g^G$	0.312	-	$S_y^C$	1.6	$GPa$

Tab. 4.1 Geometric and mechanical properties utilized for the analysis of the influence of nonlinear material behavior

MODEL	BEAM		TRUSS
	Girder	Pylon	Cable
EMB	Elastic		Elastic
CMI	Elastic		Inelastic

---

BMI	<i>Inelastic</i>	<i>Elastic</i>
FMI	<i>Inelastic</i>	<i>Inelastic</i>

**Tab. 4.2** Models utilized for the analysis of the influence of nonlinear material behavior

The first model (EMB) allows to investigate the structural response of the bridge due to the geometric nonlinearity effects only. The second and the third models are partial nonlinear problems which add to the geometric nonlinearity effects a single source of material nonlinearity, relative to cables (*CMI*) or girder and pylons (*BMI*). The last one is the fully nonlinear model (*FMI*) which takes into account all nonlinearity sources. Models defined above have been analyzed for load cases described in the previous section and the maximum load was estimated by the load–displacement curve of the global bridge systems as illustrated in Figs. 4.8 and 4.9.



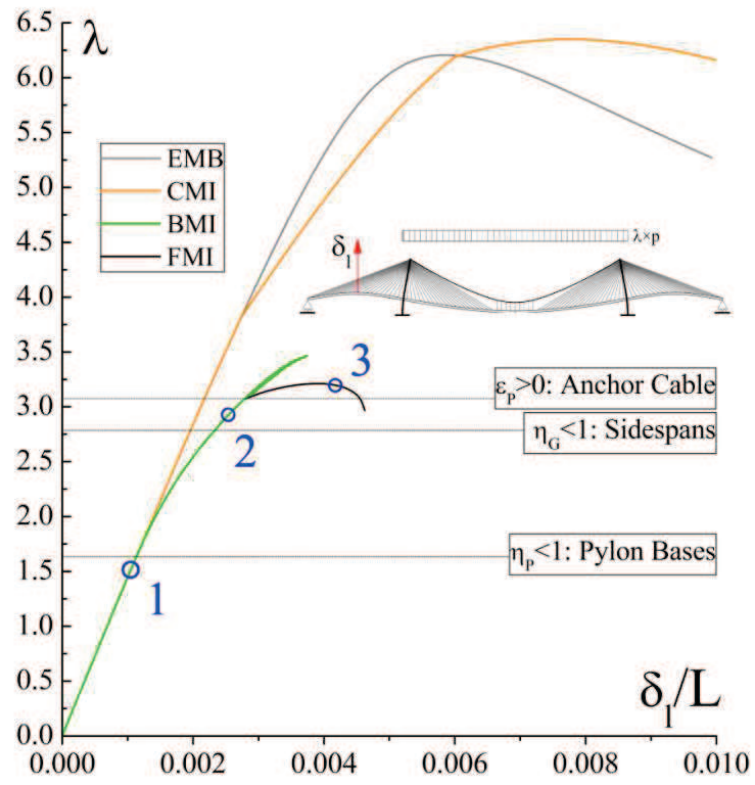


Fig. 4.8 Load-displacement curve for LC1: Analysis on material nonlinear behavior

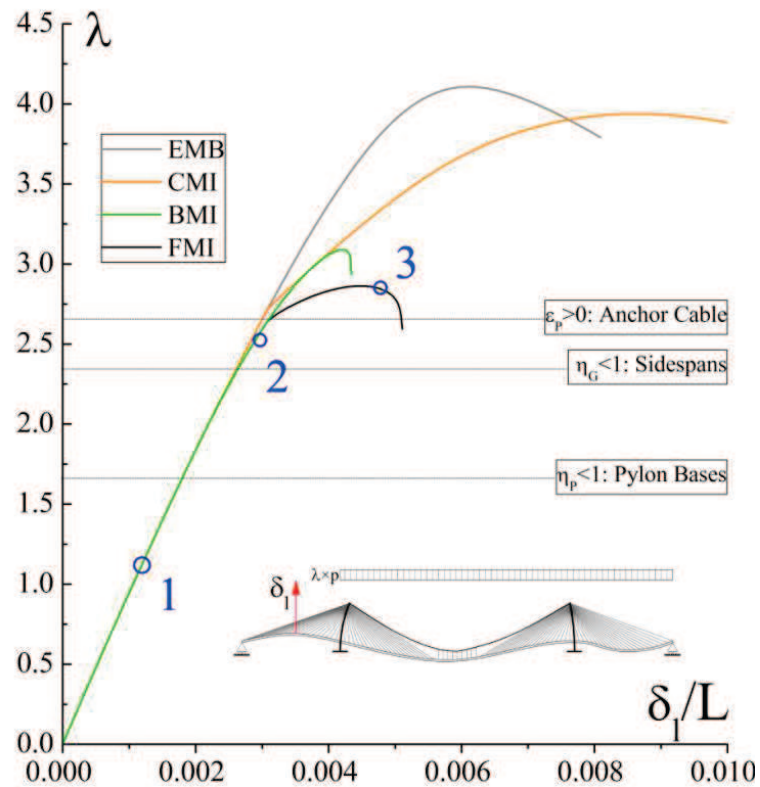


Fig. 4.9 Load-displacement curve for LC2: Analysis on material nonlinear behavior

The vertical axis indicates the load multiplier ( $\lambda$ ), whereas in the horizontal axis is reported the dimensionless control point displacement.

For both load cases, the lateral midspan deflection ( $\delta_1$ ) has been chosen as control point and it was divided by midspan length.

The corresponding evolution of bridge deformed shapes for the FMI model is illustrated in Fig. 4.10, with reference to the three load levels illustrated in Figs. 4.8-4.9 by blue circles. The evolution of the bridge deformation is shown by using a color map of the displacements. All load-displacement curves exhibit an initial linear behavior which changes with increasing live loads, depending on both geometrical and material nonlinearities effects.

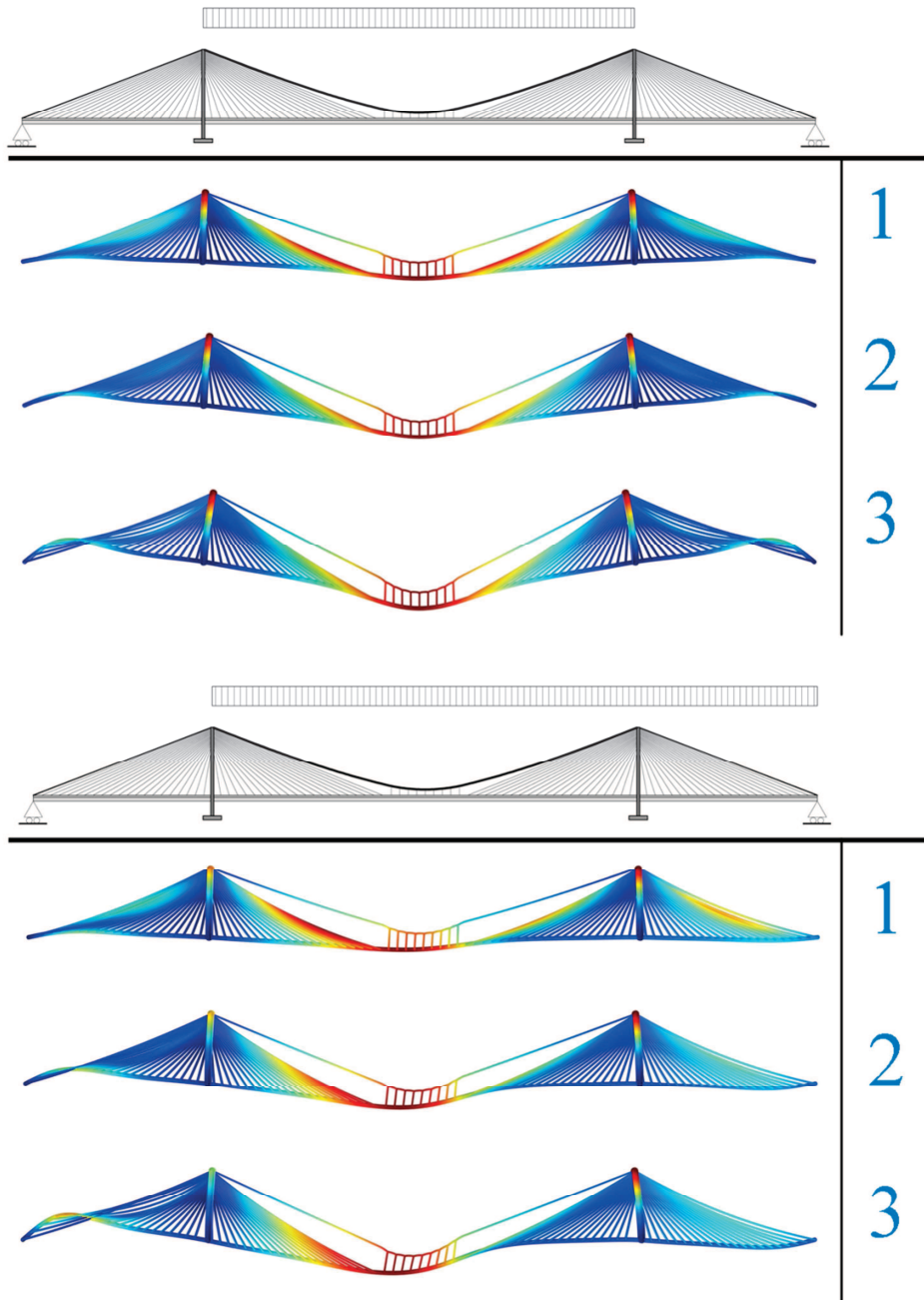


Fig. 4.10 Evolution of the bridge deformed shapes – FMI

In particular, it can be seen that EMB model leads to a maximum load highly overestimated with respect to the FMI model about 93% and 43%, respectively, for LC1 and LC2. Partial inelasticity models, CMI and BMI, leads to different result. As a matter of fact, if the difference between the BMI and FMI models is about 12% and 9%, respectively, for LC1 and LC2, on the other hand, comparing CMI to FMI, the difference is about 95% and 41%, respectively, for LC1 and LC2.

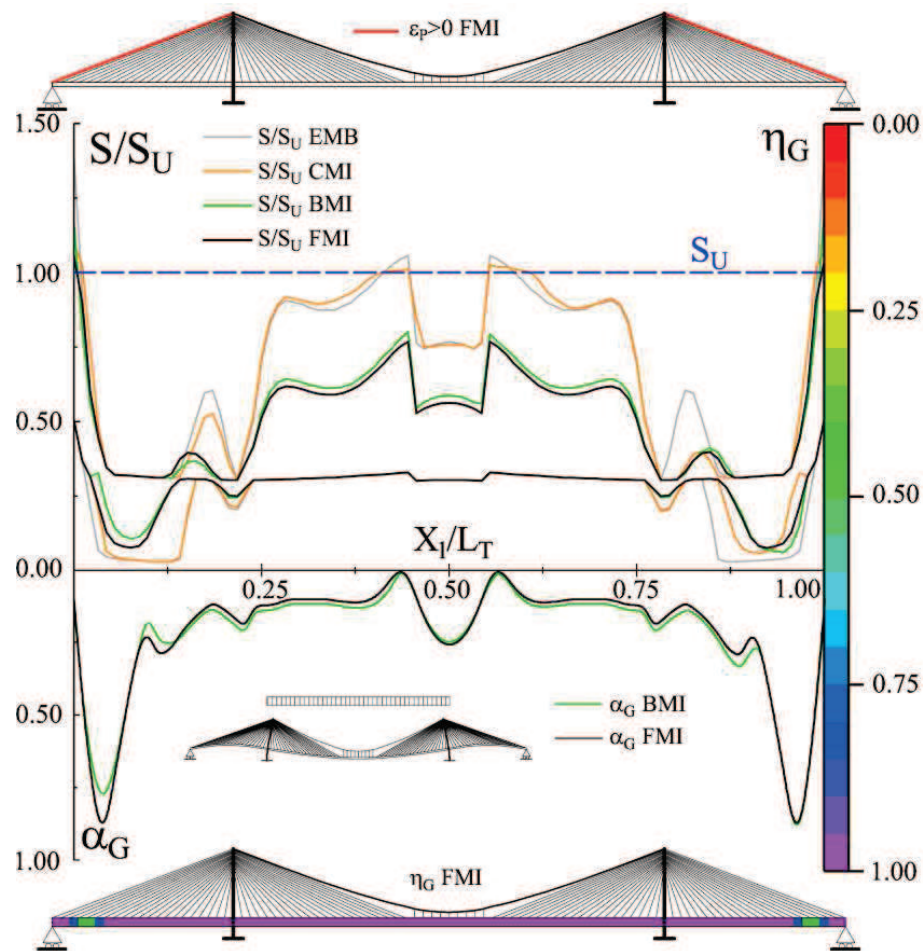


Fig. 4.11 Force-state parameter  $\alpha^G$  and dimensionless reduction parameters  $\eta^G$ ; Maximum cable stresses – LC1

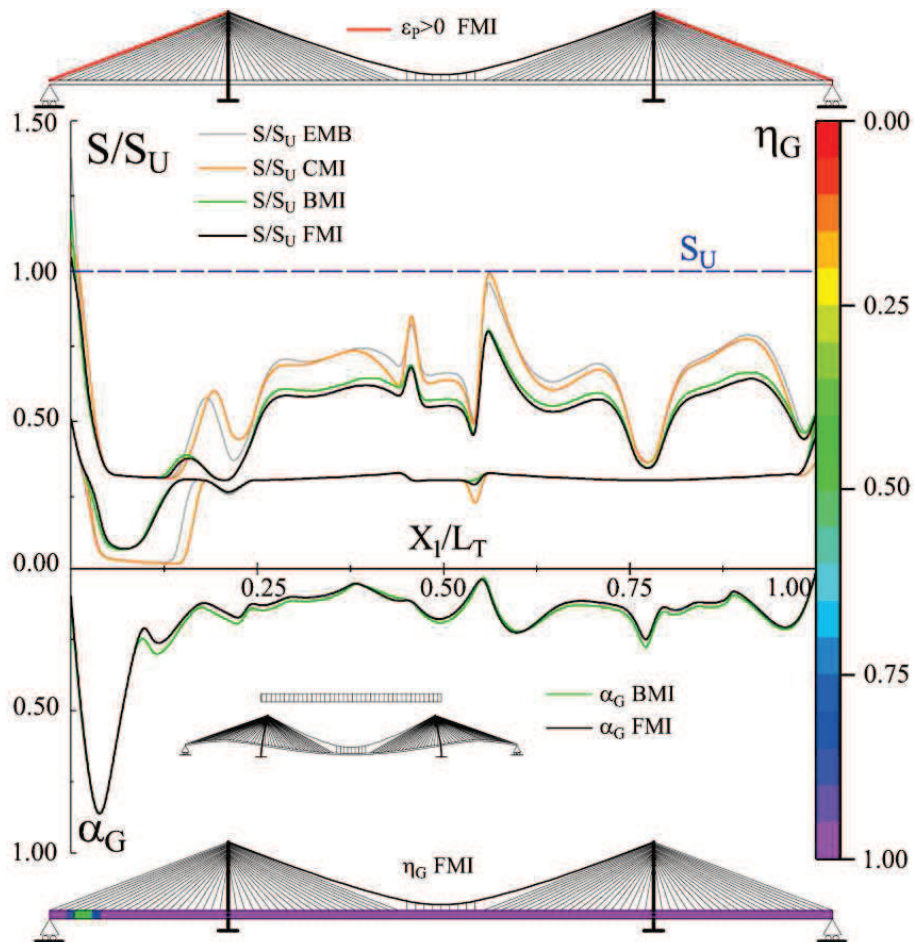


Fig. 4.12 Force-state parameter  $\alpha^G$  and dimensionless reduction parameters  $\eta^G$ ; Maximum cable stresses – LC2

The least value of the load parameter  $\lambda$  was obtained for LC2 resulting smaller than that related to LC1 about 11%. However, both LC1 and LC2 have similar features characterizing the collapse mechanisms.

As a matter of fact, in both load cases the bridge behavior was characterized by plastic phenomena occurred firstly at the pylon bases, subsequently at side spans of the girder and finally at the anchor cable.

Once that the anchor cable became plastic, the structure suffered a sudden drop in stiffness, as can be seen from the abrupt change in the slope of the load-displacement curves, and as a consequence, it can't withstand further load increments.

This aspect can be better appreciated by examining plastic state variables with reference to the ultimate configuration of the bridge. Figs 4.11-4.12 show the values of the force-state parameter  $\alpha^G$  and dimensionless reduction parameters  $\eta^G$  for girder as well as the maximum stress reach in each cable, with reference, respectively, to LC1 and LC2. Moreover, Fig. 4.13 shows plastic state variable of pylons, that is  $\alpha^P$  and  $\eta^P$ , with reference to both load cases. As before, comparisons between models defined in Tab.4.2 are proposed.

It can be seen that, the girder and pylons material inelasticity mainly influences the structural response of the bridge since there are no significant differences between FMI and BMI models in term of parameter  $\eta^G$  and  $\eta^P$  as well as maximum cable stress.

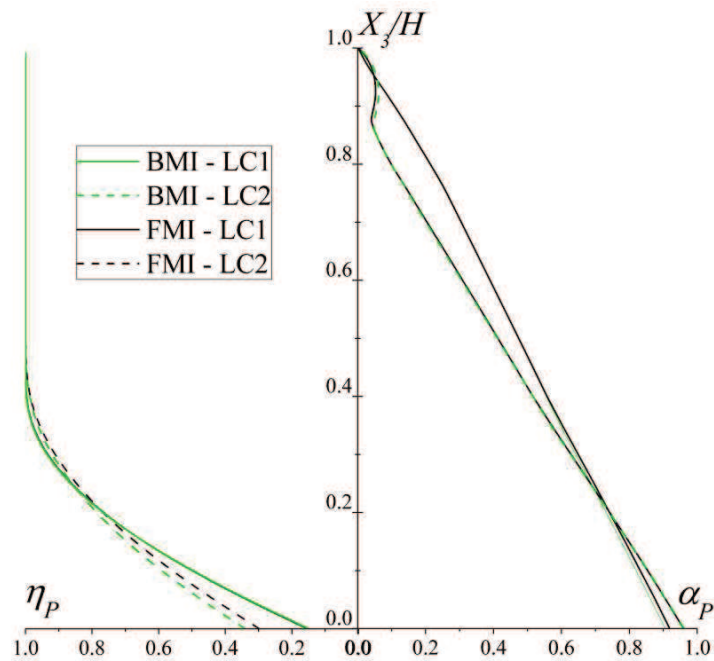
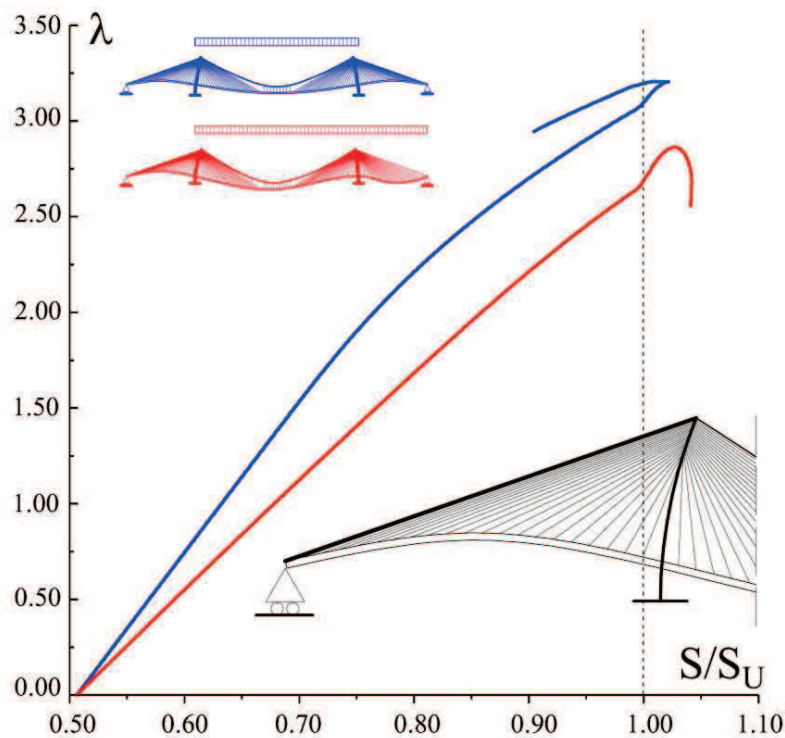


Fig. 4.13 Force-state parameter  $\alpha^P$  and dimensionless reduction parameters  $\eta^P$  for LC1 and LC2

In particular, all cable remain elastic with the exception of the anchor cable, which exceed the yield stress about 4.2% and 6.7%, respectively, for LC1 and LC2. Furthermore, in both load case, same values of plastic rates for girder and pylons located at the beginning of the side spans are observed.

With reference to the girder, this imply an increase in the girder curvature as can be also seen by the ultimate bridge deformation reported in Fig. 4.10. This aspect seems to be the causes that involves the greater loss of stiffness of the structure since plastic phenomena occurred close to the anchor zone of the bridge. However, the anchor cable plays a crucial role. As a matter of fact, the different response between FMI and BMI models in term of anchor cable material behavior, which is elastic plastic for the first and simply elastic for the latter, leads to further reduction of bearing capacity. Such aspect also explains why a lower value of load multiplier  $\lambda$  was obtained for LC2 with respect to LC1.



**Fig. 4.14** Load-anchor cable stress curve for LC1 and LC2

In Fig. 4.14 a comparison between the anchor cable stress as a function of the load multiplier for both load cases is reported. It can be seen that for LC2, the anchor cable reached the yield stress for a lower value of  $\lambda$  with respect to LC1.

Finally, in Tab.4.3 values of main cable maximum stress for models and load conditions considered above are reported. For all load cases, the main cable remains elastic, so do not influence the structural response. However, results obtained was influenced by the dimensioning parameters adopted as c parameter whose involves a system with a reduced suspended system.

Analysis	Load Arrangement	
	LC1	LC2
EMB	0.685	0.623
CMI	0.730	0.641
BMI	0.544	0.556
FMI	0.539	0.552

**Tab. 4.3** Influence of nonlinear material behavior: main cable dimensionless maximum stress (S/Su)

### Parametric Study

In the previous section, the influence of the material nonlinearity on the bearing capacity of a self-anchored cable-stayed suspension bridge was analyzed. Comparison results obtained by different types of numerical models, which are illustrated in Tab. 4.1, have shown that a fully nonlinear numerical model can offer a good description of the maximum load capacity and ultimate behavior of a self-anchored cable-stayed suspension bridge.

In this section, a parametric study is presented, which describes self-anchored cable-stayed suspension bridge in terms of dimensionless variables, strictly related to bridge characteristics.



At first, cable system properties were studied. In particular, analysis focused on size and extension of the cable-stayed system portion.

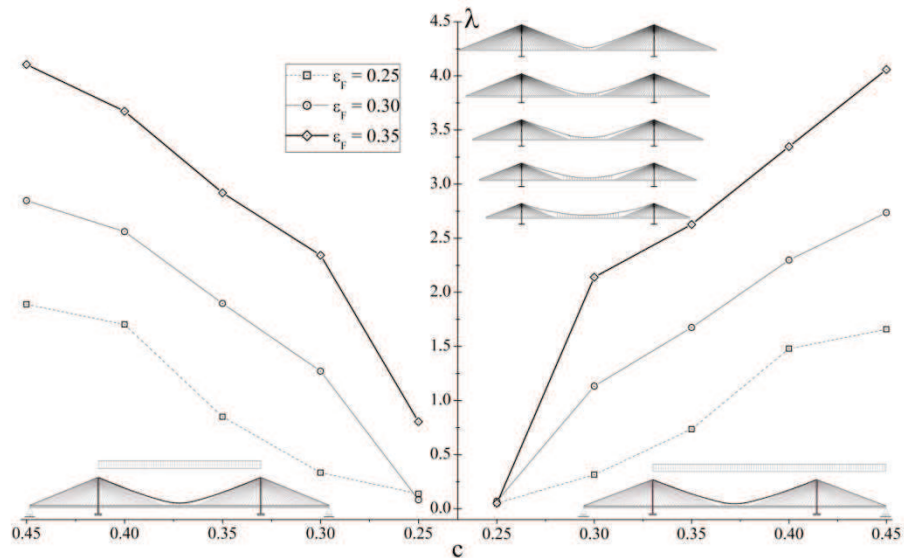


**Fig. 4.15** Variability of the length of cable-stayed portion, for several values of relative bending stiffness  $\mathcal{E}_F$

In Fig. 4.15 the variability of the load multiplier  $\lambda$ , obtained for LC1 and LC2, as a function of the length of cable-stayed portion, express by  $c$  parameter, for several values of the relative bending stiffness  $\mathcal{E}_F$  is presented.

Results were carried out considering a self-anchored cable-stayed suspension bridge with height-span ratio ( $\mu$ ) and tower to girder bending stiffness ratio ( $I_r$ ), respectively, equal to 0.4 and 25.

It can be seen that the value of  $\lambda$  increased with high values of  $c$ .

As a matter of fact, short cable-stayed portion imply short side spans and a cable system more similar to a suspension system which increases the deformability of the central span. Such configurations make the structure suitable to local buckling instability of the girder due to a lower stiffness offered by the cables system and a lower stabilizing effect due to the counterweight of the side spans.

On the other hand, long cable-stayed portion leads to bigger side spans and a structure more similar to a cable-stayed system which improve the structural performance avoiding buckling instability problem.

Values related to LC1 and LC2 are quite similar and differed by an average ranging from 10% to 15% for each value of  $c$  and  $\varepsilon_F$ .

It is worth nothing that, improvement in the structural performance were obtained by increasing the relative girder bending stiffness. As a matter of fact, for each value of  $c$ , the difference between load multipliers corresponding to the values of  $\varepsilon_F$  considered vary with an average about 44-46 %.

Further results were obtained analyzing the variability of the cable-stayed portion length by numerical models introduced in the previous section Tab. 4.1. The values of  $\lambda$  are reported in Tab. 4.4 while in Fig. 4.16 the percentage error (e %) of EMB, CMI and BMI models with respect to the FMI model is shown.

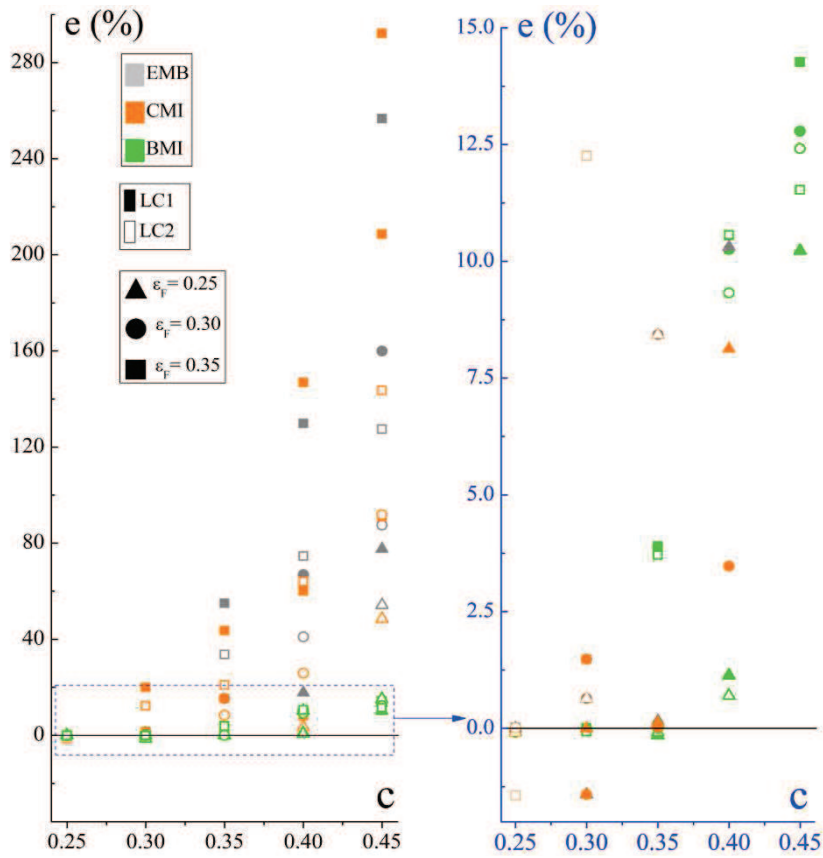


Fig. 4.16 Percentage error (e %) of EMB, CMI and BMI models with respect to the FMI model

$c$	MODEL	$\epsilon_F$					
		0.25		0.3		0.35	
		LC1	LC2	LC1	LC2	LC1	LC2
0.25	EMB	0.14	0.08	0.08	0.07	0.80	0.05
	CMI	0.14	0.08	0.08	0.07	0.80	0.05
	BMI	0.14	0.08	0.08	0.07	0.80	0.05
	<b>FMI</b>	<b>0.14</b>	<b>0.08</b>	<b>0.08</b>	<b>0.07</b>	<b>0.80</b>	<b>0.05</b>
0.30	EMB	0.33	0.31	1.29	1.14	2.81	2.40
	CMI	0.33	0.31	1.29	1.14	2.81	2.40
	BMI	0.33	0.31	1.27	1.13	2.34	2.14

	<b>FMI</b>	<b>0.33</b>	<b>0.31</b>	<b>1.27</b>	<b>1.13</b>	<b>2.34</b>	<b>2.14</b>
	EMB	0.85	0.74	2.19	1.81	4.52	3.51
0.35	CMI	0.85	0.73	2.19	1.81	4.19	3.18
	BMI	0.85	0.73	1.90	1.67	3.03	2.72
	<b>FMI</b>	<b>0.85</b>	<b>0.73</b>	<b>1.90</b>	<b>1.67</b>	<b>2.92</b>	<b>2.63</b>
	EMB	2.00	1.63	4.28	3.24	8.44	5.84
0.40	CMI	1.84	1.53	4.10	2.89	9.07	5.49
	BMI	1.72	1.49	2.82	2.51	4.06	3.70
	<b>FMI</b>	<b>1.70</b>	<b>1.48</b>	<b>2.56</b>	<b>2.30</b>	<b>3.67</b>	<b>3.35</b>
	EMB	3.36	2.56	7.40	5.13	14.65	9.23
0.45	CMI	3.61	2.46	8.79	5.25	16.10	9.89
	BMI	2.08	1.91	3.21	3.08	4.69	4.53
	<b>FMI</b>	<b>1.89</b>	<b>1.66</b>	<b>2.85</b>	<b>2.74</b>	<b>4.11</b>	<b>4.06</b>

**Tab. 4.4** Load multiplier as a function of  $c$  parameter and relative bending stiffness for  $I_r = 25$  and  $\mu = 0.4$

Results show that the percentage error increase with the length of cable-stayed portion. In particular, it is almost zero for  $c$  equal to 0.25, that is for short cable-stayed portion, which means that the whole bridge structural response is mainly dominated by local buckling instability without plastic structural members.

On the other hand, for  $c$  equal to 0.45, that is for long cable-stayed portion, the structural response is affected by plastic strain since differences about 297 %, 260 % and 14.5 %, respectively, for CMI, EMB and BMI, were obtained. The smallest error percentages is relative to BMI model, which confirm what observed in the previous section.

It is worth noting that, the difference between BMI and FMI model has grown exponentially for values of  $c$  between 0.3 and 0.45, which means that as the cable system becomes stiffer, the inelastic behavior of cables plays a relevant role in maximum load capacity of the bridge structure.

The self-anchored cable-stayed suspension bridge considered in the previous analysis was employed to analyze the variability of the stay step size

along the pylon height. In particular, a constant relative bending stiffness  $\varepsilon_F$  equal to 0.3 was assumed. Four types of cable-stayed layout, namely, a fan system, two semi-fan system, respectively, with  $\Delta^P = L/500$  and  $\Delta^P = L/200$ , and a harp system was considered. Fig. 4.17 shows results relative to LC1, while in Tab. 4.5, further results relative to LC2 are reported.

	$\mu$	$\lambda$	
		LC1	LC2
FAN	0.4	2.52	2.46
	0.45	3.06	2.99
	0.5	3.65	3.59
SEMI-FAM $\delta P = L/500$	0.4	2.58	2.29
	0.45	3.12	2.81
	0.5	3.67	3.40
SEMI-FAM $\delta P = L/200$	0.4	2.65	1.71
	0.45	3.17	2.33
	0.5	3.76	2.96
HARP	0.4	2.60	1.61
	0.45	3.31	2.56
	0.5	4.06	3.69

**Tab. 4.5** Variability of load multiplier with respect of cable-stayed system configuration

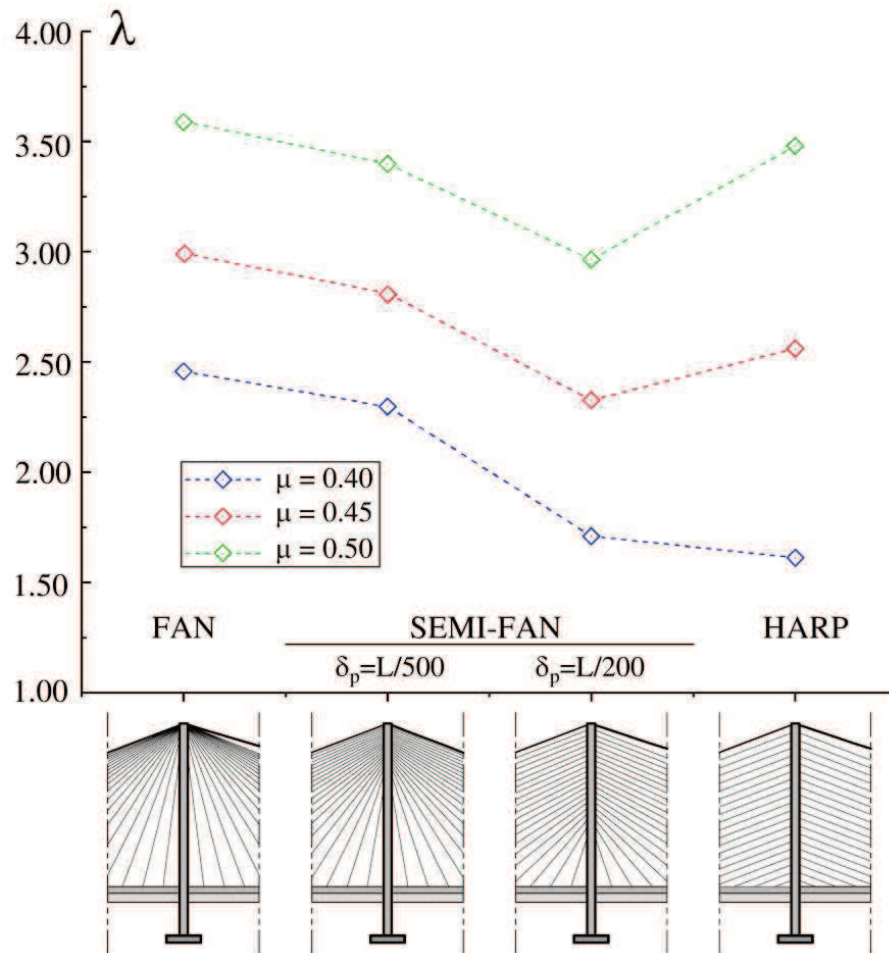


Fig. 4.17 Variability of the cable-stayed system configuration

The cable-stayed system layout affected the bridge response and, in particular, the fan system offered the best performance.

More in detail, reduced values of the load multiplier  $\lambda$  were observed for the semi-fan system with  $\Delta^p = L/200$  which differ with respect to the fan configuration about 62-65%. The differences between the fan and the harp systems depend on the values of the height-span ratio  $\mu$ . As a matter of fact, such difference is about 68%, 39% and 2% for  $\mu$  equal, respectively, to 0.40, 0.45, 0.50.

This can be explained considering that higher values of the height-span ratio  $\mu$  implies higher pylons and, this aspect improves the performance of an harp cable-stayed system. On the other hand, with reference to the values of load multiplier reported in Tab. 4.5, obtained for LC2, it seems that the configuration of the cable-stayed system portion didn't affect the structural behavior since the no relevant differences were obtained between the models.

The girder and tower main properties were analyzed in term of stiffness properties. Results reported in Fig. 4.18 (a-b) show the variability of load multiplier  $\lambda$  in terms of the tower to girder bending stiffness ratio  $I_r$ , for several values of the relative girder bending stiffness  $\mathcal{E}_F$ .

In particular, Fig. 15-a and fig. 15-b refer, respectively, to 0.4 and 0.5 values of height-span ratio  $\mu$ .

For sake of brevity, only results related to LC1 load case are presented, however conclusions obtained can be extended to LC2 load case.

It can be seen that high values of  $\lambda$  were obtained for high values of  $I_r$  and  $\mathcal{E}_F$  for a fixed value of  $\mu$ . Such bridge configurations involves smaller pylon deflections and, as a consequence, reduced nonlinearity effects.

As a matter of fact, higher values of pylons and girder stiffness avoid local buckling instability and plastic strain so that the entire structure still remain elastic for higher value of  $\lambda$ .

It is worth nothing that, there were abrupt changes in patterns of load multiplier values at  $I_r = 5$  since the difference of values of  $\lambda$  between  $I_r = 1$  and  $I_r = 5$  is about 63%, whereas it is about of 4% between  $I_r = 5$  and  $I_r = 10$ .

Values of  $I_r$  less than 5 imply that the bridge behavior is dominate by local buckling pylons, whereas values higher than 5 avoid these kind of problem and the structural behavior is similar to that described in the previous section.

The structural performance of the bridge was improved by increasing height-span ratio  $\mu$  since the value of load multiplier increase with an average ranging from 46 % to 58%.

Furthermore, higher values of the height-span ratio  $\mu$  and higher values of the relative girder bending stiffness  $\mathcal{E}_F$  avoid local buckling phenomena of pylon for less values of  $I_r$  since no abrupt changes in the distribution of the values of load multipliers were observed.

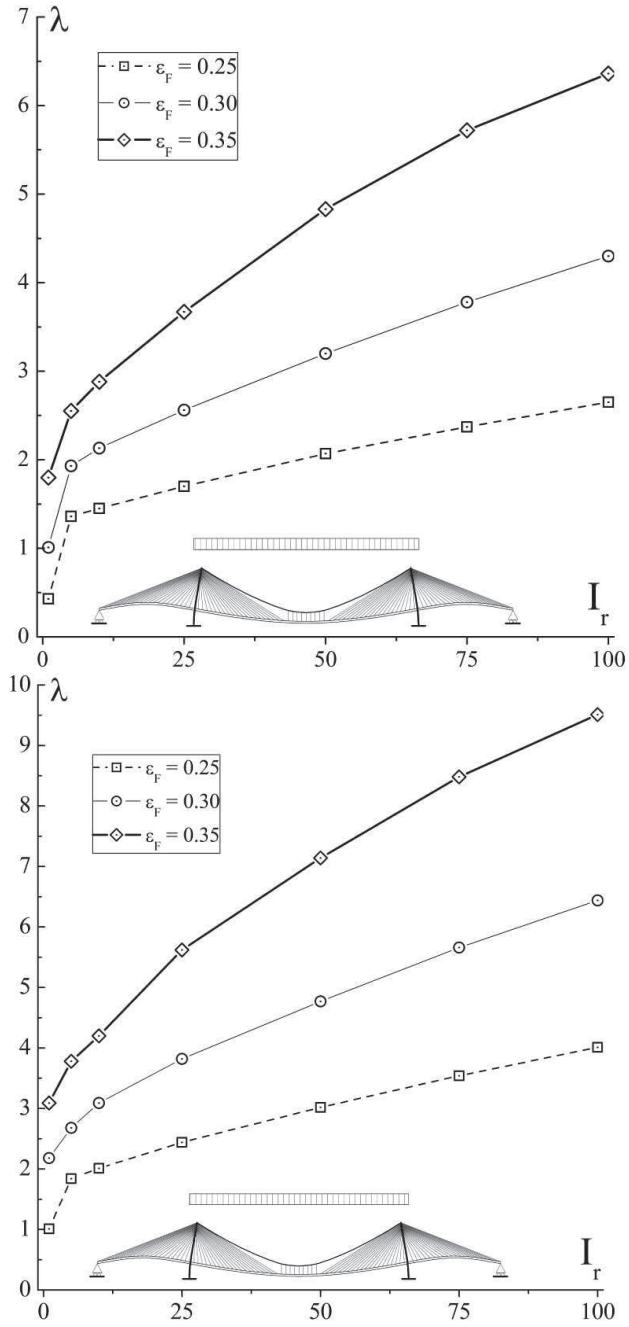


Fig. 4.18 Variability of tower to girder bending stiffness ratio  $I_r$ , for several values of relative girder bending stiffness  $\epsilon_F$  and height-span ratio  $\mu$ .



Finally, the variability of the midspan length was analyzed.

Three self-anchored cable-stayed suspension bridges with midspan lengths, respectively, equal to 500, 1000 and 1500 m, each of them characterized by cable-stayed portion  $c$ , relative bending girder stiffness  $\varepsilon_F$  and tower to girder bending stiffness ratio  $I_r$ , respectively, equal to 0.4, 0.3 and 25, were considered.

As before, the variability of the height-span ratio  $\mu$  was taken into account considering height-span ratio respectively, equal to 0.4, 0.45 and 0.50. Fig. 4.19, shows the values of the load multiplier  $\lambda$  as a function of the midspan lengths.

The self-anchored cable-stayed suspension bridge scheme seems to offer good performance in the field of short, medium and long spans. As a matter of fact, it can be observed that the maximum load capacity increased with an average about 16% and 4%, respectively, for LC1 and LC2. In particular, high values of the height to span ratio imply better performance regardless of the midspan lengths as for each bridge and for each load case, the values of  $\lambda$  increase about 22%.

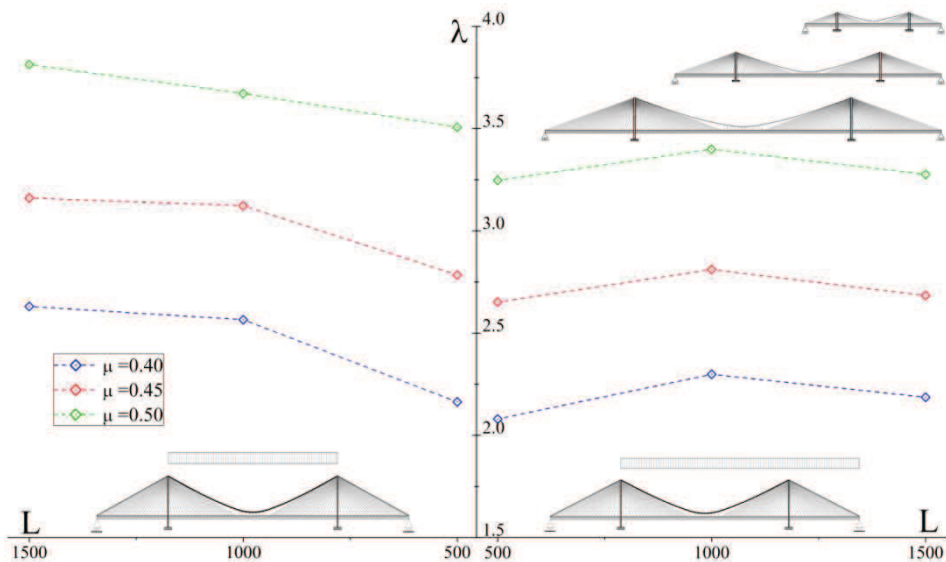


Fig. 4.19 Variability of the midspan length

# 5

## CONCLUSIONS

Cable supported bridges are typically employed to overcome medium or long spans, because of their structural, economical and aesthetic properties. During the last year, the adoption of high performance materials for structural components combined with the use of advanced analysis methodologies has resulted in great progress of cable supported bridges. In this framework, the main benefit was to increase bridge midspan lengths. However, other problems as bridges-wind interaction, moving loads effects and the analysis of structural behavior due to earthquake action have been accurately investigated and nowadays new issues are being studied. Costs reduction, development of more realistic analysis models, study of the structural vulnerability due to extreme loading conditions and safety assessment of existing bridges are topics which are receiving greatest interest.

The present doctoral thesis has been developed in this context. In particular, it focused on the three following distinct issues:

- Propose a design methodology to define the optimum design of cable system of cable supported bridges;
- Investigate the structural behavior of cable supported bridges due to the presence of damage mechanisms in the cable system under the action of moving loads;
- Develop a numerical model to analyze the nonlinear behavior of self-anchored cable-stayed suspension bridge.

Each of these issues has been initially investigated from a theoretical point of view defining governing equations in a differential form. Subsequently, simply converting such governing equations in a variational form, results have been carried out by means of numerical techniques. In particular, the structural problem has been simulated by a displacement-based finite element approximation implemented in a FE software, i.e. Comsol COMSOL Multiphysics. In particular, a 3D model of the bridge structure based on beam elements for girder and pylons and truss elements for the cable system has been defined in order to reduce the computational efforts in the numerical calculations. Specifically, the bridge girder is replaced by a longitudinal spline with equivalent cross-section and material properties, whereas the pylons are composed by two columns linked at their top by horizontal beam elements.

The bridge girder is connected to the suspension system by means of explicit constraint equations, which are imposed between the off-set nodes of the girder and those associated to the cable elements. The cable system, which is connected to the pylons and girder, is essentially defined by the combination of stays, hangers and main cable. In particular, the cable system is modeled according to the Multi Element Cable System (MECS) approach, in which each cable is discretized using multiple truss elements. The stiffness reduction caused by sagging is accounted by allowing the cable to deform under applied loads.

Large deformations are reproduced by using Green Lagrange formulation and the axial strain is calculated by expressing the global strains in tangential derivatives and projecting the global strains on the cable edge.

The first part of the thesis focused on the definition of a new design methodology. In this context, the finite element model of the bridge structure

has been combined with an optimization design method in order to quantify the optimum dimensioning of the cable system and the post-tensioning stress in the dead load configuration according to the so called “*performance based design*” (P.B.D.), which means the best utilization of the weight utilized in the structure and thus the lowest possible costs in the bridge construction.

The method is consistent with an two-step numerical algorithm able to evaluate the optimum solution with respect to both dead and live load configurations, taking into account design constrains concerning serviceability and ultimate limit states. In particular, under dead loads, the analysis is developed with the purpose to calculate the post-tensioning cable forces to achieve minimum deflections for both girder and pylons. Moreover, under live loads, for each cable elements, the lowest required cross-section area is determined, which verifies prescriptions, under ultimate or serviceability limit states, on maximum allowable stresses and bridge deflections. The final configuration is obtained by means of an iterative procedure, which leads to a progressive definition of the stay, hanger and main cable characteristics, concerning both post-tensioning cable stresses and cross-sections.

It is worth noting that the iteration procedure as well as the optimization problem have been developed by using an external subroutine, which combines Livelink™ for Excel package and Comsol Multiphysics. The algorithm was implemented by means of proper customized subroutines, which manage the parameters involved in the iterative procedure. However, the proposed formulation can be implemented in several computational frameworks, since it is based on data, which can be easily extracted and handled from quite standard commercial FE softwares.

The proposed model has been validated and tested by means of several studies on different bridge schemes. In particular, in order to prove the efficiency of the proposed approach to predict the cable system dimensioning and post-tensioning stresses of the cable elements, comparisons with existing optimization techniques available from the literature have been performed. Subsequently, the robustness of the design methodology has been checked performing the optimum design of a self-anchored cable-stayed suspension bridge with a small central span and a reduced number of elements. Finally,

further results have been developed for more complex structures involving several configurations of the cable system and a large number of variables such as those involved in long span bridges. This to prove the wide applicability of the proposed methodology.

From the results, the following conclusions can be drawn:

1. The proposed methodology can be considered a useful tool in the prediction of the required cable dimensioning and post-tensioning forces, since it is able by mean of a limited number of convergent iterations to provide the optimum design solution in terms of stress and displacements variables; however, in the present analysis, the optimum configuration is carried out with respect to the cable system elements only, without entering in the optimization of the pylon and girder characteristics;
2. despite existing methodologies based on pure optimization procedure, the proposed method seems to be not affected by numerical convergence problems, since it is based on a hybrid two-step algorithm, in which the solution is enforced by using physically based expressions;
3. The proposed algorithms is based on a simple procedure, which can be easily handled on the basis of data available by using standard commercial FE software packages.
4. the optimum solution is searched according to maximum utilization material criterion, for which under LL combinations, it is supposed that the worst stress should be equal to the corresponding maximum stress, leading, globally to a reduced steel quantity in the cable system;
5. the increments of the cable system stiffness is achieved by using proper performance factors based on a secant description of the cable stiffness, which are able to reduce bridge deformability, thus verifying prescriptions on maximum deflections of girder and pylons;
6. for the cable-stayed bridge scheme, the results show that cables which require larger values of steel quantity than the rest of the elements are

those associated to the anchor stays or the longest elements in the midspan;

7. the analyses for the investigated case on a long span bridge have shown that pure suspension or cable-stayed bridge schemes present values of total steel quantity larger or lower than that associated to the HCS configuration, with percentage errors equal to 108 and 76, respectively. However, for CS bridges, the reduced value of the involved steel quantity is compensated by the construction of the pylons, which present larger height with respect to conventional SP or HCS bridge schemes.

The second part of the thesis has treated the investigation on the behavior of cable supported bridge scheme subjected to damage mechanisms under the action of moving loads. The purpose of this investigation was to analyze the amplification effects of the bridge structure produced by the moving load application and damage mechanisms in the cable system. Moreover, the analysis focuses attention on the influence of the inertial characteristics of the moving loads.

The damage definition concerning the cable failure mechanisms has been formulated by using damage law based on Continuum Damage Mechanics, which, correctly, reproduce the time dependent nature of the cable failure. In particular, the presence of damage mechanisms in the cable system involved by degradation phenomena are supposed to produce a reduction of the cross-section area.

The moving system description refers to railway vehicle loads, which are reproduced by means equivalent uniformly distributed loads, perfectly connected to the girder profile which proceed with constant speed along the bridge development. As a result, the kinematic parameters of the moving system coincide with the ones defined by the girder, neglecting frictional forces arising from the external loads, roughness effects of the girder profile, and local loading distribution produced by railway load components. It is worth nothing that,

these assumptions are quite recurrent in the framework of cable supported bridges with long spans, in which, typically, such interaction forces produced by localized dynamic effects are negligible with respect to the global bridge vibration.

The study has been performed by mean of dynamic nonlinear analysis.

The purpose of the investigation was to evaluate the dynamic amplification effects of the bridge structure produced by the moving load application and damage mechanisms in the cable system. In particular, in order to quantify the amplification effects produced by the moving loads over the static solution, numerical results are proposed in terms of dynamic amplification factors for undamaged (UD) and damaged (D) bridge structures in terms of the moving loads and the bridge characteristics. It is worth noting that (UD) configurations refer to a bridge structures, in which cables are not affected by any damage mechanisms. Contrarily, damaged (D) cable system corresponds to bridge configurations, in which one or more cable elements are subjected to the explicit damage mechanism.

Two sets of results has been produced: the first one concerns the analysis of cable-stayed bridges subjected to an accidental failure in the cable system. Sensitivity analyses of typical design bridge variables as well as effects produced by the moving system characteristics, pylon typologies and the failure mode characteristics involved in the cable system have been investigated by means of comparisons between damaged and undamaged bridge configurations. Such results aims to reproduce damage cases treated by P.T.I. and S.E.T.R.A. and, as a consequence, is useful to check the accuracy and effectiveness of the suggested simplified method. The analyses have shown that the presence of damage mechanism in the cable system is able to produce larger D.A.F.s then those obtained for undamaged bridge configurations. The D.A.F.s strongly depend on the moving system speeds and the mass schematization. Underestimations in prediction of D.A.F.s and maximum design bridge variables are noted for the cases in which the inertial description of the moving mass is not properly taken into account. The results developed in terms of the damage mechanism configuration, moving mass description, and bridge properties have shown that recommendations provided by existing codes, that

is, P.T.I. and S.E.T.R.A., become unsafe in many cases. As a matter of fact, results developed in terms of the damage mechanism characteristics have shown that the damage mode which produces the worse effects on the bridge behavior is that associated with the failure of the anchor stay. In particular, the analyses have pointed out that damage mechanisms involving the failure of the lateral anchor stay are able to produce large amplifications in the investigated parameters, whose ranges with respect to the static undamaged value are equal to 2.5–3.5 for vertical midspan displacement, to 5.5–8.5 for midspan bending moment, to 1.3–2.8 for midspan torsional rotation, and to 1.9–2.3 for the anchor stay axial stress. The results developed in terms of the damage mechanism characteristics have shown that the damage mode, which produces the worse effects on the bridge behavior is that associated with the failure of the anchor stay. Comparisons developed in terms of tower topology have shown that the H-shaped tower bridge is much more affected than the A-shaped one, since the failure modes produce an unbalanced distribution of the internal stresses in the cable system, leading to larger torsional rotations and vertical displacements of the tower and the girder, respectively. It is worth noting that only the effects produced by moving loads are considered in the results. However, in the framework of cable-stayed bridges, another severe loading condition is the one related to wind effects. As a matter of fact, damage mechanisms in the cable system, among which a typical example is the one considered in the present paper, may amplify the resonance effects related to aeroelastic instability phenomena, leading to a premature bridge collapse.

In the second part of the investigation, comparisons with bridge schemes based on hybrid cable-stayed suspension, pure cable-stayed and suspension cable system are proposed. The study is conducted with the purpose of investigating the vulnerability of the structure against damage and complete failure phenomena produced in the cable system by means of comparisons between damaged and undamaged bridge configurations. In particular, the enhanced properties of the hybrid cable-stayed suspension bridges are point out, also in the light of existing codes on cable supported bridges. From the analyses, the following main conclusions can be developed.



1. For all damage scenarios, the HCS bridges present lower deformability and stress vulnerability indexes than those observed for pure cable-stayed and suspension bridge schemes. The presence of a combined cable system, formed by both hangers and stays, is able to better redistribute the additional stresses produced by internal damage mechanisms in the bridge components.
2. The analyses denote that inertial forces arising from moving loads and those involved by the damage mechanisms are able to produce relevant amplification effects with respect to the static behavior. Such results have been analyzed with respect to several descriptions of the DAFs, which quantify the increments in the design bridge variables, i.e. bending moments and displacements, with respect to the static solution. The results denote that underestimations on the prediction of maximum values of both stresses and displacements are observed, if a transient analysis with a refined description of the inertial contributions is not carried out.
3. The worst damage scenario that affects the pure cable-stayed bridge is the one associated with the failure of the anchor stay, which produces, also in the case of dead loading, displacements of the girder, which are much larger than the corresponding ones commonly recommended by serviceability limit state prescriptions.
4. For the suspension system, the damage to the main cable produces effects on the bridge behavior only for high values of the damage parameters. Contrarily, dangerous effects in the cable stress distribution with large values of the vulnerability are observed for the damage scenarios affecting the hangers elements.
5. The analyses denote that PTI prescriptions cannot be applied in the case of pure suspension and cable-stayed bridge schemes, since discrepancies in the prediction of deformability and stresses parameters are observed with respect to the analyses presented by the proposed modeling.

---

From the results obtained by the present analysis and for the investigated cases, it appears that hybrid cable-stayed suspension bridges present an enhanced behavior to reduce additional stresses produced by accidental failure mechanisms with respect to conventional bridges based on pure cable-stayed and suspension systems, producing lower deformability and stress variables in both girder, pylon and cable-system elements. However, further results are necessary to verify such behavior also in the case of short or medium span bridges. It is worth nothing that, the study of the coupled aeroelastic and damage effects was not considered in the present formulation and it could be an object of future investigation.

Finally, the last part the thesis has focused on the analysis of the nonlinear behavior of cable supported bridges considering both geometric and material nonlinearities. Geometric and material nonlinearities affect cable supported bridges behavior significantly. Material nonlinearities come from the nonlinear stress–strain behavior of materials arise when one or more bridge elements exceed their individual elastic limits. On the other hand, geometric nonlinearities may arise from different sources. The cable system is affected by nonlinear behavior of single elements, since they exhibit a different response in loading and in unloading due to the cable “sag” effect induced by self-weight. Girder and pylons are composed by shallow or slender element which are very flexible and are affected by large displacements. Moreover, nonlinear effects may arise owing to the so-called beam-column effect due to the axial force–bending moment interaction. It is worth nothing that, beam-column effect can occur in cable supported bridges whose cable system configuration includes cable-stayed portions as pure cable-stayed, hybrid cable-stayed suspension and self-anchored cable-stayed suspension schemes. In these cases, since an high pretension force exists in stays, girder and pylons are subjected to a large axial compression and bending moment under the action of dead and live loads. Lateral deflection and axial force are interrelated such that the bending stiffness is dependent on the element axial force and the presence of bending moments

will affect the axial stiffness. In particular the element bending stiffness decreases for compression axial force and increases for a tension force.

In the proposed study, the maximum load carrying capacity of self-anchored cable-stayed suspension bridges taking into account all nonlinearity sources has been investigated. To this end, the finite element model of the bridge structure described above has been enhanced with further formulations relative to the material inelastic behavior. In particular, for the girder and pylons, a gradual yielding theory based on the (CRC) tangent modulus concept and a plastic hinge model has been employed, while for cable elements the finite plasticity theory of Green and Naghdi has been adopted.

The bridge structure has been studied by a limit point instability approach based on the use of a quasi-static transient analysis with increasing live loads. By this way, the evolution of the bridge structure has been traced up to the maximum load. However, since the bridge behavior is mostly influenced by the post-tensioning cable force distribution, the Zero Displacement Method has been employed to identify the initial geometrical configuration of the bridge under the action of dead loads.

It is worth noting that the structural response is obtained by solving nonlinear and differential equations relates, respectively, to the structural response, which account for the geometric nonlinearities, and to the inelastic material behavior. For this reason, the finite element model of the structure is coupled with several equation-based models, each of them related to definition of the inelastic properties of cables, pylons and girder.

The main aim of the investigation has been to analyze the influence of the nonlinear material behavior as well as the geometrical and structural parameters of the bridge on the maximum bearing capacity of the structure.

From the results, the following conclusions can be drawn:

1. With reference to a self-anchored cable stayed bridge which has been defined by different models which differ from each other depending on the possibility that cables and/or pylons and girder can assumed an elastic or an elastic plastic behavior, results have shown that the

---

inelastic material behavior affects significantly the maximum load carrying capacity of the bridge structure.

2. The bearing capacity of the bridge structure increase with the length of cable-stayed portion. Short cable-stayed portion imply short side spans and a cable system more similar to a suspension system which increases the deformability of the central span. Such configurations make the structure suitable to local buckling instability of the girder due to a lower stiffness offered by the cables system and a lower stabilizing effect due to the counterweight of the side spans.
3. High values of girder and pylon bending stiffness lead to considerable benefits in terms of maximum load. Such parameters directly controls the geometric dimensions of structural members and, as a consequence, larger dimensions avoid local buckling instability and plastic strain so that the entire structure still remain elastic for higher value of load.
4. The cable-stayed portion, which can assume a fan, semi-fan or harp configuration affect the structural behavior. A fan system has implied the best performances specially with reference to low values of the height-span ratio parameter which implies short height pylons. The harp configuration has offered a good structural behavior for high pylon height.
5. The midspan length hasn't altered significantly the value of the maximum load, so the structural system retains its properties for any scale.

## BIBLIOGRAPHY

- Adeli, H., & Zhang, J. (1995). Fully nonlinear analysis of composite girder cable-stayed bridges. *Computers and Structures*, 54(2), 267-277.
- American Association of State Highway and Transportation Officials. (2007). *Bridge design specifications*. Washington, DC: AASHTO.
- Au, F. T., Wang, J., & Cheung, Y. K. (2001). Impact study of cable-stayed bridge under railway traffic using various models. *Journal of Sound and Vibration*, 240(3), 447-465.
- Au, F. T., Wang, J., & Cheung, Y. K. (2002). Impact study of cable-stayed railway bridges with random rail irregularities. *Engineering Structures*, 24(5), 529-541.
- Baldomir, A., Hernández, S., Nieto, F., & Jurado, J. (2010). Cable optimization of a long span cable stayed bridge in la Coruña (Spain). *Advances in Engineering Software*, 41(7-8), 931-938.
- Barbero, E. J., & Lonetti, P. (2001). Damage model for composites defined in terms of available data. *Mechanics of Composite Materials and Structures*, 8(4), 299-315.

- Barbero, E. J., & Makkapati, S. (2000). Robust design optimization of composite structures. *Proceedings of the 45th International SAMPE Symposium and Exhibition*, (p. 1341-1352). Long Beach, CA, USA.
- Barbero, E. J., Sosa, E. M., Martínez, X., & Gutiérrez, J. (2013). Reliability design methodology for confined high pressure inflatable structures. *Engineering Structures*, *51*, 1-9.
- Behin, Z., & Murray, D. (1992). A substructure-frontal technique for cantilever erection analysis of cable-stayed bridges. *Computers and Structures*, *42*(2), 145-157.
- Bruno, D., Greco, F., & Lonetti, P. (2008). Dynamic impact analysis of long span cable-stayed bridges under moving loads. *Engineering Structures*, *30*(4), 1160-1177.
- Bruno, D., Greco, F., & Lonetti, P. (2009). A parametric study on the dynamic behavior of combined cable-stayed and suspension bridges under moving loads. *International Journal for Computational Methods in Engineering Science and Mechanics*, *10*(4), 243-258.
- Bruno, D., Greco, F., Lonetti, P., & Nevone Blasi, P. (2012). Dynamic interaction of cable supported bridges with traffic loads including the effect of an accidental failure in the cable system. *Bridge Maintenance, Safety, Management, Resilience and Sustainability - Proceedings of the Sixth International Conference on Bridge Maintenance, Safety and Management*, (p. 2827-2834). Stresa, Lake Maggiore; Italy.
- Bruno, D., Greco, F., Nevone Blasi, P., & Bianchi, E. (2013). A 3D nonlinear static analysis of long-span cable-stayed bridges. *Annals of solid and structural mechanics*, *5*(1-2), 15-34.
- Chatterjee, P., Datta, T., & Surana, C. (1994). Vibration of cable-stayed bridges under moving vehicles. *Structural Engineering International*, *4*, 116-121.

- Chen, D., Au, F., Tham, L., & Lee, P. (2000). Determination of initial cable forces in prestressed concrete cable-stayed bridges for given design deck profiles using the force equilibrium method. *Computers and Structures*, 74(1), 1-9.
- Cheng, Y., Au, F. T., & Cheung, Y. K. (2001). Vibration of railway bridges under a moving train by using bridge-track-vehicle element. *Engineering Structures*, 23(12), 1597-1606.
- COMSOL. (2012). *Reference manual*. Stockholm: Comsol.
- De Miranda, S. (1980). *I ponti strallati di grande luce*. Roma: Edizioni scientifiche A. Cremonese.
- Enrique Luco, J., & Turmo, J. (2010). Linear vertical vibrations of suspension bridges: A review of continuum models and some new results. *Soil Dynamics and Earthquake Engineering*, 30(9), 769-781.
- Federation International du beton. (2005). *Bulletin No. 30. Acceptance of stay cable systems using prestressing steels*. Lausanne, Switzerland : Federation International du beton.
- Ferreira, F., & Simões, L. M. (2011). Optimum design of a controlled cable stayed bridge subject to earthquakes. *Structural and Multidisciplinary Optimization*, 44(4), 517-528.
- Gimsing, N. (1991). *Structural systems for cable suspended bridges*. Copenhagen, Denmark .
- Gimsing, N., & Georgakis, C. (2012). *Cable supported bridges. Concept and design*. Chichester, West Sussex, United Kingdom: John Wiley & Sons Ltd.
- Hassan, M. M. (2013). Optimization of stay cables in cable-stayed bridges using finite element, genetic algorithm, and B-spline combined technique. *Engineering Structures*, 49, 643-654.

- Hassan, M. M., Nassef, A., & El Damatty, A. (2012). Determination of optimum post-tensioning cable forces of cable-stayed bridges. *Engineering Structures*, 44, 248-259.
- Irvine, M. (1981). *Cable structures*. New York: Dover Publications Inc.
- Janjic, D., Pircher, M., & Pircher, H. (2003). Optimization of cable tensioning in cable-stayed bridges. *Journal of Bridge Engineering*, 8(3), 131-137.
- Kawashima, K., Unjoh, S., & Tunomoto, M. (1993). Estimation of damping ratio of cable-stayed bridges for seismic design. *Journal of structural engineering*, 119(4), 1015-1031.
- Kim, K., & Lee, H. (2001). Analysis of target configurations under dead loads for cable-supported bridges. *Computers and Structures*, 79(29-30), 2681-2692.
- Konstantakopoulos, T., & Michaltsos, G. (2010). A mathematical model for a combined cable system of bridges. *Engineering Structures*, 32(9), 2717-2728.
- Kwaśniewski, L. J., Li, H., Wekezer, J. W., & Małachowski, J. (2006). Finite element analysis of vehicle-bridge interaction. *Finite Elements in Analysis and Design*, 42(11), 950-959.
- Lee, T., Kim, Y., & Kang, S. (2008). Optimization of tensioning strategy for asymmetric cable-stayed bridge and its effect on construction process. *Structural and Multidisciplinary Optimization*, 35(6), 623-629.
- Lemaitre, J., & Chaboche, J. L. (1994). *Mechanics of Solid Materials*. Cambridge, UK: Cambridge University Press.
- Lemaitre, J., & Desmorat, R. (2005). *Engineering Damage Mechanics*. New York: Springer Berlin Heidelberg.



- Lepidi, M., Gattulli, V., & Vestroni, F. (2007). Static and dynamic response of elastic suspended cables with damage. *International Journal of Solids and Structures*, 44(25-26), 8194-8212.
- Materazzi, A. L., & Ubertini, F. (2011). Eigenproperties of suspension bridges with damage. *Journal of Sound and Vibration*, 330(26), 6420-6434.
- Meirovitch, L. (1986). *Elements of vibration analysis*. Southhampton, UK: McGraw-Hill.
- Nagai, M., Iwasaki, E., & Nogami, K. (2003). Effect of inelastic behavior of cables on ultimate behavior and strength of a 600-m steel cable-stayed bridge. *Proceedings of second MIT conference on Computational Fluid and Solid Mechanics* (p. 506-508). Elsevier.
- Nieto, F., Hernández, S., & Jurado, J. (2009). Optimum design of long-span suspension bridges considering aeroelastic and kinematic constraints. *Structural and Multidisciplinary Optimization*, 39(2), 133-151.
- Ohsaki, M. (2011). *Optimization of Finite Dimensional Structures*. Boca Raton, FL: CRC Press. Taylor & Francis Group.
- Petrini, F., & Bontempi, F. (2011). Estimation of fatigue life for long span suspension bridge hangers under wind action and train transit. *Structure and Infrastructure Engineering*, 7(7-8), 491-507.
- Post-Tensioning Institute. (2007). *Recommendations for Stay Cable Design, Testing and Installation*. Phoenix, Ariz, USA: Post-Tensioning Institute.
- Pugsley, A. (1968). *The theory of suspension bridges*. London: Edward Arnold Ltd.
- Ren, W. (1999). Ultimate behavior of long-span cable-stayed bridges. *Journal of Bridge Engineering*, 4(1), 30-37.

- Sacco, E., & Lebon, F. (2012). A damage-friction interface model derived from micromechanical approach. *International Journal of Solids and Structures*, 49(26), 3666-3680.
- Service d'Etudes Techniques des Routes et Autoroutes. (2001). *Haubans—Recommandations de la Commission Interministérielle de la Précontrainte*. Bagneux, France: Service d'Etudes Techniques des Routes et Autoroutes.
- Sih, G. C., & Tang, X. (2008). Fatigue crack growth rate of cable-stayed portion of runyang bridge: Part I - Cable crack growth due to disproportionate cable tightening/loosening and traffic loading. *Solid Mechanics and its Applications*, 152, 209-247.
- Sih, G. C., Tang, X., Li, Z., Li, A., & Tang, K. (2008). Fatigue crack growth behavior of cables and steel wires for the cable-stayed portion of Runyang bridge: Disproportionate loosening and/or tightening of cables. *Theoretical and Applied Fracture Mechanics*, 49(1), 1-25.
- Simões, L. M., & Negrão, J. J. (2000). Optimization of cable-stayed bridges with box-girder decks. *Advances in engineering software*, 31(6), 417-423.
- Starossek, U. (2009). Avoiding disproportionate collapse of major bridges. *Structural Engineering International: Journal of the International Association for Bridge and Structural Engineering (IABSE)*, 19(3), 289-297.
- Thai, H. T., & Kim, S. (2011). Nonlinear static and dynamic analysis of cable structures. *Finite Elements in Analysis and Design*, 47(3), 237-246.
- Thai, H. T., & Kim, S. (2012). Second-order inelastic analysis of cable-stayed bridges. *Finite Elements in Analysis and Design*, 53, 48-55.
- The European Committee for Standardisation. (1993). *EN 1993 - Eurocode 3: Design of steel structures - Part 1-11: Design of Structures with tension components*. The European Committee for Standardisation.

- The European Committee for Standardisation. (2003). *EN 1991 - Eurocode 1, Actions on structures - Part 2: Traffic loads on bridges*. The European Committee for Standardisation.
- The European Committee for Standardisation. (2005). *EN 1991 - Eurocode 1: Actions on structures - Part 1-7: General actions - Accidental Actions*. The European Committee for Standardisation.
- Troitsky, M. (1988). *Cable-stayed bridges. Theory and design*. Boston: BSP Professional Books.
- Walther, R., Houriet, B., Isler, W., Moia, P., & Klein, J. (1999). *Cable-stayed bridges*. London: Thomas Telford Publishing.
- Wang, H.-L., Qin, S.-F., Zhang, Z., Huang, C.-L., & Xu, W.-J. (2010). The basic differential equations of self-anchored cable-stayed suspension bridge. *Mathematical Problems in Engineering*(Article ID 805195), 12.
- Wang, H.-L., Tan, Y.-B., Qin, S.-F., & Zhang, Z. (2013). Geometric nonlinear analysis of self-anchored cable-stayed suspension bridges. *The Scientific World Journal*(Article ID 734387), 5.
- Wang, P., Tang, T., & Zheng, H. (2004). Analysis of cable-stayed bridges during construction by cantilever methods. *Computers and Structures*, 82(4-5), 329-346.
- Wang, P., Tseng, T., & Yang, C. (1993). Initial shape of cable-stayed bridges. *Computers and Structures*, 47(1), 111-123.
- Wang, Y., Vlahinos, A., & Shu, H. (1997). Optimization of cable preloading on cable-stayed bridges. *Smart Systems for Bridges, Structures, and Highways* (p. 248-259). San Diego, CA: Norris Stubbs.
- Warnitchai, P., Fujino, Y., & Susumpow, T. (1995). Non-linear dynamic model for cables and its application to a cable-structure system. *Journal of Sound and Vibration*, 187(4), 695-712.

- Wickert, P., Canfield, A., & Reddy, J. (2010). Least-squares continuous sensitivity shape optimization for structural elasticity applications. *American Institute of Aeronautics and Astronautics Inc. (AIAA)*, 48(12), 2752-2762.
- Wilson, J., & Gravelle, W. (1991). Modelling of a cable-stayed bridge for dynamic analysis. *Earthquake Engineering and Structural Dynamics*, 20(8), 707-721.
- Wolff, M., & Starossek, U. (2009). Cable loss and progressive collapse in cable-stayed bridges. *Bridge Structures*, 5(1), 17-28.
- Wriggers, P. (2008). *Nonlinear Finite Element Methods*. Berlin, Germany: Springer.
- Xia, H., Xü, Y., & Chan, H. (2000). Dynamic interaction of long suspension bridges with running trains. *Journal of Sound and Vibration*, 237(2), 263-280.
- Xu, Y., Chen, Z., & Xia, Y. (2012). Fatigue assessment of multi-loading suspension bridges using continuum damage model. *International Journal of Fatigue*, 40, 27-35.
- Yamaguchi, H., & Ito, M. (1997). Mode-dependence of structural damping in cable-stayed bridges. *Journal of Wind Engineering and Industrial Aerodynamics*, 72(1-3), 289-300.
- Yang, F., & Fonder, G. A. (1998). Dynamic response of cable-stayed bridges under moving loads. *Journal of Engineering Mechanics*, 124(7), 741-747.
- Yoo, H., & Choi, D. (2008). New method of inelastic buckling analysis for steel frames. *Journal of Constructional Steel Research*, 34(10), 1152-1164.
- Yoo, H., & Choi, D. (2009). Improved system buckling analysis of effective lengths of girder and tower members in steel cable-stayed bridges. *Computers and Structures*, 87(13-14), 847-860.

- 
- Yoo, H., & Choi, D. (2012). Approximate method for estimation of collapse loads of steel cable-stayed bridges. *Journal of Constructional Steel Research*, 72, 143-154.
- Zhang, H., & Xie, X. (2011). Dynamic responses of cable-stayed bridges to vehicular loading including the effects of the local vibration of cables. *Journal of Zhejiang University: Science A*, 12(8), 593-604.
- Zhang, J., & Au, F. T. (2013). Effect of baseline calibration on assessment of long-term performance of cable-stayed bridges. *Engineering Failure Analysis*, 35(15), 234-246.
- Zhang, Y. (2003). The concept and development of smart structures technologies for long-span cable-supported bridges. *Marine Georesources and Geotechnology*, 21(3-4), 315-331.
- Zhang, Z., Wang, H., Qin, S., & Ge, X. (2009). Limit span of self-anchored cable-stayed suspension cooperation system bridge based on strength. *Frontiers of Architecture and Civil Engineering in China*, 3(3), 286-291.
- Zhu, J., Ye, G., Xiang, Y., & Chen, W. (2011). Dynamic behavior of cable-stayed beam with localized damage. *Journal of Vibration and Control*, 17(7), 1080-1089.